Environment Canada

Environmental Protection Service

Environnement Canada

Service de la protection de l'environnement

Microwave Systems for Detecting Oil Slicks in Ice-infested Waters:

Phase 1 - Literature Review and Feasibility Study

Economic and Technical Review Report
EPS 3-EC-81-3

Environmental Impact Control Directorate
September 1981

ENVIRONMENTAL PROTECTION SERVICE REPORT SERIES

Economic and Technical Review Reports relate to state-of-the-art reviews, library surveys, industrial inventories, and their associated recommendations where no experimental work is involved. These reports will either be undertaken by an outside agency or by the staff of the Environmental Protection Service.

Other categories in the EPS series include such groups as Regulations Codes, and Protocols; Policy and Planning; Technology Development; Surveillance; Training Manuals; Briefs and Submissions to Public Inquires; and Environmental Impact and Assessment.

Inquiries pertaining to Environmental Protection Series should be directed to the Environmental Protection Service, Department of the Environment, Ottawa, Ontario, Canada, K1A 1C8.

Minister of Supply and Services Canada 1981

Catalogue No. En 46-3/81-3E
ISBN: 0-662-11657-7

MICROWAVE SYSTEMS FOR DETECTING OIL SLICKS IN ICE-INFESTED WATERS: PHASE 1 - LITERATURE REVIEW AND FEASIBILITY STUDY

by

C-CORE
Centre for Cold Ocean Resources Engineering
Memorial University of Newfoundland
St. John's, Newfoundland

for the

Environmental Emergency Branch
Environmental Impact Control Directorate
Environmental Protection Service
Environment Canada

EPS 3-EC-81-3
September 1981

Disponible en français

s'adresser au:

Coordonnateur des publications
Direction générale du contrôle des incidences environnementales
Service de la protection de l'environnement
Environnement Canada
Ottawa (Ontario)
K1A 1C8

ABSTRACT

A study was undertaken to ascertain the possibilities and problems associated with the use of microwave techniques in detecting oil pollution in the ice environment. A comprehensive investigation into the microwave emission and scattering properties of sea ice, oil on water, and the ocean surface was made and the results of analyses are presented. Available information on the electrical properties of oil and the behaviour of oil in the ice environment is included. A selected, annotated bibliography of the published literature on microwave scattering and emission from sea ice, water and oil on the water surface is attached as Appendix 6. The design and data requirements of an experiment have been outlined. Possible radar data processing and analyses methods are given. In recommending required future efforts, it is suggested that theoretical and laboratory studies, as well as experiments under controlled conditions, are likely to produce quantitative information on the microwave emission and scattering from oil in the ice environment.

The results show that only a qualitative assessment of a limited nature can be made on the performance of active and passive microwave systems in detecting oil slicks in the ice environment from the limited information available on microwave emission and scattering from sea ice, oil on water, and the ocean.

It appears that either Ku- or X-band active measurements, along with L-band measurements, are suitable for detecting oil when it is present on and in the top surface of the ice. Both VV and HH polarizations seem equally likely to succeed, with cross-polarization providing additional useful information.

The passive systems operating at frequencies of around 37 GHz with horizontal polarization and at angles of incidence of 30° to 45° from nadir seem appropriate. The use of a lower frequency in the range from 8 to 14 GHz may provide additional information.

Active and passive systems operating in the frequency range from 100 to 300 MHz may be able to detect oil when it is present under ice, or is contained within the lower regions of sea ice.

The presence of oil in the ice environment is likely to be detected through indirect subtle clues (i.e., changes in texture and tone such as those produced by increased melting of oil covered areas in comparison with oil free areas).

RÉSUMÉ

La présente étude évalue les possibilités et les limites des techniques micro-ondes utilisées pour la télédétection des hydrocarbures en milieu glaciel. Elle rapporte les résultats de recherches approfondies sur les propriétés d'émission et de rétrodiffusion de micro-ondes de la glace de mer, des hydrocarbures sur l'eau, et de la surface de la mer. Le lecteur trouvera aussi des renseignements sur les propriétés électriques des hydrocarbures et sur leur comportement en milieu glaciel. L'annexe 6 offre une bibliographie critique sur la rétrodiffusion et l'émission de micro-ondes par la glace de mer, l'eau et les hydrocarbures à la surface de l'eau. Les auteurs donnent des indications relatives à la conception et aux données requises pour une expérience. Les méthodes de traitement et d'analyse de données radar sont définies. Enfin, les recommandations laissent entrevoir que des études théoriques et en laboratoire ainsi que des expériences contrôlées fourniront probablement des données quantitatives sur les propriétés d'émission et de rétrodiffusion micro-ondes des hydrocarbures en milieu glaciel.

Les résultats montrent que seule une évaluation qualitative d'une portée limitée peut être faite sur le rendement des télédétecteurs à micro-ondes (passifs et actifs) dans la détection des nappes d'hydrocarbures en milieu glaciel à partir des rares renseignements accessibles sur l'émission et la rétrodiffusion de micro-ondes par la glace de mer, les hydrocarbures sur l'eau et la mer.

Les mesures de détection active dans des bandes Ku ou X ainsi que dans la bande L paraissent convenir pour des hydrocarbures qui se trouvent à la surface de la glace ou dans la couche supérieure. Les deux types de polarisation VV et HH semblent avoir les mêmes chances de succès et la polarisation croisée permettra d'obtenir d'autres renseignements utiles.

Les appareils passifs fonctionnant à des fréquences d'environ 37 GHz en polarisation horizontale et à des angles d'incidence de 30° à 45° du nadir semblent appropriés. On peut obtenir des renseignements additionnels en utilisant une fréquence inférieure dans la gamme de 8 à 14 GHz. Les appareils actifs et passifs fonctionnant dans la bande de fréquence entre 100 et 300 MHz peuvent détecter les hydrocarbures qui se trouvent sous la glace ou dans les couches inférieures de la glace de mer.

La présence d'hydrocarbures en milieu glaciel peut vraisemblablement être décelée grâce à des indices indirects tels les changements de texture et de niveau au moment de la fonte accélérée qui distingue les zones recouvertes d'hydrocarbures des zones non polluées.

FOREWORD

This is phase one of a report which outlines the results of a study concerning the detection of oil slicks in ice-infested waters, utilizing microwave systems. A feasibility study and literature review are included in this phase of the report. The work in this report was executed by C-CORE, under the supervision of Dr. R.A. O'Neil of the Canada Centre for Remote Sensing (CCRS), who acted as scientific authority. The report was supported by CCRS as part of the Arctic Marine Oilspill Program (AMOP), sponsored by the Research and Development Division, Environmental Emergencies Branch, Environmental Protection Service, Environment Canada.

TABLE OF CONTENTS

LIST OF FIGURES

CONCLUSIONS AND RECOMMENDATIONS

Only a qualitative assessment on the possibilities and problems associated with the detection of oil in the ice environment can be made from the available data. The total lack of information in certain cases, and gaps in others, does not permit a more quantitative investigation. It appears that microwave systems may be more useful under certain situations than others, however, the numerous variables involved and lack of information does not permit a better identification of favourable or unfavourable situations. The investigation shows that the nature of microwave scatter and emission from sea ice is poorly understood. Some parameters of sea ice which affect the radar return and microwave emission have been isolated, but information on how these parameters interact to produce the changes in radar return and emission is lacking. The quantitative relationship between sea ice parameters and scattering and emission levels has yet to be established. The utility of active and passive microwave systems for ice reconnaissance, however, is well established. The relationship between wind speed and microwave emission and scattering from temperate oceans is established to a certain extent. The applicability of these results to the colder environment, especially in the leads where wind induced surface roughness effects may be reduced, can only be assumed. No information is available on the electrical properties of oil at near freezing and below freezing temperatures. The role of active and passive microwave systems for oil pollution surveillance in the temperate oceans is well established and these are being used operationally by the U.S. Coast Guard. But there is a lack of quantitative information on the microwave scattering and emission from oil polluted waters. The information available on the behaviour of oil in the ice environment is mostly based on theoretical and laboratory investigations.

The need to conduct a controlled, well defined experiment where oil is spilled intentionally into the ice environment is clear. One experiment, however, is unlikely to be definitive, as it will not be possible to cover the various situations in which oil is going to be present under actual accidental circumstances. The microwave systems such as imaging radars, radiometers, and scatterometers will only be useful when oil is present in or over the top surface of ice. For detecting oil under ice, probing radars or radiometers operating at longer wavelengths will be needed. It appears the presence of oil is likely to be detected through indirect subtle clues such as a change in texture, tone and the occurrence of melt pools.

The information available on microwave scattering from the ocean, ice and oil on ice is unlikely to be conclusive with regard to the possibilities of oil detection in an ice environment. The oil interacts with sea ice and its detection is influenced by how this interaction changes the physical and electrical properties of the medium as a whole, and how these changes affect the microwave scattering and emission.

In view of the above, it is clear that even a full-scale experiment is unlikely to be conclusive, so theoretical studies, laboratory investigations, and controlled experiments need to be undertaken. Recommendations for specific work related to the problem of detection of oil in the ice environment through microwave techniques are:

(a) The measurement of electrical properties of various types of oil as a function of frequency for various temperatures especially at, near and below freezing temperatures;

(b) Theoretical and laboratory investigation into the electrical properties of heterogeneous mixtures such as oil/ice, oil/snow, and oil/water mixtures, and how these change as a function composition, temperature, and frequency;
(Various models are available for computing electrical properties of heterogeneous mixtures).

(c) Theoretical and laboratory investigations into the changes in the microwave emission and scattering due to the presence of oil in and over sea ice;
(Models are available for computing brightness temperatures and the value of σ^{o} for sea ice. The models do provide results which are in general agreement with the experimental results. At the very minimum these models can provide data of a relative nature when oil is introduced into sea ice. At the present time, even the changes produced in the reflection coefficient due to the presence of oil in sea ice are not known.)

(d) Studies of the effect of changes in temperature and salinity, especially for temperatures near freezing, on microwave scattering and emission from the ocean;
(These can easily be achieved through theoretical investigations.)

(e) Investigations should be undertaken to ascertain microwave emission and scattering from oil covered cold water surfaces, and oil under sea ice;
(These can be more readily ascertained from controlled laboratory experiments. In addition, theoretical studies can be conducted to extrapolate to experimental results.)

(f) An investigation to ascertain if the changes in the emission and scattering levels produced due to the presence of oil over and in various types of sea ice fall within the variance produced by a sea ice type;

(The radar return from sea ice and from any other target is statistical in nature due to fading. As a result the observed mean value over a target can fluctuate over a large dynamic range. In addition, signal fluctuations also occur due to the changes in the characteristics of the medium from one place to another. If the two parts can be separated then the changes in the level due to the variation in the characteristics may provide a clue to the identity of the target. Some ice types are more homogeneous than others and, therefore, likely to produce less variance. An analysis of variance produced by various types may enable the classification of ice types. Moreover, if the variance introduced by the sea ice types and the ocean surface is known, then any slight change due to the presence of oil may be detectable. It is for this reason that it is considered important to determine the statistics of radar backscatter from sea ice and ocean surfaces. Such a study should be undertaken.)

(g) Studies to ascertain the "true" texture of various ice types should be conducted;

(The texture exhibited on a SAR image is partly dependent on the system design and averaging, and partly on the characteristics of the target. Such a study can also provide information on how degrading resolution influences the interpretability of a radar image. The use of both texture and tone has to be incorporated into the classification and interpretative process. If the texture introduced by the sea ice can be ascertained then the change in texture due to the presence of oil can be more fully identified. It is for this reason that texture discrimination studies should be carried out on the available SAR data of sea ice).

(h) Investigations to ascertain the effect of using various parameters in processing SAR data; and,

(i) Studies into the use of various image enhancement techniques such as tone enhancement, texture enhancement, averaging, and channel addition and subtraction.

In terms of priorities, recommendations (b), (c), (d), and (f) are more important than others. The recommendations (g), (h), and (i) should be implemented when SAR data collected under AMOP (Arctic Marine Oilspill Program) are analyzed.

C-CORE has been able to collect good quality multi-channel SAR imagery of sea ice under its SAR '77 program using ERIM's radar system. Part of this imagery has been selected under Phase II of the present contract to undertake studies related to recommendations (f) through (i). Some aspects of the recommendations can be accomplished under Phase III and will produce valuable information on the processing and analysis of SAR data.

1 INTRODUCTION

Petroleum exploration in northern regions has increased the potential for oil spills in ice-infested waters. The harsh environment of this area influences the risk of oil pollution through equipment failure and human error; as well as by hampering clean-up operations. Oil spills may be caused by collision between oil carrying tankers and other vessels, leaks, pipe rupture or blowouts at well drilling sites. Ice and icebergs present a hazard to oil exploration, production and transportation, especially off the coast of Labrador.

Oil spilled in this ecologically fragile environment could cause serious harm, especially if the spill is large. It is necessary, therefore, that a means for locating, detecting, identifying, monitoring, containing, and recovering oil spilled in the ice environment be provided. The techniques used will differ from those required in temperate regions because of the presence of ice, icebergs, uncertain weather and long periods of darkness.

1.1 Background

Oil in the ice environment is subject to the same processes of spreading, evaporation, dissolution, emulsification, sinking, microbial modification, photochemical modification, and biological degradation as that in temperate regions. There can be, however, considerable differences between the rate of these processes in the cold and ice environment and that of the temperate region. The colder climate of the Arctic and sub-arctic increases the longevity of spilled oil by decelerating natural degradation processes. Depending on the sea and ice conditions, spilled oil may spread over the ice, under the ice, on the water, or in several modes at once. In addition, oil may become absorbed and entrapped in ice, covered with snow, or a mixture of snow and oil may result on the top surface of the ice. Oil spilled under ice may rise to the top of the surface in spring and summer through brine channels. Oil pools combined with ice melt pools may be present in summer and spring, and refreeze in winter.

It has been found that the roughness of the top and bottom surfaces of ice may act as a natural barrier for the containment of the oil; however, oil spilled may be dispersed over a large area due to opening and closing of leads, ice drift, and currents. Remote sensing techniques may provide viable means of locating, detecting and monitoring oil pollution in regions where there is a possibility of oil dispersal over a large area and an uncertainty of its behaviour in ice-infested waters.

The role of remote sensing techniques in locating, detecting (the type), and monitoring oil pollution over the temperate oceans is established to a certain extent. A number of sensors such as laser fluorosensors, active and passive microwave systems, low light level television cameras, and ultraviolet sensors operating in different parts of the electromagnetic spectrum are being operationally used for oil pollution surveillance and monitoring. The microwave systems are unique among remote sensors in providing almost all weather, day/night operational capability and large areal coverage.

1.2 Purpose

The purpose of this study was to investigate the possibility of using microwave systems in locating, detecting (the type), and monitoring oil slicks over ice and ice-infested waters. Remote sensors, including microwave systems, have yet to be tested for their ability to locate, detect, and monitor oil pollution in ice and ice-infested waters.

Both active and passive microwave systems have proven their capability for ice reconnaissance and monitoring, wind speed measurement over the oceans, imaging of ocean waves and currents, determination of ocean temperature and salinity, snow pack mapping, and locating, detecting, and monitoring oil pollution over ice-free temperate oceans. Some of these systems are operational; however, in certain cases, operational use is being explored.

In this study, an attempt was made to ascertain the contrast in readings from an oil spill and the surrounding water, ice and snow surfaces, using microwave emission and radar scanning techniques. Operating parameters under which this contrast could be enhanced were studies, as well as conditions which could cause "false alarms", so that these could be reduced. The objectives were accomplished using available information on microwave emission and scattering from ice, oil, and water.

1.3 Scope

The scope of this study is limited to the extent of information available on the microwave emission and scattering properties of ice, oil, and water. Limited quantitative information is available on the changes in microwave characteristics with changes in the properties of sea ice. The nature of radar scattering and microwave emission from sea ice has yet to be fully understood. Some parameters of sea ice which play a dominant role in affecting emission and scattering have been isolated, but information on how these parameters interact to produce changes in scattering and emission is limited. Sea ice is a complex medium which is formed and found under diverse and variable conditions. As a

result, the strength of microwave emission and scattering signals from sea ice varies over a wide, dynamic range. The same ice conditions may appear differently on imagery produced with different systems.

There is little information documented on the electrical and physical properties of oil and snow as a function of frequency and temperature. More quantitative data are available concerning the emission of oil on water than scattering from oil on water. The microwave characteristics of the ocean surface are known to a certain extent. The behaviour of oil in ice and ice-infested waters, however, is still being investigated.

Some information is available individually on the microwave characteristics of sea ice, oil on water, and water alone. The task is to combine this information and assess if oil over ice and oil in ice-infested waters will present measurable changes in scattering and emission. The assumption inherent in this approach of combining and predicting is that the microwave emission and radar scattering are linear phenomena, and thus the microwave characteristics of oil over ice and ice-infested waters can be ascertained by linear manipulation and comparison. Oil, however, does interact with ice, snow, and water and in certain cases produces mixtures; as a result, the study can only be qualitative in nature, and thus limited in scope.

No attempt is made to model the changes produced in the microwave emission and scattering due to the interaction of oil with snow and ice and the resulting changes in their electrical and physical properties. To help fulfill the objectives of this study, a library search was undertaken and an annotated bibliography of some of the available literature on microwave scattering and emission from sea ice, water and oil was compiled (see Appendix 6).

The information available in the literature was reviewed and analyzed and results are presented in Appendices 1 through 5. The material in the appendices consists of discussions on the behaviour of oil in the ice environment (Appendix 1); the electrical properties of oil (Appendix 2); microwave emission and scattering from water (Appendix 3); microwave emission and scattering from ice and snow (Appendix 4); and microwave emission and scattering from oil on water (Appendix 5).

Section 2 of the main report contains a brief outline of the theory and operational characteristics of microwave systems. The effect of atmospheric attenuation on microwave signals is also discussed in Section 2.

The summary of results from the material presented in Appendices 1 through 5 is provided in Section 3. Section 4 contains a discussion on the detection and monitoring of oil in the ice environment based on the available information.

A discussion on the optimum systems and operating parameters required for detecting and monitoring oil in the ice environment through microwave techniques is presented in Section 5.

The design of a remote sensing experiment to test the ability of microwave systems to detect and monitor oil in the ice environment is outlined in Section 6. A discussion on the data requirements of this experiment including the possible modes of data processing and analyses is found in the conclusions and recommendations of this study.

2 MICROWAVE SYSTEMS

The microwave spectrum extends approximately from 1 mm to 1 m in wavelength (300 MHz to 300 GHz frequency). The frequency range from 100 to 300 MHz is of interest for ice probing radars. Microwave sensors can measure through cloud cover and some rain with the measurements being almost independent of weather at the lower microwave frequencies. As a result, microwave systems can provide timely information under both day and night conditions when other systems become inoperable due to weather and lack of incident light.

Microwave responses are functions of the frequency (or wavelength), polarization, and look angle which are dependent on the electrical and physical properties of the target. Surface roughness and subsurface structure are examples of these.

Active microwave systems transmit their own signal and measure the energy returned back from the target. Passive microwave systems measure the natural radiation emitted by the target plus the energy from other sources reflected from it, and are, therefore, more sensitive to atmospheric conditions than active systems. The spatial resolution achieved by the passive systems is inherently poorer than that achieved by active systems. In addition to the antenna beamwidth limitation, active systems may achieve spatial resolution through doppler-angle, range-angle, and range-doppler configurations. The best resolution is achieved through range-doppler techniques as in the case of synthetic-aperture radar (SAR). Spatial resolution can be limited only through the antenna beamwidth, in passive systems.

The theories and operations of both active and passive microwave systems are presented in detail by Skolnik (1970) and Moore (1975).

2.1 Active Microwave Systems

Radar is an active system, as it transmits its own electromagnetic energy and measures the energy reflected or scattered from a target. Radar can produce an output in an imaging format (called imaging radar such as Side-Looking Airborne Radar (SLAR), or a non-imaging format such as a scatterometer line trace.

SLAR is designed as a side-looking instrument, to permit better resolution than otherwise possible. The SLAR system transmits a beam in a fixed direction perpendicular to the line of flight. Coverage of ground features is accomplished by the forward motion of the vehicle carrying the radar, which allows successive transmitted beams to cover new areas. These continuous line scans result in a composite coverage of

a wide swath of the surface. The energy reflected back to the radar from the targets is recorded on a photographic film. The amount of backscatter returned by ground features is determined by the radar frequency, angle of incidence, the surface roughness on the scale of the radar wavelength, the dielectric properties of the target, and the aspect angle.

The ability of a radar system to image an individual target depends on the range to the target, the radar backscatter of the target, and the sensitivity of the receiver. Discrimination between two closely spaced targets is a function of the system resolution, since resolution, in general, is defined as the ability to distinguish between two adjacent objects on the ground. Imaging radar is characterized by each area the size of one resolution cell producing one point on the image.

In both non-coherent (real-aperture radar) and coherent (synthetic-aperture radar, SAR) modes, the resolution in the across-track is achieved by transmitting a short pulse; shorter pulses means smaller resolution cells. For "real-aperture" radar, in the along-track or azimuth direction, the resolution is limited by the antenna beamwidth and increases with increasing range. The narrower the beamwidth, the smaller is the size of the resolution cell. A narrower beamwidth can be obtained by increasing the size of the antenna or increasing the frequency. In the case of SAR the length of the antenna is increased synthetically, by storing both the amplitude and phase of the return signal and adding the signals coherently (Skolnik, 1970). The length available for generating a synthetic-aperture is the distance over which a target is within the physical beamwidth of the antenna. A longer length is available at longer ranges. In theory, therefore, a fully focussed case, (azimuth resolution), which is equal to half the physical antenna length independent of the wavelength and range, can be obtained by synthetic-aperture techniques (Brown and Porcello, 1969).

The image produced by a radar is somewhat similar, although not identical to an optical photograph. The difference is caused by the use of longer wavelengths and distortion resulting from various geometric differences.

The density, brightness, or grey-tone on a radar image is proportional to the received power, which in turn depends on the radar backscatter coefficient; σ^{o} (radar cross section normalized to the illuminated area), and the system and flight parameters. Essentially, it is the variation of σ^{o}, which is depicted as variation in density or brightness on an image. The linking parameter between the brightness on a radar image and the properties of a target is the quantity, σ^{o}.

All of the SLAR systems in operation today are uncalibrated. Thus, the grey-tone, brightness or density on a radar image is a relative and not an absolute quantity. As a result it is not possible to compare images obtained from two different systems or to compare images produced by the same system at different times unless a common reference point is established for calibration purposes.

A radar scatterometer, in contrast to an imaging radar, is by design a calibrated system and permits a more detailed and quantitative observation of radar scattering behaviour (Moore, 1966). The radar scatterometer is an instrument designed to measure 'σ^{o}' as a function of the illuminated angle, 'θ' (angle measured from the vertical). The data obtained from the scatterometer is of great value for understanding the nature of the radar return from different targets and for the design of future radar systems.

As pointed out by Moore and Thomann (1971), a trade-off exists between the grey-tone resolution and spatial resolution in a radar system. The grey-tone resolution is dependent on the number of independent samples averaged because of the statistical nature of the radar return. In general, more independent samples are averaged in a non-coherent, real-aperture radar, than in a synthetic aperture radar. As a result, the "speckled" texture exhibited on a synthetic aperture radar image may not be due to the properties of the target but rather to the system design (Moore, 1976).

In addition to the above, radar systems may be designed to probe glaciers, snow, and sea ice. These ice probing radars may prove valuable in detecting oil under sea ice. The possibilities of using probing radars to measure sea ice thickness have been explored (Parashar et al.1977).

2.2 Passive Microwave Systems

Any object which has a temperature above $0^{o}K$ emits (and absorbs) electromagnetic energy in different parts of the frequency spectrum. The relationship between the frequency of emittance (or absorption) and the amount of energy emitted (or absorbed) is given by Planck's Black-Body Radiation Law (Chandrasekhar, 1960).

The temperature equivalent to the energy measured by a radiometer (a passive microwave system) is termed the "Apparent Temperature". In a practical situation a radiometer viewing the surface of the earth measures contributions from surface emission, emission and partial absorption, by the intervening atmosphere emitted and the atmospheric radiation reflected by the surface in the direction of the radiometer.

The apparent temperature (T_{ap}) of the surface when measured by the radiometer at an angle Θ from the vertical is given by:

$$T_{apj}(\Theta) = L(\Theta)\left[T_{Bj}(\Theta) + T_{sj}(\Theta)\right] + T_{atm}(\Theta) \qquad (1)$$

In the above equation "j" represents vertical or horizontal polarization and $L(\Theta)$ is the atmospheric transmittance determined by atmospheric absorption between the surface and the radiometer in the direction Θ. $L(\Theta)$ can be written as:

$$L(\Theta) = \exp\left[-\text{Sec}\ \Theta \int_o^H \alpha(z)\, dz\right] \qquad (2)$$

$T_{atm}(\Theta)$ represents the contribution from the atmosphere and is given by:

$$T_{atm}(\Theta) = \text{Sec}\ \Theta \int_o^H T_{air}(z)\, \alpha(z) \cdot \exp\left[-\text{Sec}\ \Theta \cdot \int_z^H \alpha(x)\, dx\right] dz \qquad (3)$$

Equation (3) gives the emittance by the atmosphere and subsequent attenuation by the intervening atmosphere.

Parameters appearing in equations (1), (2), and (3) are defined as follows:

$\alpha(z)$ = the atmospheric attenuation coefficient per unit length at an altitude of 'z' Km.

$T_{air}(z)$ = thermometric temperature of air (atmospheric temperature) at an altitude of 'z' Km above the surface.

H = height of the radiometer from which the measurement is made.

$T_s(\Theta)$ = the emitted atmospheric radiation reflected by the surface of the earth in the direction of the radiometer.

x = a dummy variable.

$T_B(\Theta)$ = brightness temperature of the surface of the earth = εT.

where: ε = emissivity of the surface.

T = thermometric temperature of the surface.

In order to compute the value of the apparent temperature measured by the radiometer we need to know three quantities:

(1) The variation of the absorption coefficient with height;

(2) The temperature profile, that is, the variation in the temperature with altitudes; and,

(3) The brightness temperature of the surface.

The actual signal received and measured by the radiometer is in fact dependent on the antenna radiation efficiency, atennna power pattern, and the main beam efficiency. If the antenna radiation efficiency corrections are made on the received signal, the corrected signal is termed the antenna temperature. The antenna temperature is the weighted average of apparent temperature over the antenna power pattern and is dependent on the main beam efficiency.

The distinction among the antenna temperature, apparent temperature and brightness temperature is not normally made by some researchers but should be when reporting radiometric measurements. Thus, to determine brightness temperature from the radiometric signals, the effects of the antenna power pattern and atmospheric attenuation should be taken into account. For a loss-less atmosphere and measurements made with a radiometer having a main beam efficiency of one, the output signal is the same as the brightness temperature. The emissivity of the target for the frequency of interest can be obtained from the brightness temperature if the thermometric temperature of the target is known. The calibration in a radiometer is achieved by comparing the received signal with cold and hot reference temperatures. Radiometers can be operated in a scanning mode, providing output in an image format or a non-imaging mode.

2.3 Atmospheric Attenuation

The attenuation (absorption and emission) of microwaves in the atmosphere is caused primarily by gas molecules (having different magnetic and electric dipole moments), fog, water vapour, and clouds. In the microwave region attenuation in the atmosphere is mainly due to the presence of oxygen and water vapour; the attenuation by other gases is small. As the density and percentage (approximately 21%) of oxygen in the atmosphere remains constant all the time, the attenuation by oxygen is mainly dependent on wavelength. The density and percentage of water vapour keeps changing in the atmosphere, so attenuation is dependent on both wavelength and density.

The absorption coefficient $\alpha(z)$ may be written as a sum of the contributions from each source:

$$\alpha(z) = \alpha_{O_2}(z) + \alpha_{H_2O}(z) + \alpha_{cloud}(z) + \alpha_{rain}(z)$$

where z is the altitude, α_{O_2}, α_{H_2O}, α_{cloud}, and α_{rain} are the absorption coefficients of

oxygen, water vapour, condensed water droplets (liquid or ice) in clouds, and rain, respectively.

The equations for calculating absorption coefficients for water vapour, oxygen, and cloud given by Edgerton et al. (1973) are based on Van Vleck (1947a and b) for oxygen and water vapour, and on Gunn and East (1954) for cloud.

A summary of atmospheric attenuation as a function of frequency is provided in Figure 1. The one way attenuation through standard atmosphere due to oxygen and water vapour is presented in Figure 2 (Moore, 1975). The brightness temperature as a function of frequency over water and land is presented in Figure 3 (Staelin, 1966). The attenuation of radar signals for various rain fall rates is presented in Figure 4 (Medhurst, 1965).

As shown in these figures, serious atmospheric effects on radar are confined to the shorter wavelengths. The atmosphere only slightly absorbs radar signals at most of the wavelenghts used, and usually wavelengths longer than 3 cm are relatively unaffected. Radar echoes from precipitation and clouds present more of a problem than absorption as these mediums might obscure a desired echo. Cross-polarized returns from clouds and rain are normally smaller than the ground echo; so, this mode may be used in such cases. Even a heavy rain fall has a negligible effect on radar signals for wavelengths beyond about 8 cm. Snowfall may affect the radar signals but measurements under such conditions are not available.

Radiometers are more sensitive to atmospheric conditions than radars because the strength of the signal is considerably smaller. Depending on the temperature and type of cloud, a radiometer may indicate a higher or lower value of brightness temperature for the target than exists.

Edgerton et al. (1971) used aircraft meteorological data (pressure temperature, and water vapor density), together with visual estimates of cloud height and density, obtained during microwave measurements, to compute estimates of the effects of atmospheric attenuation (and re-radiation). Two different atmospheric models were investigated: one derived from measured meteorological data incorporating clouds and another using an Arctic Summer Atmosphere model having no clouds. In both cases, the computed brightness temperatures of sea water (0^{o}C and a salinity of 35^{o}/oo) due to atmospheric contributions between sea level and a 9 km altitude were 3 to 4^{o}K at 2.81 cm, 10 to 12^{o}K at 1.55 cm, 10 to 18^{o}K at 1.35 cm (nadir), 8 to 10^{o}K at 0.96 cm, 15 to 17^{o}K for horizontal polarization at 0.81 cm (45^{o} from nadir) and 10 to 13^{o}K for vertical

polarization at 0.81 cm (45^{o} from nadir). Also, increases in the computed brightness temperature of seawater due to increases in cloud water content (0 to 0.3 kg/m^2) at a 9 km altitude were $4^{o}K$ at 2.81 cm, $7^{o}K$ at 1.55 cm (nadir), $9^{o}K$ at 1.35 cm, $15^{o}K$ at 0.96 cm, and $30^{o}K$ and $18^{o}K$ at 0.81 cm for, respectively horizontal and vertical polarization (45^{o} from nadir). It was noted that the effect of the atmospheric contribution is significantly reduced when viewing substances whose emissivities are larger than that of seawater. For example, the increases noted above when viewing seawater at a range of 0 to 9 km are greatly reduced when viewing a substance whose low altitude brightness temperature is $230^{o}K$: 1 to $2^{o}K$ at 2.81 cm, 2 to $3^{o}K$ at 1.55 cm, 5 to $6^{o}K$ at 1.35 cm, 2 to $3^{o}K$ at 0.81 cm, and 4 to $5^{o}K$ at 0.96 cm.

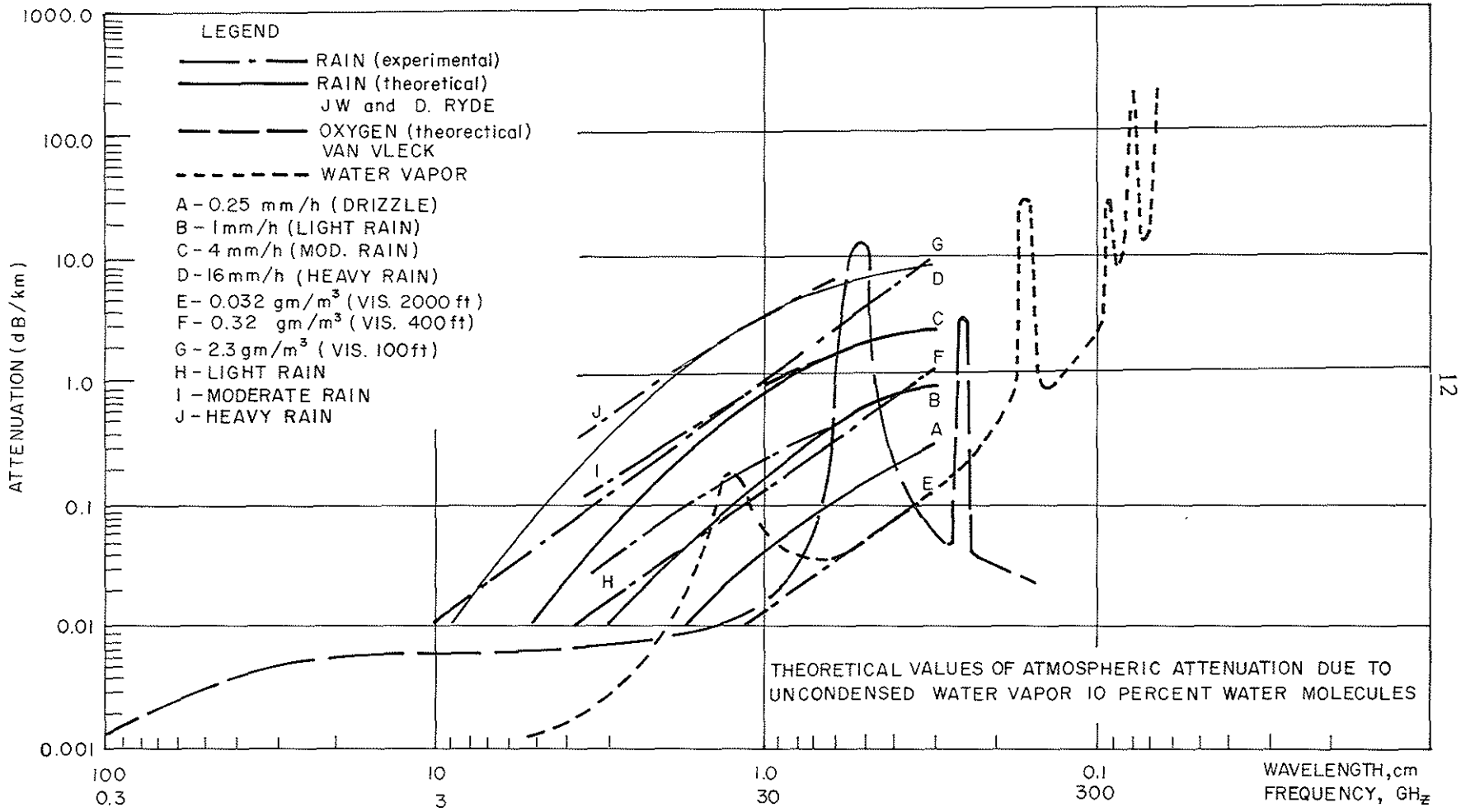

FIGURE 1 ATMOSPHERIC ATTENUATION SUMMARY

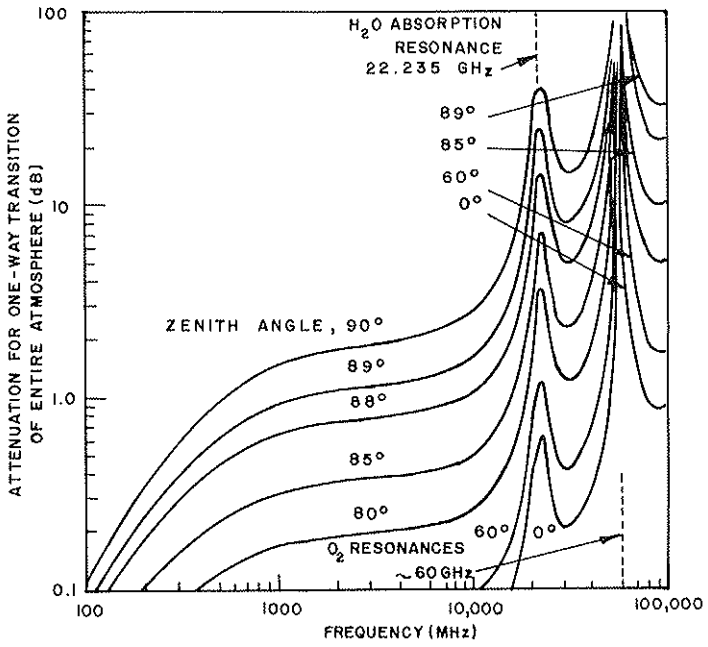

FIGURE 2 ONE WAY ATTENUATION THROUGH THE STANDARD SUMMER ATMOSPHERE DUE TO OXYGEN AND WATER VAPOR (Moore, 1975).

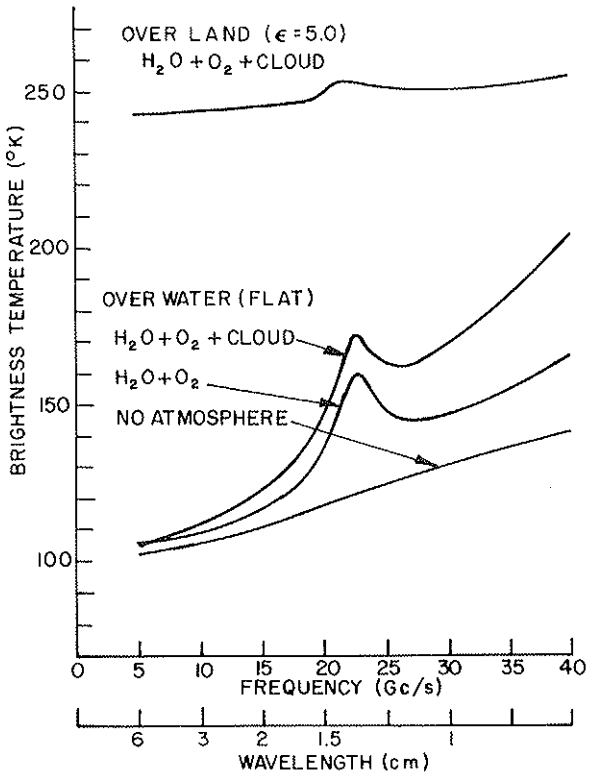

FIGURE 3 BRIGHTNESS TEMPERATURE VS FREQUENCY (Staelin, 1966).

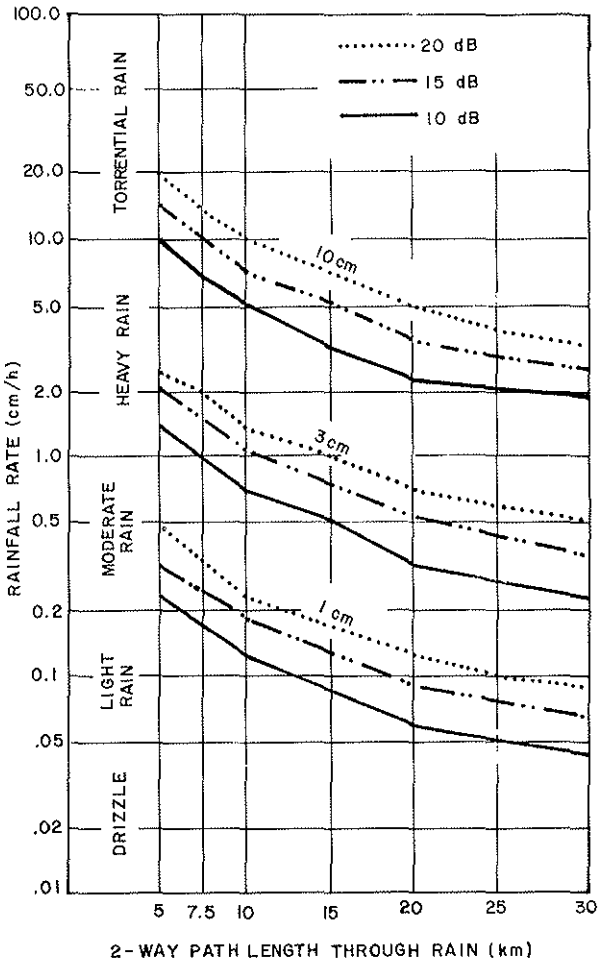

FIGURE 4 ATTENUATION OF 1, 3, AND 10 cm, RADAR BY RAINFALL. THE ATTENUATIONS GIVEN ARE VERY CONSERVATIVE, BEING THE MOST EXTREME DETERMINED BY MEDHURST (1965).

3 SUMMARY OF RESULTS

The microwave scattering and emission characteristics of water, ice and oil over water were investigated on the basis of available literature, and detailed results are presented in the appendices. Summaries of the behaviour of oil in the ice environment and the electrical properties of oil are also included. An annotated bibliography of the published literature available on the microwave scattering and emission properties of oil, water, and ice was compiled and provided in Appendix 6.

It should be pointed out that whatever radar and radiometer data are available are of limited use because of the nonavailability of corroborative "ground truth" information. Moreover, most of the data had been gathered with uncalibrated systems which makes the task of evaluation and comparison difficult.

The following sections contain a summary of the material presented in Appendices 1 through 5.

3.1 Oil in the Ice Environment

Most research to date on the behaviour of spilled oil over and under sea ice has involved experiments in laboratory cold rooms or in stationary first-year ice. More research is needed on the behaviour of oil in regions where ice conditions are more dynamic and where multi-year ice is present. Significant points on the behaviour of oil in the ice environment are:

(a) The density of seawater is approximately 1.03 g/cm^3 and salt free; pure ice can have a density of about 0.91 g/cm^3. Sea ice has a variable density ranging from perhaps 0.70 g/cm^3 to 0.91 g/cm^3, the latter value being associated with old ice containing very little brine. The actual density of sea ice depends on the way it is formed and its subsequent history. In contrast, the density of North Slope crude oil is 0.89 and, after aging for two weeks in the arctic summer, the density rises to about 0.95. Hence, oil can be either lighter or heavier than sea ice.

(b) The spreading of oil on water surfaces in the temperate region occurs in three phases: inertial-gravity, viscous-gravity, and surface tension. The second phase reduces the slick thickness to approximately one millimeter and the third phase often reduces it to a monomolecular layer. In the cold environment, the slick may not reduce to monomolecular layer as the third, surface tension phase, does not occur for most of the oil types. Slick thicknesses from 1 mm to 1 cm have been

observed but, generally, slick thicknesses of about 0.5 cm are found. Thicker oil slicks are obtained due to herding of the oil by wind action and the natural roughness of the sea ice surface.

(c) Oil spilled on the upper surface penetrates summer ice, whereas virtually no oil penetration occurs on winter snow and ice. The temperature differences between the oil and snow or ice cause an immediate melting and refreezing at the interface. During winter conditions, falling or driven snow may saturate oil up to 80 percent by water volume, forming a cohesive oil/snow mixture.

(d) Oil spilled on the surface of the ice under summer conditions is light enough to spread into the lower topographic levels, and eventually migrates to melt pools already formed. The minimum oil layer thickness is about 0.5 cm. A model for the spreading of oil on an ice surface has been developed based on the statistics of the surface roughness.

(e) Oil spilled under ice becomes trapped in the uppermost irregular pockets at the ice-water interface. The equilibrium thickness of a continuous oil film is about 1 cm and the maximum thickness is determined by the depth of depressions or variations in the ice thickness. The free flow of oil is restricted by the roughness of the underside of ice. If oil and gas are released together, gas will replace oil at the ice-water interface and the oil thickness may be on the order of 1 mm.

During the ice growth season, oil may penetrate between 5 and 10 cm into the loose skeletal structure on the underside of ice. The oil may also adhere to the surface and become sandwiched between ice layers. Oil has an insulating effect which slows the formation of a second layer of ice.

(f) Oil enclosed in brine channels and trapped under areas of ice will remain essentially in its original state through winter. During the spring and summer, after the first-year ice surface melts and the brine channels open up, the oil may migrate to the surface of the ice. As the dark oil absorbs heat from the sun the rate of migration increases and oil forms a melt pool on the surface. Multi-year ice does not contains brine channels so oil may remain trapped for up to 3-4 years or longer. However, some studies have shown that, during early summer oil may be able to reach to the top of the ice surface, even in multi-year ice.

(g) The ice environment increases the longevity of spilled oil by decelerating natural degradation processes.

(h) Ice fields may provide natural barriers for ice containment.

(i) Oil dispersal over large areas may occur due to lead matrix pumping, melting of oiled hummocks, under ice transport through currents, and ice drift.

(j) There is a controversy as to whether a major oil spill will change the Arctic heat balance.

The behaviour of oil in the ice environment is fairly complex and depends on a number of conditions such as wind speed, air/ice temperature, type of ice, type and temperature of the spilled oil. Depending on the sea and ice conditions, spilled oil may spread or become absorbed into the surface and bottom layers of the ice, spread on the water, or spread in several modes at once.

3.2 Electrical Properties of Oil

There is little information documented regarding the dielectric properties of petroleum oils. There are a number of gaps in the dielectric property and frequency relationship. Most of the data available are for refined oils, not the types of oil likely to be involved in a major oil spill. Data for the less refined oils are available at very few frequencies. The significant electrical properties of oil are:

(a) One data set for refined oils shows that in the frequency range from 10^5 to 10^{10} Hz, the real part of the complex permittivity varies from 1.9 to 2.25 depending on the oil type. The corresponding imaginary part shows more fluctuations with frequency, and may vary in range from 1 to 140 ($x10^{-4}$).

(b) Another measurement at 4-4.5 GHz shows the real part to be between 2.27 and 2.43 depending on the oil type.

(c) The measurements at 37 GHz for crude oils indicate the real part to be between 1.82 and 3.01 and the corresponding imaginary part to be between 0.0148 and 0.3 depending on the oil type and age. Both real and imaginary parts seem to increase with decreasing gravity of crude oils. The effect of aging appears to increase the real and imaginary part of the complex permittivity of oil. The major change occurs in the imaginary part and an increase of two orders of magnitude has been reported for Bunker 'C' fuel oil.

(d) Measurements at 19.3 GHz for crude oils show the real part to be between 2.4 and 2.10 and the imaginary part to be between 0.01 and 0.05.

(e) The real part of the complex permittivity for crude oils has been reported to vary from 1.85 to 2.94 with 2.0 being the average value. The loss tangent ($x10^4$) has been reported to be 3 at 1 MHz, 15 at 10 GHz and 20 at 25 GHz.

During experimentation a different type of oil was used by each researcher. The effect of temperature on the dielectric properties of oil, however, has not been studied and all measurements have been made in the temperature range of 19°C to 26°C, where reported. Oil spilled in ice-infested waters is subject to temperatures lower than 0°C and its dielectric properties may be quite different. Only theoretical calculations have been undertaken to examine the effect of mixing oil and water. Formulae are available for computing dielectric properties of such heterogeneous mixtures as oil and water and oil and sea ice. No attempt has been made to use these formulae for oil/sea ice mixtures. An anomaly in the dielectric properties of oil seems to exist around 100 MHz, the frequency region found suitable for measuring sea ice thickness through ice probing radar, and this may prove to be useful for detecting oil under sea ice.

3.3 Microwave Scattering and Emission from Oceans

It has been demonstrated through experimental observation that ocean surface waves and patterns can be imaged with synthetic aperture imaging radars. A radar scatterometer is used for measuring ocean wind velocity. Passive microwave systems may be used for determining ocean temperature and salinity variations. The significant points related to microwave scattering and emission from the ocean are:

(a) The complex permittivity of seawater is dependent on salinity, temperature, and frequency, and may be computed by equation. The real part decreases and the imaginary part increases with increasing salinity and temperature. The dielectric properties of pure, fresh, and seawater seem to be identical for frequencies above 20 GHz.

Active

(b) Radar scattering from the ocean may be described through two scattering processes. For incidence angles less than 20°, the contribution to scattering from long wavelength ocean gravity waves is dominant and for angles greater than 20° capillary waves produce the dominant effect. The scattering from capillary waves is produced through "Bragg resonances" in which the radar return from adjacent crests of the most important ocean components of the sea spectrum add in phase. This condition provides a relationship between the ocean wavelength and the radar wavelength and is dependent on the angle of incidence. For the first order interaction "Bragg wavelength" for the ocean is the same as the probing radar wavelength at an incidence angle of 30°. A composite model based on smaller

wavelength capillary waves superimposed on longer wavelength gravity waves is being used to compute radar scattering from the ocean.

(c) A power law relationship exists between wind speed and σ^o (radar backscatter coefficient) for wind speeds greater than about 3 m/s and less than 20 m/s, and, for incident angles beyond 25^o, σ^o changes about one-half dB per 10 log change in wind speed (m/s). There is some argument as to whether this rate is 1/2 or 1/4.

(d) The σ^o_{VV} values can be as much as 10 dB higher than σ^o_{HH} values for large incidence angles.

(e) Both Ku- and X-band frequencies are preferred for sensitivity to local wind speed. Ku-band appears to be more sensitive to wind speed and weather in general than X-band.

(f) The σ^o sensitivity to wind speed variation seems to be about the same for up-wind, down-wind, and cross-wind conditions but the magnitude of σ^o for cross-wind is less.

(g) As yet, a single theory which fully explains the imaging of ocean waves using synthetic aperture radar, does not exist.

(h) Rain, snow, and ice can dampen and smooth the ocean waves, but quantitative data are not available.

(i) An oil slick may simulate a reduction in the wind velocity by a factor of two in the high wind seed region.

Passive

(j) Increases of 1.1^oK per m/s of the horizontally polarized brightness temperature with wind speed have been measured at 19.3 GHz and incidence angle of 55 degrees.

(k) Microwave radiometer sensitivity to wind speed increases with observational wavelength and is most pronounced for horizontal polarization at larger incidence angles. Surface roughness effects dominate the brightness temperature of the ocean at low wind speeds and sea foam effects dominate at very high wind speeds, with the transition occurring in the region between 15 and 20 m/s.

(l) The emissivity of foam (about 0.8 and greater) is about twice that of water, and foam may produce brightness temperatures approaching the thermometric temperature of the ocean.

(m) Microwave emission increases with the root-mean-square (rms) of the wave slope.

(n) Vertically polarized emitted radiation is much less affected by wind speed, and at angles of about 50^o, is almost independent of sea state.

(o) Emission at long wavelengths seems to be more responsive to water temperature changes.

(p) Salinity variations only affect microwave emission at long wavelengths ($\geq$4 cm).

(q) A theoretical model for computing microwave emission from the ocean surface is available.

The microwave emission and scattering results obtained from the ocean are based on measurements made in the open temperate region. The dominant factor influencing the radar return and microwave emission from the ocean surface seems to be surface roughness, which can be related to the wind speed. Whether these results are applicable in the cold ocean environment, especially where sea ice is predominant, must be investigated. The areas of open water which are likely to be present are small leads and polynyas. The effect of the wind speed in changing the surface roughness characteristics of these open water areas is small as compared to the effect in open ocean. The presence of sea ice may also dampen the surface roughness effects to some unknown degree. The freezing temperatures will produce some changes in the electrical properties of water, thereby influencing the microwave characteristics.

3.4 Microwave Scattering and Emission from Sea Ice

Both active and passive microwave systems have demonstrated their capability in the mapping of sea ice. The nature of radar scattering and microwave emission is not yet fully understood and optimum operating techniques and system parameters need to be established. The quantitative relationships between the microwave scattering and emission characteristics and sea ice parameters which play an important role in influencing the radar scattering and microwave emission have been isolated. But how these parameters interact to produce the changes in the scattering and emission is far from clear. The important physical properties of sea ice are its temperature and salinity, both of which vary with depth and ice thickness. The brine volume, related to both salinity and temperature, determines the electrical properties of sea ice. The surface roughness is dominant in affecting radar scattering in higher frequency bands (X- and Ku-bands). Only the characteristics of the top layer of ice influences the radar scattering and emission at these frequencies. The skin depth is of the order of a wavelength. For measuring the ice thickness, ice probing radars operating in the 100 to 300 MHz region are required. These systems appear to be more appropriate for detecting oil under ice.

The significant characteristics related to microwave scattering and emission from sea ice are;

(a) The complex permittivity of sea ice is dependent on temperature, salinity, and frequency. The dielectric constant of brine varies from 80 at 100 MHz to approximately 34 at 23 GHz. The dielectric constant of pure ice remains constant at about 3 within this frequency range. The dielectric constant of sea ice may vary from 3 to 5.3 and more depending on salinity and temperature. In general, the dielectric constant decreases with increasing frequency in the frequency range of interest. Signal attenuation in sea ice increases with increasing frequency, temperature and brine volume. The skin depth is of the order of a wavelength at $-10^{o}C$ for sea with a salinity of $2^{o}/oo$, and decreases with increasing frequency, temperature, and salinity.

Active

(b) Radar imaginary can be used to determine concentration, ice floe size, water openings, drift, topographic features, pressure zones, and ice age, and to infer ice thickness. In certain cases, it may not be possible to identify ice-free areas on the basis of tone alone as both open water and smooth thin ice may give a black tone. However, certain indirect clues may signify the presence of thin ice. The ability to locate and detect water openings, fractures, and ridges depends on the resolution of the system (both spatial and grey-tone) and their orientation relative to the flight track. Features parallel to the flight track are likely to show up better than those which are perpendicular. Pressure ridges give higher backscatter than the surrounding ice in certain types of ice. Multi-year ice floes are more readily identified than the first-year ice floes, although distinction between the two may not be possible in certain cases.

(c) Ice age is probably the most difficult characteristic to be determined from the SLAR imagery. It seems possible, however, to identify major ice types on good radar imagery through size, shape and texture of the imaged ice, and through the presence of puddles, drainage channels and rafting, if these are visible. Normally, at X-band and higher frequencies, multi-year ice gives as bright a return as that given by thicker first year ice. New ice or very thin first-year ice sometimes gives almost no return as in the case of open water. One reported hindrance to the interpretation of ice features on radar imagery is that the returns from open water,

'young' ice, 'grease' ice and 'slush' ice have overlapping dynamic ranges. 'Brash' ice gives a bright return but it presents a different texture.

(d) It is not possible to obtain a direct measure of the ice thickness from a radar image. For ice thickness measurements, an ice probing radar operating in the 100 to 300 MHz range is required. A rough measure of the ice thickness may be obtained by associating a mean thickness with an ice category and relating it to the brightness on a radar image or the value of σ^o on scatterometer data, thus, establishing an empirical relationship between σ^o or brightness and ice thickness.

(e) The X-band and Ku-bands appear to be optimum in discriminating sea ice types and delineating other features. Past measurements made simultaneously with more than one frequency qualitatively indicate that a two frequency system might provide more information about sea ice than a single frequency system. For example, scatterometer results show that a combination of a 13.3 GHz and a 400 MHz system definitely eliminates the ambiguity regarding very thin ice because of a reversal of the angular character of radar return from sea ice less than 18 cm thick at these two frequencies. The resolution achievable for most purposes. L-band may be another useful band, as the good quality imagery obtained by C-CORE under the SAR '77 program indicates. The frequency, or combination of frequencies required for determining the surface characteristics of sea ice is different from the one needed for direct thickness measurement or locating materials such as oil under ice.

(f) There appears to be no difference between the like polarizations (VV or HH) in their ability to discriminate sea ice, on the basis of limited evidence. There is an indication that cross-polarization alone or in combination with like-polarization may be valuable in sea ice studies.

(g) Quantitative studies have not been undertaken to examine the effect of resolution in discriminating ice types. Both grey-tone resolution and spatial resolution are important but a trade-off exists between the two.

(h) No one set of angles appears to be better than any other. The use of angles near grazing (incidence angles $>80^o$) results in return from ice edges and ridges making it more difficult to distinguish between smooth ice areas and water. Use of near vertical incidence angles with like and cross-polarized channels may help in distinguishing ice regions from open water. More contrast between ice type is presented between 20^o and 60^o.

(i) The masking effect of snow cover has still to be determined. There is a preliminary indication that Ku-band wavelengths can penetrate dry snow cover so that they are not affected by it, which suggests snow cover would not be a problem at lower frequencies. The return or masking effect of snow is dependent on the type of snow, its depth, density, temperature, water content, and observational wavelength. The size of ice and snow crystals in comparison to radar wavelength and their shape and orientation may influence radar scattering and emission from snow and ice. Attenuation in wet snow may be of enough significance to mask reflections from the snow-ice interface. Recrystallized snow is liable to show up on the radar image. The real part of the complex permittivity at high frequencies for dry fluffy snow is about 2. The values of 1.2 for dry fluffy snow and 1.8 for dense snow have been attributed for lower frequencies. As a result snow cover may act as a matching layer between air and ice.

(j) The changes produced in the appearance of ice on a radar image due to seasonal variations have yet to be studied. The radar imagery of sea ice obtained in summer may appear to be different from winter ice imagery because of the melting of snow and ice. Refrozen melt ponds can sometimes be identified on good winter ice radar imagery as are the melt pools on the summer imagery.

(k) Automatic classification techniques can be used in discriminating sea ice types when analyzing scatterometer data. An agreement of about 85 percent has been achieved in identifying and classifying four categories of sea ice, as established from stereo photo interpretation. Such automatic classification techniques have yet to be tried on radar images of sea ice. The use of not only grey-tone values, but also textural information, in discriminating sea ice images has yet to be evaluated and incorporated into both manual and automatic interpretive processes. Such an analysis is likely to provide clues as to the presence of oil in the ice environment.

(l) From the limited data which is available, icebergs can be identified on both X-band and K-band imagery. There is no indication as to which polarization will be optimum in discriminating icebergs. VV polarization seems suitable on the basis of available data, but HH should provide better discrimination against water. The range of angles should be near grazing to accentuate the shadow. The task of separating ships from iceberg targets is still being investigated.

(m) Radar scatterometer results at both 13.3 GHz and 400 MHz show that the difference in value of σ^{o} between some ice types is small, of the order of 0.25 dB. The

variances in the value of σ^o at each angle causes the σ^o versus θ curve for some ice types to overlap. The analysis of variance in the value of σ^o from sea ice has still to be investigated. The variance produced due to system design and averaging and the characteristics of sea ice need to be separated. A dynamic range of about 30 to 35 dB in the value of σ^o from sea ice is exhibited. Rough fast ice and multi-year ice give maximum values of σ^o versus θ, with 13.3 GHz being more suitable for ice identification than 400 MHz.

Passive

(n) Measured brightness temperatures can be used to delineate five or six gross categories of ice. In general, multi-year ice gives a lower brightness temperature than first-year ice, and sometimes multi-year ice can be distinguished from second year ice. Relatively thicker first year ice may give brightness temperatures between those given by new and young ice. The vertically polarized temperatures are always more than the horizontally polarized brightness temperatures. The same appears to be true for snow covered surfaces. The contrast between ice and water is more with horizontal polarization and increases with wavelength ($\geq$0.81 cm), being greatest at 2.81 cm. The horizontally polarized brightness temperatures are more sensitive to the effect of surface roughness. As the ice ages and becomes thicker, the brightness temperature increases for both the horizontal and vertical polarizations and the difference between "high" (240^oK) and "low" ($200\text{-}210^oK$) emission levels corresponding to young and weathered sea ice respectively decreases as the observational wavelength is increased from 0.51 to 3.2 cm.

(o) The microwave emissivity of "new" ice is about 0.95 and that of "old" ice about 0.75 in the 5 - 40 GHz frequency region, and the difference between the two increases with frequency. The emissivity differences observed at 45^o (at 0.8 and 1.55 cm wavelengths) off vertical are somewhat less than at nadir.

(p) A relationship seems to exist between brightness temperature and ice porosity. A linear relationship of about a 2^oK decrease in brightness temperature per one percent increase in average porosity exists for multi-year ice. For pure ice or compressed snow as in glaciers, there is a relationship between emissivity and crystal size on the wavelength scale. The horizontally polarized brightness temperature for sea ice can vary from 100^oK to 260^oK and vertically polarized temperature from 150^oK and 265^oK with giving the lowest value and first-year ice

giving the highest value. Other ice types give temperatures in the upper part of the range.

(q) Theoretical models for computing σ° and brightness temperatures from sea ice are available. The results from these models show reasonable agreement with the experimental results but the models need to be tested further for validity.

Simultaneous use of active and passive microwave systems may provide more information about the ice environment than use of one system alone. The variability of ice conditions and the use of different, uncalibrated systems makes the task of comparing results difficult. The use of texture in discriminating ice types has still to be incorporated in the interpretive process. The texture presented by the system design and averaging has yet to be separated from that caused by the characteristics of the ice. The quantitative evaluation of multi-channel data has yet to be attempted.

3.5 Microwave Scattering and Emission from Oil on Water

The use of active and passive systems in oil pollution surveillance over the temperate oceans is fairly well established. The U.S. Coast Guard is already using such sensors as part of their AOSS (Airborne Oil Surveillance System) operation.

There are two mechanisms by which the presence of oil on a water surface may be detected. Both of these mechanisms create anomalies in the microwave emission and radar scattering when oil is present. It is the presence of this local anomaly in the relative uniform background of the sea surface that signifies the detection of oil pollution. The first mechanism is the smoothing effect of oil which reduces the ocean surface roughness, thus reducing emissivity and increasing specular reflection. It is felt that this is the primary detection mechanism enabling the detection of oil films on relatively rough seas. The second mechanism is the direct change in the emission and scattering of water surface due to the presence of oil. Oil in general has a larger value of emissivity than that of calm ocean and a smaller reflection coefficient value. This is due to oil having a lower dielectric constant ($\sim$2) than that of water ($\sim$49) at micro-wavelengths. The second mechanism is slightly the weaker of the two, but offers the promise of measuring oil thickness. The above mechanisms affect the emission or scattering in two opposite and unequal ways, and are independent of each other.

The significant observations related to microwave scattering and emission from oil on water surfaces are:

(a) Water-waves influenced by oil films are in the range of 0.01 to 10 m.

(b) An oil layer always results in a damping action on capillary waves and so is detectable by the relative weakening of the wave induced scattering or emission.

(c) Thin oil films (μm thickness) only indicate their presence by their damping action on capillary waves; the nature of the oil (viscosity and layer thickness) cannot be deduced from this observation directly.

(d) The extent to which thick oil films (mm thickness) dampen the water waves provides an opportunity for the estimation of the product of the oil viscosity and layer thickness.

(e) The dampening of the waves that are influenced by an oil layer, takes place over a distance of typically 50 to 100 m from the edge of the oil slick.

Passive

(f) The emissivity of petroleum oils in the microwave region has been found to be typically around 0.8 while water has an emissivity of about 0.4.

(g) The minimum detectable oil film thickness on a calm water surface using a 37 GHz microwave radiometer is from 0.1 to 0.3 mm. The microwave brightness temperature of an oil film is inversely proportional to sensor wavelength. The horizontally polarized signatures are more responsive to an oil film than the vertically polarized component. For vertical polarization at an incidence angle of about 55° the emissivity is independent of oil slick thickness. All oil film signatures are positive (radiometrically warmer than unobscured water) for specular water surfaces. Antenna viewing angles of 30° to 45° above nadir afford best all-around sensor performance. Microwave emission levels observed in the laboratory increase with increasing film thickness.

(h) The microwave emission characteristics of oil slicks vary with oil type and film thickness. The mass of oil per unit area is the parameter of most importance.

(i) In rough seas the dominant method enabling oil spills to be detected is the dampening of the capillary waves by the oil film. This causes a reverse effect as far as brightness temperature is concerned since the brightness temperature of a rough sea is greater than that of a calm sea and could be greater than that of the oil slick. The oil slick, by reducing the roughness, lowers the effective brightness temperature of the polluted area, creating a contrast, enabling detection. Detection by passive microwave techniques in this situation is dependent on the frequency of the sensor. As only the capillary (<0.025 m) and very short gravity waves (>0.05 m) are

attenuated, only sensors operating at wavelengths comparable to or shorter than these will detect any change. For longer wavelengths this alteration in small roughness will not have any significant effects. Thus, under rough sea conditions the increased emissivity of the oil may be counteracted by the increased ocean surface emissivity but the dampening effect still allows the slick to be detected.

(j) The reduction effect of surface roughness has been reported to be able to produce a negative temperature anomally of up to $10^{o}K$. At an operating frequency of 38 GHz, the crossover point between the increased brightness temperature caused by an oil slick and decreased temperature effect caused by the reduction in surface roughness was seen to be in the range of 0.1 to 0.3 mm oil film thickness. At 37 GHz, for the conditions encountered, the additional emission from an oil slick is overshadowed by the decrease in ocean emission associated with the reduction of surface roughness when film thicknesses were about 50 mm or more. For film thicknesses of 10 to 20 microns or less, the surface roughness phenomenon was dominant, allowing the detection of these thin slicks. This seems to confirm that a "crossover" point exists where the two opposing mechanisms cancel each other. This would of course be dependent on such things as slick thickness, oil type and sea state.

(k) Foam, with an emissivity of about 0.8 would give rise to a higher sea surface brightness temperature. The absence of foam caused by an oil slick's dampening effect on a normally foam covered sea would, therefore, increase the negative temperature anomaly and aid in the detection of oil slicks.

(l) For the temperature variation normally encountered in a given area, the change in brightness temperature between an oil polluted and oil free area would not be significant. However, the variation in the emissivity of oils and seawater with temperature has not been examined and these variations may prove to be important at temperatures around $0^{o}C$ in order to distinguish oils from surrounding water and ice. The variation in water salinity would not seem to have any significant effect on the brightness temperature of water.

Active

(m) For active systems, image contrast between polluted and unpolluted ocean surfaces is a strong function of the polarization of the radar signal. Vertically polarized signals produce maximum contrast. There is some evidence that radar may be used to determine oil thickness. There is no evidence, however, that oil type yields a

distinctive signature. The oil spreading rate may be used to gain some insight into oil type if two or more images can be acquired over a reasonable interval of time.

(n) A strong functional relationship exists between the incident radar wavelength, the sea state and the thickness of the oil film. The observed trends indicate that thin films (1 μm) are best detected in low sea states (10 knot winds or less) by low frequency transmissions (1 to 3 GHz) while there is some indication that thin films may be best detected in high sea states by higher frequency (5 GHz and above) transmissions. Streamers from the main spill region and wind blown films can also be imaged.

(o) Oil film thicknesses of about 0.5 μm should be detectable with radar. A spatial resolution of 30 to 90 m in both range and azimuth directions seems adequate for slick definitions. The radar viewing angle should be within 45° of the horizontal to avoid specular returns. Since small grazing angles yield larger swatch widths, an angular range from 2° to 20° seems suitable for radar design.

(p) On both X-band SLAR imagery and 13.3 GHz scatterometer data, a reduction of 3 to 10 dB in the value of σ° has been observed due to the presence of oil slicks. This decrease occurs for incidence angles greater than 25° and is attributed to the oil dampening of small gravity or capillary waves. A local reduction of the order of 5 dB in the value of σ° is considered a reasonable oil spill detection threshold. The critical wind speed below which false alarm risks could be of importance in an operational system using X-band radar appears to be order of 3 to 5 m/s in summer and 8 m/s in winter. Sea surface temperature variations resulting in a surface roughness pattern alone do not seem to be important as false alarm risks, and surface currents should not cause problems. Natural fish oils and other chemicals may cause false alarms but their extent will be limited.

To obtain the thickness distribution within an oil spill, the resolution of the systems used is important. Both active and passive microwave systems seem able to detect and monitor oil spills in the temperate oceans. Whether the results presented here are equally applicable in ice-infested waters where temperatures are at freezing or below, and the roughness effects produced by wind may be reduced because of the relatively small water openings and the presence of sea ice, need to be fully investigated.

4 DETECTION AND MONITORING OF OIL POLLUTION IN THE ICE ENVIRONMENT

Testing the ability of various remote sensors to detect and monitor oil pollution in the ice environment has not been previously attempted. A qualitative assessment of the role of various remote sensors for oil pollution surveillance is found in a report on combatting oil spills in the Beaufort Sea (Philip Lapp Limited, 1975). The present study provides an account of the nature of radar scattering and microwave emission from ice, water and oil on water. An attempt is made in this section to assess the ability and limitations of microwave systems for oil pollution surveillance and monitoring in the ice environment. This assessment is only qualitative due to the nature of the information available.

4.1 Physical Considerations

The investigation into the behaviour of oil in the ice environment shows spilled oil may spread over the ice, under the ice, on the water, or in several modes at once depending on the sea and ice conditions. In addition, oil may become incorporated into the top and bottom surfaces of sea ice through absorption and may get trapped between ice layers. Oil spilled under ice, especially first-year ice, may rise to the top of the ice surface in the spring and summer through brine channels. Oil pools combined with ice melt pools may be present in summer and spring, and these may refreeze in winter. A mixture of snow and oil may be produced in the winter. As a result, the situations under which oil is likely to be present in the ice environment are:

(a) Oil on water surface - Two situations may be encountered:

i presence of oil in leads and polynyas and,

ii oil over larger water surfaces such as near the edges of shorefast ice and in and around loose ice pack where the concentration of ice is relatively small. The freezing conditions of winter present a different situation from that of summer. For wind generated capillary waves in deep water the initial growth rate is determined by the difference between the amplification rate and attenuation rate. The attenuation rate for a clean water surface is determined by the molecular viscosity of the water, its density and wave number. The molecular viscosity of water is highly temperature dependent whereas the density is essentially independent of the water temperature, and thus the dampening rate depends on the temperature. As the presence of oil is

detected through its wave dampening action, the false alarm threshold will be dependent on temperature.

(b) Oil on the top of the ice surface - The summer and winter conditions must be considered separately. In summer conditions oil is likely to be present in depressions and melt pools. Oil covered areas melt faster than the oil free ice areas. Oil having risen from under the ice, will also produce melt pools. Near the freezing temperature of water, oil is light enough to flow freely, but at colder temperatures it may freeze. Under winter conditions oil will be incorporated into refrozen melt pools, or a snow/oil mixture may result.

(c) Oil absorbed in the snow and ice surface - A distinction should be made for the situation when oil becomes incorporated into hummocks. Hummocks and ridges which contain oil melt faster than those which are oil free. Both winter and summer conditions need to be considered.

(d) Oil adhering to the ice - This is the situation in which oil may adhere to the bottom of the ice and the ice itself is overturned.

(e) Oil incorporated into the ice structure - This situation may occur when oil migrates upward through brine channels.

(f) An oil layer sandwiched between two ice layers.

(g) Oil incorporated into the bottom transition layer of ice.

(h) An oil layer at the ice/water interface.

(i) An oil layer on the underside of the ice with a layer of gas on top of it.

The situations outlined above although they have been idealized to a certain extent, represent various ways in which oil may be present in an ice environment. It is not clear which situations are more likely to occur than others as are based on laboratory observations. The likelihood of these situations occurring depends on method, location, and rate of oil spill; time of observation after spill; and rate of ice freezing and melting. The potentials and limitations of microwave techniques in detecting oil when it is present in these circumstances are addressed next.

4.2 Detection of Oil Through Microwave Scattering and Emission

In the light of the material presented in the preceding sections, a qualitative assessment of the possibilities and problems associated with detecting oil through microwave techniques can be made for the various situations under which oil is going to

be present in an ice environment. Each of the situations which are likely to be encountered are discussed below:

(a) The work done to date on the microwave scattering and emission properties of oil indicates that in temperate oceans oil films can be detected. The detection of oil is more readily obtained in conditions where the wind produces waves on the unpolluted water surface. It is found that oil, by dampening capillary waves, produces a detectable anomaly on the radar scattering area, such as in a loose ice pack and at the edge of shorefast ice, and wind can have an appreciable effect in changing the water surface roughness, oil can likely be detected just as in temperate oceans. In summer, however, the critical wind speed below which false alarms could be of importance is 3-5 m/s, whereas in winter it could be about 8 m/s for X-band radar. The attenuation rate of wind generated capillary waves on a clean water surface is determined by the molecular viscosity of the water which in turn is highly dependent on temperature. As a result the probability of not getting excitation of capillary waves will be greater for lower surface temperatures. At low average wind speed, a mixture of areas with ripples and no ripples can be expected with relatively more "no ripples" at a lower temperature. When evaluating averages (time or space) of σ^o, this will give a lower value of σ^o at lower temperatures at a given wind speed. The σ^o measurements at X-band show temperature dependencies of this kind.

The effect of an oil slick is to reduce the value of σ^o by as much as 10 dB and the brightness temperature can be increased by as much as 70^oK. The key to recognition of the oil slick is the contrast between it and the surrounding water. But if the water itself cannot be recognized, then detection of oil will be difficult. False alarms can occur because certain ice types give the value of σ^o and brightness temperature in the same range as given by oil polluted water. This is especially true in the case of new or thin first-year ice, but the texture, size, and location may provide a clue to the discrimination of oil polluted water regions.

The problem of detecting oil slicks in small water leads, where the effect of wind may be reduced because of the small surface area and dampening of the waves by surrounding sea ice, is different from the one mentioned above. Moreover whole leads may be covered by an oil slick so that the contrast with surrounding unpolluted water may not exist. Experiments have shown, however, that oil will be driven in the direction of the wind, piling up at near ice edges. In this event there could be

some open water available to allow discrimination against polluted water or indication of change in textures towards the thicker oil at the edges. The key to the detection of oil is the resolution of the system and orientation of the lead in relation to the look direction. As mentioned earlier, it sometimes becomes difficult to distinguish an open water lead from a frozen one, but texture may provide a clue as to whether a lead is frozen. The possibilities of a false alarm in the case of detection of oil in leads will be higher than when larger water surfaces are present.

Detecting the presence of oil on a water surface in an ice environment depends on the surface area of water, resolution of the system, prevailing wind speed and temperature, look direction, and the surrounding ice type. In certain cases, as outlined, detection will be easier than in others and the false alarm risk can be reduced by learning more about the scattering and emission from relatively thin first-year ice types.

(b) To be able to detect oil on the top of the ice surface depends on a number of situations such as resolution of the system, time of the year, and type of ice. It is likely that the presence of oil on the ice surface will be inferred through indirect clues such as the presence of melt ponds, which is especially true in summer. Because of the higher amount of melting, both in rate and quantity, of the oil covered regions in relation to the oil free regions, the clue is to look for such instances. In the case of first-year ice these clues may be apparent on radar imagery. The passive systems have a relatively poor spatial resolution so that detection utilizing these systems would be more difficult.

In cases where there is no melting, the presence of oil is likely to change the surface roughness, thereby affecting the radar return. The oil may act as a matching layer between air and ice, just as snow does. In winter, it seems the detection of oil on top of a sea ice surface would be more difficult than in summer, but the electrical properties of oil at, near and below freezing temperatures are not known, so qualitative or quantitative assessment cannot be made. But again the clues are the oil/snow mixture and refrozen melt ponds, which may produce variable textures and can be detected on radar imagery and radiometers data.

The false alarms in this case are likely to be produced in situations where thin ice areas are present, especially when the ice surface is relatively smooth. The smooth thin ice areas appear relatively black on radar imagery. The presence of oil on the

top of ice surface will not change the surface roughness but will effect the electrical properties.

(c) The detection of oil when it is absorbed by snow or ice depends on how the inclusion of oil changes the electrical properties of sea ice. If the oil replaces brine in sea ice, the electrical properties of polluted ice may change because the dielectric constant of oil is about 2.2 and that of brine is about 34. The dielectric constant of oil is between that of fluffy dry snow (~1.8) and pure ice (~3.2). The variations in the electrical properties of oil with temperature are not known, but the electrical properties of oil/ice combination will be different from the surrounding ice/brine medium. This difference is going to be more pronounced in the case of first-year ice. This change may be detectable on both radar imagery and radiometer data.

It has been found that the brightness temperature of sea ice may be related to its porosity. The presence of oil may change the porosity, thereby, increasing its possibility of detection. It should be pointed out that both radar scattering and emission for frequencies above about 10 GHz is influenced by only the top layer of sea ice. Thus, the presence of oil in only the top layer may be detectable at such frequencies. The salinity of the sea ice will determine the penetration in the surrounding sea ice. But, when brine is replaced by oil, more penetration may be possible. The melting of oiled hummocks and ridges will provide similar clues, as in the case of oil over ice. The detection of cracks and fractures is important, as these may allow the oil spilled under ice to rise to the surface.

There is more penetration of electromagnetic waves in winter than in summer, because of lower temperatures. Wave penetration in summer ice is restricted because of surface melt water, and the oil spilled below winter ice will not rise to the surface where it might be detectable at microwave frequencies.

(d) When oil is spilled under the ice, it may adhere to relatively small pieces of ice and these may later overturn, and drift into unpolluted waters. The detection of oil in such cases is of course contingent on the size of the pieces in relation to the resolution of the system. In most cases it may not be possible to detect these pieces or the oil adhering to them.

(e) The problem of detecting oil when it is incorporated into the total ice structure is similar to when oil is absorbed in the top surface of the ice. However, in this case the oil may not be present in the top layer, so the penetration capabilities of the

radar becomes more important. The use of longer wavelengths may provide the required detection capability.

(f) When the oil layer is sandwiched between two ice layers, or oil layers occur on the underside of ice, the use of high frequency radars and radiometers would not be of value. For such cases, ice probing radars operating in the 100 to 300 MHz region may provide the required detection capability. It may be possible to more easily detect oil when it is present as a layer on the underside of ice than when it is incorporated into the bottom transition layer. In the first case, a sharper change in electrical properties occurs.

5 OPTIMUM DETECTION PARAMETERS

On the basis of the available information it seems difficult to ascertain optimum parameters for detection of oil in the ice environment. The parameters which are useful for ice reconnaissance, detection of oil on water and wind speed measurement may be equally applicable in the case of oil detection in the ice environment. The parameters which are optimum for one situation may be different from the ones for another situation. The task is to seek an increase in the contrast between oil-free and oil-polluted areas. It appears that simultaneous use of active and passive systems would increase the possibilities of oil detection and decrease the false alarm risk.

5.1 Active Microwave Systems

From the microwave scattering results of sea ice, it appears both X and Ku-band frequencies are suitable for discriminating various sea ice types and conditions. Ku-band frequencies appear to be better than those in the X-band, but these are more sensitive to weather conditions. Dual frequency systems seem to provide more information about the ice environment than single frequency systems. The frequency in the L-band appears suitable. L-band frequencies will provide more penetration capability than the X- or Ku-band frequencies alone. It appears that both spatial and grey-tone resolutions are important in detecting subtle indirect clues for the presence of oil. The spatial resolution which can be conveniently achieved at frequencies lower than L-band may not be suitable for sea ice studies.

Both VV and HH polarizations appear equally suitable for sea ice studies. It seems that cross-polarization alone or preferably, in combination with like-polarization may be of better utility. One set of angles does not appear to be better than another, however, more contrast between ice types is presented between incidence angles of 20° to 60°. Angles less than 20° may help in distinguishing ice regions from water. For angles near grazing, the return is basically from ice edges and ridges and it is difficult to distinguish smooth ice regions from open water.

The results from microwave scattering of unpolluted ocean surfaces shows that both X-band and Ku-band radar signals are sensitive to wind speed. The scattering at L-band frequencies is less sensitive to changes in wind speed. The return from the ocean surface for angles greater than about 20° is from capillary waves and is related to wind speed. The surface roughness effect becomes prominent for wind speeds greater than about 3 m/s. The VV signals are as much as 10 dB higher than HH signals but both like

polarizations are sensitive to changes in the wind speed. At grazing angles greater than about 60° from the horizontal very little difference is noted in the sea echo for different polarizations. Significant differences exist at low grazing angles. In calm seas with little wind, the echo obtained with horizontal polarization is considerably less than with vertical polarization. The echo with horizontal polarization increases with increasing wind speed at a faster rate than the increase with vertical polarization, so that with rough sea conditions there is less difference in the magnitude of the sea echo from the two polarizations. The up-wind and down-wind situations produce a larger magnitude of sea echo than the cross-wind situation.

The microwave scattering measurements from oil polluted oceans indicate that vertically polarized signals produce maximum contrast, and that thin films (1 μm) are best detected in low sea states (10 knot winds or less) at low frequencies (1 to 3 GHz), while in high sea states higher frequencies (5 GHz and above) seem more suitable. Incidence angles greater than about 25° seem more appropriate.

Icebergs can be detected at both X- and Ku-band wavelengths. The SAR data recently obtained by C-CORE indicates that L-band signals also provide discrimination capability. The angles near grazing are certainly preferable and both VV or HH polarizations seem equally suitable. The discrimination against open water may be more easily obtained at HH than at VV polarization.

On the basis of sparsely available data, the electrical properties of oil do not show an appreciable change in the frequency range of interest. Information on the variation of the electrical properties of oil is lacking.

By considering the available information as presented here, the use of X- or Ku-band frequencies, along with L-band measurements seem appropriate for detection of oil in the ice environment. The long wavelength ocean gravity waves can also be imaged with synthetic aperture radars at these frequencies. Both like and cross polarization measurements seem desirable. It is not clear if VV polarization is to be preferred over HH polarization. In certain situations VV may be better than HH and in others vice versa. Measurements made in different angular ranges may provide different information. Incidence angles greater than 25° and less than 70° may be suitable. Angles less than 25° may provide additional information useful for separating water from ice regions and also in the detection of oil.

The range of frequencies desirable for detecting oil under sea ice is different from the one needed for surface detection. To achieve the penetration capabilities,

frequencies in the 100 to 300 MHz region are more suitable. At these frequencies, however, it may not be possible to achieve a suitable horizontal resolution.

5.2 Passive Microwave Systems

The spatial resolution achievable with passive microwave systems is generally poorer than that which can be achieved for active systems. The microwave emission measurements of sea ice indicate that the contrast between ice and water is more with horizontal polarization and increases with wavelength ($\geq$0.81 cm), being greatest at 2.81 cm. The contrasts between ice types decrease as the wavelength is increased from 0.51 to 3.2 cm. The optimum frequency seems to be around 30 GHz (1 cm wavelength) but measurements at 10.6 GHz (2.81 cm) also show good discrimination. The vertically polarized temperatures are always more than the horizontally polarized brightness temperatures. Horizontally polarized brightness temperatures are more sensitive to changes in the surface roughness.

Microwave emission measurements from the ocean show that horizontal polarization is preferable. Horizontal polarization is more sensitive to wind speed than vertical polarization. Vertically polarized emission is insensitive to changes in sea state at viewing angles of about 50° to 55°. Emission associated with surface roughness increases with observational frequency. Frequencies around 19GHz and 37 GHz seem suitable. It seems a frequency of about 5 GHz is more responsive to water temperature changes. The salinity variations only effect microwave emission at long wavelengths ($\geq$ 4 cm), with 21 cm being appropriate for salinity measurements.

The microwave emission properties of oil polluted oceans indicate that the microwave brightness temperature of an oil film is inversely proportional to sensor wavelength, with the contrast between oil covered and oil free surfaces being more for horizontal polarization than for vertical polarization. Antenna viewing angles of 30 to 45° above nadir seem to provide more information. Frequencies around 37 GHz and from 8.35 to 14.5 GHz seem suitable.

In view of the above, it seems that frequencies around 37 GHz are suitable for detection of oil in the ice environment. But a lower frequency, probably in the range from 8.35 to 14.5 GHz, will definitely provide more detailed information. A still lower frequency may provide information about the oil imbedded in the bottom layer of sea ice and underneath sea ice. The angular range from 30 to 45° is definitely preferred and vertical polarization may also provide useful information.

6 EXPERIMENT DESIGN

It is evident that a need exists to conduct a well designed, well thought out experiment which will ascertain the ability of various remote sensors, especially microwave sensors, to detect and monitor oil in the ice environment. Such an experiment, in addition, should provide valuable information on the behaviour of oil in the ice environment. The complexities involved and the problems associated with conducting a large scale experiment are tremendous. As a result it will not be possible to undertake many experiments of this nature. It is for this reason that an experiment involving intentional oil spills in an ice environment must be well defined in terms of its objective and purpose and what is likely to be achieved through the measurements.

6.1 Physical Considerations

It will be desirable to have available as many various types and conditions of ice as possible in the test area. The ice types which are particularly important are various forms of new ice, young forms of ice, relatively thicker first-year ice types and, if possible, multi-year ice. In addition, both small leads, and polynyas and open water surfaces of a relatively larger area, such as in a loose ice pack, should also be present. It certainly will be helpful to monitor oil spills in the test area through various seasons so as to test the affect of ice growth, different sea states, and various other situations as outlined earlier.

6.2 Data Requirements and Specifications

It is realized that all the possible and desirable situations under which oil may be present in an ice environment will not exist in the test area. The situations for which microwave data can and should be obtained are:

(a) oil spilled over various types of ice,
(b) oil spilled in leads,
(c) oil absorbed in snow and ice,
(d) oil spilled over a relatively larger water surface and surrounded by ice, where the effect of wind is noticeable, and,
(e) oil embedded in the ice structure.

In terms of priority, situations (b) and (d) seem more important for consideration than others.

It may not be possible to use very many varieties of oil but varieties of crude oils should be tried. The oils used should be ones which are more likely to be spilled. For the collection of remote sensing data the considerations are:

(a) Both active and passive microwave systems should be used. The remote sensing Convair-580 aircraft will carry the multi channel Environmental Research Institute of Michigan (ERIM) SAR, a 13.3 GHz radar scatterometer, and possibly a radiometer, in addition to an multispectral scanner (MSS) and RC-10 cameras.

(b) The test area should be well marked and be large enough to contain a variety of ice types and conditions. Ground truth information should be obtained for areas representative of various ice types and features, and oil conditions. The ground truthed areas should be large enough to be identified on the aerial photographs and radar imagery. Measurements of salinity, temperature, density, ice thickness, snow cover, surface roughness, and height and spatial extent of ridges should be made. In addition, the visual state of the surface due to the presence of oil should be noted. A record of humidity, air temperature, cloud cover and wind speed should be kept. Ground truthed areas should be marked with corner reflectors so that these may be identified on the radar imagery.

(c) Test areas should be monitored under a variety of wind speed and sea state conditions.

(d) Test areas should be mapped for various temperature and weather conditions. Mapping should be done before, during, and after a snowfall.

(e) SAR mapping should be done with both the available antenna depression angles at various altitudes, and flown in both the 8 km and 25 km swath configurations.

(f) The spilled area, which is going to be relatively small, should be mapped from all four sides as in a box so that all incidence and aspect angles are covered.

(g) Mapping of the same area on successive days should be undertaken to see if changes in ice conditions, drift, and the growth pattern of the ice cover have an effect on the ability to detect oil.

(h) It must be ensured that the SAR and other sensors are working properly. The quality of the obtained imagery should be checked during the experiment to see if the system is functioning properly. It certainly will be helpful to fly over the test area with another radar system such as the Motorola SLAR.

(i) SAR data with all the four polarizations (HH, VV, HV, VH) should be obtained.

(j) Data should be obtained under summer and winter conditions.

(k) A flight to calibrate the SAR system should be established. Corner reflectors with a known radar scattering cross section should be assembled in a pattern over the whole swath width of the imaged area. This will provide the data for calibration.

(l) The electrical properties of the oil spilled at near and below freezing temperatures for the wavelengths of the sensors to be used, should be known.

In terms of priority considerations (b), (e), (h), (i), and (l) appear to be more important for implementation than others.

6.3 Data Processing and Analysis

The inital SAR data can be processed for a moving or stationary target. The focussing requirement is influenced by the velocity of the moving target. The targets whose velocity differences are below a certain value cannot be discriminated because of the depth of focus. The likelihood of waves showing up on a synthetic aperture radar image, if these are physically present, is influenced by their velocity and on the way SAR data is processed initially. Thus, the initial processing of SAR data has some bearing on the detection of oil in the ice environment. The wavelength of the ocean gravity wave and its velocity are related to each other in open water. The velocity of the surface water introduces a proportionate doppler shift on the received signal. Thus, waves of different velocities are likely to appear when the same scene is processed for different parameters, initially. The SAR data, collected by C-CORE under the SAR '77 program illustrates that waves when present in sea ice do show up on the radar image, and under certain conditions the presence of sea ice or its boundaries cannot be ascertained on the radar imagery. These SAR data had been processed for a moving target. The results may likely be different when processing is done for a stationary target. As a result, the SAR data obtained under the experiment should be processed for various parameters. The specification of these parameters can be more readily ascertained if the SAR data obtained by C-CORE is processed differently. The SAR data obtained during the experiment should be processed for the best possible resolution. The imaged data should be digitized to permit digital analysis and enhancement of the images.

Those techniques of data processing and subsequent image processing (both optical and digital) should be considered which are likely to enhance the possibility of detection of oil and reduce the false alarm rate. Some of these techniques are:

(a) Tonal contrast enhancement,

(b) Texture enhancement,

(c) Averaging (single look and multi-look imagery),

(d) Channel addition and subtraction.

Such techniques could be tested on the SAR data obtained by C-CORE. The results obtained after the completion of this work provide an indication of the techniques likely to be successful.

REFERENCES

Brown, W.W. and L.J. Porcello, "An Introduction to Synthetic Aperture Radar", IEEE Spectrum, Vol. 6, pp. 52-61, (September 1969).

Chandrasekhar, S., Radiative Transfer, Dover Publications, New York, (1960).

Edgerton, A.T., A. Stogryn, D.P. Williams, and G. Poe, "A Study of the Microwave Emission Characteristics of Sea Ice," Aerojet General Corporation, Azusa, California, Summary Report 1741R-2, 35 pp. (1971).

Edgerton, A.T., F. Ruskey, D. Williams, A. Stogryn, G. Poe, D. Meeks, and O. Russel, "Microwave Emission Characteristics of Natural Materials and the Environment" (A Summary of Six Years Research), Aerojet General Corporation, Azusa, California, Final Technical Report 9016R-8, 301 pp. (1973).

Gunn, K. and T. East, "The Microwave Properties of Precipitation Particles", Quarterly Journal of Royal Meteorological Society, London, Vol. 80, pp. 522-545, (October-December 1954).

Medhurst, R.G., "Rainfall Attenuation of Centimeter Waves: Comparison of Theory and Measurement," IEEE Transactions on Antenna and Propagation, Vol. AP-13, pp. 550-564, (July 1965).

Moore, R.K., "Radar Scatterometry - An Active Remote Sensing Tool," in Proceedings Fourth International Symposium on Remote Sensing of Environment, Ann Arbor, Michigan, pp. 339-374, (April 1966).

Moore, R.K., and G.C. Thomann, "Imaging Radars for Geoscience Use," IEEE Transactions on Geoscience Electronics, Vol. GE-9, pp. 155-164, (July 1971).

Moore, R.K., (Ed.), "Microwave Remote Sensors," Chapter 9, Manual of Remote Sensing, Vol. I, American Society of Photogrammetry, Falls Church, Virginia, pp. 399-538, (1975).

Moore, R.K., "SLAR Image Interpretability - Trade-Offs Between Picture Element Dimensions and Non-coherent Averaging," University of Kansas Centre for Research, Inc., Remote Sensing Laboratory, RSL Technical Report 287-2, pp. 41, (January 1976).

Parashar, S.K., B. Dawe, and R.D. Worsfold, "Evaluation of Potential Sea Ice Thickness Measuring Techniques - Development of a Remote Sea Ice Thickness Sensor - Phase I," C-CORE Publication Report 77-6, 84 pp. (1977).

Philip A. Lapp Ltd., "An Investigation of Systems for the Surveillance and Monitoring of Oil Spills in the Beaufort Sea", Prepared for the Canada Centre for Remote Sensing, Ottawa, Under Contract Serial No. OSS4-0276, pp. 177, (August 1975).

Skolnik, M.I., (Ed.) Radar Handbook, McGraw-Hill Book Company, New York (1970).

Staelin, D.H., "Measurements and Interpretation of the Microwave Spectrum of the Terrestrial Atmosphere Near 1 cm Wavelength", Journal of Geophysical Research, Vol. 71, pp. 2875-2884, (November 1966).

Van Vleck, J.H., "The Absorption of Microwaves by Oxygen," Physical Review, Vol. 71, pp. 413-424, (April 1947a).

Van Vleck, J.H., "The Absorption of Microwaves by Uncondensed Water Vapor," Physical Review, Vol. 71, pp. 425-433, (April 1947b).

APPENDIX 1

APPENDIX 1 - OIL IN AN ICE ENVIRONMENT

A1.1 INTRODUCTION

Oil in an ice environment is subject to the same processes as those in the temperate regions. These processes are: spreading, evaporation, dissolution, emulsification, sinking, microbial modification, photochemical modification, and biological degradation. There can be, however, considerable differences between the rate of these processes in the Arctic region and those in the temperate regions. The colder climate of the Arctic and subarctic regions increases the longetivity of spilled oil by decelerating natural degradation processes. Depending on the sea and ice conditions, spilled oil may spread over the ice, under the ice, on the water, or in several modes at once.

The behaviour of oil spills in the Arctic, and cold environments in general, is being studied with increasing urgency because of increasing oil and gas exploration in such regions. It is felt that any oil spilled in such regions, especially on a large scale, would upset the fragile ecological balance and do irreparable harm to the environment. The studies are being conducted with a view towards providing means for location, detection, monitoring, containment, and retrieval of oil spilled in the ice environment because these means differ from those required in the temperate regions.

The presence of oil in the environment may occur as a result of ship accidents, pipe rupture, or blowout of a drilling well. The purpose of this appendix is to present the general behaviour of oil in the ice environment from the point of view of the possibility of its detection and monitoring through remote sensing means.

A1.2 Oil In Ice

The observations of the behaviour of oil spills in ice-infested waters and the results obtained from complementary laboratory studies of oil spills under ice have been reported by, amongst others, Green and MacKay (1975), Rosenegger (1976), Mackay and Thornton (1976), Chen et al.(1976 a and b), Scott and Chattergee (1975), Hoult et al. (1975), and Glaeser and Vance (1971). The first extensive study of the interaction of crude oil with shorefast sea ice was undertaken during the winter of 1974-75 as a part of the Beaufort Sea Project at Cape Parry, N.W.T. The results were presented by NORCOR Engineering and Research Limited (1975).

Glaeser and Vane (1971) have presented results obtained from an experiment conducted by the U.S. Coast Guard (USCG) during July, 1970 to investigate the behaviour

and spreading rate of Prudhoe Bay Crude Oil when spilled on water and ice. The interaction of spilled crude oil with ice over a period of time and the physical and chemical changes which occur in the crude oil as a result of aging were also studied. The results indicate that the upper layer of recrystallized ice in the test area absorbed up to 25 percent of its volume in oil which had been released on the surface. The ice surface had gradual undulations ranging up to approximately six inches and generally sloped downward from the area of the spill centre. The upper surface consisted of recrystallized ice with an average thickness of approximately two inches, having a density range from 0.46 to 0.61 g/m^3, and appeared like snow. The oil seeped to the lowest possible level of this layer, eventually migrating to the melt ponds present. It was found that the spreading of the crude oil on water was significantly affected by the wind. The crude oil would not spread out as a thin film but would gather in thick films when forced by the wind against ice. Crude oil released under ice rose to the ice/water interface, where it remained without dispersing to any great extent. Glaeser (1971), on the basis of this experiment, had observed that the viscosity of the tested crude oil was low enough for it to spread easily under summer Arctic conditions, but, colder temperatures in winter will increase the viscosity of the crude oil sufficiently to cause it to apparently freeze. It was pointed out that the natural roughness of the ice will act to contain spilled oil at all times. The oil spread on water attained a minimum thickness of 5 mm. For the spreading of oil under water, it was observed that in all cases oil rose to the underside of the ice and formed in pockets because the crude oil had a specific gravity of approximately 0.89. Multi-year ice in general has a specific gravity of 0.85 as compared with 0.91 for pure, salt free ice. Sea ice is of a lower density because of a brine migration process which leaves the ice with a porous structure. Thus, in comparison with sea ice, crude oil will almost always be more dense, resulting in its flow under multi-year sea ice because of hydrostatic considerations. This flow will be restricted by the very rough and rugged underside of ice. It was observed that oil exhibited an increase in viscosity with age attributed chiefly to a loss of volatiles. The specific gravity of oil was also correspondingly raised. It was also pointed out by Glaeser (1971), that an oil spill on the ice surface will result in a greater than normal absorption of solar radiation and thus melting of ice.

On the basis of the above experiment and subsequent experiments conducted by USCG during February, 1972, it was observed by Koburger and Getman (1974), that oil penetrates summer ice whereas virtually no oil penetration occurs on winter snow and ice. The temperatures difference between the oil and snow or ice causes an immediate melting

and refreezing at the interface. It was pointed out that during winter conditions, falling or driven snow will saturate oil up to 80 percent by water volume forming a cohesive oil/snow mixture. The detailed results and analysis of the February, 1972 experiment conducted by the USCG are presented by Chen (1972).

The ways in which ice fields may provide natural barriers for oil containment were presented by Barber (1971). Campbell and Martin (1973), have suggested three processes involved in the dispersal of oil in the Arctic: lead matrix pumping, where the oil could be dispersed by the continuous opening and closing of leads in the open ice pack; oiled hummock melting, where oil particles, incorporated into ice hummocks formed during closing of oil filled leads, would have a different absorption of solar radiation; and under ice transport in the form of oil-in-water and water-in-oil emulsions. Due to these processes, oil could be dispersed over a large area, thereby affecting the heat balance in the Arctic. In response to this hypothesis, Ayers et al (1974), have reasoned that a significant alteration of the Arctic heat balance from a major oil spill probably would not occur.

The rate of spreading of oil on an ice surface and the forces involved in the spreading were studied by Chen et al (1974). It was concluded that the effect of surface roughness of the gravity-viscous spreading may be considered to be insignificant and that a chance in oil volume does not affect the correlation between spreading and time. The effect of temperature on spreading could be accounted for by changes in viscosity. The role of interfacial tension forces in assisting or retarding the spread of oil under ice was discussed by Mackay and Thornton (1976).

The results of a laboratory study conducted to determine the behaviour of oil under sea ice have been reported by Wolfe and Hoult (1974). They studied three possible modes of oil entrapment under sea ice as shown in Figure A1-1. The three principal modes of behaviour for the interaction of sea ice with oil trapped under it were hypothesized as: (A) the ice entrapping the oil in a pool and proceeding to form beneath it; (B) the ice continuing to grow, pushing the oil before it; and (C) the sea ice entrapping the oil causing the formation of a matrix of oil and ice. It was observed that a combination of (A) and (C) was the actual method of oil entrapment in sea ice. The bulk of the oil was pocketed in a pool below the original ice subsurface while more sea ice proceeded to grow under it. A small amount of oil does rise into the pores of the skeletal layer, and into small vertical shafts, such as air bubbles, which rise from the lower

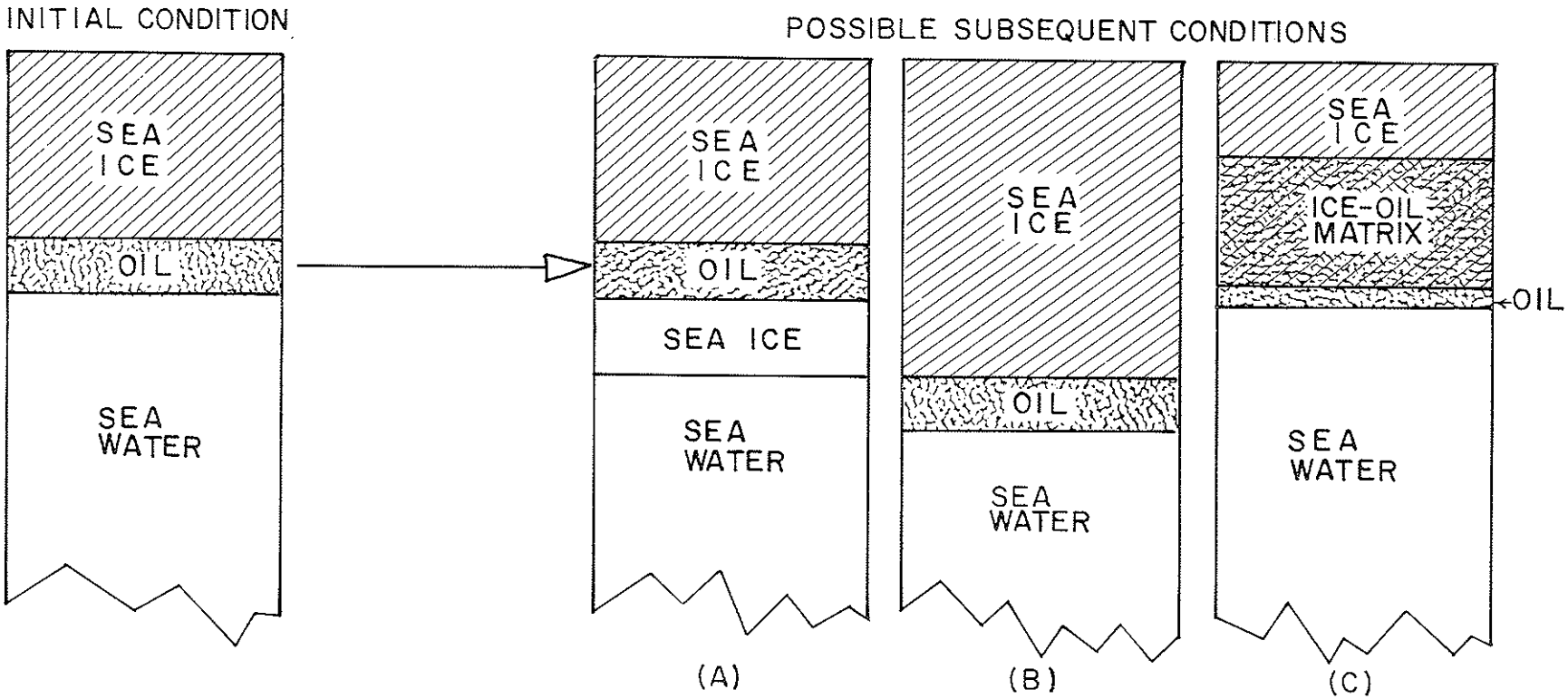

FIGURE A1-1 POSSIBLE MODES OF OIL ENTRAPMENT IN SEA ICE.
(Wolfe and Hoult, 1974)

surface of the ice. A larger amount of oil, in comparison with the oil contained in these air bubbles, was contained in the lower most inch of the ice. During the ice melting experiment, a considerably greater amount of oil rose into the ice, due to an increase in the ice porosity because of melting, reaching as a high of 8 cm above the lower surface of a 13 cm thick block.

A detailed investigation into the behaviour of oil in the Arctic was presented by Hoult et al.(1975). Both, oil under and over the ice, situations had been considered. A model of oil spreading on the surface of ice was developed considering the statistics of the surface roughness. In laboratory experiments, it was observed that North Slope oil, at the temperature of freezing sea water, is a good insulator compared to the sea ice itself.

In a report prepared for the University of Toronto, Greene and Mackay (1975) presented results of an experimental spill of crude oil in an ice covered freshwater pond. It was pointed out that the behaviour of oil in fresh ice differs from that in saltwater ice because of the existence of brine drainage channels which cause saline ice to be more porous. The results also show that when oil spilled under the ice was allowed to escape to the surface through two cracks, oil slicks of 1 cm thickness were formed with a stable edge having a thickness of 0.5 cm. The behaviour of crude oil under freshwater was discussed by Chen et al.(1976a), confirming the findings of Wolfe and Hoult (1974) that the oil can be sandwiched between ice layers. Siu et al.(1977), presented results of an experiment conducted to see the effect of continuous spilling of hot oil on ice. It was found that the oil slick area was proportional to elapsed time to the power 0.8. Chen et al. (1976b), have shown that the behaviour of oil spilled in ice-covered rivers is difficult to predict but observations show that oil spilled in ice free rivers will quickly be dispersed downstream.

The behaviour of oil in ice-infested waters has been studied by NORCOR (1977). It was observed that oil released into the water column under a solid ice cover will rise and gather in pools and lenses at the bottom of the ice sheet. The oil will be contained by the natural roughness of the underside of ice. Some oil may escape to the surface through cracks. Most of the oil and gas is likely to be contained by all but the smaller floes when the ice is not a solid pack. In the case of a first-year ice floe, the bulk of the oil will migrate to the surface of a first-year ice floe, the bulk of the oil will migrate to the surface of the ice during the first summer, whereas with a multi-year floe it could take a number of years for the oil to be released. The results indicate that solar radiation penetrates snow and that underlying oil will absorb heat through a snow covering.

The formation and growth of sea ice in the presence of waves and spilled oil has been investigated by Martin (1976), in laboratory experiments. Two kinds of sea ice grew in the wave field: grease ice which appeared as a thick soupy, flexible layer on the sea surface and pancake ice consisting of solid, circular pieces of ice with raised rims. Diesel oil released 20 cm under 6 cm thick grease ice rose rapidly and spread out on the sea surface and no signs of oil absorption below the grease ice surface was evident. Most of the oil released under pancake ice appeared to penetrate the ice surface.

The permeability of multi-year ice in relation to sea water has been studied by Milne et al.(1977). It was hoped that this may provide insight into the permeability of multi-year ice with respect to oil. The four floes tested showed that multi-year ice is permeable to seawater and has a porosity in the range between 0.2% and 0.03%.

A review of the above indicates that the behaviour of oil in the ice environment is fairly complex and depends on a number of climatic and ice conditions such as wind speed, temperature, type of ice, and type and temperature of the oil.

A1.3 Summary of Significant Results

The spreading of oil on water surfaces in the temperate region is well understood (Hoult, 1972). As pointed out by Green (1977), at first, spreading is controlled by a balance between inertial and gravity forces. The next phase is dominated by viscous forces which tend to reduce slick spreading, and gravity which tends to incease spreading. The latter phase reduces the slick thickness to approximately one millimeter. The slick becomes thinner, often to a monomolecular layer, because of surface tension spreading, due to a large positive spreadings coefficient. It was found that the spreading of oil due to surface tension may be absent in the cold environment (Glaeser and Vance (1971). Green (1977) pointed out that while this third phase does occur for some types of crude oil on near-freezing freshwater and seawater, the oil slick does not become thin. Slick thicknesses from 1 to 10 mm were observed. The transition point where an oil slick on the sea surface would stop spreading by surface forces has been determined (Garrett, 1969). Glaeser and Vance (1971) found that Prudhoe Bay crude oil spilled on the Arctic Ocean (0^{o}C water temperature) reached a stable spreading state at a thickness of 0.5 cm, after which spreading was affected only by the wind. McMinn (1972) spilled the same oil over arctic ice in tension became an important factor in spreading. It was suggested that the rough uneven surface of the ice and subsequent pocketing of the oil limited the spreading so that the transition point thickness, calculated to be about 3 mm, was never reached.

It was pointed out by Greene (1977), that oil is dispersed from a slick by wave action. Particles 1 - 2 mm in size are driven down into the water column and may remain in suspension following currents. Larger, weathered tar balls may also form (McLean, 1972). It has been estimated that approximately 7% of the oil slick volume per day is initially dispersed under three foot wave conditions. Evaporation of up to 50%, or greater, of the mass of crude oil under moderate winds and warm temperatures can occur over a period of days.

Sea ice has a variable density, ranging from perhaps 0.70 to 0.91 g/cm^3, the latter value being assoicated with old ice containing very little brine. The actual density of ice depends on the way it is formed and its subsequent history. In contrast, the density of North Slope crude oil is 0.89 and after aging two weeks in the arctic summer, this density rises to about 0.95 (Glaeser and Vance, 1971). Hence the oil can be either heavier or lighter than the sea ice. The density of sea water is approximately 1.03 g/cm^3 and for salt free ice about 0.91 g/cm^3.

Petroleum discharged below the ice cover, such as from an oil well blowout, rises to the underside of the ice in a cone shaped plume and becomes trapped in the uppermost irregular pockets at the ice-sea water interface. A rising oil plume tends to be unstable, breaking up into small spherical particles 1 cm in diameter or less. Most crude oils form sessible drops at an ice-water interface. The equilibrium thickness of a continuous oil film is about 1 cm with the minimum thickness for Normal Wells crude oil being 0.8 cm. The maximum thickness or more than equilibrium value of the entrapped oil is determined by the depth of depressions or variations in ice thickness. Studies have suggested that oil trapped under the ice is virtually indistinguishable from fresh crude oil with regard to viscosity, density, and other parameters. Regardless of the reason, the temperature of the ice at the ice-water interface will be at the freezing point. At this temperature, a typical crude oil will have a viscosity low enough to flow easily. Its free flow, however, will be restricted by the roughness of the undeside of the ice. If oil and gas are released together under ice, as in more realistic situations, gas will replace oil at the ice-water interface and the oil thickness may only be on the order of 1 mm.

Oil enclosed in brine channels and trapped under areas of ice will remain essentially in its original state through winter. During the spring and summer, after the first-year ice surface melts and the brine channels open up, the oil may migrate to the surface of the ice. As the dark oil absorbs heat from the sun, the rate of migration increases and oil forms a melt pool on top of the surface. Multi-year ice contains no brine

channels so the oil may remain trapped for up to 3 - 4 years or longer. However, some studies have shown that even in multi-year ice, during early summer, oil may be able to reach to the top of the ice surface.

The temperature of the released oil may also influence its behaviour in sea water and cause some melting of the sea ice. During the ice growth season, oil may penetrate between 5 to 10 cm into the loose skeletal structure on the underside of the ice. The oil may adhere to the surface and become sandwiched between ice layers. In certain cases, a mixture of sea water, ice, and oil can be formed (Hoult et al.,1975). Oil has an insulating effect which slows the formation of a second layer of ice.

The presence of oil on the surface of sea ice may occur when oil under ice reaches the surface through cracks and leads and between ice floes. Some oil-covered ice pieces may overturn, and, because of the banging of ice floes against one another, oil spilled in the leads may reach the top of the ice surface. As found by Glaeser and Vance (1971), Prudhoe crude oil (60^{o}F) poured onto ice and snow in the arctic spreads to a minimum thickness of 0.5 cm. The spill area was much smaller than a similar spill on water and its spreading on ice restricted by the surface roughness. (A spreading model based on roughness statistics of the ice surface was developed by Hoult et al (1975).

On snow and ice, the oil flows downslope pooling in depressions. Oil penetrates summer ice whereas virtually no oil penetration occurs on winter snow and ice; the temperature difference between the oil and the snow or ice causes an immediate melting and freezing at the inferface. It was found by Glaeser and Vance (1971), that the upper layer of recrystallized ice in the test area absorbed up to 25 percent its volume in the oil which had been released. During winter conditions falling or driving snow will saturate oil up to 80 percent by water volume, forming a cohesive oil/snow mixture. As a result, weathering of oil, particularly by evaporation, is greatly reduced.

Oil in the ice environment can be dispersed over a large area due to processes described by Campbell and Martin (1973). Oil particles may be incorporated into hummocks and ridges. Oil is absorbed by snow. Ice surfaces covered with black crude oil absorb more solar radiation than clean white ice surface. Under experimental summer field conditions, ice covered with crude oil absorbed approximately 30 percent more radiation than clear ice. As a result, oil covered ice melted approximately 2 cm per day faster than clear ice. The albedo of oil covered snow is about 4 times that of an oil film or water (NORCOR, 1975).

A1.4 Conclusions

Most research to date concerning the behaviour of oil spilled on and under sea ice has involved experiments in laboratory cold rooms or in stationary first-year sea ice. More research is needed into the behaviour of oil in regions where ice conditions are more dynamic and where multi-year ice is present.

From the point of view of remote sensing, oil needs to be detected and monitored under the following situations:

(a) Oil on water surface under freezing conditions;
(b) An oil and snow mixture on an ice surface when oil is absorbed by snow;
(c) Refrozen melt pools containing oil, snow and ice;
(d) Oil sandwiched between snow and ice;
(e) Oil on top of an ice surface;
(f) Oil absorbed in the ice surface;
(g) Oil imbedded in the underside layer of ice;
(h) Oil layers under ice;
(i) Oil on rough top and bottom ice surfaces, and;
(j) "Lead matrix pumping" and the spreading of oil between floes.

Some of the situations mentioned above will be different under summer and winter conditions.

REFERENCES

Ayers, R.C., H.D. Johns, and J.L. Glaeser, "Oil Spills in the Arctic Ocean - Extent of Spreading and Possibility of Large-Scale Thermal Effects," Letter in Science Vol. 186, pp. 843-4, (November 1974).

Barber, F.G., "Oil Spilled with Ice: Some Qualitative Aspects," Proceedings of the Joint Conference on Prevention and Control of Oil Spills, Washington, D.C., pp. 133-137, (June 1971).

Campbell, W.J., and S. Martin, "Oil and Ice in the Arctic Ocean: Possible Large-Scale Interactions," Science Vol. 181, pp. 56-58, (July 1973).

Chen, E.C., "Arctic Winter Oil Spill Test United States Coast Guard, Inland Waters Directorate," Technical Bulletin, No. 68, Department of the Environment, Ottawa, 24 pp., (1972).

Chen, E.C., J.C.K. Overall, and C.R. Phillips, "Spreading of Crude Oil on an Ice Surface," the Canadian Journal of Chemical Engineering, vol. 52, pp. 71-74, (February 1974).

Chen, E.C., B.E. Keevil, and R.O. Ramseier, "Behaviour of Crude Oil Under Fresh Water Ice," Journal of Canadian Petroleum Technology, Montreal, pp. 79-83, (April-June, 1976a).

Chen, E.C., B.E. Keevil, and R.O. Ramsierer, "Behaviour of Oil Spills in Ice Covered Rivers," Scientific Series No. 61, Inland Waters Directorate, Ottawa, pp. 41, (1976b).

Garrett, W.D., "Confinement and Control of Oil Pollution on Water with Monomolecular Surface Films," Proceedings of the Joint Conference on Prevention and Control of Oil Spills, pp. 257-261, (December 1969).

Getmet, J.H., and L.A. Schultz, "Tests of Oil Recovery Devices in a Broken Ice Field," Proceedings of the Offshore Technology Conference, Dallas, Texas, Paper No. OTC 2695, pp 18, (May 1976).

Glaeser, J.L., "A Discussion of the Future Oil Spill Problems in the Arctic," Proceedings of the Joint Conference on Prevention and Control Of Oil Spills, Washington, D.C., pp. 479-484, (1971).

Glaeser, J.L. and G.P. Vance, "A Study of the Behaviour of Oil Spills in the Arctic", Project No. 714108/A/001, 002, Office of Research and Development, U.S. Coast Guard, Washington, D.C., pp 60, (February 1971).

Golden, P.C., "Oil Removal Techniques in an Arctic Environment," Marine Technology Society, Vol. 8, No. 8, pp 38-43, (January 1974).

Greene, G.D. and Mackay, "The Probable Nature and Behaviour of Oil Spills in the Beaufort Sea and the Feasibility of Clean-up," Report of the Institute of Environmental Studies of the University of Toronto, and published as a chapter in "Oil under Ice": Offshore Drilling in the Canadian Arctic, by D. Pimlott, D. Brown and K. Sam, published by the Canadian Arctic Resources Committee, Ottawa, Ontario, (December 1975).

Greene, G.D., "The Behaviour of Oil in Ice-covered and Ice-infested Seas," Proceedings of the Eleventh Congress of the Canadian Meteorological Society, Winnipeg, Manitoba, (June, 1977).

Hoult, D.P., S. Wolfe, S. O'Dea, and J.P. Patureau, "Oil in the Arctic," Unites States Coast Guard, Final Report No. CG-D-96-75, Task No. 4108.2.3, pp 218, (March, 1975).

Koburger, C.W., and J.H. Getman, "Oil Spill Problems in Cold Climates: The Coast Guard Attacks the Alaskan Oil Spill Problem," Naval Engineers Journal, Vol. 86, pp 59-64, (December, 1974).

Mackay, D. and W.Y. Shiu, "The Aqueous Solubility of Weathered Crude Oils," Bulletin of Environmental Contamination and Toxicology, Vol. 15, No. 1, (1975a).

Mackay, D., P.J. Leinonen, J.C.K. Overall, and R.B. Wood, "The Behaviour of Crude Oil Spilled on Snow," Journal of the Arctic Institute of North America, Vol. 28, No. 1, Montreal, (March, 1975b).

Mackay, M. and D.E. Thornton, "The Interfacial Behaviour of Oil under Ice," Canadian Journal of Chemical Engineering, Vol. 54, No. 72, pp 71-73, (February, 1976).

Martin, S. "A Laboratory Study of the Dispersion of Crude Oil Within Sea Ice Grown in a Wave Field," Department of Oceanography, Univeristy of Washington, Special Report 69, Washington, (1976).

McLean, A.Y., "The Behaviour of Oil Spilled in a Cold Environment," Proceedings of the Offshore Technology Conference, Dallas, Texas, Paper No. OTC 1522, pp 14, (May, 1972).

McMinn, T.J., "Crude Oil Behaviour on Arctic Winter Ice," Final Report of Project 734108, Unites States Coast Guard, (September 1972).

Milne, A.R., R.H. Herlinveaux, and G. Wilton, "A Field Study on the Permeability of Multi-Year Ice to Sea Water with Implications on its Permeability to Oil," Technology Development Report EPS-4-EC-77-11, Environmental Impact Control Directorate, Ottawa, pp 33, (October 1977).

NORCOR Engineering and Research Ltd., "The Interaction of Crude Oil with Arctic Sea Ice," Technical Report No. 27, Beaufort Sea Project, Department of Environment, Victoria, B.C., Canada, (1975).

NORCOR Engineering and Research Limited, "Probable Behaviour and Fate of a Winter Oil Spill in the Beaufort Sea," Technology Development Report EPS-4-EC-77-5, Environmental Impact Control Directorate, Ottawa, pp 111, (August 1977).

Ramseier, R.O., G.S. Gantcheff and L. Colby, "Oil Spill at Deception Bay, Hudson Strait," Scientific Series No. 29, Inland Waters Directorate, Water Resources Branch, Ottawa, (1973).

Rosenegeer, L.W., "Oil-In-Ice Studies," Lab Report L-12075, Imperial Oil Co. Ltd., Resource Production and Technical Services Laboratory, Calgary, Alberta, (1975).

Scott, B.F., and R.M. Chattergee, "Behaviour of Oil Under Canadian Climatic Conditions," Scientific Series No. 50, Inland Waters Directorate, Water Quality Branch, Ottawa, pp 27, (1975).

Siu, S.K., C.R. Philips, and E.C. Chen, "The Continuous Spilling of Hot Oil on Ice," Journal of Canadian Petroleum Technology, Montreal, pp 31-34, (January 1977).

Topham, D.R., "Hydrodynamics of an Oil Well Blowout," Beaufort Sea Project, Technical Report Nop. 33, Department of Environment, Victoria, B.C. (1975).

Wadhams, P., "Oil and Ice in the Beaufort Sea," Polar Record, Vol. 18, No. 114, pp 237-250, (1976).

Wolfe, L.P. and D.P. Hoult, "Effects of Oil Under Sea Ice," Journal of Glaciology, Vol. 13, No. 69, pp 473-488, (1974).

APPENDIX 2

APPENDIX 2 - ELECTRICAL PROPERTIES OF OIL

A2.1 INTRODUCTION

The ability to monitor remotely by microwave methods (both passive and active) any natural or artificial material (liquid or solid) in the environment is directly related to the electrical properties of the interfacing materials. There properties can vary significantly with temperature, period of exposure (for those materials not normally exposed to the environment), particular chemical composition and contamination by mixing with other materials. These properties are also frequency dependent and can vary considerably with it.

Of particular interest here are the electrical properties of oils as they affect the microwave emissivity and the radar backscatter, and these are both the real and imaginary parts of the complex permittivity.

The microwave emissivity (E_m) of homogeneous oil of constant thickness on a flat sea surface is given by (Meeks et al, 1971):

$$E_m = 1 - R_{(h,v)}(\Theta) = 1 - \left| \frac{\rho_{12_{(h,v)}} e^{2i\psi t} + \rho_{23_{(h,v)}}}{e^{2i\psi t} + \rho_{12_{(h,v)}} \rho_{23_{(h,v)}}} \right|^2$$

where $\psi = \frac{2\pi}{\lambda} \sqrt{\varepsilon_2 - \sin^2 \Theta}$

and $R_{(h,v)}(\Theta)$ is the reflectivity;

ρ_{12}, ρ_{23} are the Fresnel reflection coefficient at the air-oil and oil-water interfaces, respectively;

Θ is the angle of incidence;

(h,v) denote horizontal and vertical polarization respectively;

ε is the complex permittivity of the oil; and,

t is the thickness of the oil layer.

But from Edgerton and Trexler (1970) we have for a layered structure that,

$$\rho_{\ell n_{(h)}} = \frac{\sqrt{\varepsilon_\ell - \sin^2\Theta} - \sqrt{\varepsilon_n - \sin^2\Theta}}{\sqrt{\varepsilon_\ell - \sin^2\Theta} + \sqrt{\varepsilon_n - \sin^2\Theta}}$$

and

$$\rho_{\ell n_{(v)}} = \frac{\varepsilon_n \sqrt{\varepsilon_\ell - \sin^2\theta} - \varepsilon_\ell \sqrt{\varepsilon_n - \sin^2\theta}}{\varepsilon_n \sqrt{\varepsilon_\ell - \sin^2\theta} + \varepsilon_\ell \sqrt{\varepsilon_n - \sin^2\theta}}$$

where ℓ and n refer to the interfaces of the particular mediums, 1, 2 or 3. Thus, the emissivity is totally dependent on the complex permittivity. For the case of radar backscatter the above equations for reflectivity again apply.

A2.1.1 Oil Types. One of the more difficult tasks in examining the dielectric properties of various oil types and their relation to various parameters is relating the types to each other. The American Petroleum Institute (API) designates oil types by their specific gravity according to the formula;

$$\text{API} = \frac{141.5}{\text{specific gravity}} - 131.5,$$

and from this the oil is given an "API Gravity Number". Unfortunately not all researchers follow this code. Some have used crude oil numbers (e.g. 2, 4 and 6); others have used commercial or chemical names such as Bayol-D, gasoline, and JP-1; and still others have designated the type by its source, e.g. Long Beach, Calif., Black Oil Farm, etc. Some researchers have not designated any oil type at all. In most cases it is impossible to relate these designations to one standard type classification.

A2.2 Dielectric Properties

Von Hippel (1954) undertook the most extensive study of the dielectric properties of petroleum oils in relation to frequency. The results are summarized in Figures A2-1, -2 and -3. The highest frequency is seen to be 10 GHz, which unfortunately, is at the lower edge of the band utilized for passive microwave sensors and does not cover the complete band utilized for active microwave sensors.

One other shortcoming of the data is that only refined oils are dealt with. Crude oils are of most interest. The curves do show a trend that may be extrapolated to other oil types ad this is the general decrease of the real part of the complex permittivity with frequency. The imaginary part shows a much more complicated relationship, which, because of gaps in data, cannot be adequately described at this time.

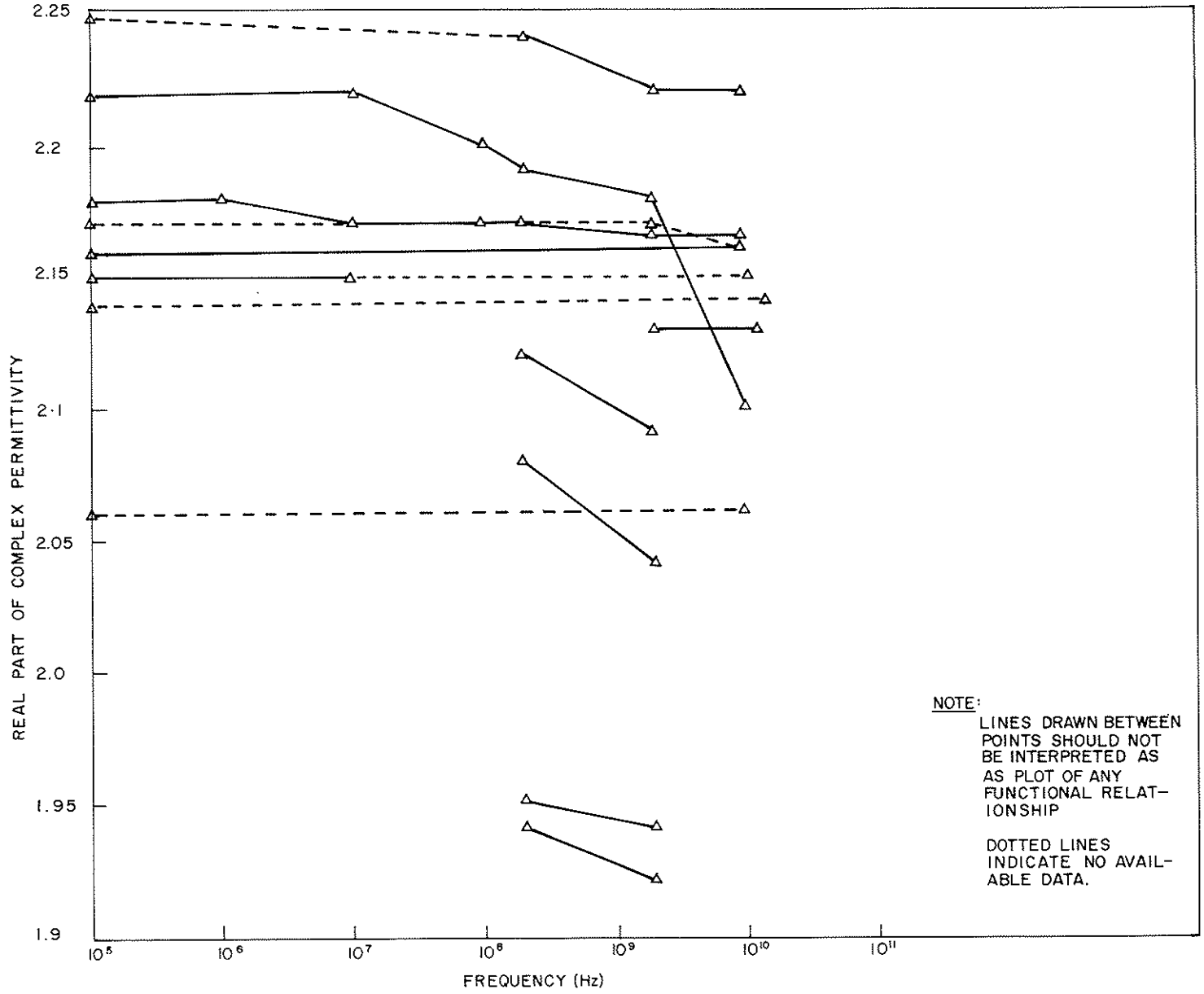

FIGURE A2-1 (Von Hippel, 1954)

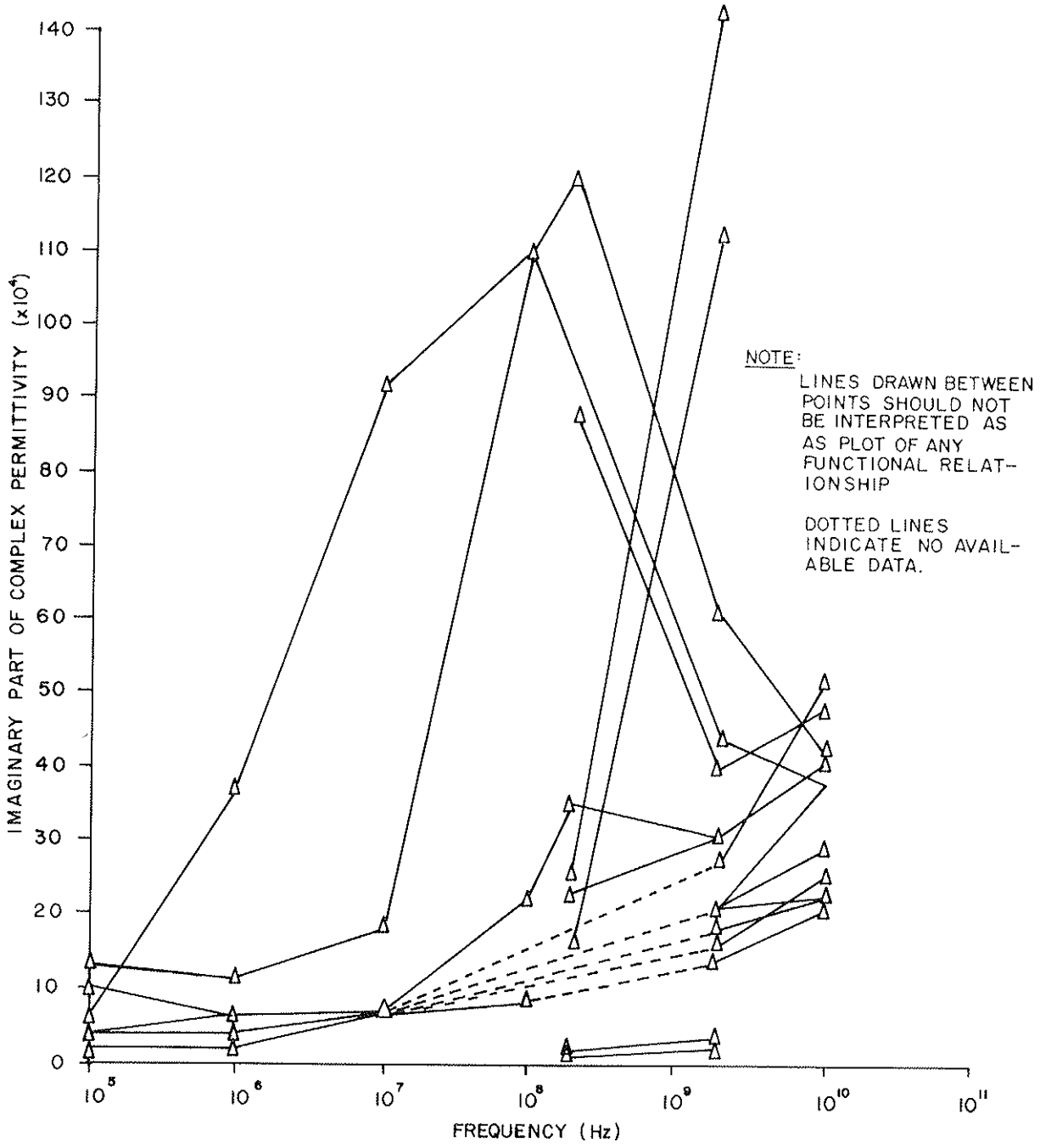

FIGURE A2-2 (Von Hippel, 1954)

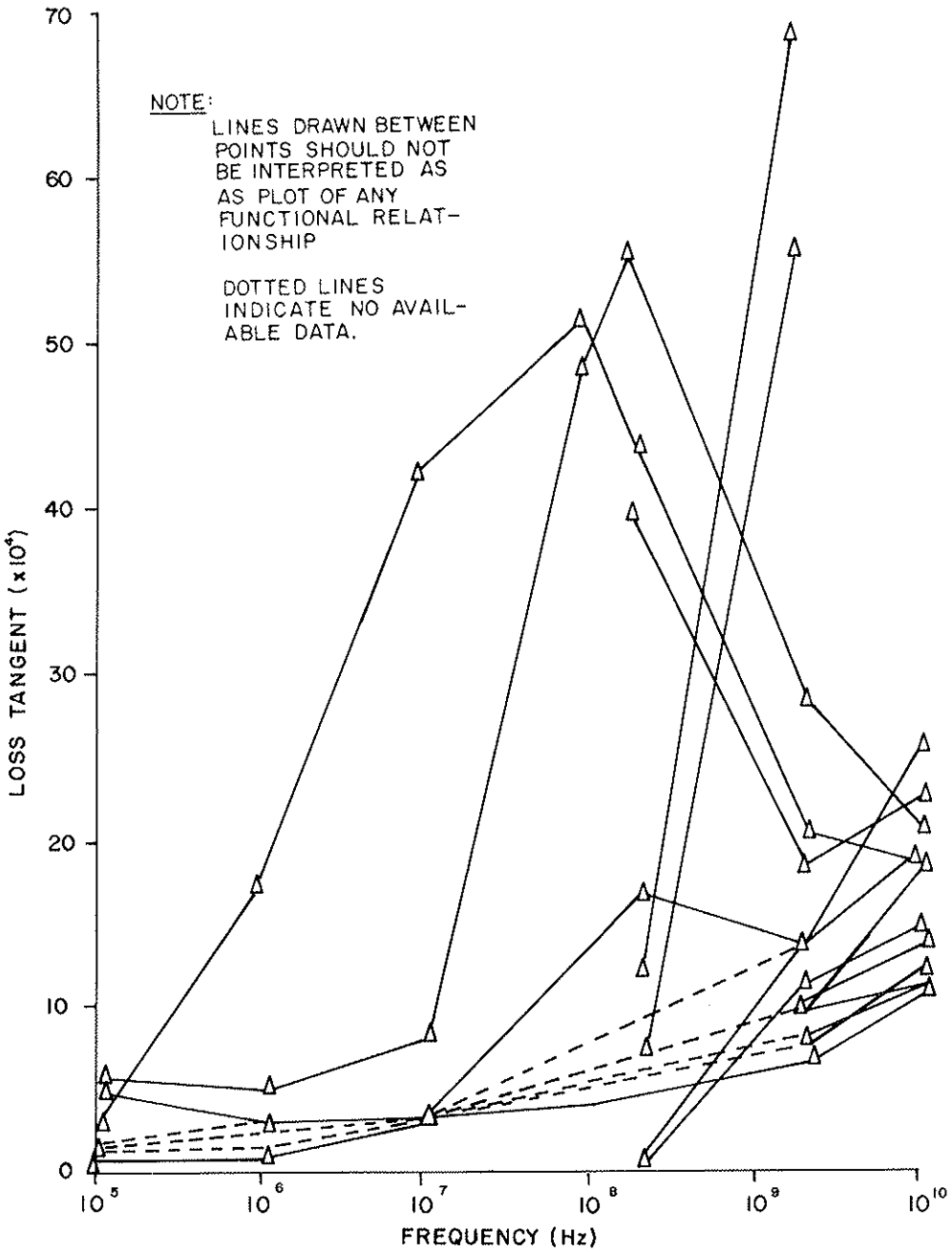

FIGURE A2-3 (Von Hippel, 1954)

Howard et al.(1967) measured the real part of the complex permittivity of a variety of fuel oils in the 4 to 4.5 GHz regions. These results are given in Table A2.1. Edgerton and Trexler (1970) undertook dielectric measurements of various oils at 37 GHz. These are summarized in Table A2.2. The effect of aging (exposure) of oils on the complex permittivity was investigated also. Figure A2-4 demonstrates the effects on the real part as well as its relationship to the API number of oil. The major difference between fresh and aged oils occurs in the imaginary part. An increase of two orders of magnitude in the imaginary part was reported for Bunker "C" fuel oils. This was attributed to the drying of the oil. Kondratyev et al.(1975) noted that the major increase occurred in the imaginary part of the oil with exposure or age as well. This was believed due to moisture absorption from the atmosphere, a seemingly opposite observation to that reported by Edgerton and Trexler. Kondratyev et al.(1975) undertook experimental work in the range from 8.8 to 12 GHz and found that the real part of the complex permittivity varied only slightly from 2.27 to 2.24 and the imaginary part decrased from 0.0150 to 0.0126. No information was supplied as to the type of oil measured. Hollinger (1974) measured three types of oils at 19.3 and 69.8 GHz. His results are summarized in Table A2.3. Finally, Klemas (1971) in a review paper reported that the real part of the complex permittivity varied from 1.85 to 2.94 with the average for crude oils being 2.0. The loss tangent ($x10^4$) was reported to be 3 at 1 MHz, 15 at 10 GHz, and 20 at 25 GHz.

The results of all the preceeding are summarized in Figures A2-5 and A2-6. Other possible sources of dielectric properties are listed in the reference section.

As there will be most likely some mixing between the oil spilled and the water, it is worthwhile considering this effect upon the complex permittivity. Hollinger (1974) states that stable emulsions with a water content between 50 and 80% can be formed from crude and residual oils. Water-in-oil emulsions would most likely have a higher dielectric constant than the pure oil because of the higher value of the dielectric constant for water. The following formula is given for the dielectric constant of such an emulsion:

$$\frac{\varepsilon - 1}{\varepsilon + 2} = \frac{\varepsilon_o - 1}{\varepsilon_o + 2} \rho_o + \frac{\varepsilon_w - 1}{\varepsilon_w + 2} \rho_w$$

where ε, ε_o and ε_w are the complex permittivities of the mixture, oil and water, respectively, and ρ_o and ρ_w are the volume fractions of oil and water. Figures A2-7 and A2-8 are representative curves of the effect of water. The effect would be very similar for other oil types (ibid). Hollinger also stated that because distillate products do not

TABLE A2.1 DIELECTRIC MEASUREMENTS MADE BY HOWARD ET AL.(1967) BETWEEN 4 AND 4.5 GHz

Oil Source	Real Part of the Dielectric Constant
Middle East via Bayonne, N.J.	2.41
Long Beach, Calif.	2.46
Long Beach, Calif.	2.43
Long Beach, Calif.	2.30
Ras Tanura, Saudi Arabia	2.30
Sasebo Arabian American Oil Company, Saudi Arabia	2.30
Black Oil Farm, Ras Tanura, Saudi Arabia	2.30
Standard Oil Co., Richmond, Calif.	2.43
Mobil Oil Co., Terminal Island, Calif.	2.38
Arabian American Oil co., Saudi Arabia	2.33
Mixture - 75% Awali - Bahrein - 25% Ainway - Venezuela	2.37
Bahrein Petrol Ltd.	2.33
NSCO Point Molate, Richmond, Calif.	2.41
Arabian American Oil Company, Ras Tanura, Saudi Arabia	2.33
Arabian American Oil Company, Hokosaki Terminal, Japan	2.30
Black Oil Farm, Ras Tanura, Saudi Arabia	2.30
Texaco Oil co., Norfolk-Trinidad, B.W.I.	2.33
Long Beach, Calif.	2.43
Long Beach, Calif.	2.44
Middle East via Bayonne, N.J.	2.27

TABLE A2.2 DIELECTRIC CONSTANTS AT 37 GHz
(Edgerton and Trexler, 1970)

Oil Type	Dielectric constant
40 Gravity Crude Oil 23°C	$\varepsilon' = 1.85 + 0.03$ $\varepsilon'' < 0.01\overline{4}8$
30 Gravity Crude Oil 23°C	$\varepsilon' = 2.06 + 0.05$ $\varepsilon'' < 0.01\overline{5}0$
20 Gravity Crude Oil 23°C	$\varepsilon' = 2.29 + 0.05$ $\varepsilon'' < 0.01\overline{9}8$
Bunker "C" Fuel Oil 23°C	$\varepsilon' = 2.41 + 0.05$ $\varepsilon'' < 0.02\overline{1}3$
Gasoline	$\varepsilon' = 2.08 + 0.05$ $\varepsilon'' < 0.00\overline{1}7$
40 Gravity Crude Oil 20°C aged 3 days in open air	$\varepsilon' = 2.10 + 0.05$ $\varepsilon'' = 0.22\overline{9} \pm 0.02$
Bunker "C" Fuel Oil 20°C aged 3 days in open air	$\varepsilon' = 2.94 + 0.07$ $\varepsilon'' = 0.29\overline{8} \pm 0.02$

TABLE A.2.3 MEASURED COMPLEX DIELECTRIC CONSTANT OF OIL
(Hollinger, 1974)

Oil Type	Temperature	Frequency 19.3 GHz	69.8 GHz
No. 2 Fuel (34.1 API Gravity)	19°C	$\varepsilon' = 2.10 \pm 0.5$ $\varepsilon'' = 0.01 \overline{+} 0.02$ $- 0.01$	2.10 ± 0.05 $0.01 \overline{+} 0.01$ $- 0.01$
No. 4 Crude	26°C	$\varepsilon' = 2.4 \pm 0.1$ $\varepsilon'' = 0.06 \pm 0.04$	2.2 ± 0.1 0.07 ± 0.04
No. 6 Crude	26°C	$\varepsilon' = 2.6 \pm 0.2$ $\varepsilon'' = 0.05 \pm 0.05$	2.6 ± 0.2 0.05 ± 0.05

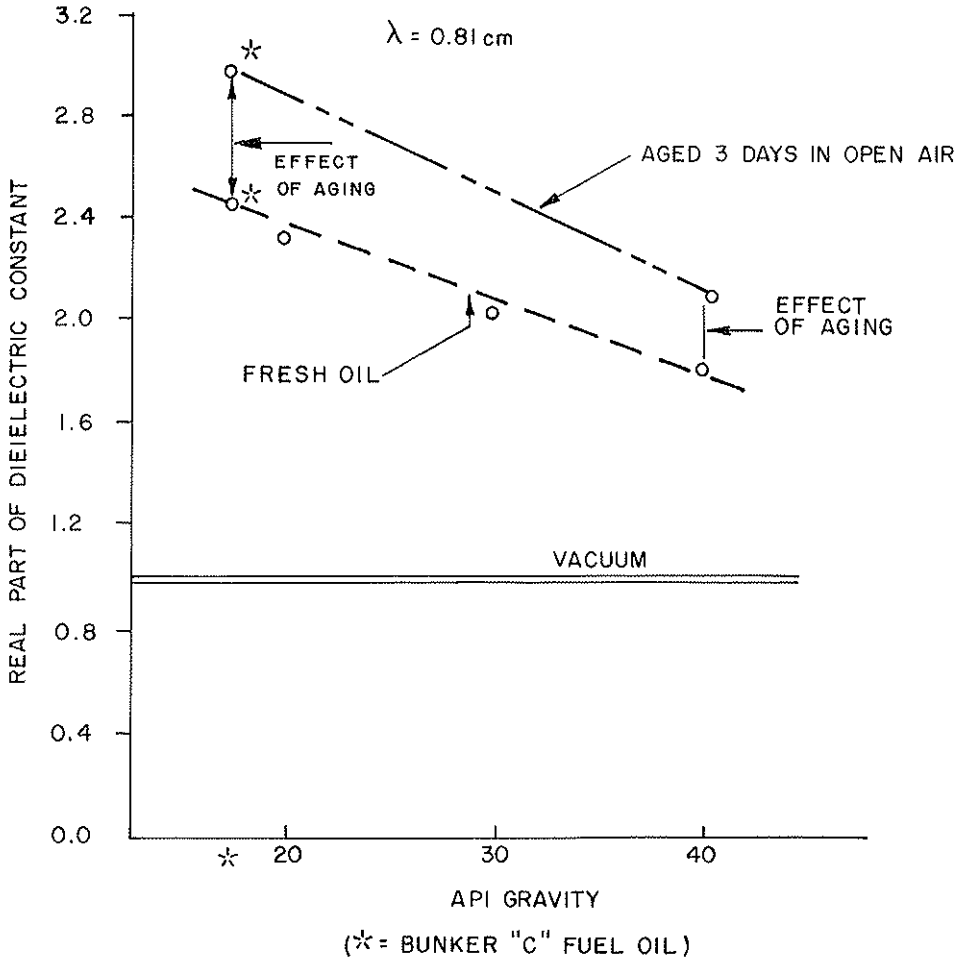

FIGURE A2-4 DIELECTRIC CONSTANT OF CRUDE OILS VERSUS API GRAVITY (Edgerton and Trexler, 1970)

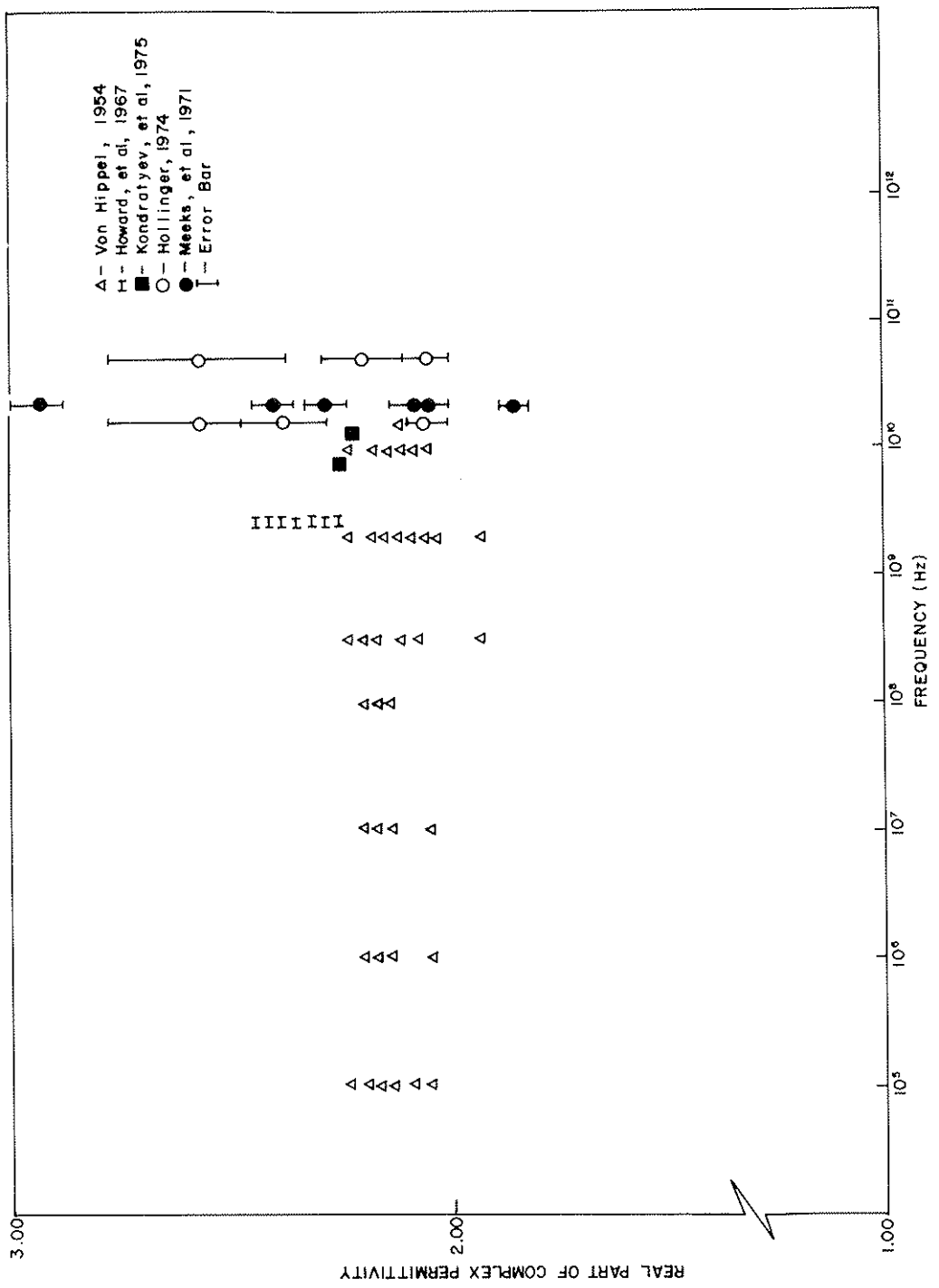

FIGURE A2-5 (Von Hippel, 1954)

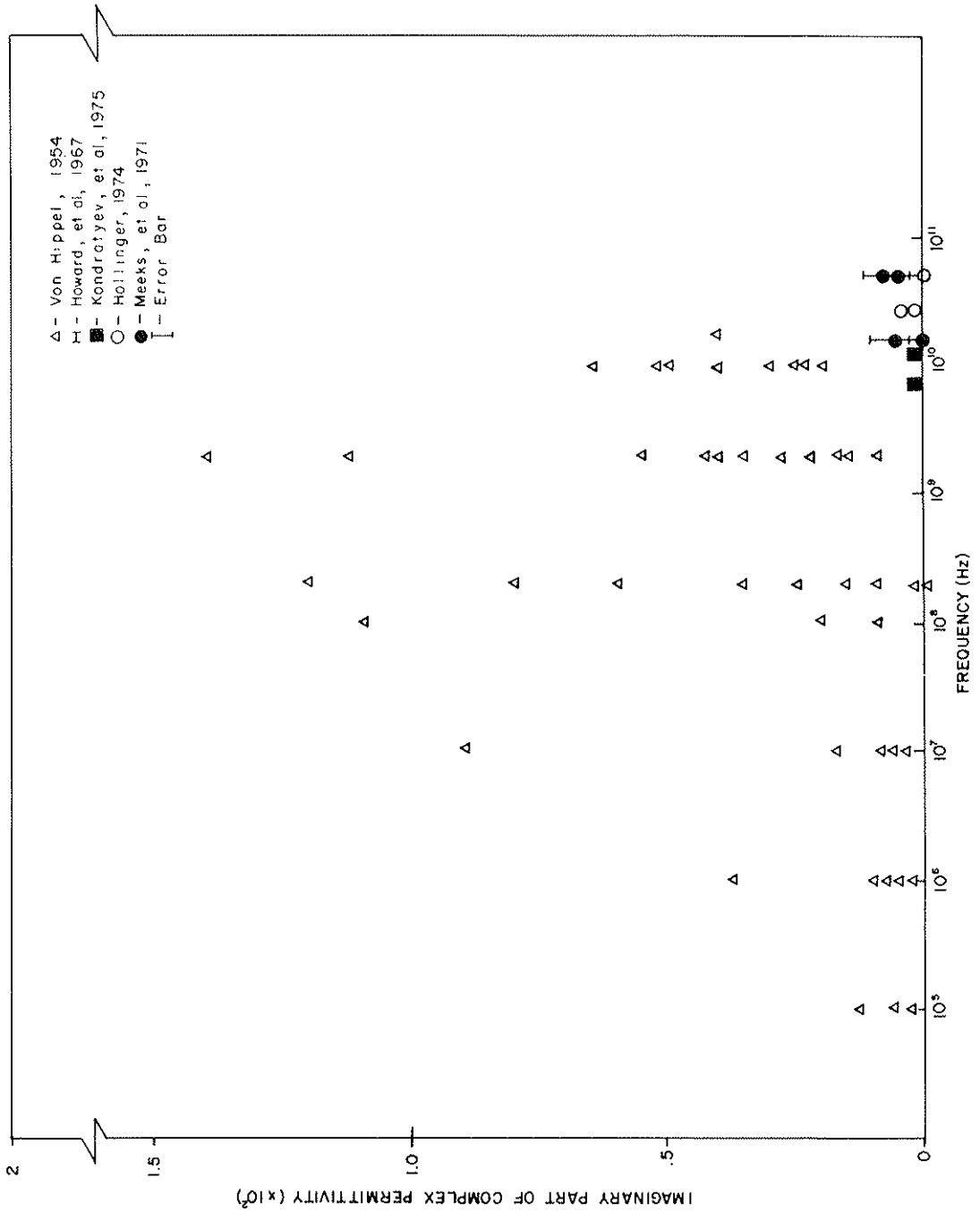
Δ - Von Hippel, 1954
H - Howard, et al, 1967
■ - Kondratyev, et al, 1975
○ - Hollinger, 1974
● - Meeks, et al, 1971
I - Error Bar
IMAGINARY PART OF COMPLEX PERMITTIVITY (x10²)
2
1.5
1.0
.5
0
FREQUENCY (Hz)
10⁵
10⁶
10⁷
10⁸
10⁹
10¹⁰
10¹¹

FIGURE A2-6

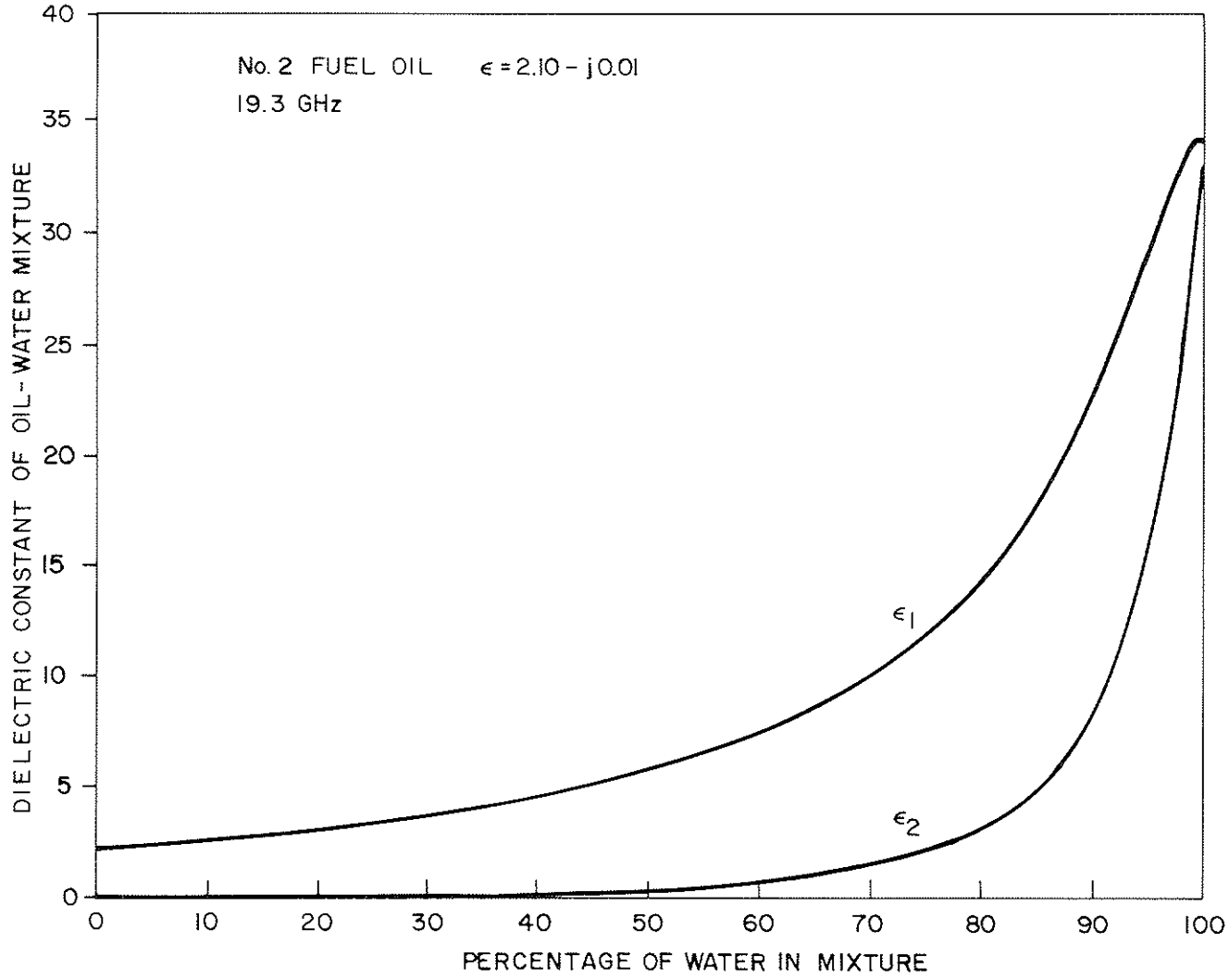

FIGURE A2-7 (Hollinger, 1974)

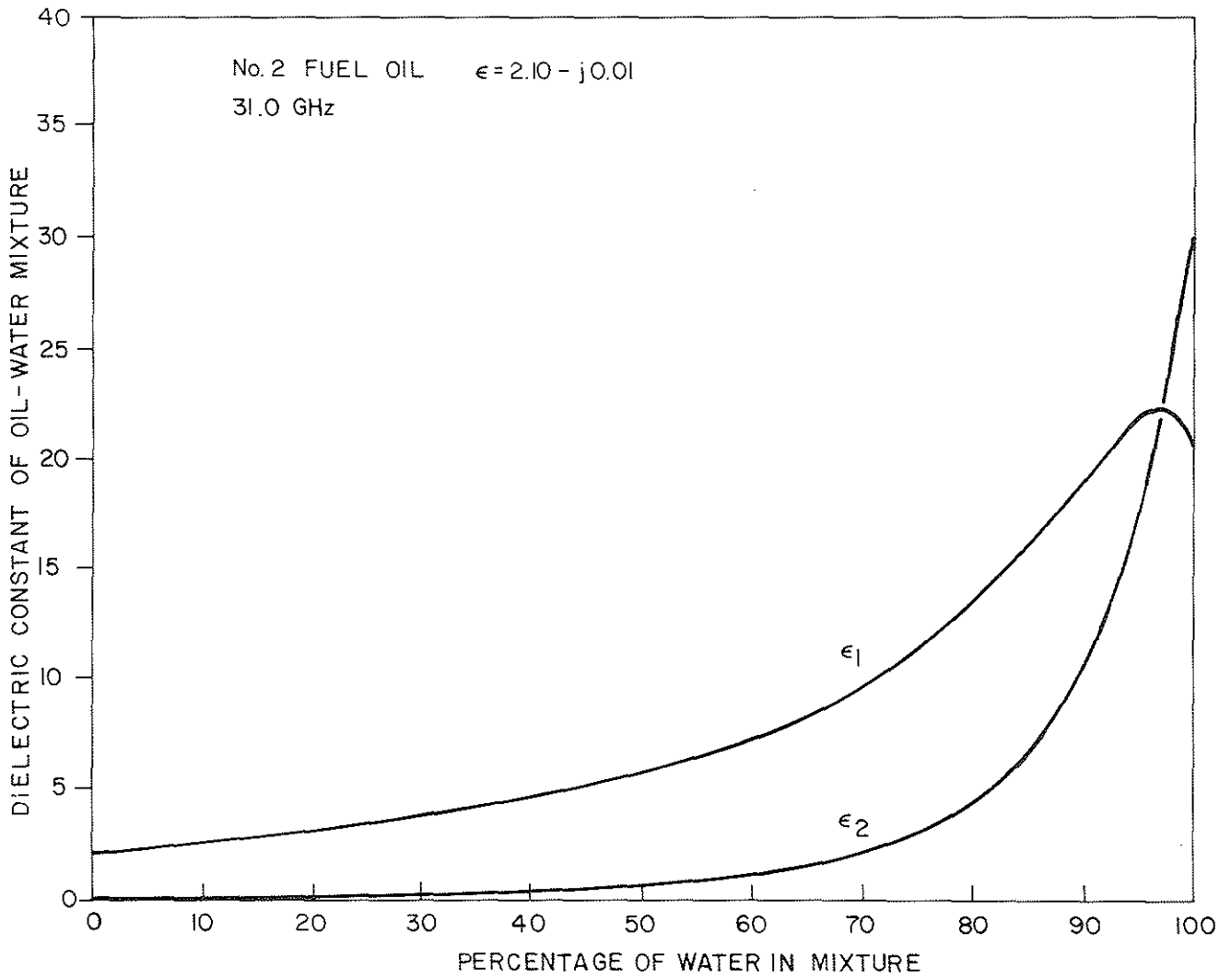

FIGURE A2-8 (Hollinger, 1974)

form stable emulsions the effect should only be significant for heavy lubricating oils and crude and residual oils. Even, then this would occur only after a period of possibly days. The above equation which was successfully used for calculations for water-bearing rocks should be applicable to oil-bearing ice.

A2.3 Conclusions

It is clear from the data presented that there is a lack of information regarding the dielectric properties of petroleum oils. From Figures A2-5 and A2-6 there are a number of gaps in the dielectric property versus frequency relations. The most comprehensive study was undertaken using refined oils, not the types likely to be involved in a major spill. The less refined oils have only been analyzed for their dielectric properties in the X- and L-band regions, usually at one specific frequency. It seems no two researchers have worked with the same oil type. As the imaginary part of the complex permittivity shows a significant anomally in the megahertz region, particularly around 100 MHz, a great deal more information is required for the purpose of evaluating microwave attenuation. It should be noted that the optimum frequency suggested for sea ice thickness sensing is in this region (Parashar et al, 1977) making it crucial that detailed information be obtained for the imaginary part if active microwave sensors are to be used to detect oil under the ice.

The effect of temperature on the dielectric properties of various oil types has apparently not been addressed to date. The temperature range of the data presented here, where available, is 19°C to 26°C. Oil spilled in ice-infested waters will be subjected to temperatures ranging around and well below freezing and its dielectric properties may be different.

Only theoretical calculations have been undertaken to examine the effects of mixing of oil and water. No actual tests have been made on the amount of mixing and the actual result. No information is available on the mixing of oil and sea ice and the resultant dielectric properties.

Aging of exposed oil has only been tentatively examined for its affect on the dielectric properties. Two seemingly contradictory reasons for the resultant effect have been given. More work is required to examine this effect in the arctic and subarctic environment, particularly when the oil is mixed with sea ice.

In summation, there is a general lack of data for specific oil types over the frequency range of interest at temperatures to be expected in ice infested waters. Also, the effect of mixing with sea ice and sea water needs to be investigated. Finally, the effect of aging must be examined.

REFERENCES

Edgerton, A.T., and D.T. Trexler, "Radiometric Detection of Oil Slicks," Aerojet General Corporation Report No. SD1335-1, pp 130, (January 1970).

Hollinger, J.P., "The Determination of Oil Slick Thickness by Means of Multifrequency Passive Microwave Techniques," NRL Report No. 2953, pp 144, (July 1974).

Howard, D.D., N.A. Thomas, and M.C. Licitra, "Microwave Monitoring of Sea Water Contamination of Navy Fuel Oil," NRL Report No. 6552, pp 15, (June 1967).

Klemas, V., "Detecting Oil on Water: A Comparison of Known Techniques," Proceedings of the Joint Conference on Remote Sensing of Environmental Pollutants, Palo Alto, Cal., pp 6, (1971).

Kondratyev, K. Ya, Yu Rabinovich, V.V. Nelenteyev, and E.M. Shulgina, "Remote Sensing of Oil on the Sea Surface," Proceedings of the Tenth International Symposium of Remote Sensing of Environment, Vol. 1, Ann Arbor, Michigan, pp 251-252, (1975).

Meeks, D.C., Williams, P.M., Wilcox, A.T., Edgerton, "Microwave Radiometric Detection of Oils Slicks," Aerojet General Corporation, Report No. 1335-2, pp 177, (March 1971).

Parashar, S., B. Dawe and R.D. Worsfold, "Stage - 1, Evaluation of Potential Sea Ice Measurement Techniques - Development of a Remote Sea Ice Thickness Sensor," Phase 1, C-CORe Technical Report, Publication No. 77-6 (Contracted to Transportation Development Centre, Ministry of Transport), pp 84, (December 1977).

Von Hippel, A.R. (editor), Dielectric Materials and Applications, The M.I.T. Press, Cambridge, Mass., (1954).

Other Possible Sources of Oil Dielectric Properties
Chemical Abstracts Condensates

3
E8118; 1Ø8158U
AUTOMATIC MONITORING OF WATER IN A PETROLEUM STREAM
KODRAT'EU, N.A.; BONDARENKO, P.M.
USSR
TRANSPORT I KHRANENIE NEFTI I NEFTERPRODUKTOU (FORMERLY NNKNA) - CISTI
1971, 6; 27-31.ARTC
TKNTA
WATER DETN PETROLEUM DIELEC CONST; PETROLEUM ANALYSIS WATER DIELEC CONST
RUS

6
E8608; 45402Z
CAPACITANCE DENSITY MEASUREMENT OF REFRIGERATED HYDROCARBON LIQUIDS
WEITZ, PAUL G., JR.; LAMPHERE, DAVID
SIMMONDS PRECIS. INSTRUM. SYST. DIV., IND. INSTRUM. SYST., VERGENNES, UT.
ADVANCES IN INSTRUMENTATION (FORMERLY ANICA)
1976: 31, PT. 2,; 605, 6 PP;
AVINB
ALKANE LIQ DENSITY DETN: HYDROCARBON LIQ DENSITY DETN: DIELEC CONST HYDROCARBON DENSITY DETN: NATURAL GAS LIQUEFIED DENSITY DETN, PETROLEUM GAS LIQUEFIED DENSITY DETN
CAØ51009
ENG

7
E8706; 41444N
MEASUREMENT OF THE SALT CONTENT OF PETROLEUM
DENIN, S.D.; BYKOVA, Z. YA.; KLUGMAN, I. YU.
USSR
IZMERITEL,NAYA TEKHNIKA-CISTI
1977, 1; 75-7; ARTC
IZTEA
SALT DETN PETROLEUM; DIELEC DETN SALT PETROLEUM; CONTENT
CAØ51ØØ3
RUS

8
E8712; 874910
CAPACITANCE DENSITY MEASUREMENT OF REFRIGERATED HYDROCARBON LIQUIDS
WEITZ, PAUL G., JR.; LAMPHERE, DAVID
INSTRU. SYST. DIV., SIMMONDS PRECIS. PROD. INC., VERGENNES, VT.

INSTRUMENTATION IN THE CRYOGENIC INDUSTRY-CISTI
1976: 1; 605, 1-6; ARTC
ICIND
DENSITY LIQ HYDROCARBON DETN; NATURAL GAS LIQ DENSITY; PETROLEUM GAS LIQ
DENSITY: DIELEC CONST HYDROCARBON DENSITY; CAPACITANCE HYDROCARBON LIQ DENSITY
CA051009
ENG

2
E7916; 94234K
STANDARDIZATION OF A DIELECTRIC CONSTANT-MEASURING DYNAMIC METHOD FOR TRACE WATER DETECTION IN PETROLEUM
KLUGMAN, I. YU.; SOKOLOV, I.L.
USSR
FROM REF. ZH.; SEE PRINTED ISSUES OF CHEMICAL ABSTRACTS FOR COMPLETE BIBLIOGRAPHY DETAILS.
1972: 136,; 90-7. ARTC
D8MMY
WATER DETECTION PETROLEUM: DIELEC CONST WATER DETECTION
RUS

8
E8712; 87392X
USE OF FREQUENCY CHARACTERISTICS OF DIELECTRIC LOSSES OF PETROLEUM AND A WATER-PETROLEUM EMULSION FOR MONITORING WATER CONTENT
KURKOVA, Z.E.; BONDARENKO, P.M.
USES. NAUCHNO-ISSLED. INST. SOBORU, PODGOT. NEFTI NEFTEPROD., UFA, USSR
TRANSPORT I KHRANENIE NEFTI I NEFTEPRODUKTOV (FORMERLY NNKNA) - CISTI
1977; 4; 23-6; ARTC
TKNTA
PETROLEUM WATER DETN DIELEC LOSS
CA051003
RUS

9
E8718; 138277Y
APPLICABILITY OF THE DIELECTRIC LOSS MEASUREMENT METHOD FOR DETERMINING WATER CONTENT IN PETROLEUM PRODUCTS
ZWIERZUCKI, WIESLAW
POLITECH. POZNAN., POZNAN, POL.
NATA (KATOWICE, POLAND)
1977: 33,5; 166-9; ARTC
NAFPA
PETROLEUM PRODUCT WATER DETN: DIELEC LOSS WATER DETN
CA051009
POL
@

3
E7916; 98124X
COMPLEX DIELECTRIC CONSTANT OF DISPERSE SYSTEMS
KLUGMAN, I. YU.
SARATOV, USSR
ELEKTROPOVERKHNOSTNYE YAVLENIYA V DISPERSNYKH SISTEMAKH
MOSCOW, USSR. "NAUKA"; 1972; 49-55 GRIGOROV, O. N.PROC
26TFA
DIELEC PROPERTY PETROLEUM WATER EMULSION; SALT EMULSION DIELEC PROPERTY
RUS
@
P, *,1,4

5
E8224; 158423T
FREQUENCY-DIELECTRIC CONSTANT MEASURING METHOD FOR DETERMINATION OF SALT CONTENT IN PETROLEUM AND PETROLEUM PRODUCTS
BENIN, S.D.; KLUGMAN, I. YU.; ROMAN'KO, K.S.; SOLOLOV, I.L.
USSR
IZMERITEL "NAYA TEKHNIKA-CISTI
1974, 1Ø; 7Ø-2.ARTC
IZTEA
FREQUENCY DIELEC CONST APP; PETROLEUM SALT CONTENT DETN
RUS

196139H
APPARATUS FOR DETERMINING THE DEGREE OF POLLUTION OF A LIQUID FR. SOFRANCE S.A.
PATENT - FRANCE
Ø4 APR 1975; 11 PP.; PATENT: FR. DEMANDE, 2243624, 12 SEP 1973 PR,9673 32,733.PATS
FRXXB
LUBRICATING OIL CONTAMINATION MONITOR; INDUSTRIAL OIL CONTAMINATION MONITOR;
DIELEC CONST LUBRICANT MONITOR; OIL INDUSTRIAL MONITOR APP
CAØ51ØØ7
***

Engineering Index

1
Q71Ø3
EØ15482
EFFECTS OF CONDUCTION COLLOIDAL MATERIALS ON THE DIELECTRIC PROPERTIES OF CRUDE OILS
THOMPSON DD: MICKSIC SW
CHEVRON OIL FIELD RES CO, LA HABRA, CALIF
AMER CHEM SOC, DIV PETROL CHEM, PREPR V 15 N 1 FOR MEETING HOUSTON, TEX, FEB
22-27 197Ø P A118A12Ø

ACPCA
PETROLEUM CRUDE
ØØ-A512

2
Q7109
EØ584Ø5
FREQUENCY CHANGE CAN HELP IMPROVE BS & W MONITOR,S ACCURACY
THOMPSON DD; NICKSIC SW
OIL GAS J V 68 N 47 NOV 23 1970 P 69-71
OIGJA
PETROLEUM; CRUDE; OIL WELL PRODUCTION; CONTROL; DIELECTRICS; MEASURMENTS; ELECTRIC CAPACITANCE
ØØ-A511; ØØ-A512, ØØ-A701

3
Q75Ø8
ØØ54Ø83
FREQUENCY DIELECTRIC METHOD OF DETERMINING SALT CONTENTS ON CRUDE PETROLEUM AND PETROLEUM PRODUCTS
BENIN, S.D.; KLUGMAN, I. YU.; ROMAN'KO, K.S.; SOKOLOV, I.L.
MEAS TECH V 17 N 1Ø OCt 1974 P 1589-1592
MSTCA
PETROLEUM ANALYSIS; SODIUM CHLORIDE
A445; A8Ø1; A8Ø4

1
Q7ØØ6
EØ23226
INFLUENCE OF FLOW VELOCITY AND FIELD INTENSITY ON DIELECTRIC CONSTANTS OF EMULSIONS
BYKOVA ZYA; KLUGMAN IYU
SARATOV POLYTECHNICA INST, SOVIET UNION
COLLOID J OF USSR (ENGLISH TRANSLATION OF KOLLOIDNYI ZHURNAL) V 31 N 1 JAN-FEB 1969 P 17-2Ø
EMULSIONS; ELECTRIC MEASUREMENTS; DIELECTRICS; FLOW OF FLUIDS; ELECTRIC FIELDS: PETROLEUM RESEARCH
ØØ-A803

4
Q7209
EØ55976
MEASUREMENT IN THE MILLIMETER RANGE OF WAVELENGTHS OF THE WATER CONTENT OF PETROLEUM
DEM,YANOV AA
MEAS TECH V 14 N 8 AUG 1971 P 126Ø-1
MSTCA
PETROLEUM PRODUCTS; MOISTURE; MEASUREMENT; DIELECTRICS
ØØ-A513; ØØ-A944

6
Q7508
ØØ54083
FREQUENCY DIELECTRIC METHOD OF DETERMINING SALT CONTENTS ON CRUDE PETROLEUM AND PETROLEUM PRODUCTS
BENIN, S.D.; KLUGMAN, I. YU.; ROMAN'KO, K.S.; SOKOLOV, I.L.
MEAS TECH V 17 N 10 OCt 1974 P 1589-1592
MSTCA
PETROLEUM ANALYSIS; SODIUM CHLORIDE
A445; A8Ø1; A804

Information Services In Physics
Electrotechnology, Computers & Controls

3
P7624
B48997
CHARACTERISTICS OF MEASUREMENTS PERTAINING TO THE TEMPERATURE COEFFICIENT OF DIELECTRIC PERMEABILITY AND PECULIAR TO PETROLEUM (MOISTURE CONTENT DETERMINATION)
DENIN, S.D.; KLUGMAN, I.YU.; KOBYLOV, N.B. ROMAN'KO, K.S.
IZMER. TEKH. (USSR)
OCT. 1975; 18(10); 59-61
MEAS. TECH. (USA)
OCT. 1975; 18(10); 15ØØ-3
IZTEA; MSTCA
PERMITTIVITY MEASUREMENT; MOISTURE MEASUREMENT; ORGANIC COMPOUNDS; MOISTURE CONTENT; PETROLEUM; DIELECTRIC HYGROMETERS; DIELECTRIC PERMITTIVITY COEFFICIENT; INTRINSIC TRANSDUCER CAPACITANCE
B4428; C7428; B4448; C7448
ENG
ARTC
X
@

National Technical Information Services

U7622; N76-26716/ØSL
THE THERMAL RADIO EMISSION OF A CONTAMINATED SEA SURFACE.
RAYZER, V.Y.; SHARKOV, Y.A.; ETKIN, V.S.
KANNER (LE) ASSOCIATES, REDWOOD CITY, CALIF.
MAY 76; 32P; TRAN-TRANSL. INTO ENGLISH FROM THE RUSSIAN REPORT PR-237
REPT. NASA-TT-F-17033; PR-237
CONT. NASW-2790
*OCEAN SURFACE; *WATER POLLUTION; CONTAMINANTS; DIELECTRICS; FLUID FILMS; OCEAN MODELS; OIL SLICKS; REMOTE SENSORS; TEMPERATURE EFFECTS; TRANSLATIONS; USSR; RADIANT FLUX DENSITY; *OIL POLLUTION DETECTION; *THERMAL RADIATION 13B 17H; 68D; 63F; 47
@

APPENDIX 3

APPENDIX 3 - MICROWAVE SCATTERING AND EMISSION FROM THE OCEAN

A3.1 INTRODUCTION

Microwave scattering and emission from the ocean surface has been a subject of much recent research. The 14.6 GHz, multi-polarized radar scatterometer onboard the SEASAT-A satellite provides global measurements of ocean surface winds. The operational use of passive microwave systems in determining ocean temperature and salinity variations seems feasible. Experimental observations have demonstrated that ocean surface waves and patterns can be imaged with synthetic aperture imaging radars. Features such as ocean swells, oil slicks, wind slicks, currents, internal waves, eddies, and ship wakes have been imaged under a variety of conditions.

The purpose of this appendix is to review and document the significant results and features related to scattering and emission of electromagnetic waves from the ocean surface in the microwavelength region. To help understand the nature of radar return and passive microwave signatures, properties of saline water and the terminology used in describing ocean phenomena are provided.

A3.2 Description of the Ocean Surface

A wave resulting from the action of the wind on a water surface is termed a wind wave. It is a "sea" while the wind is acting on it and a swell thereafter. A wave whose velocity of propagation is controlled primarily by gravity is termed a gravity wave, and water waves of a length greater than 2 inches are considered such. Capillary waves, also called ripples, are waves of lengths less than 1 inch whose velocity of propagation is controlled primarily by the surface tension of the liquid in which the wave is travelling. Fetch or generating area is an area of the sea surfcae over which "sea" waves are generated by a wind having a constant direction and speed. Sea state is the numerical or written description of ocean surface roughness. Ocean sea state may be defined more precisely as the average height of the highest one third of the waves observed in a wave train and is presented in a numerical code. A fully developed sea is described as an area in which the maximum height to which ocean waves can be generated by a given wind force blowing over sufficient fetch is attained, regardless of duration (the length of time the wind blows is essentially the same direction over the fetch), as a result of all possible wave components in the wave spectrum being present with their maximum amount of spectral energy. Significant wave height (SWH) is the average height of the one-third

height waves of a given wave group, with height being defined as the vertical distance between a crest and trough. The numerical scale to describe sea state and a detailed description of the above terminology, is to be found in Skolnik (1970).

It is now generally accepted that a unique relationship exists between ocean surface roughness and wind speed. A qualitative relationship describing sea state as a function of wind speed, and other relationships pertaining to a description of rough seas, is exhibited in Table A3.1 (Stogryn, 1967). This relationship has been given a more quantitative basis by Cox and Munk (1954 a and b), who have determined a two-dimensional slope distribution function of Gaussian form for the sea surface on the basis of sun-glitter measurements. In investigating the effect of oil slicks, it was found that, for slicks of the order of 10^{-4} cm thick, the mean-square slopes of the surface for rough seas are reduced by a factor of two or three.

In view of the above, ocean waves can be defined as the undulations of the surface with time scales in the range from 0.025 to 25 s, corresponding to wavelengths in the region of 0.02 to 1000 m. These can be sub-classified, as gravity waves (including both wind-generated sea waves and swells) with time scales in the range of 0.1 to 25 s, length scales from 2 cm to 500 m and heights to 30 m, and as capillary waves (generated by wind but surface tension controlled) with time scales in the range of 10^{-1} to 10^{-2} s, length scales of 0.5 to 2.0 cm and heights of less than 1 cm (Matthews, 1974). A time record of the surface displacement of the ocean may contain the entire range of waves mentioned above.

A3.3 Electrical Properties of Seawater

The complex dielectric constant of seawater, which is dependent on salinity and temperature, can be found from the Debye expression (Klein and Swift, 1977):

$$\varepsilon = \varepsilon_\infty + \frac{\varepsilon_s - \varepsilon_\infty}{1 + (jw\tau)^{1-\alpha}} - \frac{j\sigma}{w\varepsilon_0}$$

where $w = 2\pi f$ is the radial frequency with f in hertz; ε_∞ is the dielectric constant at infinite frequency; ε_s is the static dielectric constant; τ is the relaxation time in seconds; σ is the ionic conductivity in mhos/m; α is an empirical parameter that describes the distribution of relaxation times; and $\varepsilon_0 = 8.854 \times 10^{-12}$ is the permittivity of free space in farads per metre.

It was found by Saxton and Lane (1952) that the static dielectric constant, ε_s, of sea water is about 75 and 69 at 0°C and 20°C respectively, compared with values of 88

TABLE A3.1 WIND AND SEA SCALE FOR A FULLY DEVELOPED SEA (Stogryn, 1967)

Sea - General		Wind				Sea				
						Wave Height (Feet)				
Sea State	Description	Wind Force (Beaufort)	Description	Range (knots)	Wind Velocity (knots)	Average	Significant	Avg $\frac{1}{10}$ Highest	Minimum Fetch (nmi)	Minimum Duration (hours)
	Sea like a mirror	0	Calm	<1	0	0	0	0	...	...
0	Ripples with the appearance of scales are formed; but without foam crests	1	Light Air	1-3	2	0.05	0.08	0.10	5	18 min
1	Small wavelets, still short but more pronounced; crests have a glassy appearance, but do not break	2	Light Breeze	4-6	5	0.18	0.29	0.37		38 min
——	Large wavelets, crests begin to break. Foam of glassy appearance. Perhaps scattered white horses.	3	Gentle Breeze	7-10	8.5	0.6	1.0	1.2	9.8	1.7 h
2					10	0.88	1.4	1.8	10	2.4
	Small waves, becoming larger; fairly frequent white horses	4	Moderate Breeze	11-16	12	1.4	2.2	2.8	18	3.8
——					13.5	1.8	2.9	3.7	24	4.8
3					14	2.0	3.3	4.2	28	5.2
					16	2.9	4.6	5.8	40	6.6
4	Moderate waves, taking a more pronounced long form; many white horses are formed. (Chance of some spray.)	5	Fresh Breeze	17-21	18	3.8	6.1	7.8	55	8.3
——					19	4.3	6.9	8.7	65	9.2
5					20	5.0	8.0	10	75	10

TABLE A3.1 WIND AND SEA SCALE FOR A FULLY DEVELOPED SEA (Stogryn, 1967) (cont'd)

Sea - General		Wind				Sea				
						Wave Height (Feet)				
Sea State	Description	Wind Force (Beaufort)	Description	Range (knots)	Wind Velocity (knots)	Average	Significant	Avg $\frac{1}{10}$ Highest	Minimum Fetch (nmi)	Minimum Duration (hours)
5	Large waves begin to form; the white crests are more extensive everywhere (probably some spray.)	6	Strong Breeze	22-27	22	6.4	10	13	100	12
					24	7.9	12	16	130	14
					24.5	8.2	13	17	140	15
					26	9.6	15	20	180	17
6	Sea heaps up and white foam from breaking waves begins to be blown in streaks along the direction of the wind. (Spindrift begins to be seen	7	Moderate Gale	28-33	28	11	18	23	230	20
					30	14	22	28	280	23
					30.5	14	23	29	290	24
					32	16	26	33	340	27
7	Moderately high waves of greater length; edges of crests break into spindrift. The foam is blown in well marked streaks along the direction of the wind. Spray affects visibility.	8	Fresh Gale	34-40	34	19	30	38	420	30
					36	21	35	44	500	34
					37	23	37	46.7	530	37
					38	25	40	50	600	38
					40	28	45	58	710	42

and 80 for pure water at these temperatures. The reduction in relaxation time from 10.1 x 10^{-12} s to 9.2 x 10^{-12} s for seawater and from 18.7 x 10^{-12} s to 17.0 x 10^{-12} s for pure water from 20°C and 0°C, respectively. The value of ε_α is about 4.9 for pure water and $\sigma = 0$ and $\alpha = 0$ can be taken for a first-order interation as suggested by Klein and Swift (1977).

The calculated variation of ε' and ε'' (real and imaginary part, respectively, of the complex permittivity) for sea water (salinity 3.6°/oo over the frequency range from 1 to 10^5 MHz for temperatures of 0° and 20°C is shown in Figures A3-1 (a) and (b), respectively. The corresponding values for pure and fresh water are added for purposes of comparison (Saxton and Lane, 1952). It is clear that the dielectric properties of pure, freshwater and seawater are identical for frequencies above 20 GHz. The value of ε' and ε'' for pure distilled water as a function of temperature for 2.653 GHz and 1.43 GHz are given in Tables A3.2a (Ho and Hall, 1973) and A3.2b, (Ho et al, 1974), respectively (Klein and Swift, 1977).

Based on past experimental results, Stogryn (1971) presented empirical relationships for computing the complex permittivity of sea water as a function of salinity and temperature. The measurements made by various researchers are compared by Edgerton et al.(1973) and calculations based on empirical results show that an accuracy of 1 or 2% may be achieved in estimating dielectric properties of seawater. A modified model for improving this accuracy was presented by Klein and Swift (1977).

A3.4 Radar Scattering from the Ocean

There are two types of scattering processes produced by the ocean at microwave frequencies. The larger ocean waves behave as an ensemble of specular reflectors such that the strength of the scatter is proportional to the slopes of gravity waves. For radar returns at near normal incidence (angles less than about 20°), the results indicate that the dominant contributor to sea returns are gravity waves which act as quasi-specular reflectors. For incidence angles greater than 20°, it is found that the primary factor governing ocean radar backscatter is the amplitute of the capillary portion of the sea spectrum. In the small pertubation theory, these components are related to the radar wavelengths by the Bragg scattering conditions that the radar return from adjacent crests of the most important ocean components add in phase producing the condition:

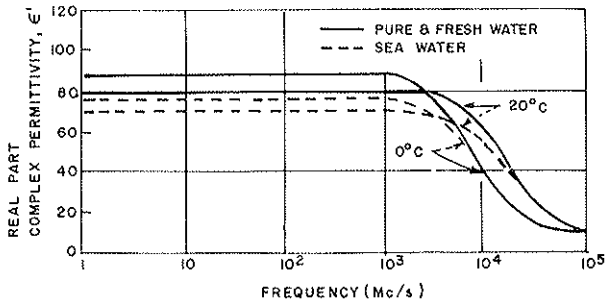

FIGURE A3-1(a) DIELECTRIC PROPERTIES OF PURE, FRESH AND SEAWATER (Saxton and Lane, 1952)

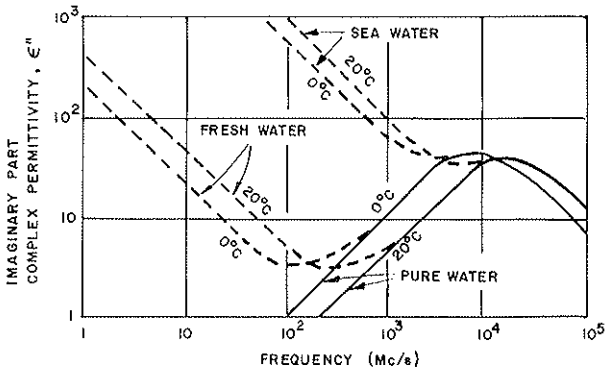

FIGURE A3-1(b) DIELECTRIC PROPERTIES OF PURE, FRESH AND SEAWATER (Saxton and Lane, 1952)

TABLE A3.2a ε' AND ε'' FOR DISTILLED WATER AS FUNCTION OF TEMPERATURE (f = 1.43 GHz) (Ho et al., 1973)

Temperature (^{o}C)	ε'	ε''
5	84.54	10.742
10	82.96	8.888
20	79.56	6.285
30	76.14	4.783

TABLE A3.2b ε' AND ε'' FOR DISTILLED WATER AS FUNCTION OF TEMPERATURE (f = 2.653 GHz) (Ho et al., 1974)

Temperature (^{o}C)	ε'	ε''
5.5	80.52	20.03
15	79.57	13.75
24	77.44	10.18
30	75.88	8.61

$$\Lambda \text{ Sin } \Theta_i = n\lambda/2$$

where Λ = ocean wavelength (component of spectrum)

λ = radar wavelength

Θ_i = angle of incidence (from local vertical)

The first order perturbation theory only accounts for n=1, although higher order "Bragg resonances" may also be important. The "Bragg wavelength" for the ocean is the same as the probing radar wavelength at an incidence angle of 30^{o}.

The modern theories of radar backscatter from the sea describe the ocean surface as consisting of two scales of roughnesses, one for that portion of the ocean spectrum having wavelengths much larger than the radar wavelength (gravity waves) and other for the part of the ocean spectrum comparable with the radar wavelength (capillary waves). Wright (1966) and Bass and Bocharav (1958) used the small perturbation method to compute the backscatter from the ocean. Wright (1968) later modified the model by

considering the effect of the perturbed surface laying on titled planes caused by the larger structures. Valenzuela (1968) used a similar approach and later (Valenzuela and Laing, 1971) developed a model for the statistics of sea clutter from scattering theory and the composite surface-scattering model. An empirical identification of the statistics of sea clutter was obtained from the Four-Frequency NRL radar data. A backscatter model was developed by Chia (1968) using the Kirchoff tangent plane approximation, but real autocorrelations based on wave spectra were used rather than the usual mathematically convenient function. Jackson (1971) extended the range of validity of the Kirchoff method by taking into account the curvature. Some researchers (Semyonov, 1966a, Barrick and Peake, 1967, and Krishen, 1970) used the Kirchoff method for part of the spectrum and added in the contribution from small perturbation theory applicable over a different angular range. A correction factor for interrelating the two parts of his solution was later added by Semyonov (1966b). A method for modifying the Krichoff theory in terms of a small perturbation solution for the undulating surface was developed by Fung and Chan (1971) and Chan and Fung (1973) by considering both coherent and non-coherent approaches. This model enabled the coupling of results from the two methods applicable to different parts of the wave spectrum and angular range.

On making recommendations for the design of the SEASAT-A scatterometer, Grantham et al (1975) have pointed out that none of the theories of backscatter presently account for breaking waves, sea foam, white caps and flying drops of spray because of the difficulties involved.

Radar backscatter measurements have beem made both in the laboratory and over the open ocean for a range of wind speeds. The preliminary analyses have indicated an increase of backscatter with wind and wave development. The wave spectrum in the capillary region can be expressed in terms of(Grantham et al, 1975):

$$S(k) = \frac{(4.05 \times 10^{-3})\, D}{k^3}$$

where k is the wave number in cm^{-1} and D is a variable depending on wind speed.

The indication from the experimental data is that S(k) continues to grow with increasing wind speed above about 3 m/s. Below that speed the capillary waves die away rapidly. It was pointed out by Grantham et al (1975) that good observations are rare for high winds although the available data show an increase in backscatter up to 20 m/s or so.

Measurements of capillary waves on the open sea are extremely difficult, so knowledge on capillary waves is based on theory and on measurements in wind-wave tanks (Pierson et al, 1971, Pierson and Stacy, 1973, and Pronk, 1975).

The correlation between the radar backscattering coefficient, σ^o, and ocean surface wind velocity has been studied extensively by many researchers (Crombie, 1955; MacDonald, 1956; Grant and Yaplee, 1957; Daley et al, 1970; Bradley, 1971; Krishen, 1971; Moore and Pierson, 1971; Glaassen and Fung, 1972; Jones et al, 1972; Newton and Rouse, 1972; Swift and Jones, 1974; Jones et al, 1977). Both aircraft and satellite data show that for wind speeds less than 20 m/s and incidence angles beyond 25^o the ocean radar scattering coefficient, σ^o, changes about one-half dB per 10 log change in wind speed (m/s). There is some argument as to whether the rate is 1/2 or 1/4 dB/10 log wind speed, but the sensitivity of σ^o to wind speed is still sufficient (even to gale-force winds) to make the scatterometer a viable remote sensor of wind speed and direction measurements.

The power law relationship between the wind speed U and σ^o is such that

$$\sigma^o = AU^{\nu}$$
$$10 \log \sigma^o = 10 \log A + \nu (10 \log U)$$
$$\sigma^o \text{ (dB)} = A \text{ (dB)} + \nu (10 \log U)$$

where A is constant and ν is the wind speed power coefficient. The variations of the value of the exponent with angle, polarization, and upwind, downwind, or cross-wind configuration is given by Grantham et al.(1975) and Jones et al.(1977). According to the aircraft data, σ^o_{VV} values can be as much as 10 dB higher than σ^o_{HH} values for large incidence angles. Most of the results show that Ku-band frequencies are preferred for maximum sensitivity to local wind speeds; however, results by Sittrop (1974) show a more rapid increase of σ^o with wind velocity at X-band, compared with Ku-band. The low frequencies (X-band) are also less sensitive to adverse weather conditions. The σ^o sensitivity to wind speed variation is about the same for upwind, downwind, or cross-wind conditions, by the magnitude for σ^o for cross-wind is less. The value of the exponent, ν, at 8.9 GHz (Daley, 1973), 13.3 GHz (Bradley, 1971 and Claassen and Fung, 1972), and 13.9 GHz (Jones et al, 1972 and Swift and Jones, 1974) are given in Table A3.3, A3.4, and A3.5, respectively (Grantham et al, 1975).

Many of the measurements of the backscatter of radar waves from the sea were summarized in Bechmann and Spizzichino (1963), Skolnik (1970) and Long (1975). The variations of sea echo and its properties as a function of frequency, polarization, and

TABLE A3.3 WIND SPEED POWER COEFFICIENT (Daley, 1973) AND (Grantham et al, 1975)

Frequency	Direction	Polarization	Exponent	Incidence Angle 20°	25°	30°	40°	50°
8.9 GHz	Upwind	VV	υ	0.20	0.25	0.37	0.66	0.73
	Downwind	VV	υ	0.20	0.29	0.36	0.80	0.80
	Upwind	HH	υ	0.00	0.33	0.58	0.87	1.03
	Downwind	HH	υ	0.00	0.29	0.52	1.04	1.30

TABLE A3.4 WIND SPEED POWER COEFFICIENT (Bradley, 1971, Classen and Fung, 1972) AND (Grantham et al, 1975)

Frequency	Direction	Polarization	Exponent	Incidence Angle θ_i 25°	35°
13.3 GHz	Upwind	VV	υ	1.12	1.49
	Downwind	VV	υ	1.15	1.60
	Crosswind	VV	υ	1.00	1.40

TABLE A3.5 WIND SPEED POWER COEFFICIENT (Jones et al, 1972) AND (Grantham et al, 1975)

Frequency	Direction	Polarization	Exponent	Incidence Angle, θ_i 20°	25°	30°	40°	50°
13.9 GHz	Upwind	VV	υ	1.00	1.53	1.90	1.90	1.90
	Downwind		υ	0.99	1.51	1.90	1.89	1.90
	Crosswind		υ	0.99	1.54	1.90	1.90	1.90
13.9 GHz	Upwind	HH	υ	0.94	1.48	1.90	2.00	2.00
	Downwind		υ	0.94	1.48	1.85	1.98	1.98
	Crosswind		υ	0.76	1.24	1.69	1.95	1.95

angle were presented for various sea state conditions. It was pointed out by Skolnik (1970) than rain, snow, and ice can smooth ocean waves. It has been observed that rain dampens the capillary wave structure and reduces σ^o at microwave frequencies. As a result rain and localized clouds often produce effects that appear as targets or they can change the sea-echo character. Breaking waves result in spikes of echo, and fish or schools of fish breaking water, and flights of birds have been observed to produce discernible echo signals.

It has been shown that ocean surface waves and currents can be imaged with a synthetic aperture radar (Brown et al, 1973, Brown et al, 1974, Brown et al, 1976, Elachi, 1976, Moskowitz, 1973, Larson and Wright, 1974 and Shuchmann et al, 1977). Ocean waves have also been imaged with the ERIM four channel synthetic aperture radar during Project SAR '77 (Worsfold, Strong and Wedler, 1977). The results are being analyzed. As shown by Elachi and Brown (1977), none of the models considered corresponding to four sources of radar backscatter modulation: tilt modulation, roughness variation, the wave orbital velocity and parametric effects, individually, fully explain the experimental results.

A study to investigate the characteristics of sea clutter using oil slicks has been conducted by Busch et al, 1959. It was felt that by making simultaneous measurements over oil free and oil covered sea, the properties of an oil free sea can be estimated since oil affects the sea surface in a known way. It was found that threre are similarities between the nature of σ^o for the clean sea and σ^o for a slick. The power amplitude (measured in dB) was observed to approximate a normal distribution for both but the "normal fit" was better for the clean sea data than for the slick data. An equation was developed for the ratio of the average value of the clutter from the clean sea to the average clutter for a slick. It was hypothesized that the width of the distribution of σ^o would be proportional to the wind speed and that the slick "acts" like a reduction in the wind velocity by a factor of two which would imply that the computed value of the standard deviation for the slick distribution of σ^o would be roughly one half that for the clean sea. No such variation was observed in the standard deviation of the experimental data possibly because of the low wind speeds, but such a relation might exist in the high wind speed region (15 to 26 knots).

A3.5 Microwave Emission from the Ocean

The brightness temperature of an infinitely extended, perfectly smooth, calm sea, neglecting atmospheric effects, was calculated by Hollinger (1973), as a function of frequency for various salinities and temperatures by using the equation:

$$T_B = (1 - R^2)\, T,$$

where T_B is the brightness temperature in degrees Kelvin; T is the thermometric temperature of water in degrees Kelvin; and R is the Fresnel reflection coefficient for the air-water interface. The dielectric properties of water as a function of the salinity and temperature of the water and frequency of observation were given. Based on these dielectric properties, the propagation characteristics of mircowave radiation in water such as skin depth and absorption were calculated. The values of the real part (ε') and imaginary part (ε'') of the complex permittivity as a function of frequency are presented in Figures A3-2 and A3-3, respectively. The skin depth as a function of frequency for pure and sea water is presented in Figure A3-4. The brightness temperatures at normal incidence are given in Figures A3-5 and A3-6 for temperatures of 0^{o} and 20^{o}C, respectively.

It has been shown by Hollinger (1971a) that surface roughness effects dominate the brightness temperature of the ocean at low wind speeds and that sea foam effects dominate at very high speeds. The transition wind speed between the two effects was thought to lie in the region between 15 and 20 m/s. It was found that the brightness temperature of the sea depends on wind speed and this dependance decreases with decreasing observational frequency. Increases of 1.1^{o}K per m/s of the horizontally polarized brightness temperature at 19.3 GHz, and a 55 degrees incidence angle, with wind speed have been measured (Hollinger, 1971b). It was suggested that the surface waves shorter than the observational wavelength were relatively unimportant in influencing the brightness temperature. It was seen that the sensitivity to wind speed increases with observational frequency and is most pronounced for horizontal polarization at larger incidence angles. Foam is known to have a very high brightness temperature approaching the physical temperature of the sea. It was suggested that the brightness temperature of the foam is apparently independent of polarization and incidence angle, and should decrease with decreasing observational frequency for foam layers whose depth is less than about one fourth of the observational wavelength. Stogryn (1967) made an interesting observation that the brightness temperature of vertically polarized radiation is

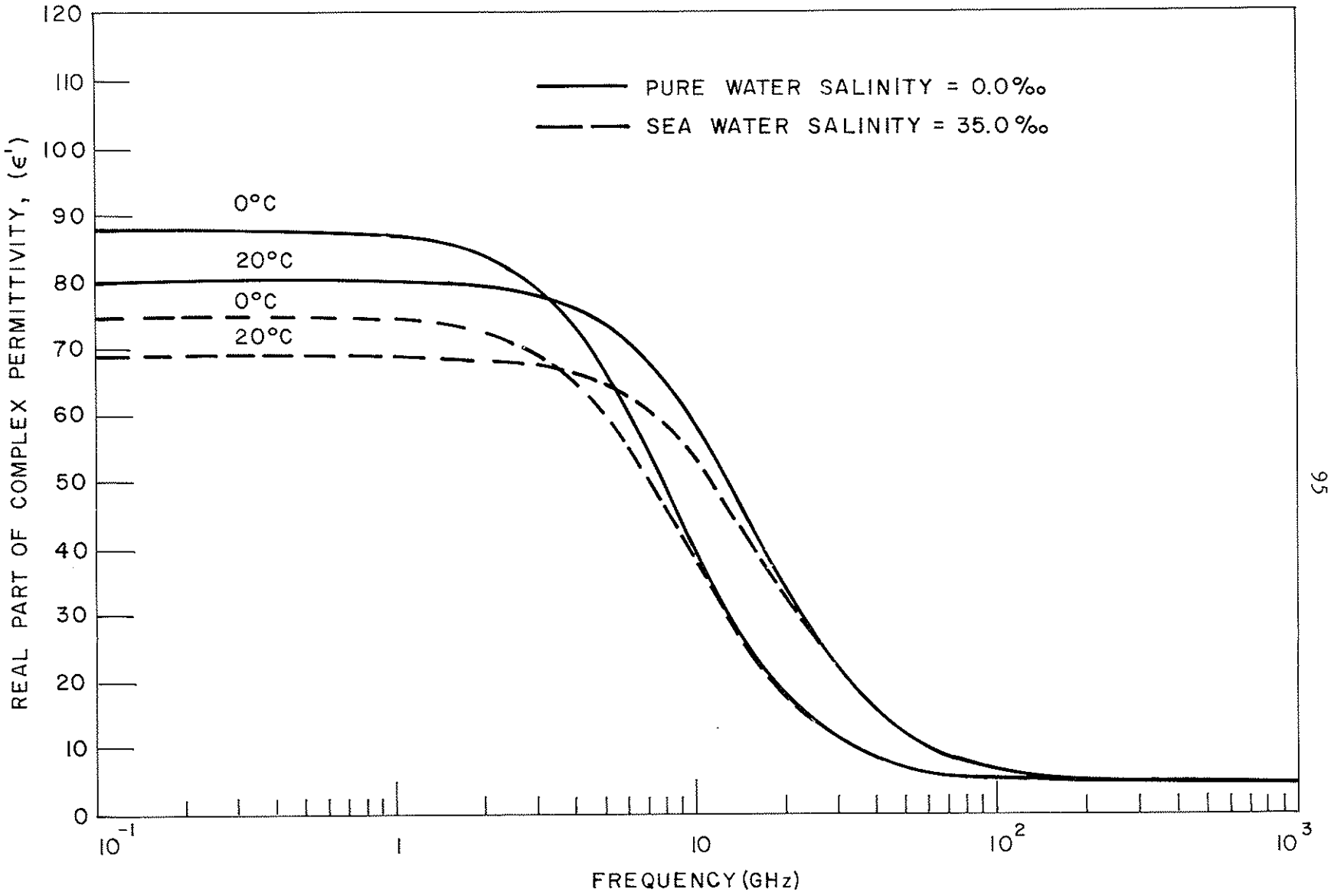

FIGURE A3-2 REAL PART OF COMPLEX PERMITTIVITY. (Hollinger, 1975)

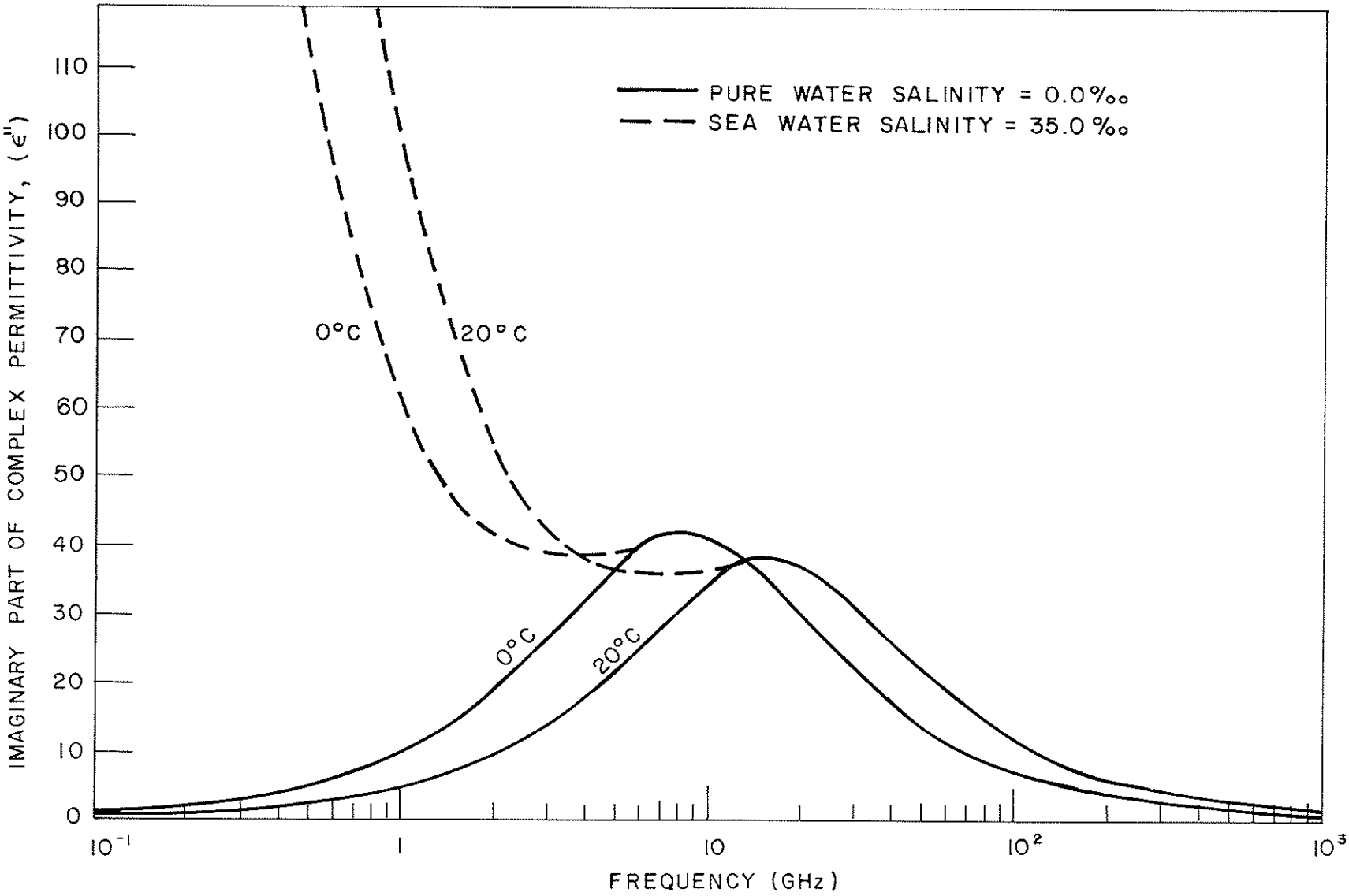

FIGURE A3-3 IMAGINARY PART OF COMPLEX PERMITTIVITY
(Hollinger, 1973)

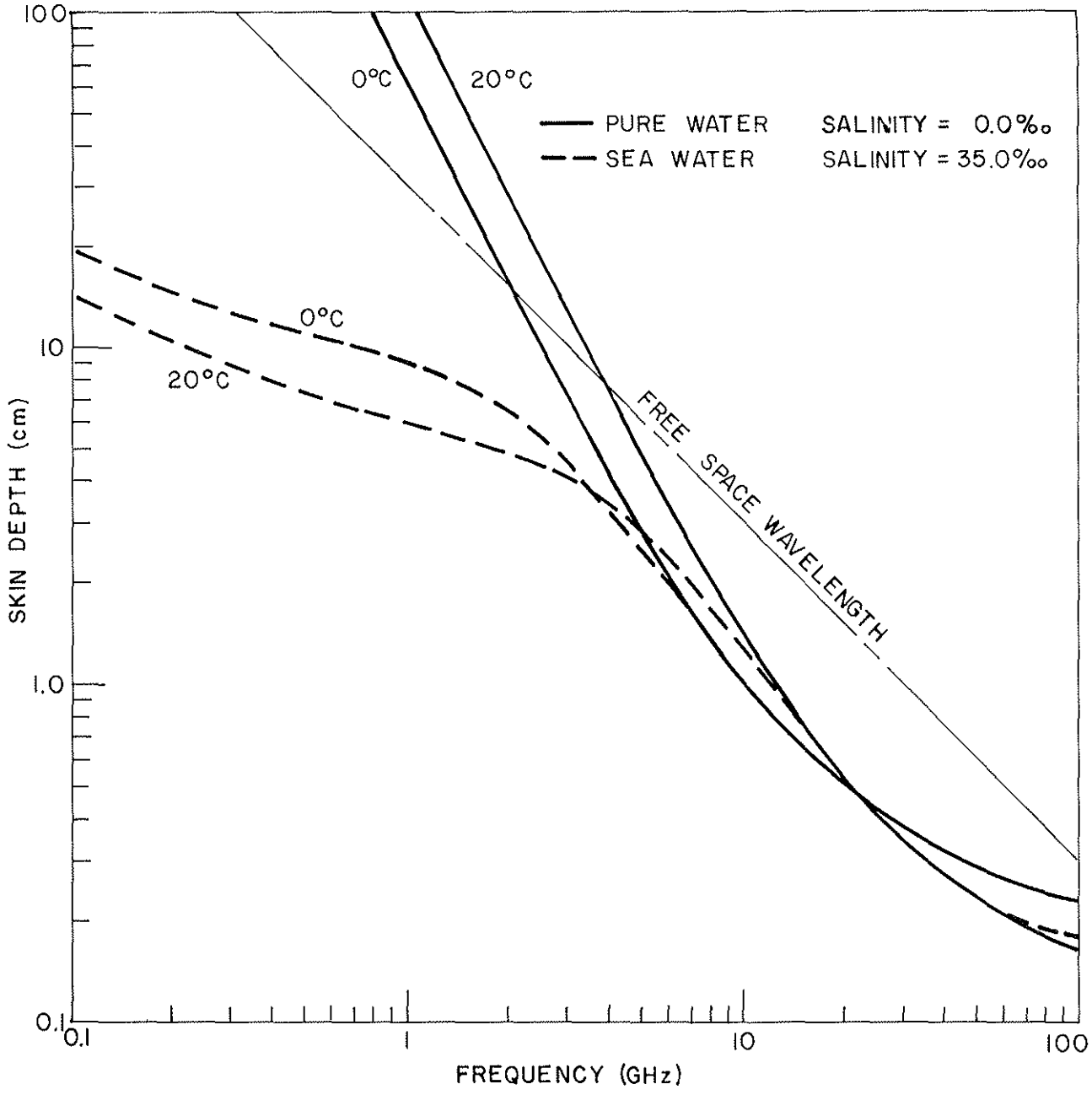

FIGURE A3-4 SKIN DEPTH (Hollinger, 1973)

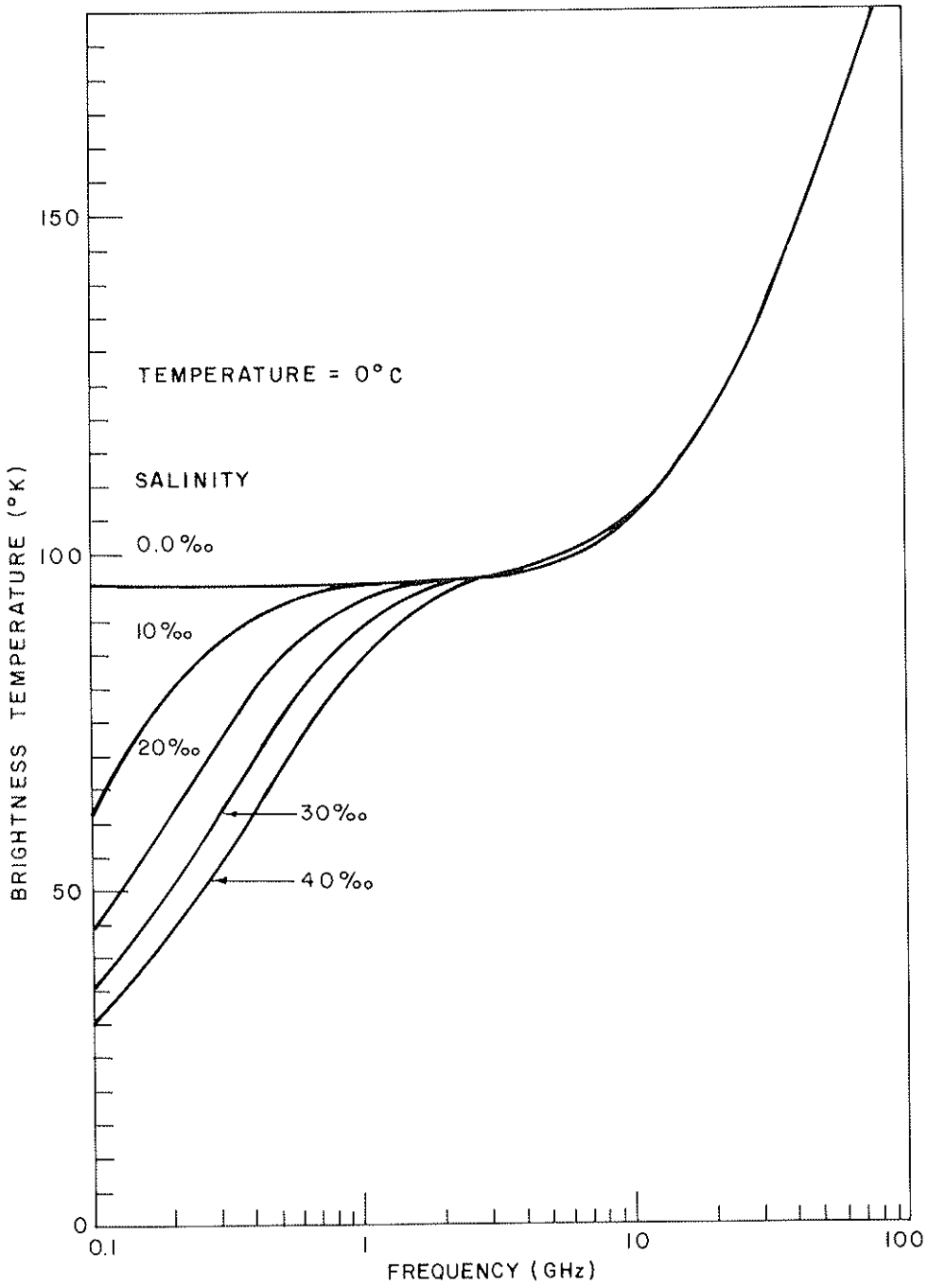

FIGURE A3-5 BRIGHTNESS TEMPERATURE AT NORMAL INCIDENCE (Hollinger, 1973)

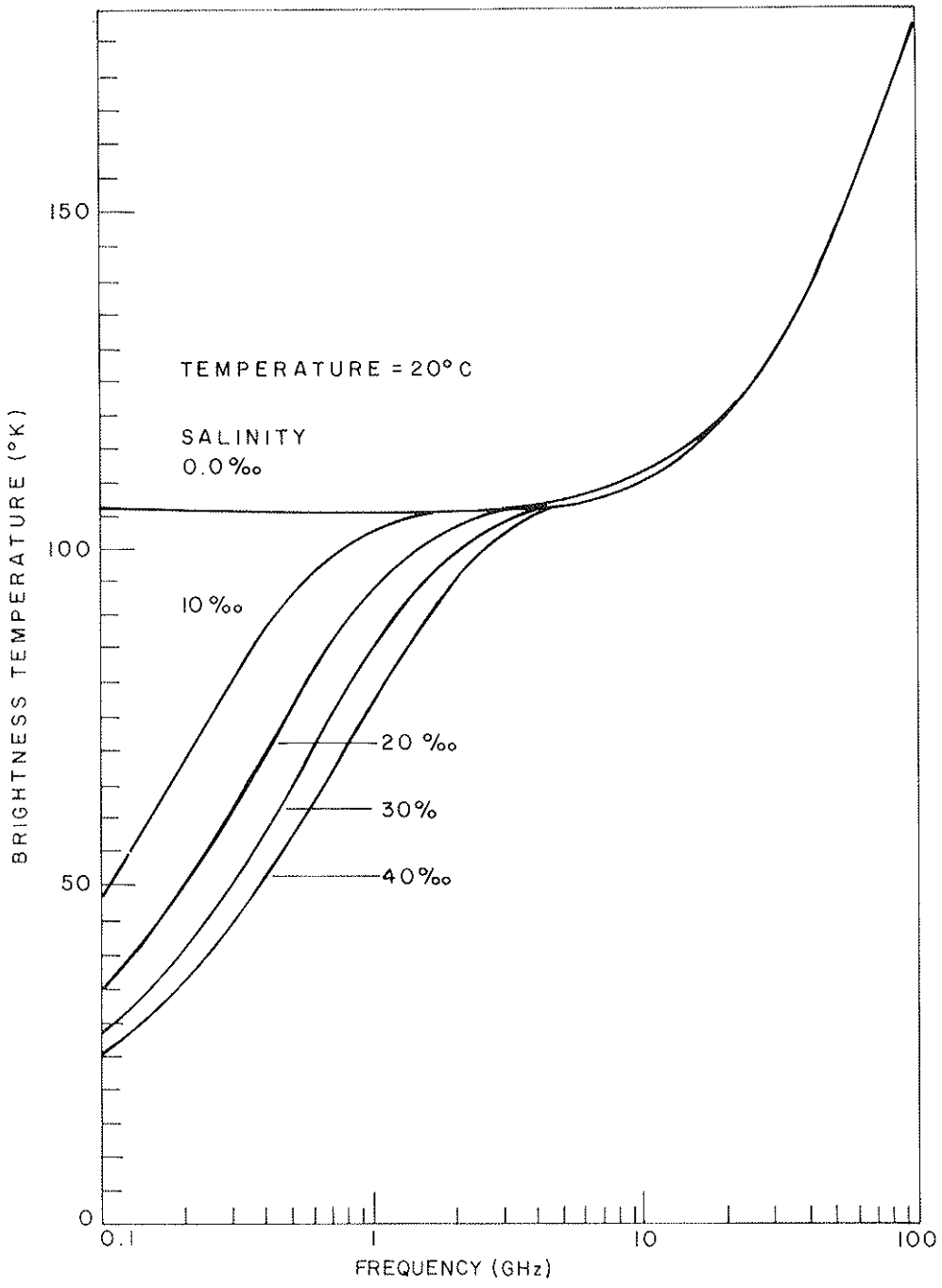

FIGURE A3-6 BRIGHTNESS TEMPERATURE AT NORMAL INCIDENCE (Hollinger, 1973)

much less affected by wind speed and, at an angle of 50^{o} (at 19.4 GHz), is almost independent of the state of the sea. A theory of microwave emission from the ocean surface was also presented by Stogryn (1967).

To ascertain the microwave characteristics of the ocean environment, the Aerojet General Corporation conducted a series of experiments over a number of years. Edgerton et al.(1973) have presented the following summary of the results:

(a) Microwave emission increases with root-mean-square (rms) wave slope.

(b) Horizontally polarized emission increases with wind speed over the range of observation angles from 20 to 70 degrees with a slightly greater increase at larger angles. Measurements of non-breaking waves and swells show a near linear increase in horizontally polarized emission with rms wave slope.

(c) Vertically polarized emission is invariant at viewing angles of 50^{o} to 55^{o}.

(d) Emission associated with the rms wave slope increases with observational frequency.

(e) Emission associated with non-breaking waves and swells is directional (that is, emission in direction of propagation is different from emission perpendicular to direction of propagation).

(f) The emissivity of foam (about 0.8) is about twice that of water and, therefore, microwave emission increases significantly with the presence of foam.

(g) Emission at long wavelengths is more responsible to water temperature changes.

(h) Salinity variations only effect microwave emission at long wavelengths ($\geq$4 cm).

The results of measurements at 1.41, 8.36 and 19.34 GHz reported by Hollinger (1970) were compared with the theory proposed by Stogryn (1967) in Figure A3-7 (excluding atmospheric effects, Edgerton et al, (1973)). Airborne and ground-based measurements (Nordberg et al, 1969 and Williams, 1968) indicate that the presence of surface foam enhances the apparent emissivity of sea water from values near 0.3 to 0.4 to values approaching 1.0 at wavelengths ranging from 0.8 to 25 cm at zero observational angle. Nordberg et al.(1970), from aircraft measurements made at a 1.55 cm wavelength, have reported that brightness temperature in the nadir direction increased almost linearly with wind speed from 7 to 25 m/s at a rate of about 1.2^{o}C per m/s. At 70^{o} from nadir the rate was 1.8^{o}C per m/s. The increase was reported to be directly proportional to the occurrence of "white" water on the sea surface. Essentially no "white" water was present at wind speeds less than 7 m/s and the observed brightness temperatures in the nadir direction were about 120^{o}K. "White" water cover was on the order of 30 percent at wind

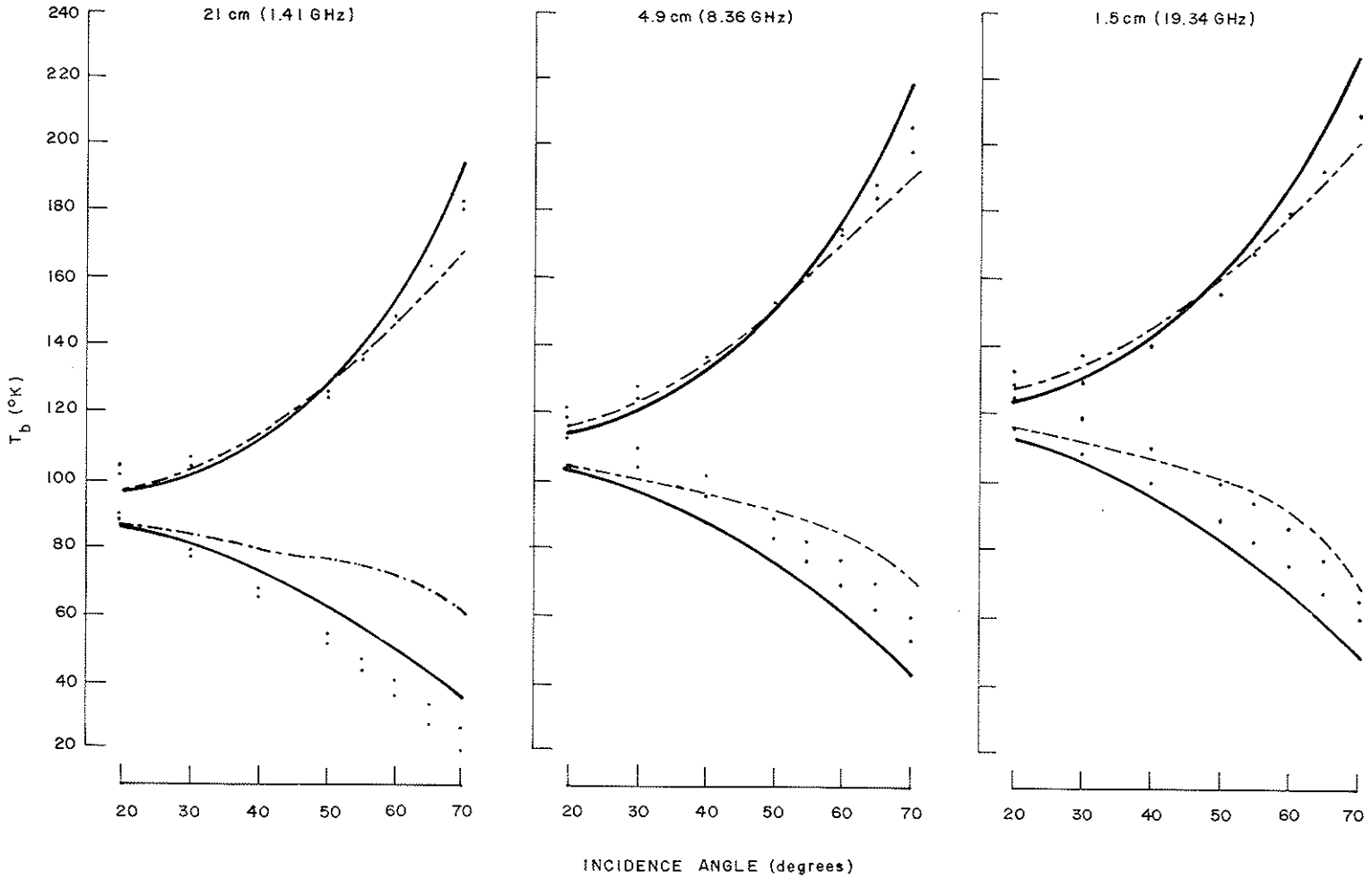

FIGURE A3-7 OCEAN SURFACE BRIGHTNESS TEMPERATURES AT THREE WAVELENGTHS (Hollinger, 1970). DOTS AND CROSSES ARE AVERAGE MEASUREMENTS AT WIND SPEEDS OF 0.5 AND 13.5 m/s; RESPECTIVELY, SOLID AND DOTTED CURVES HAVE BEEN CALCULATED FOR WIND SPEEDS OF 0 AND 15 m/s, RESPECTIVELY, BY MEANS OF STOGRYN'S THEORY. (Stogryn, 1967)(Edgerton et al, 1973).

speeds of 25 m/s and average brightness temperatures at nadir were about 142°K. A maximum brightness temperature of 220°K was observed for foam patches large enough to fill the entire radiometric beam.

The microwave radiometric results obtained from the Bering Sea Expedition (BESEX), conducted jointly by the U.S. and U.S.S.R., were reported by Wilheit and Fowler (1977). It was shown that determination of wind speed at the ocean surface and liquid water content of the cloud may be made from such data. Blume et al.(1977), have reported that measurements with a 2.65 GHz radiometer corresponded well with that calculated from the known sea surface and atmospheric properties over a fairly wide range of surface salinity values (0.2 to 25°/oo). Paris (1972) and Thomann (1973) have shown the possibilities of measuring surface salinities with a 21 cm wavelength radiometer. Hollinger et al (1975) have indicated that the optimum observation frequency for the determination of sea surface temperature lies between about 3 and 6 GHz.

A3.6 Conclusions

Measurements made with the active and passive microwave systems indicate that both the radar scattering coefficient, σ^o, and brightness temperature from the ocean are dependent on surface roughness and increase linearly with wind speed in the region from about 3 to 20 m/s. The vertical-vertical polarization is more sensitive to wind speed for the active systems and horizontal polarization for the passive systems. Both sea surface temperature and salinity can be measured through the passive microwave systems. Radiometers operating between about 3 to 6 GHz with vertical polarization and at an angle of about 53° appear suitable for sea surface temperature measurements. Salinity measurements require passive systems operating at a wavelength of about 2 cm. Radar scatterometers operating in the Ku-band are being used for determination of wind speed and direction over the oceans. Synthetic aperture radars can be used to image ocean surface waves, currents and patterns.

REFERENCES

Apel, J.R., "A Hard Look at Oceans From Space," AIAA 9th Annual Meeting, Washington, D.C., Paper No. 73-11, (January 8-10, 1973).

Bass, F.G.,a dn V.G. Bocharov, "On the Theory of Scattering of Electromagnetic Waves from a Statistical Uneven Surface," Radioteknika i electronika, Vol. 3, pp 251-258, (1958).

Bass, F.G., I.M. Fuks, A.I. Kalmykov, I.E. Ostrovsky, and A.D. Robenberg, "Very High Frequency Radiowave Scattering by a Disturbed Sea Surface," IEEE Transactions on Antennas and Propogation, Vol. AP-16, No. 4, pp 560-568, (September 1968).

Bass, F.G., S.Y. Braude, I.M. Fuks, A.I. Kalmykov, A.V. Megn, I.E. Ostrovsky, and R.D. Rosenberg, "Radiophysical Investigations of Sea Roughness (Radiooceanography) at the Ukrainian Academy of Sciences," IEEE Journal of Oceanic Engineering, Vol. OE-2, vol. 1, pp 43-52, (January 1977).

Barrick, D.E., and W.H. Peake, 1967, "Scattering from Surfaces with Different Roughness Scales: Analysis and Interpretation," Reserach Report, Batelle Memorial Institute, Ohio, (1967).

Beckmann, P., and A. Spizzichino, The Scattering of Electromagnetic Waves from Rough Surfaces, MacMillan Publishers, New York, (1963).

Blume, H.J.C., A.W. Love, M.J. Van Melle, and W.W. Ho, "Radiometric Observations of Sea Temperature at 2.65 GHz over the Chesapeake Bay," IEEE Journal of Oceanic Engineering, vol. OE-2, No. 1, pp 121-128, (January 1977).

Bradley, G.A., "Remote Sensing of Ocean Winds Using a Radar Scatterometer," Ph.D. Thesis, Univeristy of Kansas Center for Research, Inc., (September 1971).

Brown, W.E., Jr., C. Elachi, and T.W. Thompson, "Oceanographic Observations with Imaging Radar," U.R.S.I. Fall Meeting, Boulder, Colorado, (1973).

Brown, W.E., Jr., C. Elachi, and T.W. Thompson, "Radar Imaging of Ocean Surface Pattterns," U.R.S.I. Fall Meeting, Boulder, Colorado, (1974).

Brown, W.E., Jr., C. Elachi, and T.W. Thompson, "Radar Imaging of Ocean Surface Patterns," Journal of Geophysical Research, vol. 81, pp 2657-2667, (1976).

Buch, J.Z., J.W. Crispin, R.G. DeLosh, F.T. Johnson, E.E. Lamphiear, O.L. Tiffany, and B.W. Wentworth, "Sea Clutter Using Oil Slicks, Bendix Aviation Corporation, Ann Arbor, Michigan, ONR contract No. 2349 (00), Report BSR-139, pp 125, (October 1959).

Chanm H.L., and A.K. Fung, "Backscattering from a Two-Scale Rough Surface with Application to Radar Sea Return," NASA Contractor Report CR-2327, (November 1973).

Chia, R.C., "The Theory of Radar Scatter from the Ocean," University of Kansas Center for Research, Inc., technical Report 112-1, (October 1968).

Claassen, J.P. and H.S. Fung, "The Wind Response of Radar Sea Return and its Implication on Wave Spectral Growth," Technical Report 186-5, University of Kansas Center for Research, Inc., (March 1972).

Cox, C., and W. Munk, "Measurements of the Roughness of the Sea Surface from Photographs of the Sun's Glitter," Journal of the Optical Society of America, Vol. 44, pp 838-850, (November 1954a).

Cox, C. and W. Munk, "Sea Surface and Sea Glitter," Journal of Marine Research, Vol. 13, pp 198-227, (1954b).

Crombie, D.D., "Doppler Spectrum of Sea Echo at 13.56 Mc/s," Nature, Vol. 175, pp 681-682, (1977).

Daley, J.C., "An Empirical Sea Clutter Model," NRL Memo Report 2668, (1973).

Daley, J.C. et al, "Radar Sea Return-JOSS2," Final Report, Rep. 7539, Washington, D.C. (1962).

Droppleman, J.D., "The Apparent Microwave Emissivity of Sea Foam," Journal of Geophysical Research, Vol. 75, No. 3, pp 696, (1970).

Edgerton, A.T., F. Ruskey, D. Williams, A. Stogryn, G. Poe, D. Meeks, and O. Russel, "Microwave Emission Characteristics of Natural Materials and the Environment (A Summary of Six Years Research)," Aerojet-General Corporation, Azusa, California, Final Technical Report, 9016R-8, pp 301, (1973).

Elachi, C.' and W.E. Brown, Jr., "Models of Radar Imaging of the Ocean Surface Waves," IEEE Journal of Oceanic Engineering, Vol. OE-2, No. 1, pp 84-95, (January 1977).

Elachi, C., "Wave Patterns Across the North Atlantic on September 28, 1974, from Airborne Radar Imagery," Journal of Geophysical Research, Vol. 81, pp 2655-2656, (1976).

Fung, A.K. and H.L. Chan, "On Backscatter from Two-Scale Rough Surfaces," AGARD Conference Proceesings No. 90 on Propagation Limitations in Remote Sensing, Colorado Springs, (June 1971).

Grant, C.R. and B.S., Yaplee, "Backscattering from Water and Land at Centimeter and Millimeter Wavelengths," Proceedings of the IRE, No. 7, pp 972-982, (1957).

Grant, E., T. Buchanan, and H. Cook, "Dielectric Behaviour of Water at Microwave Frequencies," Journal of Chemistry and Physics, vol. 26, No. 156, (1957).

Grant, E.., and R. Shack, "Complex Permittivity Measurements at 8.6 mm Wavelengths over the Temperature Range 1-60^{o}C," British Journal of applied Physics, Vol. 18, pp 1807, (1967).

Grantham, W.L., E.M. Bracalente, W.L. Jones, J.H. Schrader, L.C. Schroeder, and J.L. Mitchell, "An Operational Satellite Scatterometer for Wind Vector Measurements over the Ocean," NASA TMX-72672, pp 169, (March 1975).

Grantham, W.L., E.M. Bracalente, W.L. Jones, and J.W. Johnson, "The SEASAT-A Satellite Scatterometer," IEEE Journal of Oceanic Engineering, Vol. OE-2, No. 2, pp 200-206, (April 1977).

Guinard, N.W., "The Remote Sensing of the Sea and Sea ice," Proceedings of the Sixth International Symposium on Remote Sensing of Environment, University of Michigan, Ann Arbor, Michigan, Vol. 11, pp 737-754, (October 1969).

Guinard, N.W., and J.C. Daley, "An Experimental Study of Sea Clutter Model," IEEE Proceedings, Vol. 58,, No. 4, pp 543-550, (April 1970).

Guinard, N.W., J.T. Ransone, Jr., and J.C. Daley, "Variation of the NRCS of the Sea with Increasing Roughness," Journal of Geophysical Research, Vol. 76, pp 1525-1538, (February 1971).

Ho, W., and W.F. Hall, "Measurements of the Dielectric Properties of Sea Water and NaCl solutions at 2.65 GHz," Journal of Geophysical Research, Vol. 78, pp 6301-6315, (1973).

Ho, W., and A.W. Love, and M.J. Van Melle, "Measurements of Dielectric Porperties of Sea Water at 1.43 GHz," NASA Contractor Report CR-2458, (December 1974).

Hollinger, J., "Passive Microwave Measurements of the Sea Surface," Journal of Geophysical Research, Vol. 75, No. 5209, (1970).

Hollinger, J., "Passive Microwave Measurements of Sea Surface Roughness," IEEE Transactions on Geoscience Electronics, Vol. GE-9, No. 3, pp 165-169, (July 1971a).

Hollinger, J.P., "Remote Passive Microwave Sensing of the Ocean Surface," Proceedings of the Seventh International symposium on Remote Sensing of Environment, University of Michigan, Ann Arbor, Vol. III, pp 1807-1817, (May 1971b).

Hollinger, J.P. "Microwave Properties of a Calm Sea,", Naval Research Laboratory, Washington, D.C., Report No. 7110-2, pp 69, (August 1973).

Hollinger, J.P., R.M. Lerner, and M.M. Wisler, "An Investigation of the Remote Determination of Sea Surface Temperature Using Microwave Radiometry," Naval research Laboratory, Washington, D.C., NRL Memorandum Report 3159, pp 54, (November 1975).

Jackson, F.C., "A High Frequency Correction to the Kirchoff Approximation, with Application to Rough Surface EM Wave Scattering," GSL Report TR-71-8, Department of Meteorology and Oceanography, New York University, (1971).

Jones, W.L., L.R. Shultz, and N.D. Akey, "AAFE-RADSCAT Observations of Wind-Driven Seas," USNC/URSI Fall Meeting, Williamsburg, Virginia, (1972).

Jones, W.L., L.C. Schroeder, and J.L. Mitchell, "Aircraft Measurements of the Microwave Scattering Signature of the Ocean," IEEE Journal of Oceanic Engineering, Vol. OE-2, No. 1, pp 52-61, (January 1977).

Katzin, "On the MEchanism of Radar Sea Clutter," Proceedings of the IRE, Vol. 45, No. 1, pp 44-54, (1957).

Klein, L.A., and C.T. Swift, "An Improved Model for the Dielectric Constant of Sea Water at Microwave Frequencies," IEEEE Journal of Oceanic Engineering, Vol. OE-2, No. 1, pp 104-111, (January 1977).

Krishen, K., "Correlation of Radar Backscattering Cross Sections with Ocean Wave Height and Wind Velocity," Lockheed Electronics Company, TR No. 649D.21.025, Houston, Texas, (March 1970).

Krishen, K., "Correlation of Radar Backscattering Cross Sections with Ocean Wave heights and Wind Velocity," Journal of Geophysical Research, pp 6528-6539, (1971).

Krishen, K., "Contribution to Ocean Panel Including Reports on Some Sea Return Experiments, Ocean Surface Wind Speed Sensing and Scatterometers," Technical Report. LEC-3896, Lockheed Electronics Co., Inc., (1974).

Lane, J., and J. Saxton, "Dielectric Dispersion in Pure solar Liquids at Very High Frequencies. III. The Effect of Electrolytes in solution," Proceedings of the Royal Society, Vol. A213, pp 531-545, (1952).

Larson, T.R., and J.W. Wright, "Imaging Ocean Current Gadients with Synthetic Aperture Radar," URSI Fall Meeting, Boulder, Colorado, (1974).

Long, M.W., Radar Reflectivity of Land and Sea, Lexington Books, D.C. Heath and Co., Mass., (1975).

MacDonald, F.C. "The Correlation of Radar Sea Clutter on Vertical and Horizontal Polarization with Wave Height and Slope," IRE Convention Record, Pt. 1, pp 29-32, (1956).

Malmberg, C., and A. Margott, "Dielectric Constant of Water from 0^{o} to 100^{o}C," J. Res. Nat. Bur. Standards, Vol. 56, No. 1, (1956).

Matthews, R.E., Editor, "Active Microwave Workshop Report," NASA SP-376, (1974).

Moore, K., and W.J. Pierson, J., "World Wide Oceanic Wind and Wave Prediction Using a Satellite Radar-Rariometer," Journal of Hydronautics, Vol. 5, No. 2, pp 52-60, (1971).

Moskowitz, L.J., "The Feasibility of Ocean Current Mapping via Synthetic Aperture Radar Methods," Proceedings of the Fall Convention American Society of Photogrammetry, pp 76-77, (October 1973).

Newton, W., and W.J. Rouse, "Experimental Measurements of 2.25 cm Backscatter from Sea Surfaces," IEEE Transactions on Geoscience Electronics, GE-10, No. 1, pp 2-7, (1972).

Nordberg, W., J. Conaway, and P. Thaddeus, "Microwave Observations of Sea State from Aircraft," Oceanographic Journal of Royal Meteorological Society , 95, pp 408, (1969).

Nordberg, W., J. Conaway, D.B. Ross, and T. Wilheit, "Measurements of Microwave Emission from a Foam Covered Wind Driven Sea," X-650-70-384, Preprint, Goddard Space Flight Center, Greenbelt, Maryland, (October 1970).

Paris, J.F., "Salinity Surveys Using an Airborne Microwave Radiometer, Proceedings of the Eight International Symposium on Remote Sensing of Environment," University of Michigan, Ann Arbor, Michigan, vol. 1, pp 665-676, (1972).

Pierson, W.J., Jr., F.C. Jackson, R.A. Stacy, and E. Mehr, "Research on the Problem of Radar Return from a Wind Roughened Sea," Principal Investigators Review, Advanced Applications Flight Experiments, NASA Langley Research Center, pp 83-114, (October 1971).

Pierson, W.J., Jr., and R.A. Stacy, "The Elevation, Slope and Curvature Spectra of a Wind Roughened Sea," NASA CR-2247, (November 1973).

Pronk, A.C., "Remote Sensing of Oil Pollution at the Sea Surface II, Damping of Water Waves by an Oil Layer as a Possible Indicator for SAR Observations," Netherlands Interdepartmental Working Community for the Application of Remote Sensing Techniques (NIWARS), DELFT, Netherlands, NIWARS Publication No. 22, pp 12, (July 1975).

Ross, D.B., V.J. Cardone, and J.W. Conaway, Jr., "Laser and Microwave Observations of Sea Surface Condition for Fetch-Limited 17 to 24 m/sec Winds," IEEE Transactions of Geoscience Electronics, Vol. GE-8, pp 326-336, (October 1970).

Saxton, J.A., and J.A. Lane, "Electrical Properties of Sea Water, Reflection and Attenuation Characteristics at V.H.F., Wireless Engineer, pp 269-275, (October 1952).

Schooley, A.H., "Upwind-Downwind Ratio of Radar Return Calculated from Facet Size Statistics of a Wind-Disturbed Water Surface," Proceedings of the IRE, Vol. 50, No. 4, pp 456-461, (1962).

Semyonov, B., "Approximate Computation of Scattering of Electromagnetic Waves by Rough Surface Contours," Radio Engineering and Electronic Physics, Vol. 11, pp 1179-1187, (1966a).

Semynov, B., "An Approximate Calculation of Scattering of Electromagnetic Waves from a Slightly Rough Surface," Radiotekika i Electronika (USSR) 11, (English Translation), (1966b).

Shemdin, O.H., R.J. Lai, A. Reece, and G. Tober, "Laboratory Investigators of Whitecaps, Spray and Capillary Waves," Technical Report No. 11, Coastal and Oceanographic Engineering Laboratory, Florida Univerisity, (1972).

Shuchman, R.A., P.L. Jackson, and G.B. Feldkamp, "Problems of Imaging Ocean Waves with Synthetic Aperture Radar", Environmental Research Institute of Michigan, (ERIM), Ann Arbor, Michigan, Report No. 124300-1-T, pp 111, (August 1977).

Sittrop, H., "X- and Ku-band Radar Backscatter Characteristics of Sea Clutter, Proceedings of the URSI Commission II Specialists Meeting on Microwave Scattering and Emission from Earth, Berne, Switzerland, pp 25-37, (September 1974).

Skolnik, M., "A Review of Radar Sea Echo," Naval Research Laboratory, Washington, D.C., NRL Report 2025, (July 1969).

Skolnik, M.I., ed., Sea Echo, Radar Handbook, Chapter 25, McGraw-Hill Book Co., (1970).

Stogryn, A., "The Apparent Temperature of the Sea at Microwave Frequencies, IEEE Transactions on Antennas and propagation, AP-15, 278, (1967).

Stogryn, A., "Equations for Calculating the Dielectric Constant of Saline Water," IEEE Transactions on Microwave Theory Technology, Vol. MTT-19, No.8, pp 733-736, (1971).

Sutherland, A.J., "Spectral Measurements and Growth Rates of Wind Generated Water-Waves," Standford University, Dept. of Civil Engineering, Technical Report 84, (August 1967).

Swift, C.T., and W.L. Jones, Jr., "Satellite Radar Scatterometry," IEEE International Convention and Exhibition pp 34-41 to 34-48, (1974).

Thomann, G.C., "Remote Measurement of Salinity in an Estuarine Environment," Proceedings of the Conference on Earth Resources Observation and Information Analysis Systems, University of Tennessee, Tullahoma, Remote Sensing of Earth Resources, Vol. III, pp 327-344, (March 1973).

Valenzuela, G.R., "Depolarization of EM Waves by Slight Rough Surfaces," IEEE Transaction on Antennas and Propagation, Vol. AP-15, No. 4, pp 552-557, (1967).

Valenzuela, G.R., M.B. Laing, and J.C. Daley, "Ocean Spectra for the High Frequency Waves as Determined from Airborne Radar Measurements," Journal of Marine Research, Vol. 29, No. 2, (1971).

Valenzuela, G.R., "Backscattering of Electromagnetic Waves from a Tilted Slightly Rough Surface," Radio Science, Vol. 3, No. 11, pp 1057-1066, (November 1968).

Valenzuela, G.R., and M.B. Laing, "On the Satistics of Sea Clutter," Naval Research Laboratory, Washington, D.C., NRL Report 7349, pp 38, (December 1971).

Wilheit, T.T., Jr., and M.G. Fowler, "Microwave Radiometric Determination of Wind Speed at the Surface of the Ocean During BESEX," IEEE Journal of Oceanic Engineering, Vol. OE-2, No. 1, pp 111-120, (January 1977).

Williams, G.F., Jr., "Microwave Radiometry of the Ocean and the Possibility of Marine Wind Velocity Determination from Satellite Observations," Journal of Geophysical Research, 74, 18, pp 4591-4594, (1968).

Worsfold, R.W., D. Strong, and E. Wedler, "Project SAR '77," Proceedings of Fourth International Conference on Port and Ocean Engineering Under Arctic Conditions, vol. II, Memorial University of Newfoundland, pp 1051-1063, (September 1977).

Wright, J.W., "Backscattering from Capillary Waves with Application to Sea Clutter, IEEE Transactions on Antennas and Propagation, Vol. AP-14, No. 6, pp 749-754, (November 1977).

Wright, J.W., "A New Model for Sea Clutter," IEEE Transactions on Antennas and Propagation, Vol. AP-16, No. 2, pp 217-223, (March 1968).

APPENDIX 4

APPENDIX 4 - MICROWAVE BACKSCATTER AND EMISSION FROM SEA ICE

A4.1 INTRODUCTION

A number of studies and experiments in the past have been especially directed towards determining backscatter and emission characteristics of sea ice in the microwave region of the electromagnetic spectrum. As a result of such efforts, the practicability of utilizing active and passive microwave sensors to map sea ice has been demonstrated. Studies to date have proven the capability and utility of radar and radiometer systems to measure and discriminate between sea ice types, but these studies have helped little in the understanding of the physical phenomenon of emission and radar return from sea ice. Past studies have also lacked in producing optimum design criteria for future systems and in establishing techniques for data processing and analysis. These drawbacks in most of the past research efforts have been largely due to the inability to collect complete "ground truth" information along with the experimental data. Because of this, it has not been possible to properly correlate experimental measurements with sea ice parameters to a high degree of confidence. There is also a lack of even qualitative experimental data available corresponding to different frequencies, polarizations and angles.

The inability to collect proper "ground truth" information can largely be attributed to the nature and variability of sea ice, inaccessibility of the areas, and the prevailing harsh climates. Because of the variability of sea ice conditions from one place to another and the use of uncalibrated systems, especially side-looking airborne radar (SLAR), it becomes difficult to compare the results of one experiment with another. Two attempts at conducting experiments under partially controlled conditions with a special emphasis on obtaining corroborative "ground truth" information are known. One experiment, conducted by the Aerojet General Company on the AIDJEX test site involved the use of microwave radiometers, the results of which were presented by Meeks et al. (1974a). The other one, conducted by the University of Kansas, involved the utilization of a radar scatterometer operating at numerous microwave frequencies, receive-transmit polarizations, and angles of incidence. The data from this are still being analyzed (Onstott et al, 1977).

The purpose of this appendix is to present a review of the past measurements of microwave emission and scattering from sea ice and to document significant results. A section discussing the way radar and radiometric measurements or signatures might be

influenced or affected by the electrical and physical properties of sea ice is included. The possible effects of snow cover on the ability of microwave systems to distinguish or measure sea ice characteristics, are mentioned. The problem of detecting icebergs through the use of these systems is addressed and the available results are summarized.

A4.2 Radar Measurement of Sea Ice

A Side-Looking Airborne Radar was first used to map sea ice in the early 1960's when the U.S. Army Cold Regions Research and Engineering Laboratory (CRREL) conducted experiments over the Arctic pack ice utilizing the existing real aperture AN/APQ-56 radar system operating at a 8.6 mm wavelength. It was shown by Anderson (1966) through the analysis of the obtained images that major sea ice types could be identified on the radar imagery. Anderson showed that the sea ice imagery is interpretable to the extent that winter ice (only one season old) can be differentiated from the thicker, older, polar ice. The concentration and distribution of sea ice can also be determined. The rough-surfaced polar ice, generally from 2.5 to 4 metres thick, with pressured areas being much thicker, gave a light tone on the images. The relatively dark-tones areas consisted of smooth refrozen leads and polynas with younger, thinner ice. Still darker tones belonged to open water. This experiment was conducted in winter and no corroborative "ground truth" information was obtained except aerial photographs.

In a study conducted by Bradie (1967), it was pointed out that one hindrance to the interpretation of ice features on radar imagery is the lack of great tonal variance in the return from among open water, young ice, grease ice and slush ice.

During September 1969 the U.S. Coast Guard (USCG), in conjunction with the MANHATTEN tanker test, conducted ice-mapping experiments in the Northwest Passage using a modified Philco-ford AN/DPD-2 SLAR, operating in the Ku-band region (16.5 GHz frequency). As shown by Johnson and Farmer (1971a), the results of this experiment indicated that SLAR can readily be used to detect ice concentration, floe size and number, and water openings.

It is also possible to identify, through careful image interpretation, ice age, ice drift, surface topography, fractures, and pressure characteristics. Young ice gives an even dark tone and may have bright straight lines indicating ridging. A dark-grey to black smooth tone is given by first-year ice, and ridging is indicated by light straight lines. Second year ice gives an even grey-tone and may have ridging. These ridges are more jagged and also higher than in first-year ice. An even tone denotes relatively smooth topography. Multi-year ice gives mottled tones of grey probably caused by high

weathered ridges and interconnected melt pools. Old multi-year drainage channels can also be traced sometimes. The parameters which can be most easily determined on the radar imagery are ice concentration and floe size. The most difficult characteristic of the ice to determine, other than its actual thickness, is probably its categorical age. Another important feature that can be interpreted is whether ice is or has been under pressure. It is also possible to identify topographic features such as pressure ridges, hummocks, and cracks.

It is pointed out by Johnson and Farmer (1971a) that for many purposes SLAR provided observations superior to information obtained by a visual ice observer. The same experimental data was used to determine the drift of sea ice. The results presented by Johnson and Farmer (1971b) reveal that single ice floes, as well as general ice masses, could be tracked to an accuracy of nearly one nautical mile. In the study conducted by Biache et al.(1971) of the SLAR imagery obtained in the MANHATTEN experiment, it is pointed out that major ice types, cracks and leads can be identified.

Ketchum and Tooma (1973) presented results obtained from the radar experiment conducted by the U.S. Naval Oceanographic Office during April, 1968. This experiment, conducted over the sea ice fields north of Alaska, utilized the four-frequency synthetic aperture radar (SAR) system of the Naval Research Laboratory. The results presented indicate that the shorter wavelength X-band radar appears to have the greatest potential for sea ice study when more definitive information such as mapping, distributions of stages of ice development, and fracture pattern analysis is required. The X-band radar imagery can be used to discriminate old (second-year) ice from the young ice, the old ice giving a higher return or backscatter. Yound ice (first-year ice and younger) is smooth and could not be discriminated from open water in this experiment. Pressure-ridge patterns could sometimes be identified when they were present on a low-backscatter background. There were no notable differences between horizontally and vertically polarized X-band imagery.

The potential value of L-band radar is found to be in mapping the areal distribution of surface topography. Various ice types do not give discriminatory grey-tones at this wavelength, whereas topographic features such as ridges and hummocks can be discriminated. The only targets giving significant backscatter are the new pressure ridges and other recently deformed or broken features. Returns from the new pressure ice fromations were much more pronounced on the horizontally polarized imagery. Only the most prominent features, such as large floes and fractures, could be identified on the

P-band (400 MHz) radar imagery. It was pointed out that for motion studies in which re-identification of specific features is necessary, the X-band or, preferably K-band radars, would be the best choice.

The SLAR data acquired by the USCG off the Baffin Bay and Beaufort Sea areas in February and March of 1971 utilizing a modified DPD-2 (16.5 GHz) System, were analyzed by the Raytheon Company (USCG, 1970, 1972a). Major ice types, such as new ice, young ice, first-year ice, and multi-year ice, could be identified on a radar image. It was not possible to make a finer delineation of the categories. SLAR imagery did not permit the determination of surface configurations and it was much easier to delineate the edge of a floe on the SLAR imagery than on the photo. The effects of a snow cover on sea ice could not be determined. Sea ice images did not exhibit any masking because of snow cover except for the return from ridges. The identification of the ice age could be accomplished whether covered by thick or thin snow cover.

The same data were also analyzed by the Photographic Interpretation Corporation for the USCG (1972b). In their report, an attempt was made to determine winter sea ice parameters and to compare winter sea ice pattern "keys" with the summer pattern "keys". It was pointed out that interpreters must not rely entirely on radar keys for their work but should properly assess all of the imagery parameters such as tone, textures, spatial relationships, imagery limitations, ice environment and season, and ice stress patterns. By doing this a very detailed description of sea ice can result and the predictions about the ice can be made with more reliability. Multi-year ice can be separated from othe ice types more rapidly on the radar image than through the use of aerial photos, and stress zones can also be quickly delineated. Snow cover did not present any detrimental masking effect of sea ice conditions on the Ku-band radar imagery.

Glushkov and Komarov (1971) and Loshchilov and Voyevodin (1972) demonstrated the use of SLAR imagery (wavelength of 20 mm) obtained from the TOROS system in determining the ice conditions and ice drift. The TOROS experiments (the word "TOROS" is Russian for "ice ridge") were started in 1968 and have been carried out extensively since that time. It is believed that TOROS is being used operationally for mapping ice to permit optimal ship routing for convoys along the USSR's northern sea route.

To evaluate the capabilities of a SLAR System as an ice reconnaissance tool, as SLAR test project was organized and carried out in April, 1972 by the Canadian Department of National Defence and the Atmospheric Motorola AN/APS-94D SLAR unit

operating at a wavelength of 3.2 cm, were presented in a report by Hengeveld (1972). The results indicate that it is generally possible to identify open water by low radar returns and uneven boundaries with surrounding ice that shows good contrast in tone. It was difficult to distinguish new ice from open water because the surface was generally smooth and the profile of any rafting present was low. Variations in returns from large floes was apparent in the large scale imagery. It was possible to determine floe size and concentration and to distinguish first-year ice, fast ice and multi-year ice. Floes showing good radar returns could be classed as rough first year ice. It is noted that the AN/APS-94D has an along-track resolution of 7.5 m/km and a swath width to one side of 40 km. As a result, the resolution is crude at the far range, and the incidence angle is quite near grazing over much of the swath.

The SLAR imagery of sea ice in the Nares Strait and the Arctic ocean was analyzed by Dunbar (1975). Dunbar and Weeks (1975) have presented results of radar interpretation of young ice forms in the Gulf of St. Lawrence. It was pointed out by Gray et al.(1977b) that the appearance and usefulness of radar imagery from a particular sea ice scene depends on the type of radar used. The example given is the study of sea ice in the Nares Strait between Greenland and Ellesmere Island by Anderson (1966) and, subsequently, by Dunbar (1975). The imagery analyzed by Anderson was obtained with the APQ-56 (0.8 cm, high altitude) system and showed clearly the old ice floes as bright regions in comparison to the first-year ice, some of which appeared to be quite rough in the accompanying photographs. Dunbar analyzed imagery obtained with the APS-94D (3 cm, low altitude) system, which appeared to be quite different and emphasized ridging, ice surface relief, and roughness. It was concluded by Dunbar that the differences in the imagery were due primarily to the use of different radar parameters rather than to significantly different ice morphology.

No systematic studies for relating radar return or backscatter to sea ice were undertaken until 1967 when an experiment was conducted in the Arctic ocean with the objective of verifying the ability of a 2.25 cm wavelength radar scatterometer to identify sea ice types. An analysis of the scatterometer data carried out by Rouse (1969) showed that a 2.25 cm wavelength scatterometer can be used to discriminate ice types. It was seen that multi-year ice gives a higher return than the first-year ice, and open water can be distinguished easily by its high return at near vertical incidence. An attempt was made to estimate the surface roughness for each type by comparing the experimental results with the theoretical results based on Kirchoff's tangent plane method. The experimental

data was higher for multi-year ice and pressure ridges than for first-year ice. The experimental data was limited to a single frequency (13.3 GHz) and vertical polarization; no surface truth information except aerial photographs was available.

Another experiment, designated NASA Mission 126, was carried out in the vicinity of Pt. Barrow, Alaska in April, 1970. Large amounts of data were gathered by this mission so that a systematic study of radar return from sea ice could be undertaken. This study was conducted by Parashar (1974a) in which the ability of radar to discriminate sea ice types and their thickness was presented. Radar backscatter measurements at 400 MHz, (HH, VV, VH, and HV polarizations) and 13.3 GHz (VV polarization) were analyzed in detail. The scatterometer data were separated into seven categories of sea ice according to age and thickness as interpreted from low altitude stereo aerial photographs. It was found that there is a reversal in the character of the radar return from sea ice less than 18 cm thick at the two frequencies. Multi-year ice (sea ice greater than 180 cm thick) and open water gave the strongest returns at 400 MHz. Open water could be differentiated at both frequencies. Although 400 MHz, was not found to be a satisfactory for ice identification as 13.3 GHz, combining a 13.3 GHz and a 400 MHz system definitely eliminates the ambiguity regarding very thin ice.

Four-polarization 16.5 GHz radar imagery was also analyzed. The results show that open water and three categories of sea ice can be identified on the images. The results of the imagery analysis are consistent with the radar scatterometer results. There is some indication that cross-polarized return may be better in discriminating sea ice type and thus thickness, but the quality of the images was not sufficent to guarantee the validity of this conclusion. The results obtained from the analysis of the Mission 126 data were summarized by Parashar et al.(1974b). Automatic classification techniques were applied to the scatterometer data. Using the four categories (as in the SLAR analysis), 85 percent agreement could be achieved between the radar and stereo-photo interpretations (Parashal et al, 1977a).

An attempt was also made by Parashar et al.(1978) to formulate a theory for the polarized backscatter cross-section, σ^{o}, for sea ice by taking into account the vertical and horizontal distribution of the amount of brine entrapped, temperature, and surface roughness. The computed results from the theory were shown to be in general agreement with the experimental results.

The use of a scatterometer for discriminating sea ice types was further verified by Gray et al.(1977a). Multi-polarized scatterometer measurements of sea ice at

13.3 GHz obtained during the winter and spring of 1975-76 from a number of flight lines off the east coast of Canada were analyzed. The sea ice regions studied included shorefast ice with varying degrees of snow cover and surface roughness and several varieties of floating sea ice with different thicknesses. The scattering coefficient data shows that the contrasts between different sea ice regions were often a few dB greater for HV returns than for HH returns, substantiating earlier results to some extent.

In the results presented by Gray et al.(1977b) it was observed that there existed a strong correlation between the magnitude of the scattering coefficient and major ice types, on the basis of scatterometer data obtained from both the AIDJEX and Beaufort Sea test sites. In particular, old ice gave significantly higher returns than first-year and young ice forms. The ability of cross-polarized signals in providing more grey-scale information and contrast than the equivalent like-polarized channel was again emphasized.

The requirements for and needs in the study of sea ice were presented by Campbell et al.(1975). The results from remote sensing experiments conducted over the AIDJEX test site were included. It was pointed out that the advantage of active and passive microwave sensors lies in the fact that as long as the snow is dry, it is transparent to microwave radiation. The X-band SLAR imagery obtained from a joint Swedish-Finnish experiment conducted in the Bay of Bothnia during March, 1975 has been analyzed by Morra and de Loor (1976) and Parashar (1976b). The results show that the grey-tone rendition on the imagery was not good enough to identify and classify very many ice types and features. The SLAR was operated at near grazing angles (incident angle $>80^{o}$) at which only returns from pressure ridges, ice edges, and rough ice are evident.

A review of the application of radar techniques to the study of ice and snow was presented by Page and Ramseier (1975). It was observed that radar images tend not to show reflections from snow surfaces, showing instead the stronger reflections from the surface underneath the snow. However, the ability to penetrate snow cover depends on the temperature and type of snow, its density and frequency of observation. Some masking effects can be possible in the case of old, perennial snow or recrystallized snow. It has been observed by Waite and MacDonald (1971) that this type of snow over land is sometimes visible in radar imagery presumably due to volume scattering from the inhomogeneities existing in the old snow. The dual polarized imagery obtained with a Westinghouse 35 GHz system, presented by Page and Ramseier (1975) illustrates the substantial differences in image tone which can be obtained between HH and HV system

modes. The structure of the newer grey ice is more visible on the HH image, whereas, the cross-polarized image exhibits of younger ice, often not visible with X-band or longer wavelength systems, was clearly visible with the shorter wavelength system. The state of the art in the radar measurement of sea ice, including specifications of parameters for ice mapping radar, was presented by Parashar (1975).

Four channel synthetic aperture radar (SAR) imagery of sea ice was obtained by C-CORE during February and March, 1977 off the east coast of Canada under Project SAR '77 (Worsfold et al, 1977). The SAR belonging to Environmental Research Institute of Michigan (ERIM), was flown in conjunction with a surface verification program carried out on the shorefast ice. The imagery obtained was X-(3.2 cm) and L-(24 cm) band with like (horizontal transmit - horizontal receive) and cross (horizontal transmit - vertical receive) polarization. The ice is the imaged areas consisted of various varieties of first-year ice. The preliminary analysis (Wedler et al, 1977) showed that, in general, shorefast ice gives higher returns than the other types. The X-band radar images are sharper than L-band images. The effects in each channel due to the system preformance and due to the nature of radar return are yet to be separated.

It was observed by Dunbar (1975) that icebergs show up well on the APS-94D imagery provided they are prominent enough and appear against a sufficiently uncluttered background. It was pointed out by Parashar (1976a) that the main problem in the detection of icebergs is that they sometimes give the same return as that given by ships. The icebergs can be differentiated from ships, however, depending on certain clues such as the presence and shape of the wake, edge sharpness, size and shape of the target, uneveness of tone, and the presence of a shadow.

A4.3 Summary of Radar Backscatter Results from Sea Ice

A review of the material presented above shows that radar is indeed a valuable tool in the measurement of sea ice. Past research efforts have clearly demonstrated the ability and utility of radar to map the changing nature of sea ice, however, there exists a lack of information in terms of understanding the nature of radar return from sea ice. The characteristics of radar return as a function of frequency, polarization, angle, and resolution still need to be established. The variations in radar backscatter with various parameters of sea ice such as roughness types, thickness, salinity and temperature need to be determined. The effect of snow cover has to be ascertained completely. A general technique for interpreting sea ice radar imagery, and for identifying different important features, needs to be formulated. A need also exists to evaluate different automatic

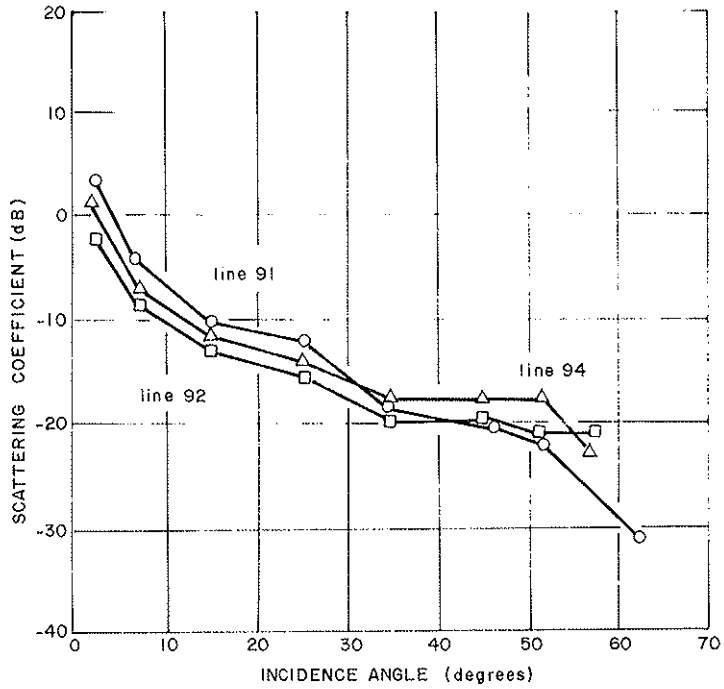

FIGURE A4-1 COMPARISON OF SCATTERING COEFFICIENT ANGLE VARIATIONS FOR FIRST-YEAR ICE (Rouse, 1969).

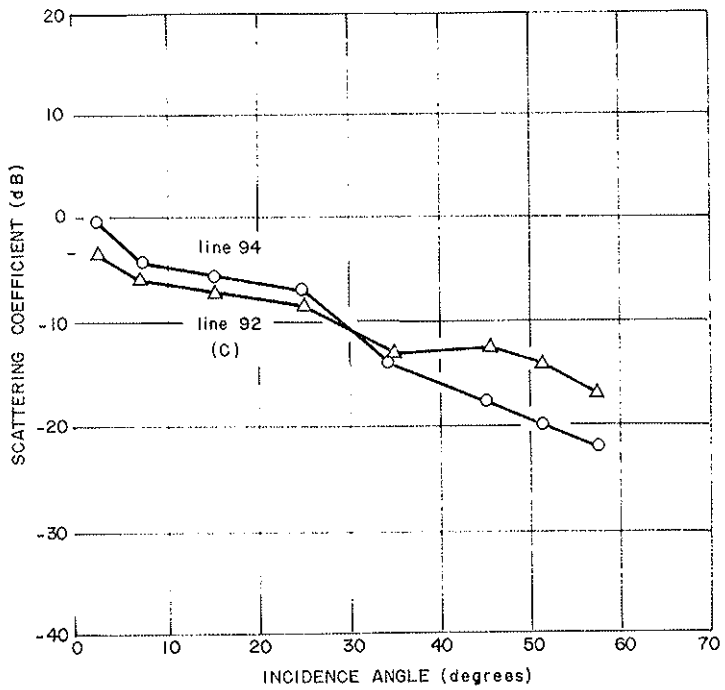

FIGURE A4-2 COMPARISON OF SCATTERING COEFFICIENT ANGLE VARIATIONS FOR MULTI-YEAR ICE (Rouse, 1969).

processing and classification techniques which will facilitate handling large amounts of sea ice data. The changes in the image because of changes in weather and/or seasonal conditions have still to be studied.

The radar scattering coefficient, σ^o, results at 13.3 GHz and VV polarization, as presented by Rouse (1969), are shown in Figures A4-1 and A4-2. A comparison of scattering coefficient angle variations for first-year ice obtained from three parallel scatterometer lines flown over different areas is shown in Figure A4-1. The first-year ice corresponding to line 92 had an average thickness of 1.35 meters and was reasonably uniform. It was covered by numerous scattered blocks of ice, and the snow cover was 1 - 2 cm thick. Both lines 94 and 91 represent pressure ridged first-year ice regions. Line 91 also had a smooth first year ice region which exhibited too great a slope near the vertical for good agreement with the block strewn first-year ice of the more northern ice regions in lines 92 and 94. In Figure A4-2 the multi-year ice measurements of line 92 are compared with multi-year ice of line 94. The agreement is good to 35^o. The multi-year ice of line 92 was noted to be several years in age with the surface being well weathered and hummocks being well rounded. The peaks of the ridges were bare ice and the depressed areas contained snow varying in depth between 20 and 60 cm. The calculated surface roughness factor based on the Kirchhoff-Huggen principle was highest for multi-year ice, followed by ridged first year ice and smooth first year ice. It was pointed out by Rouse (1969) that the data obtained on the mission were inadequate to correlate the return with salinity to a reasonable degree of accuracy.

The mean σ^o vs Θ curve at 13.3 GHz, VV polarization, obtained from radar scatterometer measurements made in NASA Mission 126 is shown in Figure A4-3. The solid lines is the actual curve obtained and the vertical bar gives $\pm$ one standard deviation at each angle. The kinks in the curve, possibly due to antenna pattern or to sampling variability, are removed by a visually-smoothed curve denoted by the dashed line.

The scatterometer data presented by Parashar (1974b) were divided into seven categories of ice based on stereo-photo interpretation. The seven categories according to thickness were: category 1, open water; category 2, new ice (>5 cm thick); category 3, thin young ice (5-18 cm); category 4, thick young ice (18-30 cm); category 5, thin first-year ice (30-90 cm); category 6, thick first-year ice (90-180 cm); and category 7, multi-year ice (180-360+ cm). The σ^o vs Θ curve at 13.3 GHz, VV polarization for each of the seven categories is shown in Figure A4-4. The corresponding σ^o vs Θ curves at 400 MHz for VV, HH and VH polarizations are given in Figures A4-5 and A4-6.

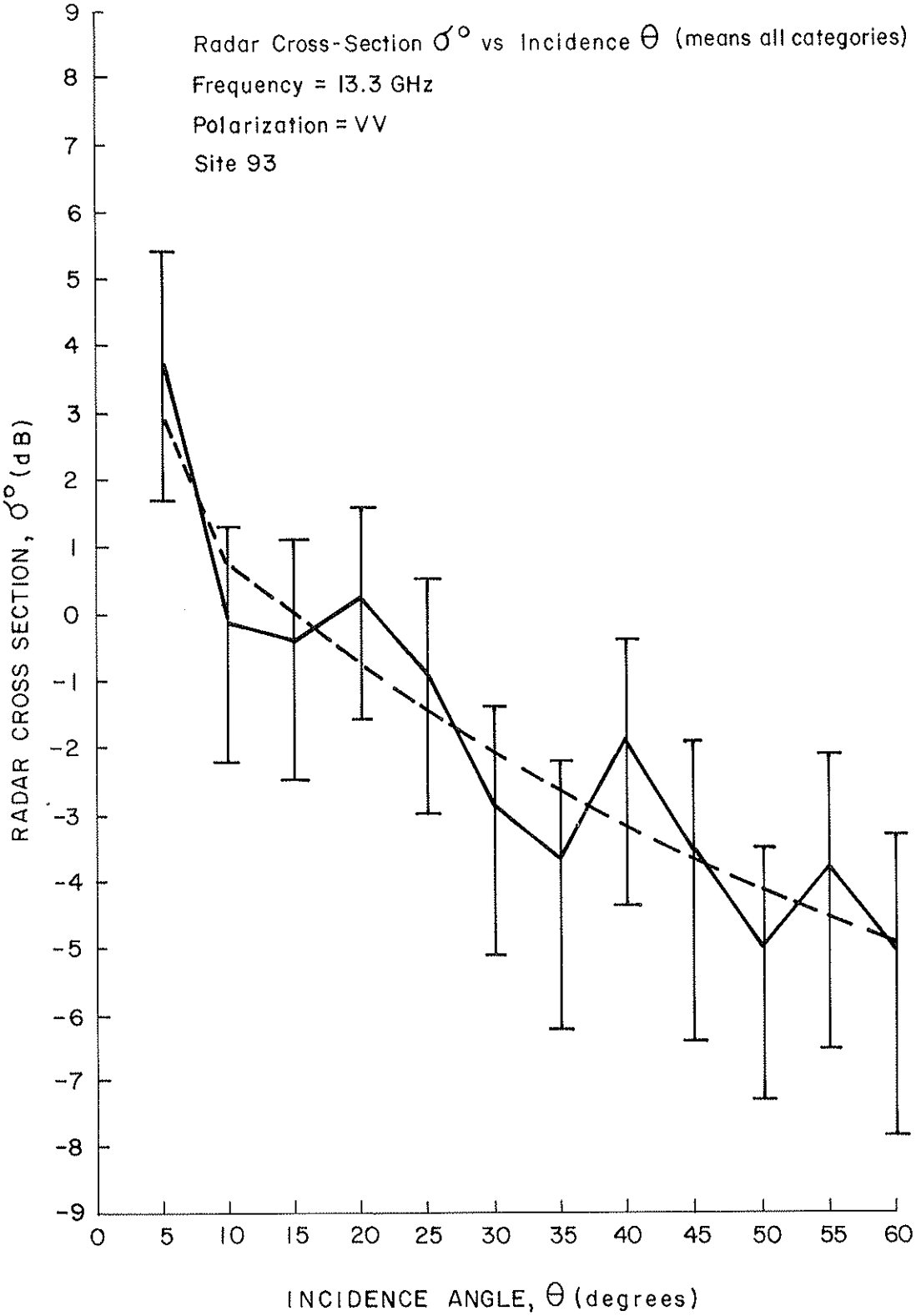

FIGURE A4-3 EXPERIMENTAL σ° vs θ MEAN OF ALL CATEGORIES
(Parashar, 1974a)

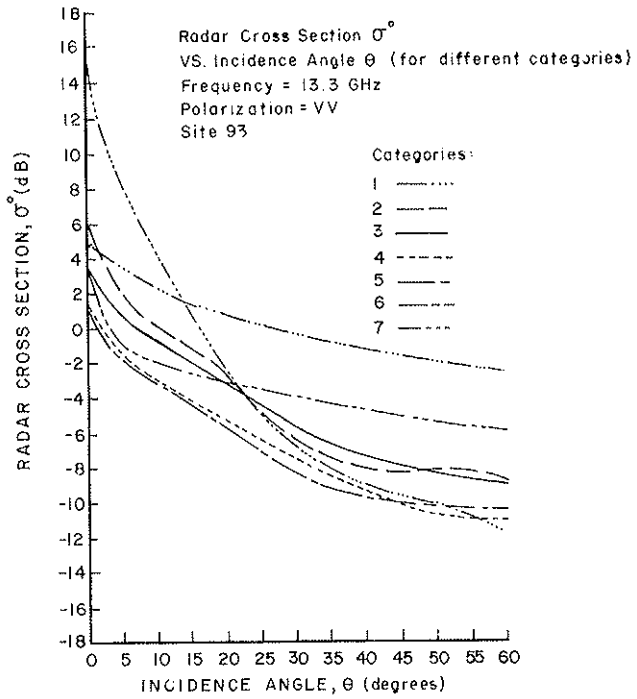

FIGURE A4-4 EXPERIMENT 0^{O} VS θ FOR DIFFERENT CATEGORIES, 13.3 GHz, W (Parashar et al, 1974)

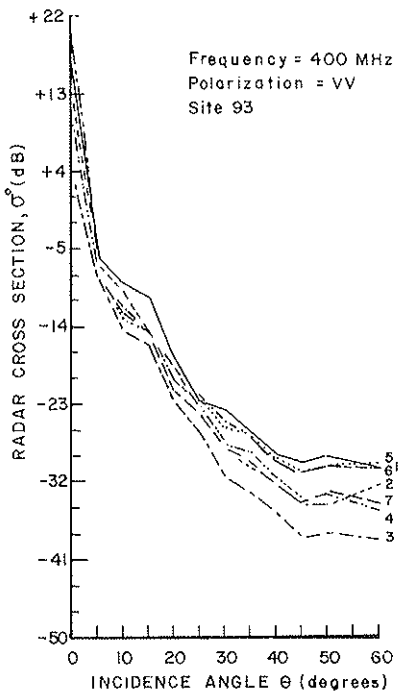

FIGURE A4-5 EXPERIMENT 0^{O} vs θ FOR DIFFERENT CATEGORIES, 400 MHz, VH (Parashar 1974)

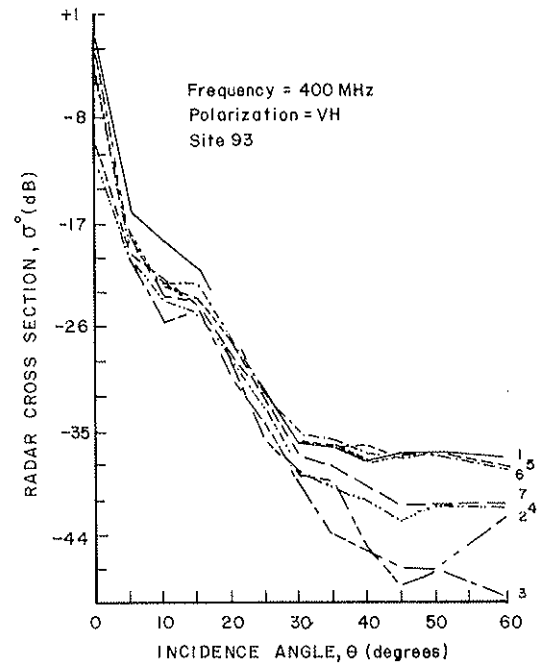

FIGURE A4-6 EXPERIMENT 0^{O} vs θ FOR DIFFERENT CATEGORIES, 400 Mhz, VV (Parashar et al, 1974)

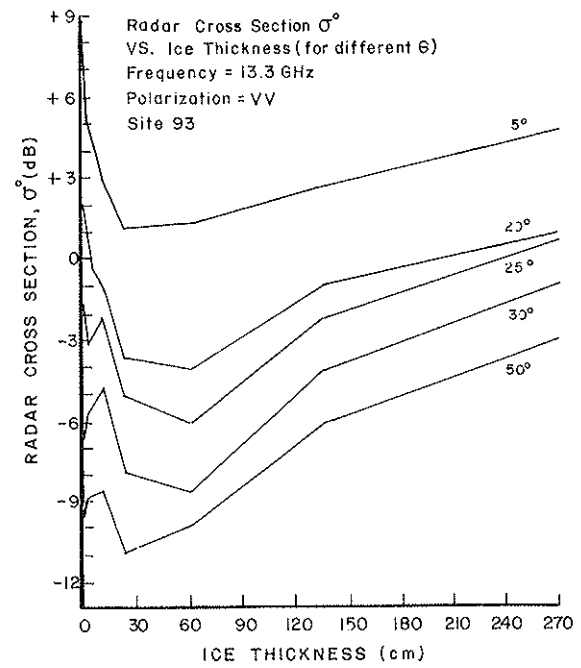

FIGURE A4-7 EXPERIMENT 0^{O} vs ICE THICKNESS FOR DIFFERENT θ, 13.3 GHz, VV (Parashar et al, 1974)

The multi-year ice does give the highest backscatter at 13.3 GHz as in the case of Rouse's data. Open water can be differentiated at both of the frequencies. First-year ice gives less return than multi-year ice at 13.3 GHz; however, thicker first-year ice types give more return than multi-year ice at 400 MHz. The σ^{o} vs ice thickness curves for various angles at 13.3 GHz using VV polarization is given in Figure A4-7. The corresponding curves at 400 MHz for VV and VH polarizations are given in figures A4-8 and A4-9, respectively. There is an ambiguity in return from thin first-year ice (categories 2 and 3) and thicker first year ice identified based on the strength of the scattering coefficient. A comparison of like and cross-polarized scattering coefficients at 400 MHz shows that more contrast between ice types is available on the cross-polarized signals than on the like-polarized signals.

The scatterometer results presented by Gray et al.(1977a) indicate that the value of σ^{o} for relatively thin ice can vary over a range of approximately 10 dB for both the like (HH) and cross (HV) polarized signals. The scattering curves at 13.3 GHz for HH and HV polarizations for Forteau Bay flight lines are shown in Figure A4-10 and A4-11, respectively. It appears that the separation between various regions is slightly more for HV than for HH and that the HV curves are flatter compared to HH curves. The order of return from various ice regions is similar for both HH and HV with rough first year shorefast ice giving maximum return at angles greater than 20^{o} followed in order by medium rough and smooth first-year shorefast ice regions. Rafted young ice gives almost the same value of σ^{o} as medium rough first-year shorefast ice although it is clear that the rafted ice is thinner. The large range of as much as 20 dB in radar return from three shorefast regions is worth noting.

The σ^{o} vs θ curves for HH and HV polarizations obtained from the Notre Dame Line 1 are shown in Figure A4-12 and A4-13, respectively. The thicker pancake ice gives maximum return for angles away from the vertical followed by thin pancake ice and rafted nilas. In this case, the rafted nilas produces less backscatter than water at all angles. The large range in radar return of as much as 15 dB from four thin ice regions appears to be related to surface roughness although surface temperature and salinity variations may also be significant.

The σ^{o} vs θ curves obtained from Notre Dame Line 2 are shown in Figures A4-14 and A4-15 for HH and HV polarizations, respectively. The maximum backscatter at incidence angles greater than 25^{o} was obtained from shorefast ice which had been broken by wave action but had subsequently been refrozen into the shorefast ice. The curves of

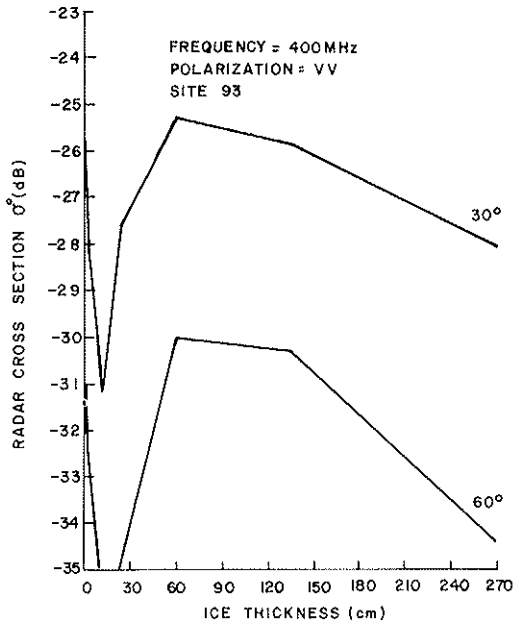

FIGURE A4-8 EXPERIMENTAL σ^o VS ICE THICKNESS FOR DIFFERENT θ, 400 MHz, W. (Parashar et al, 1974)

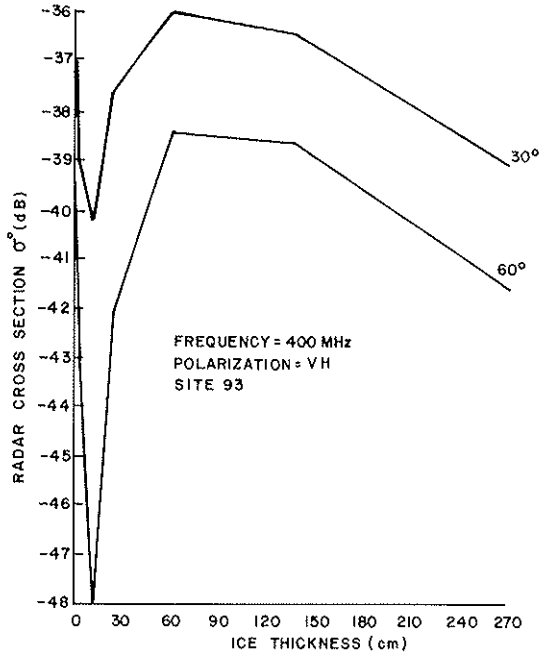

FIGURE A4-9 EXPERIMENTAL σ^o VS ICE THICKNESS FOR DIFFERENT θ, 400 MHz, VH. (Parashar et al, 1974)

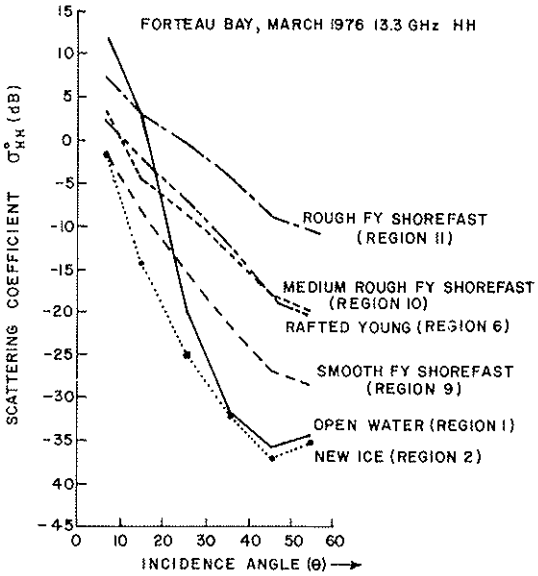

FIGURE A4-10 SCATTERING COEFFICIENT σ^o VS ANGLE θ, FORTEAU BAY, 13.3 GHz, (Gray et al, 1977a)

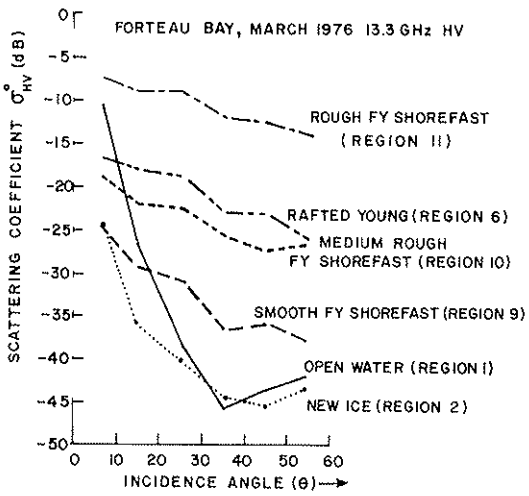

FIGURE A4-11 SCATTERING COEFFICIENT σ^o VS ANGLE θ, FORTEAU BAY, 13.3 GHz, HV (Gray et al 1977A)

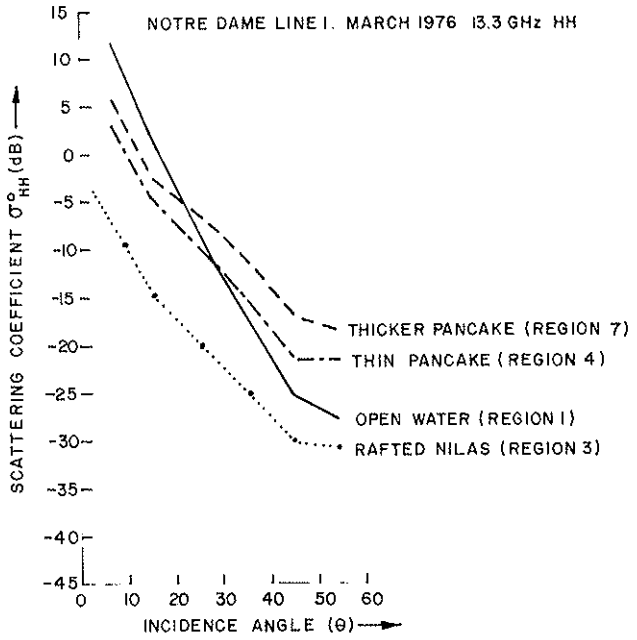

FIGURE A4-12 SCATTERING COEFFICIENT σ^o VS ANGLE θ, NOTRE DAME LINE 1, 13.3 GHz, HH (Gray et al, 1977a)

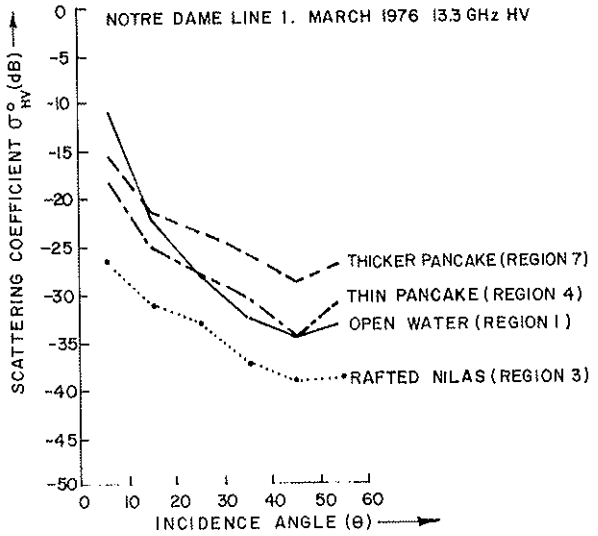

FIGURE A4-13 SCATTERING COEFFICIENT σ^o VS ANGLE θ, NOTRE DAME LINE 1,13.3 GHz, (Gray et al, 1977a)

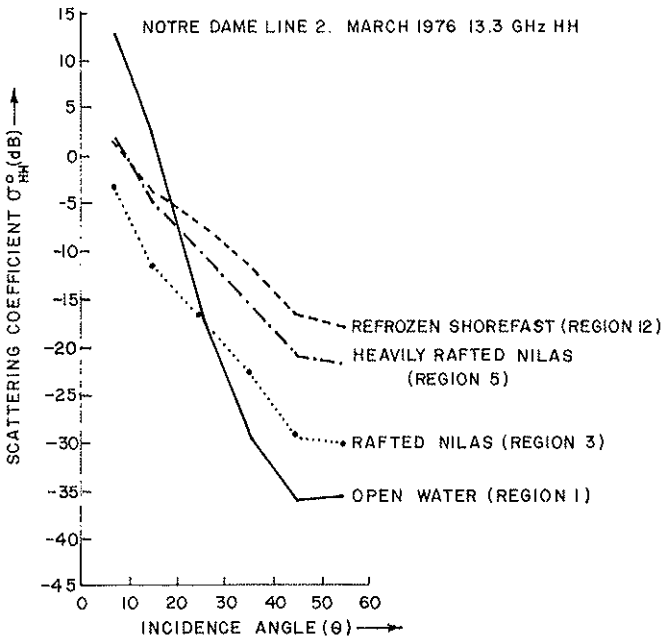

FIGURE A4-14 SCATTERING COEFFICIENT σ^o VS ANGLE θ, NOTRE DAME LINE 2, 13.3 GHz, HH (Gray et al, 1977a)

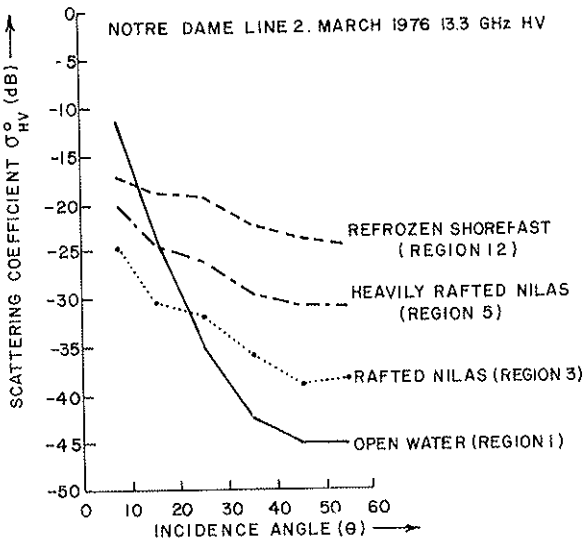

FIGURE A4-15 SCATTERING COEFFICIENT σ^o VS ANGLE θ, Notre DAME LINE 2, 13.3 GHz, HV (Gray et al, 1977a)

the back-scattering coefficient, σ^o, vs θ for HH and HV polarization, corresponding to various ice regions of the Northumberland Strait flight line, are given in figures A4-16 and A4-17, respectively. The rafted nilas region gives the lowest return at all angles except at the largest incidence angle where its return is comparable to that from open water. For incidence angles greater than 30^o, maximum return is given by thin first-year ice followed by consolidated brash ice, heavily rafted nilas and rafted young ice.

A comparison of σ^o vs θ curves from four flight lines for water indicate that the value and the slope of the curve differs from one line to another. The difference probably is due to the variation in wind speed which was not recorded. In certain cases the wind speed effects are visible on the aerial photograph when the sun glint angle is favourable.

It was pointed out by Gray et al.(1977a) that in reporting their results an effort was made to follow the existing WMO ice nomenclature and terminology (Dunbar, 1969) in identifying and classifying the sea ice. In some cases, however, it was difficult to specify a precise ice type or category and it was decided to use the term "region" in describing the area over which averaging of the scatterometer data are performed and the region was assigned the most appropriate name. This statement is particularly true in cases when first-year ice types must be divided into sub-categories such as nilas, rafted ice, young ice, and other thin categories and is probably applicable to data reported by Rouse (1969), Parashar et al.(1974b) and others.

It is difficult to compare results because of the variability of ice conditions from place to place and the use of different systems. It is difficult to compare results reported by various authors. It is possible that categories 2 and 3 (thin first-year ice categories), for which Parashar et al.(1974b) reported an ambiguous return, are similar to heavily rafted nilas and rafted young ice regions reported by Gray et al.(1977a). It has been pointed out by Bradie (1967) that the interpretation of relatively thin ice features on radar is difficult because of lack of great tonal difference within open water, young ice, grease ice and slush. But the results of Gray et al.(1977a) show that the value of σ^o for relatively thin ice vary over a wide range.

As is clear from the above, an effort to relate experimental results of radar return to various sea ice parameters such as salinity, temperature, and surface roughness is lacking. An attempt was made by Parashar et al.(1978) to formulate a theory for polarized radar backscatter cross-section, σ^o, for sea ice by taking into account the amount of brine entrapped, temperature, and surface roughness. Sea ice was considered

an inhomogeneous medium which the inhomogeneity varies continuously in the vertical direction. In addition, a small random variation in the horizontal direction was assumed. As a result, the complex permittivity, ϵ, as a function of x, y, and z coordinates can be written as:

$$\epsilon(x,y,z) = \epsilon(z) + \epsilon(x,y), \quad |\epsilon(x,y)| << |\epsilon(z)|.$$

An attempt was made to apply the developed theory to compute sea ice scatter. Numerical calculations were performed for polarized radar backscatter cross-sections (σ^o_{VV} and σ^o_{HH}) at two frequencies, 13.3 GHz and 400 MHz. These theoretical results for six ice types are presented in Figures A4-18, A4-19 and A4-20. Figure A4-18 is comparable to Figure A4-4 and A4-20 to A4-5. This comparison of theoretical and experimental results indicate that the theoretical results are in general agreement with the experimental results in terms of the absolute value of σ^o and the relative variation among the six ice types. It was found that the contribution to the value of σ^o from the surface roughness term is dominant at 13.3 GHz for all angles and for near vertical angles at 400 MHz. The contribution from the inhomogeneity term decreases at a lesser rate with angle than the surface roughness term. The validity of this model has yet to be fully tested.

In view of the above, the results of radar backscatter from sea ice and the utility of radar are summarized below:

(1) Radar can be used to measure the following parameters of sea ice:

(a) Concentration: It is not easily determined. The ability to determine ice concentration depends essentially on the abilility to separate ice areas from ice-free areas. In certain cases it may not be possible to identify ice-free areas on the basis of tone alone. More often than not the boundaries of floes are readily apparent but sometimes the surrounding ice can not be identified as such. New ice or very thin first-year ice sometimes gives almost no return as in the case of open water. Also, at near grazing angles the return is mostly from ice edges appear black, as demonstrated by a number of experiments. The ability to separate ice areas from ice-free areas depends on the grey-tone resolution of the system, the observational angles, polarizations, and frequency. Multi-year ice floes are more readily identified than the first-year ice floes although the distinction between the two may not be possible in some cases.

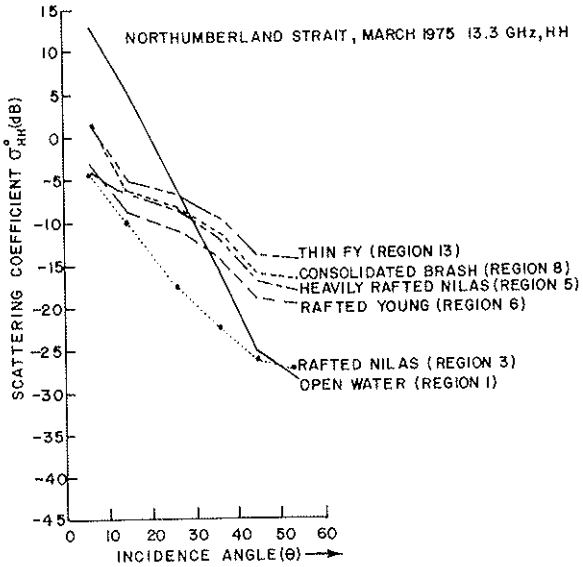

FIGURE A4-16 SCATTERING COEFFICIENT σ^{o} VS ANGLE θ, NORTHUMBERLAND STRAIT 13.3 GHz, HH (Gray et al, 1977A)

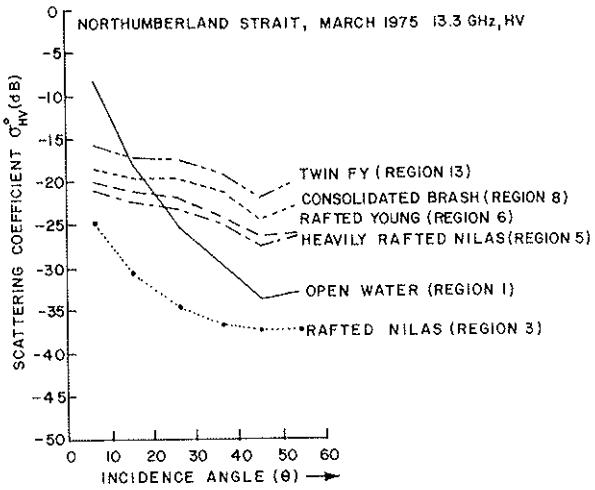

FIGURE A4-17 SCATTERING COEFFICIENT σ^{o} VS ANGLE θ, NORTHUMBERLAND 13.3 GHz, HV (Gray et al, 1977A)

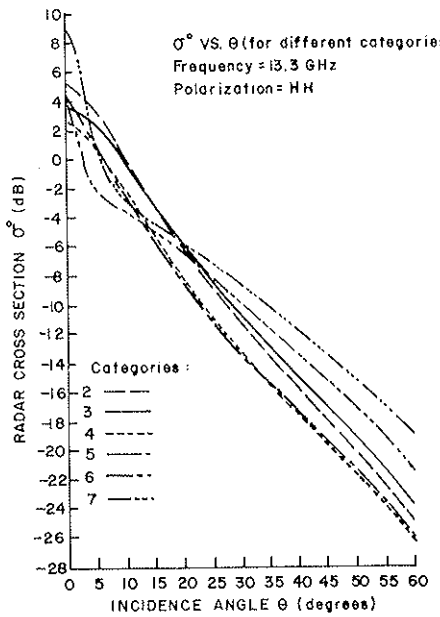

FIGURE A4-18 THEORETICAL σ^{o} VS θ FOR DIFFERENT CATEGORIES, 13.3 GHz, VV (Parashar et al, 1974)

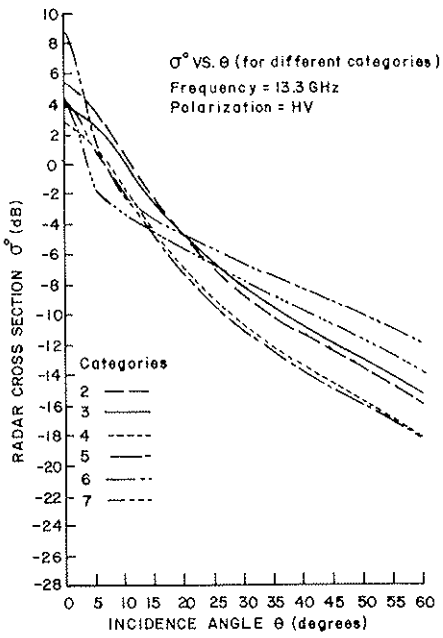

FIGURE A4-19 THEORETICAL σ^{o} VS θ FOR DIFFERENT CATEGORIES, 13.3 GHz HV (Parashar et al, 1974)

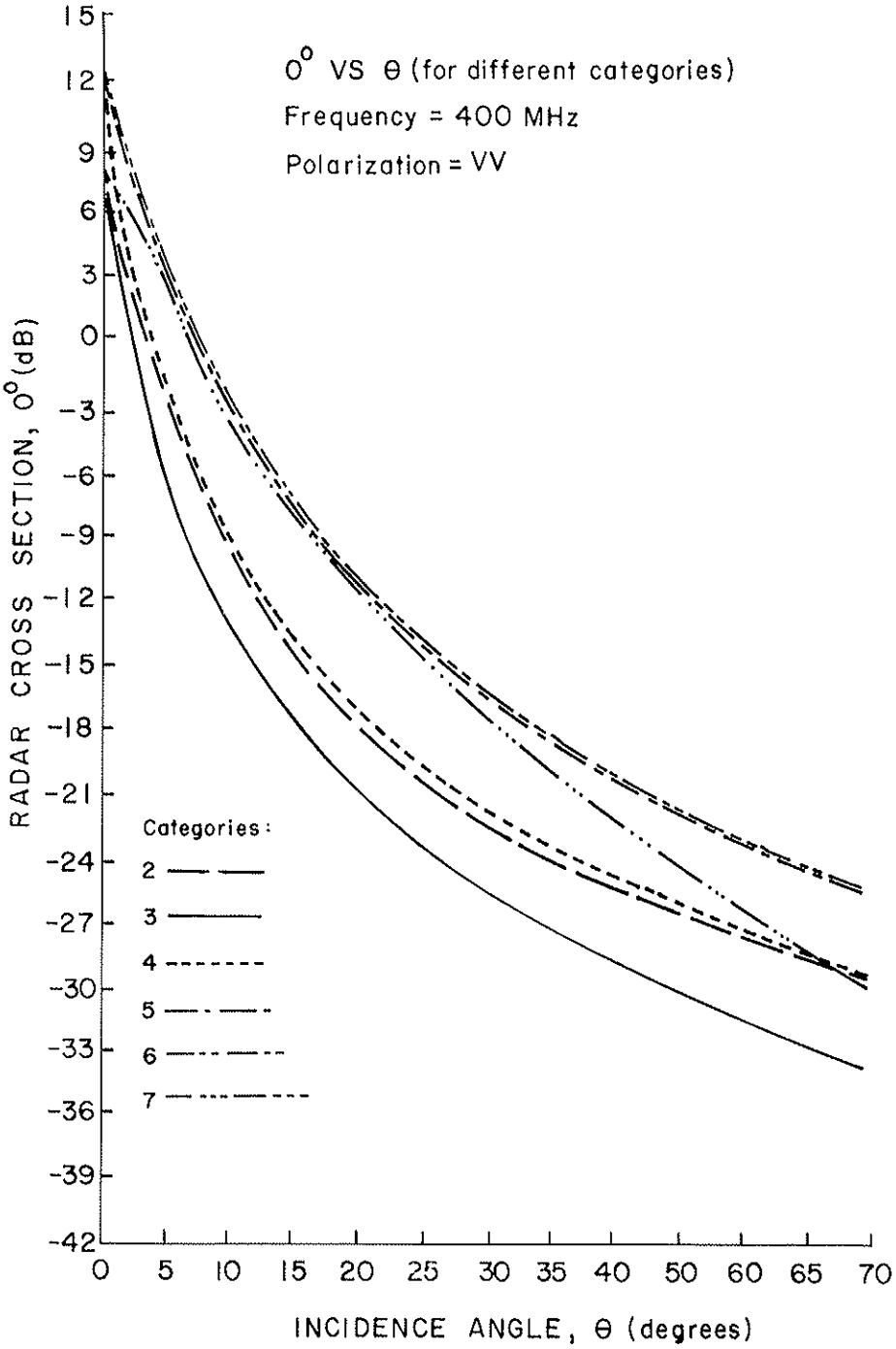

FIGURE A4-20 THEORETICAL 0^o vs θ FOR DIFFERENT CATEGORIES, 400 MHz, VV (Parashar et al, 1974).

(b) Floe size: It can be readily observed when the boundary of the floe can be located. Multi-year ice floes, because of well rounded edges, are easier delineated than first-year ice floes.

(c) Water openings: In general they are quite easily determined as black areas of no radar returns. It was reported by Dunbar (1975), however, that even the refrozen leads do give a black tone sometimes. The ability to locate water openings depends on the resolution of the system and its orientation relative to the flight tracks. The openings parallel to the flight track are likely to show up better than those which are perpendicular.

(d) Drift: It can be determined by repeated radar coverage of the same area and by identifying similar features. Single ice floes, as well as general ice masses, can be tracked to an accuracy determined by the repetition period, resolution, and navigational accuracy. It has been demonstrated by Johnson and Farmer (1971b) that the drift of individual ice floes can be determined to reasonable accuracy on DPD-2 radar imagery.

(e) Topographic features: The ability to detect pressure ridges is limited by the system resolution and the orientation of the ridge relative to the flight track. The pressure ridges are noted by their white or light grey linear images. Hummocks can be detected on good SLAR imagery. As noted by Rouse (1969), pressure ridges do give a higher backscatter, and the surface roughness factor, based on theory, is indistinguishable from multi-year ice; however, the fit of the theory to these data are poor. SLAR imagery can be used to interpret whether or not ice is or has been under pressure.

(f) Fractures: Fractures are quite often imaged as altnernate dark and light returns, depending on their width and orientation to the radar beam. Careful scrutiny of the imagery is necessary when interpreting this feature.

(g) Ice age: It is probably the most difficult characteristic that can be determined from SLAR imagery. The resolution of the SLARs used previously generally restricts their ability to discriminate between individual minute surface features such as puddles and drainage channels, and rafting, that are characteristic of certain stages of development. However, it is possible to determine categorical age or ice type by identifying certain other features such as size, shape, and texture of the imaged ice; its location as compared to the surrounding ice; the place where the imagery was obtained; and the time

of year. It it also possible to discriminate and identify different ice types from the relative grey-tones of the image as demonstrated by the scatterometer results.

Dunbar (1975) has pointed out that it is often possible to discriminate between smooth ice (which gives no return and is indistinguishable from open water on the basis of black tone alone) and water by the small roughnesses that commonly appear on the ice surface and which show as faint light lines. Very similar lines, however, occasionally appear in water openings where small amounts of brash ice are lined up by wind. Depending on the wind speed, water may not appear black in certain cases. Young ice forms are difficult to identify on the basis of tone alone as the scatterometer results show.

Normally at X-band and higher frequencies, multi-year ice gives the strongest return. New ice which is rough sometimes gives as bright a return as that given by multi-year ice, but it can be discriminated from multi-year ice because it does not have any sharp edges. Brash ice also gives a bright return but it presents a different texture.

More research is needed before a general set of guidelines can be developed for interpreting ice type or age and other features from the radar imagery. The quantitative and qualitative use of texture and tone in analyzing radar polarization, angle, resolution and seasonal variations have still to be fully understood.

(h) Ice thickness: It is not possible to get a direct measure of the ice thickness from a radar image. It is possible, though, to get a rough measure of the ice thickness by associating a mean thickness with an ice category and relating it to the brightness on a radar image or the value of σ^{o} on scatterometer data. As a result it seems possible to obtain an empirical relationship between the brightness on a radar image, or between σ^{o} on scatterometer data, and ice thickness.

(2) Frequency: X- or Ku-bands appear to be the optimum bands in discriminating sea ice types and delineating other ice features. Most of the radars in operation today operate at these bands. Radar imagery at these frequencies provides sufficient information to delineate and identify major categories of ice. Past measurements made simultaneously with more than one frequency, qualitatively indicate that a two frequency system might provide more information about sea ice. For example

the scatterometer results presented by Parashar (1974) show that by combining a 13.3 GHz and a 400 MHz system definitely eliminates the ambiguity regarding a very thin ice because of a reversal of the angular character of radar return from sea ice less than 18 cm thick at these two frequencies. The resolution achievable at a low frequency of 400 MHz, however, may not be suitable for most purposes. Ketchum and Tooma (1973) have presented radar imagery at four frequencies obtained through the Naval Research Laboratory (NRL), 4F (4 frenquency) synthetic aperture radar system and reported that at wavelengths longer than 3 cm, it tends to lose the grey-tones on the ice returns. For example, the L-band (30 cm) imagery shown was mostly black with only the major ice fractures and ridges showing as bright lines. It was also observed that younger stages of ice development, indistinguishable and unidentifiable on the X-band imagery, are often identified on band imagery, as reported by others, (Page and Ramseier, 1975). Both shorter wavelengths and more optimum parameters are probably responsible for this increased capability. The dual-frequency, synthethic aperture radar imagery obtained by C-CORE utilizing ERIM's system operating in the X (3 cm)-and L 25 cm)-bands shows a better quality of L-band imagery in certain cases than that presented by Ketchum and Tooma (1973). The better quality is probably due to better spatial resolution and system performance. The L-band imagery presented by Thompson et al.(1972) obtained with Jet Propulson Laboratory's synthetic aperture radar is also of better quality.

The best frequency or combination of frequencies for sea ice measurement still needs to be established but it appears that the use of two frequencies will be able to provide more information than the use of one. It should be pointed out that the frequency required for determining surface characteristics of sea ice is different than the one needed for direct thickness measurement or locating materials under ice. The band of frequencies from 100 to 300 MHz provide the required penetration capabilities, as reported by Parashar et al.(1977b).

(3) Polarization: There appears to be no difference between the like polarizations (VV or HH) in their ability to discriminate sea ice, on the basis of limited evidence. There is an indication that cross-polarization may be of better utility in sea ice studies as is clear from the scatterometer and radar imagery results presented above.

(4) Resolution: No quantitative study has been undertaken to see the effect of resolution in discriminating ice types. All the systems used so far in the radar measurement of sea ice have different resolutions. The best resolution was on the order of 3 m obtained with the ERIM synthetic aperture system. The DPD-2 System used by the U.S. Coast Guard has a spatial resolution of about 20 m in the along-track and the across-track direction at mid-range. The range resolution of the AN/APS-94D SLAR system is fairly constant at about 30 m, but the azimuth resolution varies with flight altitude and deteriorates across the range of the image. At a (610 m) 2000 ft flight altitude, for instance, it is 40 m at 5 km from the track and deteriorates at the rate of 8 m per kilometre. The general image quality also seems to deteriorate with range.

It should be pointed out that in addition to having a good spatial resolution it is important to have a good grey-scale resolution. There is always a trade-off between the spatial resolution and grey-scale. A combination of range and azimuth averaging of independent samples greatly improves the grey-scale of an image. The number of independent samples averaged influences the resulting speckle or texture on an image.

The scatterometer data indicate the separation of σ^{o} value between different categories is not very great; of the order of 0.25 dB. This suggests that a difference of at least 0.5 dB in the value of σ^{o} should be recognizable on the radar image. For a required dynamic range of 30 dB, as based on the scatterometer results, 60 different grey-tones would be needed with a logarithmic receiver. More would be required with a linear receiver.

(5) Angles: There appears to be no indication from past research efforts that one set of angles normally used for SLAR is better than another in sea ice studies. Some experiments have shown, however, that the use of angles near grazing (incidence angles $>80^{o}$) results in returns from ice edges and ridges, making it more difficult to distinguish between smooth ice areas and water. Scatterometer data at 13.3 GHz presented by Parashar (1974) indicate that incident angles more than 20 degrees should be used. Gray et al (1977a) have pointed out that use of near vertical incidence angles with like- and cross-polarization channels may help in distinguishing ice regions from open water.

(6) Snow Cover: The masking effect of snow cover has still to be determined. There is a preliminary indication that the waves in the K-band region can penetrate snow

cover so that they are not affected by it, which suggests that snow cover would not be a problem at lower frequencies. Parashar (1976b) presented radar imagery at X-band obtained under the Swedish-Finnish experiment in which one ice region had both snow free and snow covered surfaces. The snow-free region could not be distinguished from the snow covered region on the radar image.

The masking effects of snow, if any, are dependent on the type of snow, its depth, density, temperature, water content, and on observational frequency. The crystallized snow is liable to show up on the radar image. In the case of dry snow the reflections from the snow-ice interface are stronger than those from ice-snow interface. But, the attenuation in wet snow may be of enough significance to mask reflections from the snow-ice interface. It has been observed by Waite and MacDonald (1971) that old, perennial snow is sometimes visible on the radar image. Ketchum and Tooma (1973) have attributed some returns, in the case of multi-year ice, to recrystallized snow.

(7) Seasonal Variation: The changes produced in the appearance of ice on a radar image due to seasonal variations have yet to be studied. A preliminary indication is that the same set of guidelines can be used in interpreting winter and summer radar imagery of sea ice. The radar imagery of sea ice taken in summer may appear to be different from winter ice imagery because of the melting of snow and ice at the surface.

(8) Automatic Classification of Ice: It has been shown that automatic classification techniques can be used in discriminating sea ice types when analyzing scatterometer data (Parashar et al, 1977a). An agreement of about 85 percent has been achieved in identifying and classifying four categories of sea ice as established from stereophoto interpretation. Such automatic classification schemes have yet to be tried on radar images of sea ice. The use of not only grey-tone values but also textural information in discriminating sea ice images has yet to be evaluated and incorporated into the interpretive process. The implementation of such schemes will facilitate handling and analysis of large amounts ot radar data in real-time usage.

(9) Iceberg Identification: From the limited data which is available, icebergs can be identified on both the X-band and K-band images (Farmer, 1972; Anderson, 1966; Dunbar, 1975; and Worsfold et al, 1977). There is no indication as to which polarization may be suitable for such purposes, as the data taken so far

corresponded to this polarization, but HH should give better discrimination against water. The range of angles should be definitely near grazing so that the shadow of the iceberg can be exploited to the fullest extent. The spatial resolution depends on the minimum size of the iceberg which needs to be detected. It is important that a good grey-scale resolution be available so that the maximum contrast is achieved between the iceberg and other objects and the texture of the iceberg may be detected.

The differentiation of icebergs from ships can be made based on certain clues. If the length-to-width ratio of the target exceeds 5 to 1, it is usually a ship. If the radar shadow exceeds 25 metres, then the target is usually an iceberg. Medium and large icebergs generally have square or rectangular shaped images. Small bergs and growlers tend to have either circular or oval shaped images. The SLAR images of the icebergs are highly irregular and complex within the confines of the above shapes. Ships and fishing boats have uniformly shaped returns on the SLAR imagery and the larger vessels frequently exhibit a definitive shape.

Icebergs often exhibit a shadow or a no-return area behind them. When the iceberg is surrounded by sea ice, it almost always has a shadow, depending on the height of the iceberg and the angle of incidence. Because open water gives a black-tone, the shadow effect is not as readily apparent when icebergs are in the open water. Man-made targets, such as ships , usually give a brighter tone than icebergs. Icebergs have texture because they are many faceted and normally have a very irregular structure. Ships on the other hand, give a more even tone, although ship echoes can also be complicated. The edges of iceberg images are normally not clearly defined.

Large moving ships generally exhibit a well-defined wake on SLAR imagery with the apex at the target. Icebergs on occasion exhibit a wake, but there is generally no defined apex and the width is fairly constant with little or nor flaring.

As is clear from the above radar is a valuable tool in the study of the ice environment, but there is lack of information in understanding the nature of radar return from sea ice, and the optimum operating and system parameters have yet to be ascertained.

A4.4 Microwave Emission From Sea Ice

One of the most comprehensive and detailed analyses and studies of microwave emission from sea ice has been performed by Aerojet General Corporation of California over a number of years.

A major result of the study undertaken by Edgerton et al.(1971b) was the general classification of sea ice brightness temperature into categories of "high" (~240°K) and "low' (~200 - 210°K) emission corresponding to young and weathered sea ice, respectively. These results were based on microwave measurements performed at observational wavelengths of 0.51, 0.55, 0.81, 0.96, 1.35, 1.55, 2.81, and 3.2 cm at low (150 m) and high (9 km) altitudes, during the middle of June, 1970, near Pt. Barrow, Alaska. Only the data obtained from low altitude flights were analyzed because of a solid cloud deck existed during most of the overflights. No "surface truth" data was taken so photographic and laser data were utilized to identify the ice types. The young, unweathered ice corresponding to the "high" emission was thought to have formed within the past month or so and the weathered ice giving "low" emission was relatively old ice which appeared to have undergone weathering, such as surface melting and refreezing. The contrast in birghtness temperatures between the two ice types decreased significantly as the observational wavelength increased. The mechanism responsible with this phenomemon could not be isolated. A significant contrast in the brightness temperatures of ice and water was observed at all wavelengths greater than (or equal to) 0.81 cm. The contrast apparantly increased with wavelength and was largest at 2.81 cm. A direct quantitative comparison of measurement and theory could not be undertaken because of a lack of "surface truth" information such as salinity and temperature profiles.

Poe et al.(1972) has presented results obtained from the study into the applicability of available theories of the microwave emission properties of sea ice in explaining representative portions of the 1971 airborne passive microwave measurements taken over the Arctic-based AIDJEX camp. These results indicate the non-specular surface or volume (or both) scattering phenomena must be incorporated in theories of sea ice emissions before satisfactory explanations of the experimental results can be achieved.

It was observed that the volume scattering effects were not included in the present theories, so a theory of the scattering by random dielectric constant fluctuations (in a bounded medium) applicable to sea ice was derived. A derivation of a theory of surface scattering for slightly rough surfaces was also included. It is pointed out that one

difficulty in testing the theory adequately is the lack of information on the surface spectral density function and the three dimensional correlation function for inhomogeneity in sea ice.

A study of the microwave emission properties of sea ice based on surface-based 13.4 GHz passive microwave measurements made during the 1972 AIDJEX experiment was undertaken by Meeks et al.(1974b). The data obtained illustrate distinct decreasing microwave emissions for first-year, transitional and multi-year ice types. For transition and multi-year ice, both vertically and horizontally polarized measured brightness temperatures decreased linearly with increasing average ice porosity. The measured brightness temperatures for first year ice are comparatively uniform and appear to be more strongly influenced by high near-surface salinity concentrations combined with the occurrence of uniform porosity. It was observed that free-board height (ice above sea level) for transitional ice, refrozen melt ponds and multi-year ice can be inferred from the measured brightness temperature.

An excellent summary of a six year research effort pertaining to the microwave emission characteristics of natural materials and the environment was presented by Edgerton et al.(1973). The presented results include microwave emission from ice, snow packs, and the ocean surface. The theoretical results are compared with experimental results, including laboratory measurements of ice-water systems. It was observed that microwave emission by snow packs is wavelength dependent and is strongly dependent on liquid water content. The melting of a snowpack is readily detectable at wavelengths of 8 mm and 2.2 cm.

The results obtained from field tests conducted to explore the potential of radiometers, operating at 1400, 765, and 400 MHz, in determining sea ice thickness have been reported by Adey et al.(1972). It was observed that theoretical calculations indicate the brightness temperature is dependent on ice thickness, and, also, higher frequencies are more sensitive to thin ice while lower frequencies have greater sensitivity to thicker ice. The experimental results show that low brightness temperatures are peculiar to thin ice and higher temperatures to thicker ice, with measurements at 1400 MHz not being very sensitive to changes in ice thickness for the thickest ice type. The thickness of the snow cover, for some of the measurements reported, varied from 10 cm and 90 cm and the snow was dry and windpacked. The change in apparent brightness temperature owing to the snow (that is the temperature with snow cover minus the temperature measured after the snow was removed) was plotted against the snow thickness for the various frequencies.

The change in brightness temperature show, no apparent trend with snow thickness, and in the extreme case amounts to about 20°K. Adey (1972) also has presented a review of the use of microwave radiometry for remote sensing from aircraft and spacecraft.

The data obtained during the NASA-AIDJEX experiment in 1970 and analyzed by Wilheit et al.(1972) showed that sea ice could be distinguished from open water. Based on 1971 experiments, Gloersen et al.(1973a) showed that the observed emissivity differences of sea ice at a frequency of 19.35 GHz are associated with ice age, with multi-year ice having cold brightness temperatures (~210°K) and first year ice having warm ones (~235°K). Images depicting observed emissivities of a large ice area of the eastern Beaufort Sea were also included, in which multi-year ice floes, having an average thickness of 3-4 m, showed cold brightness temperatures while the warm temperatures were associated with first-year ice floes having average thicknesses of less than 2 m.

The results of passive microwave measurements at 0.8, 1.35, 1.6 and 3.0 cm wavelengths made during the joint U.S. - U.S.S.R. BESEX (Bering Sea Experiment) Program were presented by Gloersen et al.(1974b). It was observed that all of the first-year ice has an emissivity of greater than 0.95. Multi-year ice gives a lower emissivity and so does combinations of first-year ice and open water.

The data obtained from the ESMR (Electronically Scanned Microwave Radiometer) operating at a wavelength of 1.55 cm on board the Nimbus-5 Satellite have been used by Gloersen et al.(1973b) to make microwave maps of polar ice. The resolution cell size in the processed images was about 32 km. The distribution of multi-year ice, first-year ice, and open water would be ascertained.

A review of remote sensing activities in the study of floating ice was presented by Campbell et al.(1975), including correlation of dual-polarized 13.3 GHz scatterometer and 37 GHz passive microwave radiometer data obtained during the 1975 AIDJEX experiment. An excellent correlation between the two sets of data were achieved, with about a 60°K difference in brightness temperature between first-year and multi-year ice and about a 20 dB difference in the backscattering cross-section. A similar correlation using the same data set has been reported by Gray et al.(1977b). It was observed that the 37 GHz radiometer did not distinguish between young and first-year ice regions but there was a change in the backscatter coefficients between the two regions. There is an indication that second-year ice may be distinguishable on the basis of radiometer data, whereas, no differentiation is possible on the basis of the backscattering coefficient magnitude.

The only remote sensing experiment in conjunction with the Skylab-4 overpass related to ice was conducted during January-February 1974, in the Gulf of St. Lawrence and Atlantic Ocean. Both active and passive microwave data from airborne sensors were collected and the results were described by Campbell et al (1977). The results obtained by analyzing the Motorola APS-94D, X-band SLAR image data were presented by Dunbar and Weeks (1975). The results obtained through the use of the Passive Microwave Imaging System (PMIS), operating at 10.69 GHz with a ground resolution of 150 m from an altitude of 3050 m, were presented by Campbell et al (1977). These results show that the range of brightness temperatures for both horizontal and vertical polarizations is between $50^{o}K$ and $300^{o}K$ for sea ice images. Vertical polarization gives an average brightness temperature of $240^{o}K$ for a large grey-white ice floe with an estimated thickness of 25 cm, while the horizontal polarization gives $190^{o}K$. The ice plumes and open water mixture surrounding the floe has a representative brightness temperature of $180^{o}K$ for vertical polarization and $50^{o}K$ for horizontal polarization. The average brightness temperature of the frazil-grey ice mixture region was $200^{o}K$ for vertical polarization and $100^{o}K$ for horizontal polarization. Pancake ice gave brightness temperature of $210^{o}K$ and $160^{o}K$ for the vertical and horizontal polarization respectively. Uniform grey ice had the highest brightness temperature of $265^{o}K$ (vertical polarization) of all sea ice observed during the experiment. Shorefast ice exhibited brightness temperatures of $245^{o}K$ and $210^{o}K$ for vertical and horizontal polarizations, respectively. In summary, it was stated that the vertical polarized brightness temperature is greater than the horizontally polarized brightness temperature for all ice types and as the iced ages and becomes thicker the brightness temperature increases for both the vertical and horizontal polarizations, and the difference between the vertical and horizontal brightness temperature decreases. In conclusion, it was observed that the horizontally polarized data is the most sensitive to variations in ice types for both freshwater ice and lake ice.

The use of passive microwave images at a 1.55 cm wavelength, obtained during 1971 and 1972 from the Nimbus 5 satellite, in determining the dynamics and morphology of Beaufort Sea ice has been demonstrated by Campbell et al (1974). The satellite data in conjunction with the AIDJEX experiment permitted the delineation of first year and multi-year ice types at several scales over the entire Arctic.

It was pointed out by Hallikainen (1973) that the radiation received by a microwave radiometer is the sum of the components from seawater and sea ice, and that the contribution of the second order reflections is negligible even at moderate salinities

of sea ice. The noise temperature increases with ice thickness until the attenuation is so high that the lowest ice layers do not contribute to the radiation received by the antenna. The use of 4.7 GHz and 605 MHz radiometers in measuring sea ice thickness in the Bay of Bothnia and the Baltic Sea has been investigated by Tiuri et al. (1974). It was shown that open water (with a surface temperature close to $0^{o}C$) had a low brightness temperature of thick ice, hence rifts and open leads were easily detected using the microwave radiometer. A relatively thin ice layer increased the brightness temperature of the surface considerably and the effect of ice thickness on the brightness temperature seemed to be relatively small for thicknesses over about 50 cm. The pressure ridges had brightness temperatures about $10^{o}K$ less than those of surrounding areas with normal ice. The brightness temperatures at 605 MHz and 4.7 GHz did not differ very much and showed similar characteristics. It was observed by Tiuri et al. (1977) that the brightness temperature calculated by adding the theoretical radiometric temperatures at frequencies of 505, 870 and 1000 MHz, increases almost monotonically with the ice thickness for thicknesses exceeding 30 cm. The maximum measured brightness temperature of about $200^{o}K$ at 610 MHz corresponded to 100 cm thick ice with a surface temperature of $-3^{o}C$ and the minimum brightness temperature of about $145^{o}K$ corresponded to ice 27 cm thick.

The results obtained from the identification of sea ice using the Naval Research Laboratory's (NRL) 19.34 and 31.0 GHz nadir-looking radiometers were presented by Tooma et al. (1975). The results indicate that using two frequencies, passive microwave measurements appear capable of distinguishing between five distinct ice types and forms: open water/thin ice less than 5 cm thick, smooth first-year ice, ridged first-year ice, multi-year ice and second-year ice. The delineation between the two first-year ice categories seemed to depend on surface roughness and be independent of age or thickness. The rough multi-year ice was observed to have the same radiometric temperatures as smooth multi-year ice and the delineation of a higher-temperature multi-year ice form, hypothesized as second year ice, may be attributable to the internal structure in the ice, specifically to the presence of air bubbles.

The images of sea ice obtained by utilizing a passive microwave imaging system (MICRAD) operating in the Ka-band (33.6 GHz) were presented by Ketchum and Lohanick (1977). The images showed that the lowest brightness temperatures were exhibited by open water, some areas of new ice, which presumably had moist surfaces, and some multi-year ice floes and other forms which had experienced considerable internal stress. The relatively thicker areas of first-year ice showed a brightness between that

given by the nilas and young ice categories. The ridges in the first-year ice could not be distinguished from their background. Rafted ice appears radiometrically cooler than its background. Multi-year ice, on average, displays cooler radiometric temperatures than those given by the younger ice types, although a wide spectrum of radiometric temperatures may be present on a single multi-year ice floe. A similar observation on the variation in brightness temperature of as much as $30^{o}K$ within a single multi-year ice floe was made by Tooma et al.(1975).

The microwave emission signatures of snow and fresh water ice were presented by Schmugge et al.(1973). The measurements were made with six radiometers in the frequency range from 1.42 to 37 GHz over snow covered lake ice. It was observed that the difference between the vertical and horizontal polarizations brightness temperature at 37 GHz is $32^{o}K$. Microwave signatures of snow and ice at several wavelengths was presented by Gloersen et al (1974c). Microwave maps of the polar ice, produced by images obtained through the Nimbus - 4 satellite, were shown by Gloersen et al.(1973a).

A4.5 Summary Microwave Emission Results From Sea Ice

As is clear from the above, a comprehensive understanding into the behaviour of microwave emission from sea ice is lacking. The results, to date show that the measured brightness temperatures can be used to delineate five or six gross categories of ice. In general, multi-year ice gives a lower brightness temperature than first-year ice. In one case reported by Tooma et al.(1975), second year ice could be distinguished from multi-year ice, but in general the distinction between the two had not been possible. First-year ice may further be divided into new ice, young ice, and relatively thicker first-year ice. Sometimes a distinction can be made between rough and smooth first-year ice. Thicker first year ice may give brightness temperatures between those given by new ice and young ice. The vertically polarized brightness temperatures are always more than the horizontally polarized brightness temperatures. The contrast between ice and water is more with horizontal polarization and increases with wavelength. The horizontally polarized brightness temperatures are more sensitive to the effect of surface roughness. As the ice ages and become thicker, the brightness temperature increases for both the horizontal and vertical polarizations and the difference between "high" and "low" emission levels corresponding to young and weather sea ice, respectively, decreases as the observational wavelength is increased.

The observed variations in emissivities of "new" ice and "old" ice with frequency as obtained by Wiheit et al.(1972) are presented in Figure A4-21. The apparent

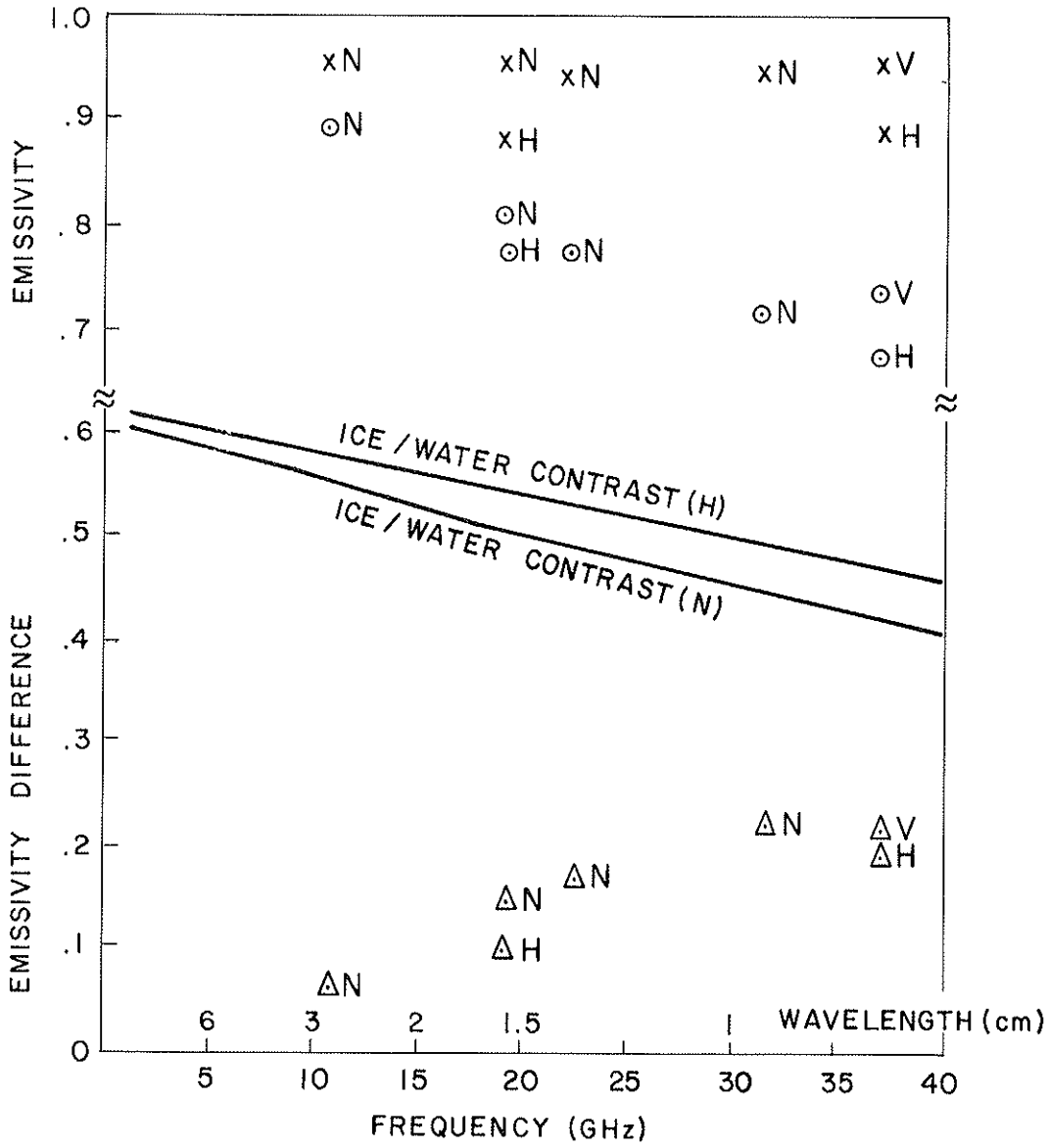

N = nadir viewing

H = viewing 45° left of nadir - horizontal polarization

V = viewing 45° left of nadir - vertical polarization

x = "New" Ice

⊙ = "Old" Ice

Δ = ϵ (new) $-\epsilon$ (old)

FIGURE A4-21 OBSERVED EMISSIVITY SPECTRUM OF "OLD" AND "NEW" ICE. (Wilheit et al, 1972)

scatter in the plots is attributed primarily to residual errors in the absolute calibration of the different radiometers. To eliminate these errors, emissivity differences between the two ice types are also plotted and these show a nearly linear dependence on wavelength. It was observed by Wilheit et al.(1972) that the emissivity differences observed at 45^{o} to nadir and at 0.8 and 1.55 cm wavelengths were somewhat less than in the nadir direction, indicating that there is less contrast of greater angles of incidence. The emissivity difference between open water and "new ice" is also shown and is largest for horizontal polarization and smallest for vertical polarization. But it should be noted that the emissivity difference between the two ice types is about the same for the two polarizations.

This same data set was analyzed by Edgerton et al.(1971b) and it is pointed out that a significant contrast in the brightness temperatures of ice and water was observed at all wavelengths greater than (or equal to) 0.81 cm. The contrast apparently increased with wavelength and was largest at 2.81 cm.

The passive microwave measurements at 13.4 GHz for several distinct ice types during the 1972 AIDJEX experiment were reported by Meeks et al.(1974a). The ice types studies were: Type A, first-year ice; Type A*, melt ponds that have grown through the ice cover; Type B, transition ice, Type C, melt ponds of different age, size and shape not connected to the sea; and Type D, multi-year ice. Types A and A* could not be distinguished radiometrically and were considered to be the first year ice, and types C and D to be multi-year ice. The summary of microwave data obtained for the five ice types is presented in Table A4.1. The number contained within the parentheses after each ice type indicates the number of stations measured. Columns 1 and 2 give the brightness temperature, T_b, at 13.4 GHz for vertical (T_b^V) and horizontal (T_b^h) polarizations, respectively. Columns 3 and 4 give average T_b values. Similarly, emissivity (ε) values are given in columns 5 through 8. Columns 10 and 11 contain T_b^h and ε^h values obtained by NASA Goddard 990 aircraft overflying first-year and multi-year sea ice types (Gloersen et al.1973a). As can be seen, good agreement exists between the emissivities obtained from both the 13.4 GHz ground based radiometers and the 19.35 GHz high altitude data. The small differences which occur between the values are primarily attributed to the difference in surface resolution. The 13.4 GHz ground based systems had a surface resolution cell of 0.31 by 0.58 m at a 40^{o} viewing angle compared to a surface resolution cell of approximately 245 by 245 m for the 19.35 GHz data obtained when utilizing a nadir viewing angle at an altitude of 10,000 m. The presence of different ice types contained

TABLE A4.1 SUMMARY OF SEA ICE MICROWAVE DATA (Meeks et al, 1974a)

	T_b^v	T_b^h	T_b^v	T_b^h	ε^v	ε^h	ε^v	ε^h	% Area	T_b^h 19.35	ε^h 19.35
A (12)	253-258	226-246	255	234	0.971-0.997	0.865-0.947	- 0.987	0.895	27.3	235-250	0.95+
A*(6)	251-259	222-229	254	224	0.951-0.998	0.842-0.868	0.981	0.853	13.6	-	-
B(7)	245-252	203-232	249	218	0.938-0.978	0.758-0.889	0.958	0.822	15.9	-	-
C(6)	235-244	199-211	239	206	0.894-0.929	0.762-0.797	0.921	0.784	13.6	-	-
D(13)	216-233	176-211	226	196	0.816-0.880	0.700-0.798	0.868	0.735	29.6	210-225	0.8
AVG			245	216			0.943	0.818	100%	-	-

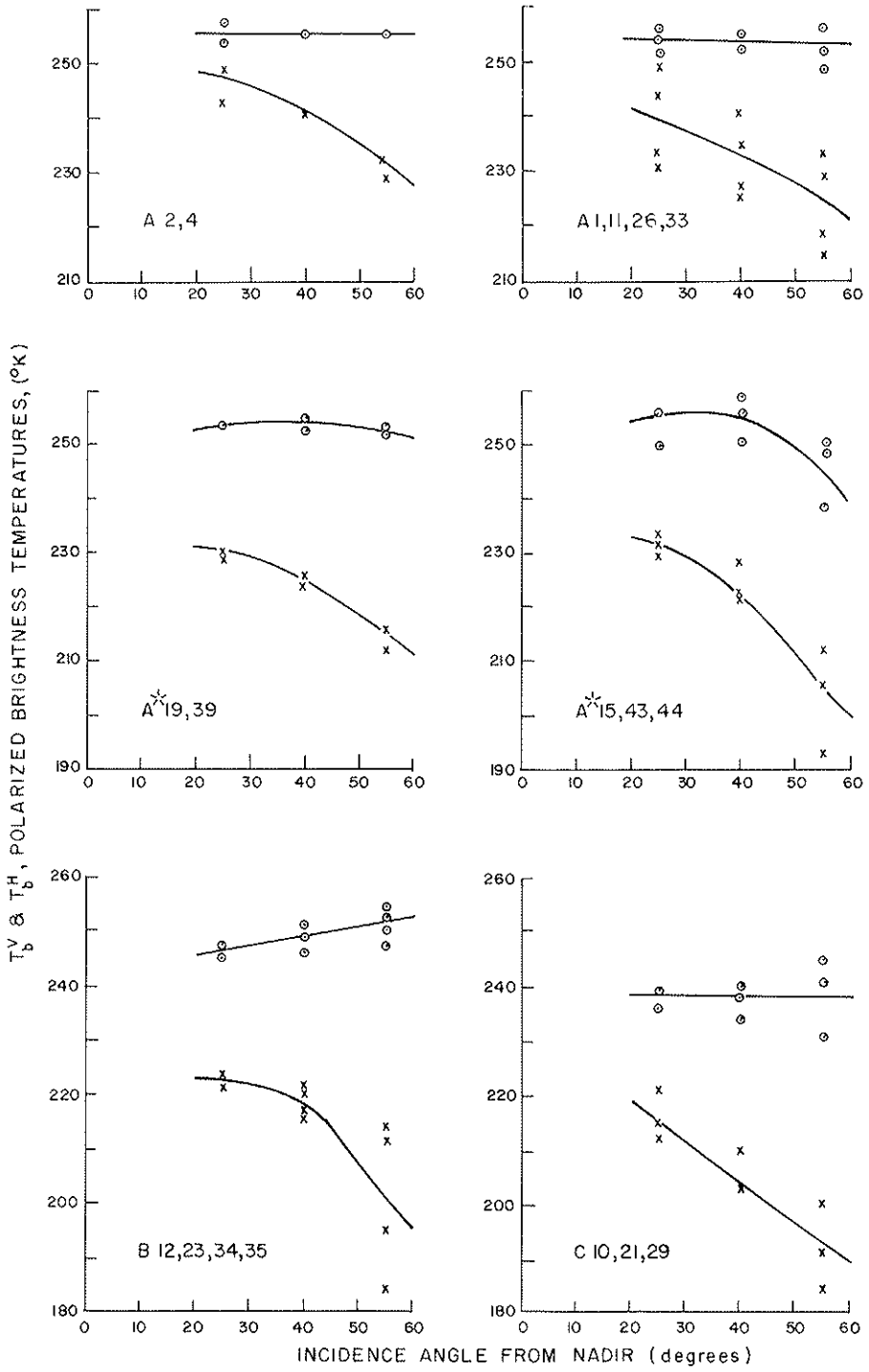

FIGURE A4-22 VERTICALLY AND HORIZONTALLY POLARIZED BRIGTHNESS TEMPERATURE GIVEN AS A FUNCTION OF VIEWING ANGLE AND ICE TYPE A, A*, B, C. THE NUMBERS AFTER EACH ICE TYPE INDICATE THE STATION NUMBER OF THE STUDY AREA. (Meeks et al, 1974a)

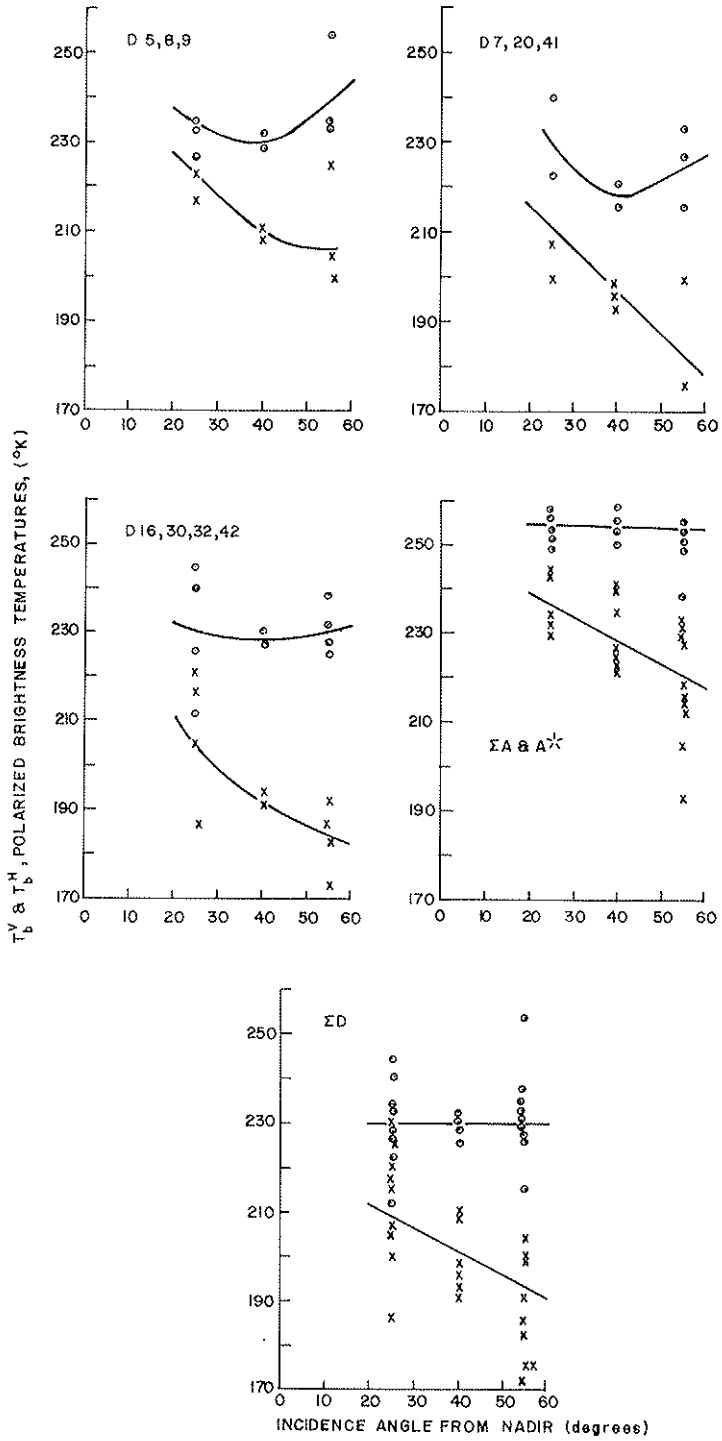

FIGURE A4-23 VERTICALLY AND HORIZONTALLY POLARIZED BRIGHTNESS TEMPERATURE GIVEN AS A FUNCTION OF VIEWING ANGLE AND ICE TYPE D INCLUDING THE AVERAGES FOR THE A AND D TYPES. The numbers after the ice type indicates the station number of the study area. (Meeks et al, 1974a).

within one 19.35 GHz resolution cell would tend to have an averaging effect on these data.

The microwave measurements with the 13.4 GHz radiometer were performed at viewing angles of 25, 40, and 55° from nadir. The T_b data obtained at each of these viewing angles for similar data groupings within each ice type are given on Figures A4-22 and A4-23. In ach plot the upper curve represents T_b and the lower curve represents T_b^h. The scatter in the plots is attributable to the observation of different ice types when rotating the radiometer from the 25 through the 55 degree viewing angles and the high degree of variability of the ice types. Comparing the first-year ice ($\Sigma(A_v \& A^*)$) with the multi-year ice (ΣD) on Figures A4-23, one sees that the T_b is independent of viewing angle, whereas T_b decreases as the viewing angle is increased from the nadir. The average polarization difference is slightly greater for multi-year ice than first-year ice (approximately 3°K).

It was observed by Meeks et al.(1974) that in addition to first-year sea ice (Type A) and multi-year sea ice (Type D), other ice types: open water (leads and polynyas), thin ice, transition ice (Type B), and refrozen melt ponds (Type C) are quantifiable when using high resolution microwave radiometry under Arctic conditions. The results are graphically summarized in Figure A4-24.

The vertically and horizontally polarized brightness temperatures and their differences at 10.69 GHz, for various ice conditions obtained on different flight lines, as reported by Campbell et al.(1977), are presented in Table A4.2. the average brightness temperatures for uniform ice types according to age are given in Table A4.3.

It was pointed out by Meeks et al.(1974) that free board height (ice height above sea level) can be inferred from measured brightness temperatures, and a relationship exists between brightness temperature and ice porosity.

It is clear from the above that microwave emission measurements can be used to discriminate sea ice types. The best frequency or combination of frequencies is still to be established. It was observed by Wilheit et al.(1972) that the optimum frequency is near 30 GHz, at which the strongest contrast between ice/water and two ice types is present. Both Edgerton et al.(1971b) and Campbell et al.(1977) have reported on achieving maximum contrast at frequencies around 10 GHz. As a result it appears that both X- and K-band are suitable for sea ice study. Simultaneous measurements at a number of frequencies seems desirable. Both horizontal and vertical polarizations are considered useful. Vertically polarized brightness temperatures appear independent of viewing angle

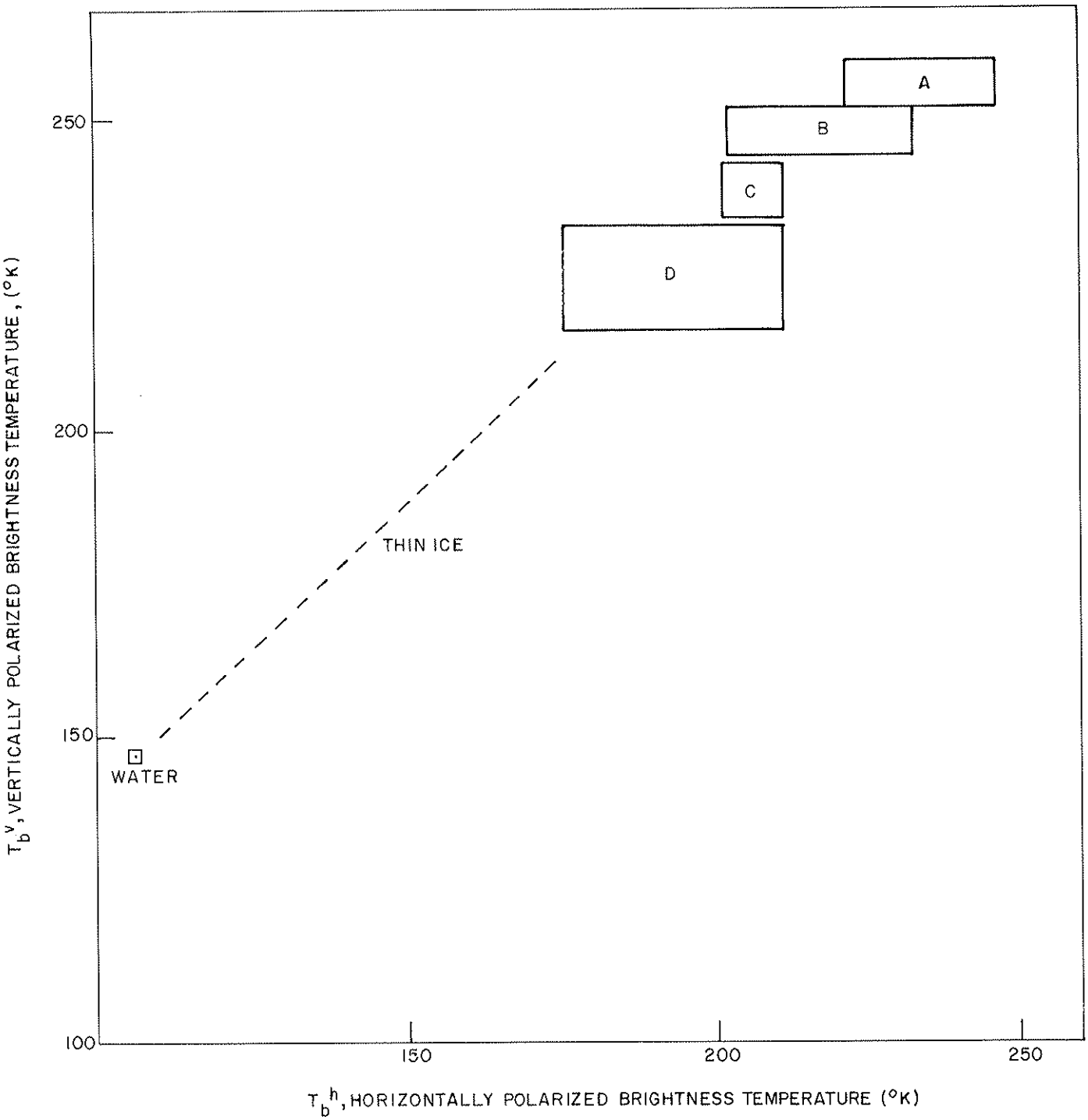

FIGURE A4-24 SUMMARY OF IDENTIFIABLE ICE TYPES AND WATER. Vertically Polarized Brightness Temperature Versus Horizontally Polarized Brightness Temperature Using the 13.4 GHz Passive Microwave Radiometer. A = First-Year Ice; b = Transition Ice (Second Year Ice); c - Melt Ponds; d - Multi-Year Ice. (Meeks et al, 1974a).

TABLE A4-2 BRIGHTNESS TEMPERATURES FOR DIFFERENT ICE CONDITIONS (Campbell et al, 1977)

Figure Number	V (^{o}K)	H (^{o}K)	V-H (^{o}K)	Ice Type
21				
b	220	120	100	Frazil
b	180	50	130	Plumes - water
c	240	190	50	Grey - white
22				
b	230	200	30	Grey - white
b	225	180	45	Consolidated Pancakes
c	210	160	50	Consolidated Pancakes
d	140	90	50	Grey slush - Open water
d	200	155	45	White Slush
d	190	140	50	Grey Slush
23				
b	250	190	60	Nilas
b	240	150	90	Dark nilas
c	245	200	45	Grey - white
c	225	145	80	Grey - white rafted
24				
b	245	185	60	Thin grey
b	255	195	60	Grey ice
b	225	175	50	Grey ice rafted
c	265	195	70	Grey ice
d	250	195	55	Grey ice
d	245	175	70	Thin grey
25				
b	245	210	35	Shorefast ice
c	225	125	100	Nilas

TABLE A4.3 AVERAGE BRIGHTNESS TEMPERATURE FOR UNIFORM ICE TYPES ACCORDING TO AGE (Campbell et al, 1977)

	V	H	ΔT
Plumes - water	180	50	130
Frazil - slush	220	120	100
Dark Nilas	225	125	100
Thin Grey	245	180	65
Grey	255	195	60
Grey-white	240	195	45
Shorefast	245	210	35

at least at one frequency (13.4 GHz). Horizontally polarized signals provide the greatest contrast between ice types, and appear to be more sensitive to surface roughness. No preference for viewing angles is exhibited but the contrast between ice types appears to be more at angles near nadir. The effect of snow cover on the measured brightness temperature is dependent on free water content in the snow and observational frequency. Microwave emission from dry snow packs decreases with increasing water equivalent (mass per unit area). A decrease of several degrees Kelvin per 0.1 metre of water equivalent has been observed. Some effects of snow cover on microwave emission were presented by Edgerton et al (1973).

A4.6 Effects of Sea Ice Parameters on Microwave Backscatter and Emission

Sea ice differs from freshwater ice in that it has impurities contained in its ice matrix. The impurities present are in the nature of liquid brine inclusions and air bubbles. The main factors which influence the formation of sea ice are the brine content of the surface water (surface salinity or the density of brine in the water), the vertical distribution of the salinity, the surface temperature and the depth of the water. The other factors which influence the formation of sea ice are wind, currents, sea state and the intensity and rate of cooling (Weeks and Assur, 1969). The salinity of sea ice is always less than the salinity of the original seawater from which it was formed. Although sea ice seldom becomes more than 2 m thick during the first winter, it may assume far greater vertical dimensions because of rafting and piling up of broken ice in the form of ridges and hummocks. In the spring and summer, the snow cover and sea ice beneath it start melting. This continued thawing results in melt water on the surface which may drain through holes in the ice. Should it survive the first year, it will begin to grow again and may achieve a thickness of more than 2 m. It may attain a greater thickness through ridging and hummocking. Therefore, first year ice (ice of one winter's growth) is always less thick and more saline than multi-year ice (ice of more than one winter's growth which has gone through at least one summer's melt).

The surface of relatively thick first year ice is generally rougher than that of multi-year ice. The difference is due to the fact that the multi-year ice has undergone at least one cycle of erosion whereas the first year ice has not. The deterioration effects on the sea ice surface caused by the ice having gone through a summer's melt are: weathering, rounding and subdividing of normally sharp, high-pressure ridges; the ablation of small pressure ridges through weathering, creating isolated hummocks on the ice; the creation of freshwater puddles or melt pools and their subsequent refreezing; and the

presence of a subdued drainage pattern on the ice surface (Anderson, 1970). There is a lack of general quantitative information available on the surface roughness parameters of sea ice. No such information is available on the micro-wavelength scales. This information is needed to compute radar return and microwave emission from sea ice utilizing theoretical scattering models. Such information will help in understanding the nature of signals received from sea ice and designing of better remote sensing systems for sea ice applications. A very general idea of the roughness parameters and the spatial variations in roughness (such as size, number and frequency of ridges) were reported by Kazo and Diachok (1973), Ling and Untersteiner (1974) and Ackley et al.(1974)

A4.6.1 Physical properties of Sea Ice. The amount of brine present in sea ice is dependent on salinity and temperature and can be found from the phase diagram given by Assur (1958). A decrease in temperature results in a decrease the relative volume of brine. The typical salinity profiles for different thicknesses of sea ice were given by Weeks and Assur (1969). Sea ice is quite saline when it is formed. The salinity of a given segment of ice gradually decreases with time, and the vertical salinity profile at any given time has a characteristic 'C' shape. The low values of the salinity at the top of the relatively thick ice indicate that it has been through a summer's melt. The salinity and temperature profiles for both first-year and multi-year ice as measured experimentally by McNeill and Hoekstra (1973) and Vant (1976) do not always show the characteristic 'C' shape and similar results were obtained in the various field measurement made by C-CORE (Wedler et al, 1977). Cox and Weeks (1973) pointed out that the salinity distribution in multi-year ice is dependent on the ice topography and cannot be adequately represented by a single average profile. From these measurements, it was found that there existed distinct differences between the profiles obtained from hummocks and depressions.

Vant et al.(1974) have made a distinction between two layers of first-year sea ice: an uppermost layer of frazil ice followed by a layer of columnar ice. Frazil ice forms from an agglomeration of ice particles which have formed in super-cooled turbulent water, whereas columnar ice forms in calm water or under an already existing ice cover. The shape of the brine pockets is approximately spherical in frazil ice, and elongated, parallel to the growth direction, in columnar ice. The transition from sea ice to water is generally not smooth and there may not be a distinct boundary at the ice-water interface. This interface may consist of a zone of concentrated liquid brine, sea ice, and water

solution. Snow and melt water on top of the ice may mask the signals originating from underneath.

A4.6.2 Electrical Properties of Sea Ice. The electrical properties of sea ice as reported in the literature show that the complex permittivity is dependent on both temperature and brine volume. The brine volume in turn depends on salinity and temperature both of which vary with the thickness of and the vertical location in sea ice.

The dielectric constant of brine varies from 80 at 100 MHz to approximately 34 at 23 GHz (Hoestra and Cappillino, 1971). The dielectric constant of the inclusions (brine) is several times larger than the dielectric constant of the continuum (ice). The dielectric constant of sea ice, which is a mixture of ice and brine, depends on the number, size and shape of the brine inclusions and air bubbles. In general, a linear relationship seems to exist between the dielectric constant and brine volume for certain ice types. The dielectric constant has been shown to increase with brine volume or with both salinity and temperature (Hoekstra and Cappillino, 1971; Vant, 1976). In general, the imaginary part of the complex permittivity increases with salinity and temperature and indications are that it decreases with increasing frequency. An empirical relationship seems to exist between dielectric loss and brine volume for first-year ice (Hoekstra and Cappillino, 1971).

The physical properties of sea ice change significantly with time and age. These in turn determine and influence the electrical properties of sea ice. The electrical properties of pure ice and freshwater ice have been investigated by many researchers and are quite well established (Auty and Cole, 1952; Cummings, 1952; and Dorsey, 1970). The most interesting properties of pure ice are its high static dielectric constant (about 100) and its long relaxation constant (about 10^{-4} seconds (s)). Both ice and water in first approximation are described by a simple behaviour of ice and water as a function of frequency is given in Figure A4-25. For frequencies much greater than 10 KHz, the dielectric constant of ice drops to about 3.

A number of different researchers have tried to measure the dielectric properties of sea ice experimentally by means of cored samples and NaCl ice grown in the laboratory. The measurements made by Fujino (1966) were in the frequency range from 0.1 to 50 KHz in various temperature ranges. Addison and Pounder (1966) measured the electrical properties of sea ice in the frequency range from 2×10^{-5} to 100 MHz. The electrical properties of sea ice presented by Wentworth and Cohn (1964) were in the frequency range of 0.1 to 30 MHz and those presented by Addison (1969) were in the

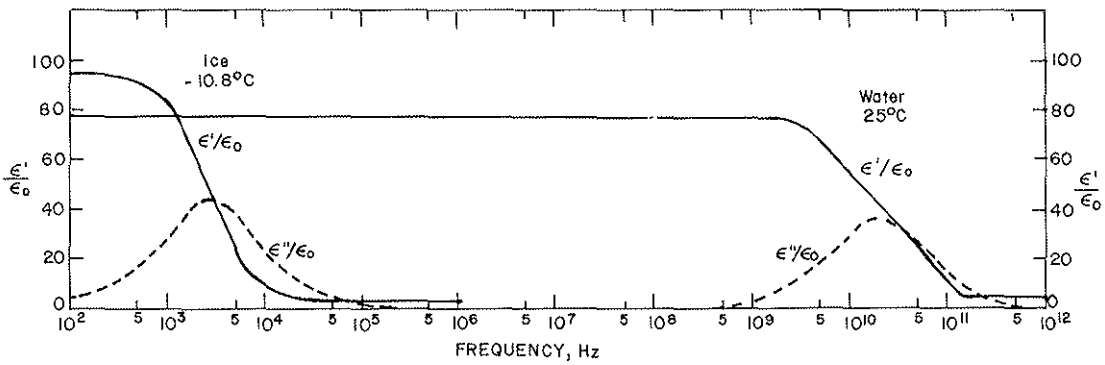

ϵ' Real part of complex permittivity

ϵ'' Imaginary part of complex permittivity

ϵ_o Permittivity of free space

FIGURE A4-25 THE DIELECTRIC BEHAVIOR OF ICE AND WATER IS A FUNCTION OF FREQUENCY (Hoekstra and Cappillino, 1971)

2×10^{-5} to 100 MHz range. Ragle et al.(1964) have quoted some electrical properties of sea ice above 100 MHz. Hoekstra and Cappillino (1971) determined the complex dielectric constant of natural sea ice and NaCl ice in the frequency range from 0.1 to 23 GHz. Byrd et al.(1972) have reported the variation of less tangent with salinity in natural sea ice at 34 GHz. Finkel'shteyn and Kutev (1972) have given values of the dielectric constant and loss without reporting the temperature. The dielectric properties of freshwater ice and sea ice at 10 and 25 GHz have been reported by Vant et al.(1974). A review of the measurements made by different workers, and a combined empirical and theoretical study of the dielectric properties of sea ice over the frequency range 0.1 to 40 GHz, were presented by Vant (1976). Vant has also reported discrepancies in measurements made by other researchers and has attributed these largely to the use of artificial as opposed to natural saline ice. It has been discovered by a number of investigators that sea ice is an anistropic material in which both attenuation and velocity are strongly dependent on the direction of propagation of the radio waves (Finkel'shteyn and Kutev, 1972).

A review of the dielectric properties of ice and snow was presented by Evans (1965). It was shown that the value of the permittivity is dependent on snow density and water constant. The real part of the permittivity at high frequencies for dry fluffy snow is about 2. The values of 1.2 for dry fluffy snow and 1.8 for dense snow were given by Mendel'son et al.(1972). A review of the dielectric properties of ice, snow and water at microwave frequencies was given by Royer (1973). The relative dielectric constant, ε'_r, of sea ice for spherically shaped inclusion particles was given by Hoekstra and Cappillino (1971) as:

$$\varepsilon'_r = \frac{\varepsilon'_{rp}}{1 - 3v_b}$$

where ε'_{rp} = relative dielectric constant of pure ice,
$\simeq 3.$

v_b = brine volume,
$$\simeq S\left|\left(\frac{49.185}{T}\right) + 0.532\right| \times 10^{-3}, \quad -0.5^{\circ} \geq T \geq -229.9^{\circ}C$$

S = salinity in parts per thousand,

T = absolute value of ice temperature in $^{\circ}C$.

The equation for brine volume was given by Frankenstein and Garner (1967) and was based on model by Weeks and Assur (1969). More exact equations were given by Frankenstein and Garner (1967) and by Stogryn (1971) for a slightly modified model. Both the models assume cylindrical, vertical brine pockets in an ice matrix.

By using various mixture formulae, Poe et al.(1972) have computed the values of the real and imaginary part of the complex permittivity of sea ice as a function of frequency, salinity, and temperature. By using these values they have also established skin depth as a function of frequency and temperature. The skin depth is of the order of the wavelength at $-10^{o}C$ for sea ice with a salinity of $2^{o}/oo$, and decreases with increasing frequency, temperature and salinity. As a result both microwave scattering and emission, which depends on the electrical properties of sea ice, are influenced by the properties of the top layer of sea ice.

Meeks et al.(1974a) have given vertically and horizontally polarized brightness temperatures as a function of snow depth. A large degree of scatter exists in the plot and no correlation can be made, tentatively suggesting that Arctic snow cover has no significant effect upon brightness temperatures when making a differentiation between ice types. This conclusion is only valid during non-melt conditions and is not applicable during summer months when free water exists within the snow cover. It was also shown that the brightness temperature is essentially independent of brine volume for multi-year ice. A linear relationship of about a $2^{o}K$ decrease in brightness temperature per one percent increase in average porosity exists, indicative of volume scattering of microwave emission taking place within multi-year ice.

A theory of microwave emission from sea ice, taking into account the vertical and horizontal variation in brine volume, was formulated by the Aerojet-General Corporation, and the theoretical results were compared with the experimental results (Poe et al, 1971 and Meeks et al, 1974). A theoretical model of microwave emission from a layer medium is developed by England (1975), which may be applicable in the case of sea ice.

A4.7 Conclusions

As is evident from the preceding, both active and passive microwave sensors are valuable tools in the study and monitoring of sea ice. The nature and characteristics of radar return and microwave emission from sea ice have yet to be fully understood and optimum operating parameters need to be established.

It appears that simultaneous use of active and passive microwave systems may provide more information about ice environment that use of one system alone.

This ability to detect and monitor oil in the ice environment will depend on how oil interacts with sea ice and behaves in such an environment and how it affects or modifies emission and scattering from sea ice in the microwave region. The main aim of this appendix has been to gather and understand all the available information about measurements of sea ice with passive and active microwave systems so as to minimize the risk of false alarm in the detection of oil.

REFERENCES

Ackley, S., W. Hibler, III, F. Kugzruk, A. Kovacs and W. Weeks, "Thickness and Roughness Variations of Arctic Multi-year Sea Ice," AIDJEX Bulletin No. 25. (July 1974).

Addison, J.R., "Electrical Properties of Saline Ice," Journal of Applied Physics, Vol. 40, No. 8, pp 3105-3114, (July 1969).

Addison, J.R., "Electrical Relaxation in Saline Ice," Journal of Applied Physics, Vol. 41, No. 1, pp 54-64, (January 1970).

Addison, J.R., and E.R. Rounder, "The Electrical Properties of Saline Ice, International Conference on Low Temperature in Science, Sapporo, Janap, Proceedings, vol. 1, Part 1, August 14-19, (1966).

Adey, A.W., R.E. Barrington, and T.R. Hartz, "Field Tests of a UHF Radiometer for Determining Sea Ice Thickness," Proceedings of the First Canadian Remote Sensing Symposium, Ottawa, pp 6, (February 1972).

Adey, A.W., "Microwave Radiometry for Remote Sensing from Aircraft and Spacecraft," Proceedings of the First Canadian Remote Sensing Symposium, Ottawa, pp 15, (February 1972).

Anderson, V.H., "High Altitude, Side Looking Radar Images of Sea Ice in the Arctic," Proceedings of the Fourth Symposium on Remote Sensing of Environment, University of Michigan, Ann Arbor, pp 847-857, (June 1966).

Anderson, V.H., "Sea Ice Pressure Ridge Study: An Air Photo Analysis," Photogrammetria, Elsevier Publishing Company, Amsterdam, (1970).

Assur, A., "Composition of Sea Ice and Its Tensile Strength, Arctic Sea Ice," N.A.S. Publication 598, Washington, pp 106-138, (1958).

Auty, R.P. and R.H. Cole, "Dielectric Properties of Ice and Solid H_2O," Journal of Chemicals Physics, Vol. 20, No. 8, pp 1039-1314, (1952).

Biache, A., Jr., C.A. Bay and R. Bradie, "Remote Sensing of Arctic Ice Environment," Proceedings of the Seventh International symposium on Remote Sensing of Environment, University of Michigan, Ann Arbor, Vol. 1, pp 523-561, (May 1971).

Bradie, R.A., SLAR Imagery for Sea Ice Studies, Photogrammetria Engineering, Vol. 33, No. 7, pp 763-766, (1967).

Byrd, R.C., M. Yerkes, W.M. Sackinger, and T.E. Osterkamp, "Millimeter Wave Reflectivity of Sea Ice, Oceans '72," IEEE International Conference on Engineering in the Ocean Environment, pp 2, (October 1972).

Campbell, W.J., P. Gloersen, W. Nordberg, and W.W. Wilheit, "Dynamics and Morphology of Beaufort Sea Ice Determined from Satellites, Aircraft and Drifting Stations," Symposium on Approaches to Earth Sciences Through Use of Scape Technology, (P. Bock.,

ed.), Konstanz, Federal Republic of Germany (23-25 May, 1973), Akademine-Verlag, pp 311-327, (1974).

Campbell, W.J., W.F. Weeks, R.O. Ramseier, and P. Gloersen, "Geophysical Studies of Floating Ice by Remote Sensing," Journal of Glaciology, Vol. 15, No. 73, pp 305-328, (1975).

Campbell, W.J., R.O. Ramseier, R.J. Weaver, and W.F. Weeks, "Skylab Floating Ice Experiment," Department of Fisheries and Environment, Ottawa, Miscellaneous Special Publication No. 34, pp 64, (1977).

Chudobiak, W.J., R.B. Gray, R.O. Ramseier, V. Makios, M. Vant, J.L. Davies, and J. Katsube, "Radar Remote Sensors for Ice Thickness and Soil Moisture Measurements," Proceedings of the Second Canadian Symposium on Remote Sensing, Guelph, Ontario, pp 418-424, (1974).

Cox, G.F.N., and W.F. Weeks, "Salinity Variations in Sea Ice," AIDJEX Bulletin No. 19, pp 1-17, (March 1973).

Cummings, W.A., "The Dielectric Properties of Ice and Snow at 3.2 cm.," Journal of Applied Physics, vol. 23, No. 7, pp 768-773, (1952).

Dorsey, N.E. "Properties of Ordinary Water Substance in all its Phases: Water Vapour, Water and all the Ices," Reinhold, New York (American Chemical Society, Nomograph Series, No. 81), (1970).

Dunbar, Moira, "A Glossary of Ice Terms (WMO Terminology)," Ice Seminar, Special Volume 10, the Canadian Institute of Mining and Metallurgy, pp 105-110, (1969).

Dunbar, M., "Interpretation of SLAR Imagery of Ice in Nares Strait and the Arctic Ocean," DREO Report No. 712, pp 33, (March 1975).

Dunbar, M., and W.F. Weeks, "Interpretation of Young Ice Forms in the Gulf of St. Lawrence using Side-looking Airborne Radar and Infrared Imagery," Cold Regions Research and Engineering Laboratory Research Report 337, pp 41, (July 1975).

Edgerton, A.T., A. Stogryn, G. Poe, "Microwave Radiometric Investigations of Snow Packs, Final Report No. 1285R-4 for U.S.G.S. Contract No. 1A-08-001-11828, Aerojet-General Corporation, Microwave Division, El Monte, California, (1971a).

Edgerton, A.T., A. Stogryn, D. Williams and G.A. Poe, "A Study of the Microwave Emission of Sea Ice," Tech. Report 1741R-1, Aerojet-General Corp, Azusa, California, pp 35, (July 1971b).

Edgerton, A.R., F. Ruskey, D. Williams, A. Stogryn, G. Poe, D. Meeks, and O. Russel, "Microwave Emission Characteristics of Natural Materials and the Environment (A Summary of Six Years Research)," Aerojet Electro Systems Co., Azusa, California, Final Technical Report No. 9016R-8, pp 171, (October 1973).

Elachi, J., and W.E. Brown, Jr., "Imaging and Sounding of Ice Fields with Airborne Coherent Radars," Journal of Geophysical Research, Vol. 80, No. 8, pp 1113-1118, (1975).

England, A.W., "Thermal Microwave Emission from a Scattering Layer," Journal of Geophysical Research, vol. 80, No. 32, (1975).

Evans, S., "Dielectric Properties of Ice and Snow - A Review," Journal of Glaciology, Vol. 5, (1965).

Farmer, L.D., "Iceberg Classification Using Side-Looking Airborne Radar, United States Coast Guard, Office of Research and Development," Applied Science Division, U.S. Coast Guard Headquarters, Washington, D.C., (May 1972).

Finkel'shteyn, M.I., and V.A. Kutev, "Probing of Sea Ice with a Sequence of Video Pulses," radio Engineering and Electronics Physics, Vol. 17, (October 1972).

Frankenstein, G., and R. Garner, "Equations for Determining the Brine Volume of Sea Ice from -0.5^{o} to -22.9^{o}C," Journal of Glaciology, Vol. 6, No. 48, pp 943-944, (1967).

Fujino, K., "Electrical Properties of Sea Ice," International Conference on Low Temperature Science, sappro, Proceedings, Vol. 1, Pt. 1, August, 14-19, (1966).

Gloersen, P., W. Nordberg, T.J. Schmugge, T.T. Wilheit, and W.J. Campbell, "Microwave Signatures of First Year and multi-Year Sea Ice," Journal of Geophysical Research, Vol. 78, No. 18, pp 3564-72, (1973a).

Gloersen, P., T.T. Wilheit, T.C. Chang, W. Nordberg, and W.J. Campbell, "Microwave Maps of the Polar Ice of the Earth," Goddard Space Flight Centre, Greenbelt, Maryland, preprint No. X-652-73-269, pp 38, (August 1973b).

Gloersen, P., T.C. Chang, T.T. Wilheit, and W.J. Campbell, "Polar Sea Ice observations by Means of Microwave Rradiometry, Proceedings of the Interdisciplinary Symposium on Advanced Concepts and Techniques in the Study of Ice and Snow Resources," Monterey, California, National Academy of Science, pp 541-550, (1974a).

Gloersen, P., R.O. Ramseier, W.J. Campbell, T.C. Chang, and T.T. Wilheit, "Variation of the Morphology of Selected Micro-Scale Test Areas During the Bering Sea Experiment," Results of the U.S. Contribution to the Joint U.S./U.S.S.R. Bering Sea Experiment, Greenbelt, Maryland, Goddard Space Flight Center, pp 104-21, (NASA X-910-74-141), (1974b).

Gloersen, P., R.O. Ramseier, W.J. Campbell, P.M. Kuhn, and W.J. Webster, Jr., "Ice Thickness Distribution as Inferred from Infrared and Microwave Remote Sensing during the Bering Sea Experiment," Results of the U.S. Contribution to the Joint U.S./U.S.S.R. Bering Sea Experiment, Greenbelt, Maryland, Goddard Space flight Centre, pp 104-121, (NASA X-910-74-141), (1974c).

Gloersen, P., T.J. Schmugge, and T.C. Chang, "Microwave Signatures of Snow, Ice and Soil at Several Wavelengths," Proceedings of the U.S.R.I. Specialist Meeting on Microwave Scattering and Emission from the Earth, Bern, Switzerland, pp 101-111, (September 1974d).

Glushkov, V.M., and V.B. Komarov, "Side-Looking Imaging Radar System TOROS and Its Application to the Study of Ice Conditions and Geological Explorations," Proceedings of

the Seventh International Symposium on Remote Sensing of Environment, University of Michigan, Ann Arbor, pp 317, (1971).

Gray, L., Cihlar, S. Parashar, and R. Worsfold, "Scatterometer Results from Shorefast and Floating Sea Ice," Proceedings of the Eleventh International Symposium on Remote Sensing of Environmennt, Ann Arbor, Michigan, vol. 1, pp 645-657, (April 1977a).

Gray, L., R.O. Ramseier, and W.J. Campbell, "Scatterometer and SLAR Results obtained over Arctic Sea Ice and Their Relevance to the Problems of Arctic Ice Reconnaissance," Proceedings of the Fourth Canadian Symposium on remote Sensing, Quebec City, pp 424-443, (May 1977b).

Hallikainen, M., "Analysis of Dielectric Properties and Noise Temperature of Sea Ice for Microwave Remote Sensing Applications," Proceedings of the European Microwave Conference, Brussels University, Vol. 2, No. C.15.3, pp 4, (September 1973).

Hengeveld, H.G., "Operation Ice Map I: Remote Sensing Trials," Transport Canada, Ottawa, (1969).

Hengeveld, H.G., "Operation Ice Map II: Side Looking Radar Trials," Canadian Department of Environment, Atmospheric Environment Science, Ottawa, (1972).

Hoekstra, P., and P. Cappillino, "Dielectric Properties of Sea ice and Sodium Chloride Ice at UHF and Microwave Frequencies," Journal of Geophysical Research, Vol. 76, No. 20, pp 4922-4931, (July 1971).

Johnson, J.D., and L.D. Farmer, "Use of Side-Looking Airbrone Radar for Sea Ice Identification," Journal of Geophysical Research, vol. 76, No. 9, pp 2138-2155, March, (1971a).

Johnson, J.D., and L.D. Farmer, "Determination of Sea Ice Drift Using Side-Looking Airborne Radar," Proceedings of the Seventh International Symposium on Remote Sensing of Environment, Ann Arbor, Michigan, pp 2155-2168, (1971b).

Kazo, Thomas L., and Orest I. Diachok, "Spatial Variability of Topside and Bottomside Ice Roughness and Its Relevance to Underside Acoustic Reflection Loss," AIDJEX Bulletin No. 19, Arctic Ice Dynamics Joint Experiment, Division of Marine Resources, University of Washington, Seattle, Washington 98105, (March 1973).

Ketchum, R.D., Jr., and S.J. Tooma, Jr., "Analysis and Interpretation of Airborne Multi-Frequency Side-Looking Radar Sea Ice Imagery," Journal of Geophysical Research, Vol. 78, No. 3, pp 520-538, (1973).

Ketchum, Jr., R.D., and A.W. Lohanick, "Passive Microwave Signatures of Sea Ice Features," Naval Ocean Research and Development Activity (NORDA), NSTL Station, Mississippi, NORDA Technical Note 9, pp 16, (September 1977).

Ling, Chi-Hai Norbert Untersteiner, "On the Calculation of the Roughness Parameter of Sea Ice," AIDJEX Bulletin No. 23, (January 1974).

Loshchilov, V.S., and V.A. Voyevodin, "Determination of Elements of Ice Cap Drift and Movement of Ice Edges by Means of the Airborne Side Scan Radar TOROS," Problems in Arctic and Antarctica, Vol. 40, pp 23-30, (1972).

McNeil, D., and P. Hoekstra, "In-situ Measurements on the Conductivity and Surface Impedance of Sea Ice at VLF," Radio Science, Vol. 8, No. 1, pp 23-31, (January 1973).

McQuillan, A.K. and D.J. Clough, "Benefits of Remote Sensing Systems to Petroleum Operations in Canadian Ice-Infested Waters," Proceedings of the Third Canadian Symposium on Remote Sensing, Edmonton, Alberta, (1975).

Meeks, D.C., G.A. Poe, and A.T. Edgerton, "Surface-Based Passive Microwave Measurements of Sea Ice During the 1972 AIDJEX Program," Final Tech. Report 174R-1, Contract No. 607476, Aerojet Electro Systems Company, Azusa, (1972).

Meeks, D.C., G.A. Poe, and R.O. Ramseier, "A Study of Microwave Emission Properties of Sea Ice - AIDJEX 1972," Aerojet Electro Systems Co., Azusa, California, Final Report 1786 FR-1, pp 103, (January 1974a).

Meeks, D.C., R.O. Ramseier, and W.J. Campbell, "A Study of Microwave Emission Properties of Sea Ice - AIDJEX 1972," Proceedings of the Ninth International Symposium on Remote Sensing of Environment, Ann Arbor, Michigan, Vol. I, pp 307-322, (April 1974b).

Mendel'son, V.L., A.I. Kozlov, and M.I. Finkel'shteyn, "Some Electrodynamics Models of Ice Sheets, Useful in Radar Sounding Problems," Atmospheric and Ocean Physics, Vol. 8, No. 4, pp 225-229, (1972).

Morra, R.H.J., and G.P. deLoor, "Ice Detection by SLAR," Winter Navigation Research Board, Swedish Administration of Shipping and Navigation, Finnish Board of Navigation, Sea Ice - 75, Research Report, No. 16:3, pp 31, (1976).

Murphy, E.J. "The Temperature Dependence of the Relaxation Time of Polarizations in Ice," Transactions of the Electro-chemical Society, Vol. 65, pp 133-142, (1934).

Onstott, R.G., G.J. Dome, R.A. Hand, J. Hague, H. Pape, and R.K. Moore, "Backscatter Properties of Sea Ice with Radar," Arctic Operations Descriptions and Preliminary Data Summary, The University of Kansas Centre for Research, Inc., Lawrence, Kansas, Remote Sensing Laboratory RSL T' 331-1, pp 150, (October 1977).

Parashar, S.K., "Investigation of Radar Discrimination of Sea Ice," (Ph. D. Dissertation), University of Kansas Centre for Research, Inc., CRES Technical Report 185-13, pp 403, (May 1974).

Parashar, S.K., A.W. Biggs, A.K. Fung, and R.K. Moore, "Investigation of Radar Discrimination of Sea Ice," Proceedings of the Ninth Symposium on Remote Sensing of Environment, Ann Arbor, Michigan, Vol. 1, pp 323-332, (April 1974).

Parashar, S.K., "State of the Art - Radar Measurement of Sea Ice," University of Kansas Centre for Research, Inc., Lawrence, Kansas, Remote Sensing Laboratory, RSL Technical Report 291-1, pp 42, (December 1975).

Parashar, S.K., "State of the Art - Radar Measurement of Icebergs," University of Kansas Centre for Research, Inc., Lawrence, Kansas, Remote Sensing Laboratory, RSL Technical Report 291-2, pp 8, (January 1976a).

Parashar, S.K., "Analysis of Sea Ice - 75 SLAR Data," Winter Navigation Research Board, Swedish Administration of Shipping and Navigation, Finnish Board of Navigation, Sea Ice - 75, Research Report No. 16:4, pp 65, (April 1976b).

Parashar, S.K., R.M. Haralick, R.K. Moore, and A.W. Biggs, "Radar Scatterometer Discrimination of Sea Ice Types," IEEE Transactions on Geoscience Electronics, Vol. GE-15, No. 2, (1977a).

Parashar, S.K., B.R. Dawe, and R.D. Worsfold, "Evaluation of Potential Sea Ice Thickness Measuring Techniques - Development of a Resmote Sea Ice Thickness Sensor - Phase I, C-CORE report 77-6, pp 84, (December 1977b).

Parashar, S.K., A.K. Fung, and R.K. Moore, "A Theory of Wave Scatter from an Inhomogeneous Medium with a Slightly Rough Boundary and its Application to Sea ice," Remote Sensing of Environment, Vol. 7, No. 1, pp 37-50, (1978).

Poe, G., A. Stogryn, and A.T. Edgerton, "A Study of the Microwave Emission Gharacteristics of Sea Ice," Aerojet Electro Systems Co., Azusa, California, Report No. 1749R-2, pp 141, (September 1972).

Ragle, R.H., R.B. Blair, and L.E. Persson, "Ice Core Studies of Ward Hunt Ice Shelf, 1960," Journal of Glaciology, Vol. 5, No. 37, pp 39-59, (1964).

Ramseier, R.O., P. Gloersen, and W.J. Campbell, "Variation in the Microwave Emissivity of Sea Ice in the Beaufort and Bering Sea," Specialist Meeting on Microwave Scattering and Emission from the Earth (E. Schanda, ed.), Proceedings of the URSI Commission II, Institute of Applied Physics, University of Bern, Switzerland, pp 87-93, (1974).

Rouse, J.W., Jr., "Arctic Ice Type Identification by Radar," Proceedings of the IEEE, Vol. 57, No. 4, pp 605-611, (April 1969).

Royer, G.M., "The Dielectric Properties of Ice, Snow and Water at Microwave Frequencies and the Measurement of the Thickness of Ice and Snow Layers with Radar," Communication Research Centre, (CRC) Report No. 1242, Department of Communications, Ottawa, (June 1973).

Schmugge, T., T.T. Wilheit, P. Gloersen, M.F. Meier, D. Franks, and I. Dirmhirn, "Microwave Signatures of Snow and Fresh Water Ice," NASA Goddard Flight Centre, Greenbelt, Maryland, Report X-652-73-335, pp 12, (1973).

Stnogryn, A., "Equations for Calculating the Dielectric Constant of Saline Water at GHz Frequencies," IEEE Transactions on Microwave Theory and Techniques, Vol. 19, No. 8, pp 733-736, (1971).

Thompson, T.W., R.J. Bishop, and W.E. Brown, "Progress Report on 25 cm Radar Observations of the 1971 AIDJEX Studies," Arctic Ice Dynamics Joint Experiment (AIDJEX), Division of Marine Resources, University of Washington, Seattle, Washington, AIDJEX Bulletin No. 12, pp 1-15, (February 1972).

Tiuri, M., M. Hallikainen, and K. Kaski, "Experiments on Remote Sensing of Sea Ice Using a Microwave Radiometer," Proceedings of the URSI Specialist Meeting on Microwave Scattering and Emission from Earth, Berne, Switzerland, pp 95-100, (September 1974).

Tiuri, M., M. Hallikainen, and A. Laaperi, "Remote Sensing of Sea Ice by Microwave Radiometry," Sahko, vol. 50, No. 4, pp 149-152, (April 1977).

Tooma, S.G., R.A. Mennilla, J.P. Hollinger, and R.D. Ketchum, Jr., "Comparison of Sea Ice Type Identification between Airbrone Dual-Frequency Passive Microwave Radiometry and Standard Laser/Infrared Techniques," Journal of Glaciology, vol. 15, No. 73, pp 225-239, (1975).

United States Coast Guard, "Data Reduction of Airborne Sensor Records," Report No. DOT-CT-01-800-A, Department of Transportation, Office of Research and Development, Washington, D.C. 20591, pp 196, (July 1970).

United States Coast Guard, "Interpretation of Winter Ice Conditions from SLAR Imagery," Report No. DOT-CT-14486-1A, Department of Transportation, Office of Research and Development, Washington, D.C. 20591, pp 100, (February 1972b).

United States Coast Guard, "Analysis of SLAR Imagery of Arctic and Lake Ice," Report No. DOT-CG-14486-A, Department of Transportation, Office of Research and Development, Washington, D.C. 20591, pp 169, (July 1972a).

Vant, M.R., R.B. Gray, R.O. Ramseier, and V. Makios, "Dielectric Properties of Fresh and Sea Ice at 10 and 35 GHz," Journal of Applied Physics, Vol. 45, No. 11, pp 4712-4717, (1974).

Vant, M.R., "A Combined Empirical and Theoretical Study of the Dielectric Properties of Sea Ice over the Frequency Range 100 MHz to 50 GHz," PhD Thesis, Carleton University, Ottawa, pp 470, (June 1976).

Vickers, R.S., J. Heighway, and R. Gedney, "Airborne Profiling of Ice Thickness using a Short Pulse Radar," In Advanced Concepts and Techniques in the Study of Snow and Ice Resources, (H.S. Santeford and J.L. Smith, eds.), National Academy of Science, pp 422-431, (1973).

Waite, W.P., and H.C. MacDonald, "Snowfield Mapping with K-band Radar in Short Course," Radar Remote Sensing for Geoscientists, University of Kansas, Lawrence, Kansas, pp 5.4-1 -5.4-26, (1971).

Welder, E., R.D. Worsfold, B. Roberts, and R. Miller, "Ice Characteristization Ground Truth Report," Twillingate, Newfoundland, Project SAR '77, Field Data Report No. 3, C-CORE Publication No. 77-32, (July 1977).

Weeks, W.F., and A. Assur, "Fracture of Lake and Sea Ice," Research Report 269, Cold Regions Research and Engineering Laboratory, Hanover, New Hampshire, (September 1969).

Weeks, W.D., Hibbler III., and S.F. Ackley, "Sea Ice: Scales, Problems and Requirements," Interdisciplinary symposium on Advanced Concepts and Techniques in the Study of Snow and Ice Resources, Monterey, California, (December 1972).

Wentworth, F.L., and M. Cohn, "Electrical Properties of Sea Ice at 0.1 to 30 M c/s," Radio Science, Journal of Research, NBS/USNC-USRI, Vol. 68D, No. 6, pp 681-691, (June 1964).

Wilheit, T.T., W. Nordberg, J. Blinn, W.J. Campbell, and A.T. Edgerton, "Aircraft Measurements of Microwave Emission from Arctic Sea Ice," Remote Sensing of Environment, Vol. 2, No. 3, pp 129, (1972).

Worsfold, R.D., D. Strong, and E. Wedler, "Project SAR '77," Proceedings Fourth International Conference on Port and Ocean Engineering Under Arctic Conditions, Memorial University of Newfoundland, St. John's, Newfoundland, pp 1051-1063, (1977).

Zagorodnikov, A.A., V.S. Loshchilov, and K.B. Chelyshev, "Two-Dimensiontal Statistic Analysis of Radar Imagery of Sea Ice," Proceedings of the Eighth International Symposium on Remote Sensing of Environment, University of Michigan, Ann Arbor, Vol. I, (1972).

APPENDIX 5

APPENDIX 5 - MICROWAVE EMISSION AND SCATTERING FROM OIL ON WATER

A5.1 INTRODUCTION

The detection of oil slicks on the sea surface is made possible through the interaction of electromagnetic radiation with the air - oil and oil - water boundaries. The two interface reflections interact to produce additive and subtractive electromagnetic interference values for an active microwave system. Additive signals are received when reflections from the air - oil interface. Subtractive interference occurs when these reflections are 180 degrees out of phase resulting in the reduction of signal amplitude. The oscillations, thus produced, approach a sine wave configuration that can be associated with oil thickness on a quarter wavelength basis. For a passive microwave system, the signal is entirely generated by the oil/water system. The occurrence of constructive and destructive emission levels should make it possible to determine oil thickness on water to at least a fraction of a wavelength. However, in spite of the above mentioned analytical basis, the relationships between the scattering and emission values and the type and thickness of oil have not been well established.

There are two mechanism by which the presence of oil on a water surface may be detected. Both of these mechanisms create anomalies in the microwave emission and radar scattering when oil is present. It is the presence of these local anomalies in the relatively uniform background of the surface that signifies the detection of oil pollution. The first mechanism is the smoothing effect of oil which reduces the ocean surface roughness, thus reducing emissivity and increasing specular reflection. It is felt that this is the primary detection mechanisms for thin oil films in other than flat calm seas. The second mechanism is the direct change in the emission and scattering of a water surface due to the presence of oil. Oil, in general, has a larger value of emissivity than that of a calm ocean and a smaller reflection coefficient value. This is due to oil having a lower dielectric constant (~2) than that of water (~49) at micro-wavelengths. The second phenomena is slightly the weaker of the two, but offers the promise of measuring oil thickness. The above mechanism affect the emission or scattering in two opposite and unequal ways, and are independent of each other.

A5.2 Emissivity and Brightness Temperature

A5.2.1 Flat Surface Conditions (Laboratory Experiments and Theory). The emissivity of petroleum oils in the microwave region has been found to be typically around

0.8 while water has an emissivity of about 0.4 (Van Kuilenburg, 1975). Many researchers have undertaken studies of the brightness temperature, which is directly proportional to the emissivity, as can be seen by the following equations (Meeks et al, 1971):

$$T_b = E_m T_o + (1 - E_m) T_s \quad \text{----------(A5-1)}$$

where E_m is the microwave emissivity;

T_o is the surface (oil) thermometric temperature; and

T_s is the temperature characterizing the sky radiation incident on the surface.

The equations relating the emissivity to the dielectric properties of a layered medium are given in Appendix 2. The parameters of equation A5-1 are dependent on surface roughness, frequency, incidence angle, and whether vertical or horizontal polarization is observed.

The Aerojet General Corporation undertook extensive combined theoretical and experimental studies of the emissive properties of petroleum oils. Edgerton and Trexler (1970) conducted one of these studies at 13.4 and 37 GHz. Their relevant conclusions are:

(a) The microwave brightness temperature of an oil film is inversely proportional to sensor wavelength.

(b) Minimum detectable oil film thickness on a calm water surface using the 37 GHz microwave radiometer was of the order of 0.1 to 0.3 mm.

(c) The horizontally polarized signatures were more responsive to oil film than the vertically polarized component.

(d) All oil film signatures were positive (radiometrically warmer than unobscured water) for specular water surfaces.

(e) Antenna viewing angles at 30 to 45^{o} from nadir afford best all-around sensor performance.

(f) Microwave signatures observed in the laboratory increase with increasing film thickness.

Figures A5-1 to A5-4 summarize their brightness temperature results for varying viewing angles, thicknesses, and two frequencies using horizontal polarization. The effect of aging and the difference occurring between day and night observations are shown. Figures A5-5 and A5-6 are examples of the emissivity values versus incidence angles for various film thicknesses, calculated from complex permittivities measured in

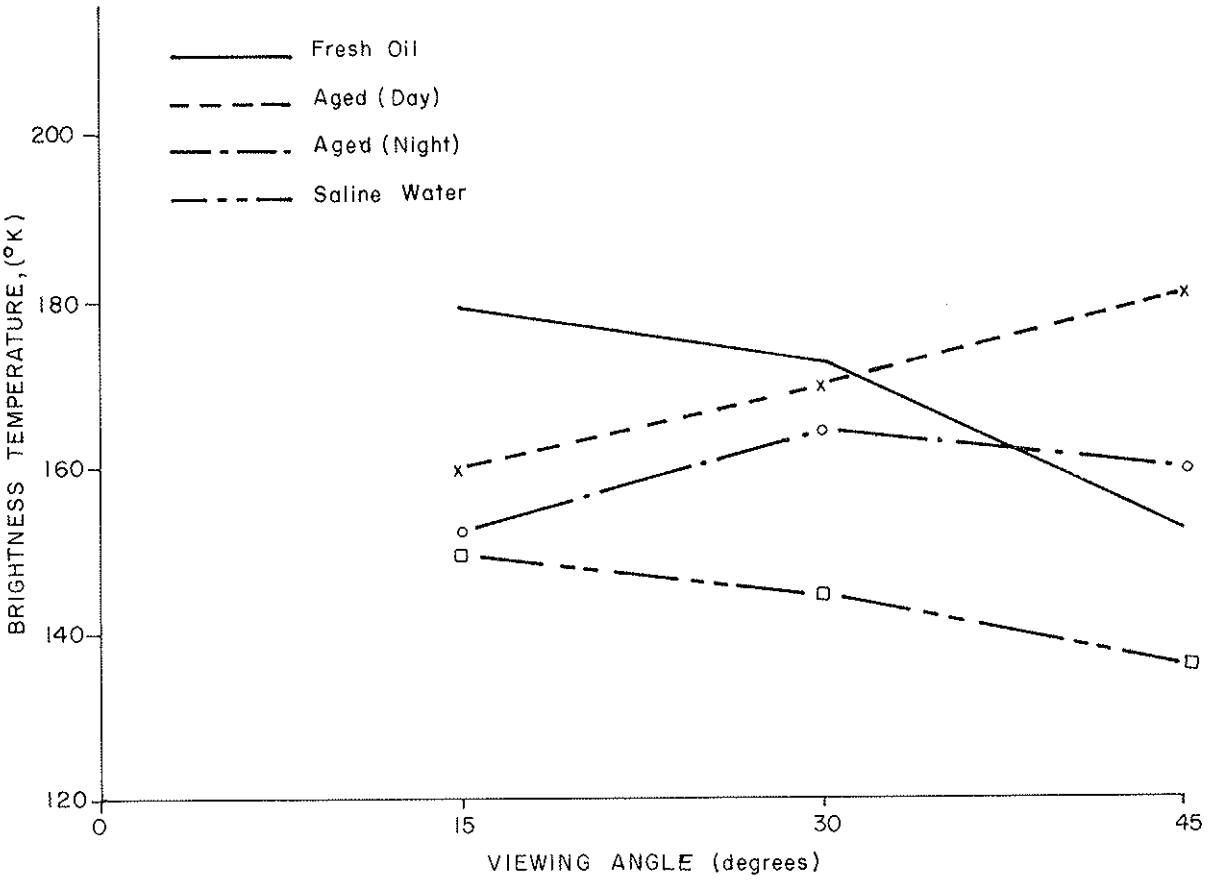

FIGURE A5-1 0.8 cm HORIZONTAL POLARIZATION BRIGHTNESS TEMPERATURE FOR FRESH 20 API GRAVITY CRUDE OIL, AGED 20 API GRAVITY (Day & Night) AND SALINE WATER (Edgerton and Trexler, 1970).

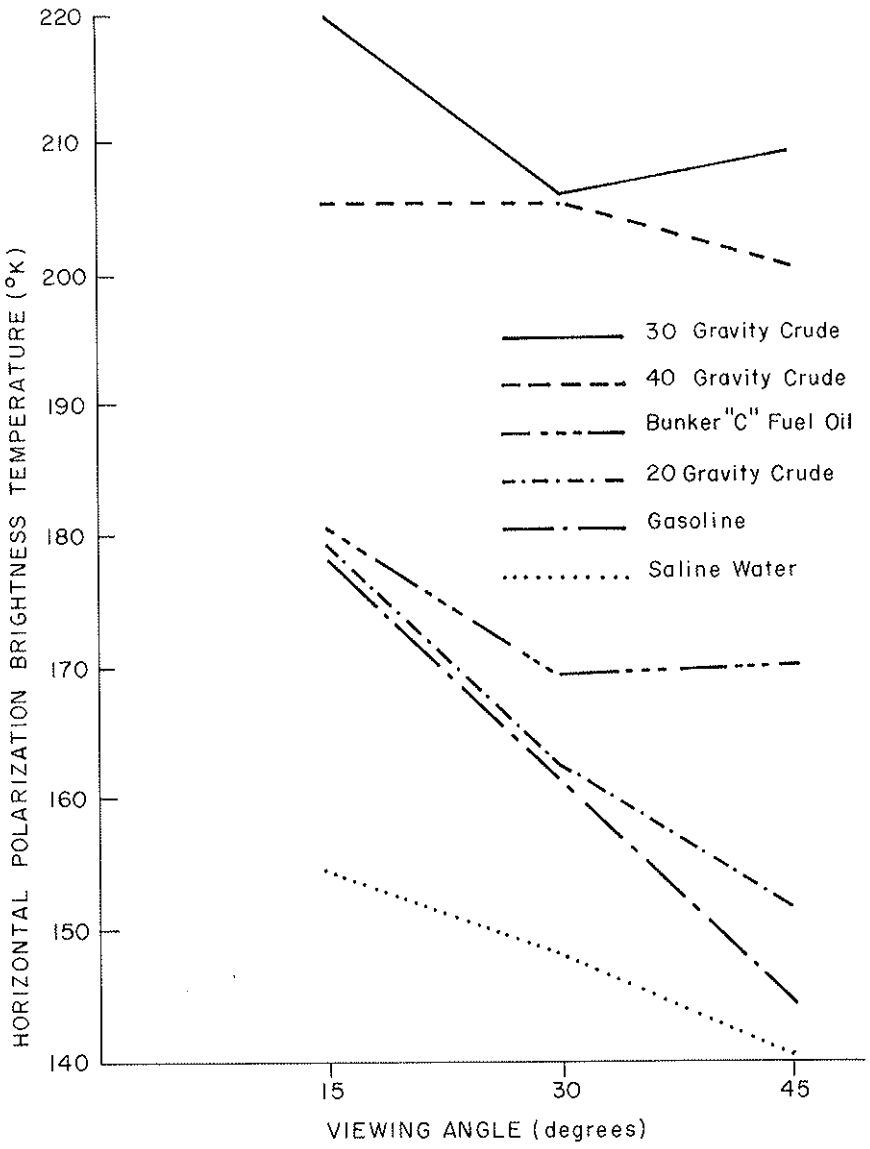

FIGURE A5-2 0.8 CM HORIZONTAL POLARIZATION BRIGHTNESS TEMPERATURE FOR POLLUTANTS USED IN LABORATORY MEASUREMENT PHASE (Edgerton and Trexler, 1970).

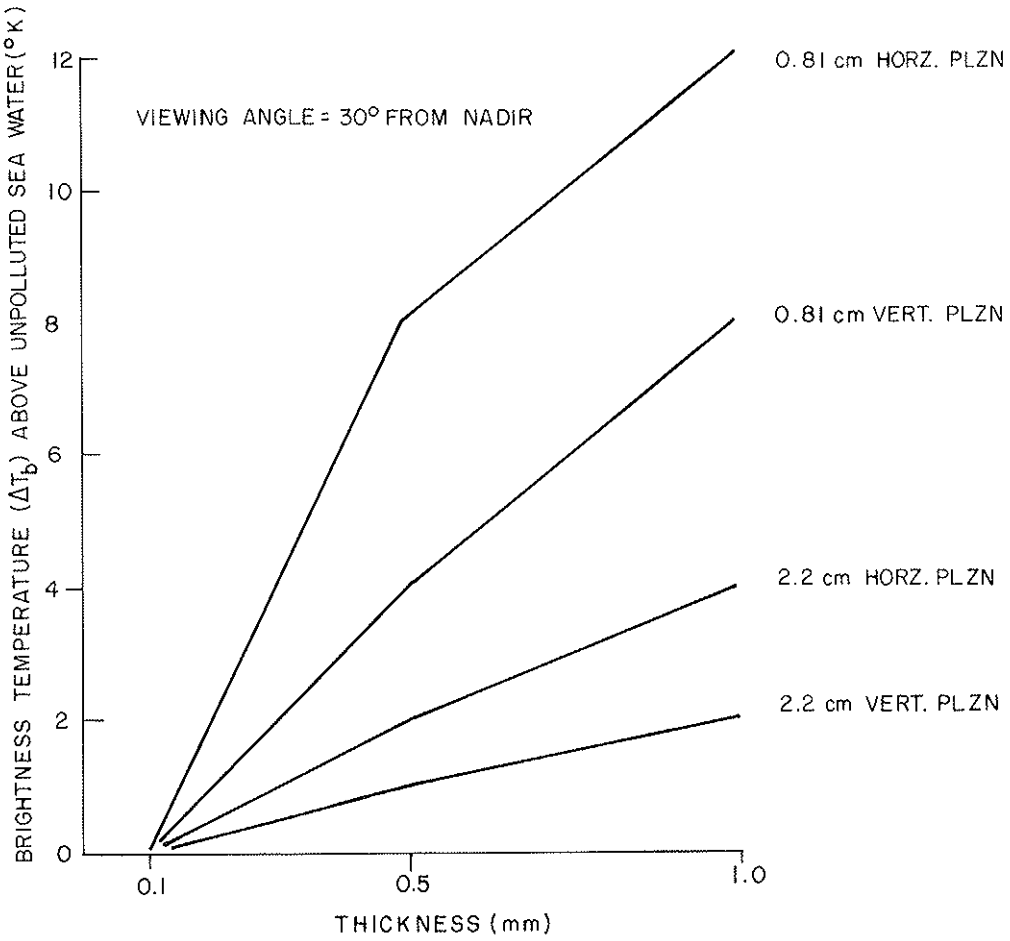

FIGURE A5-3 RELATIVE RESPONSE OF 0.81 cm AND 2.2 cm BRIGHTNESS TEMPERATURE TO GASOLINE FILM THICKNESS (Edgerton and Trexler, 1970).

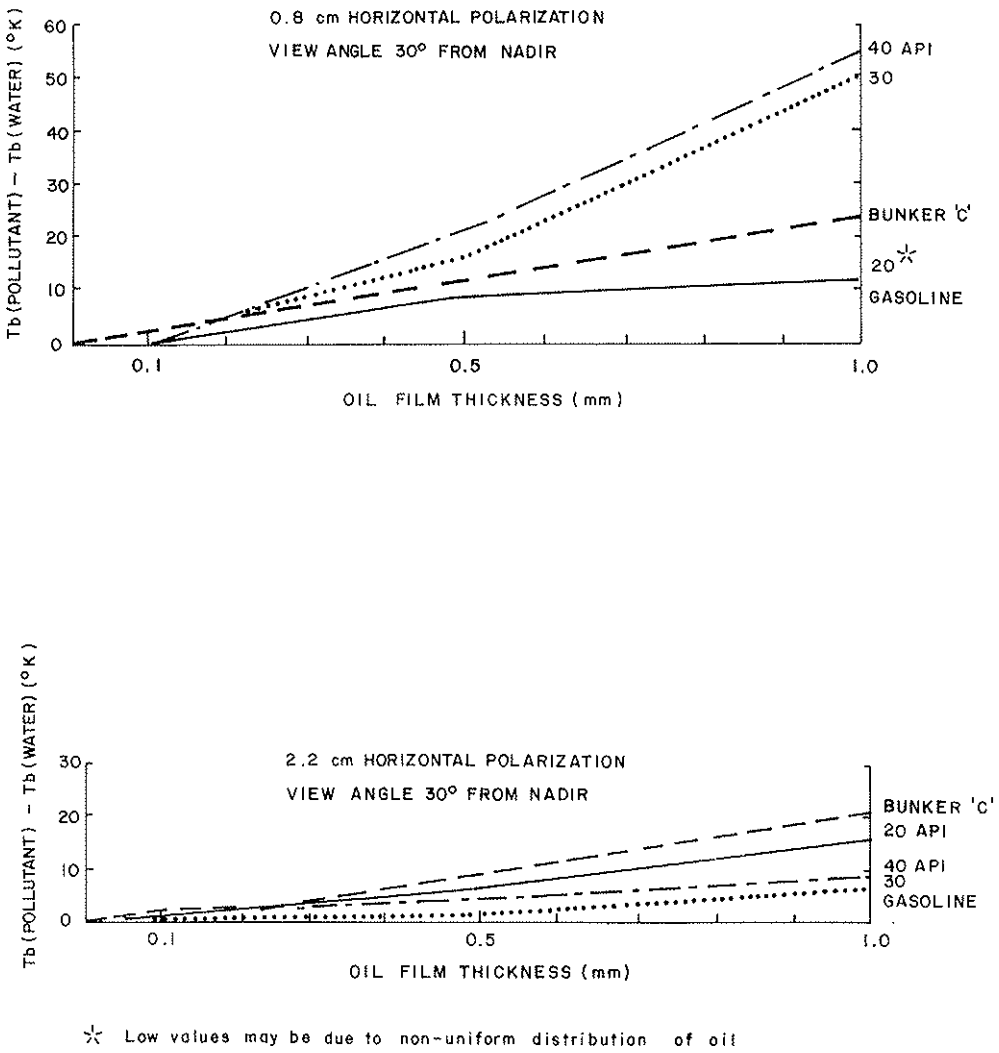

FIGURE A5-4 SUMMARY OF MICROWAVE RESPONSE TO PETROLEUM SAMPLES EXAMINED DURING LABORATORY EXPERIMENTS (Edgerton and Trexler, 1970).

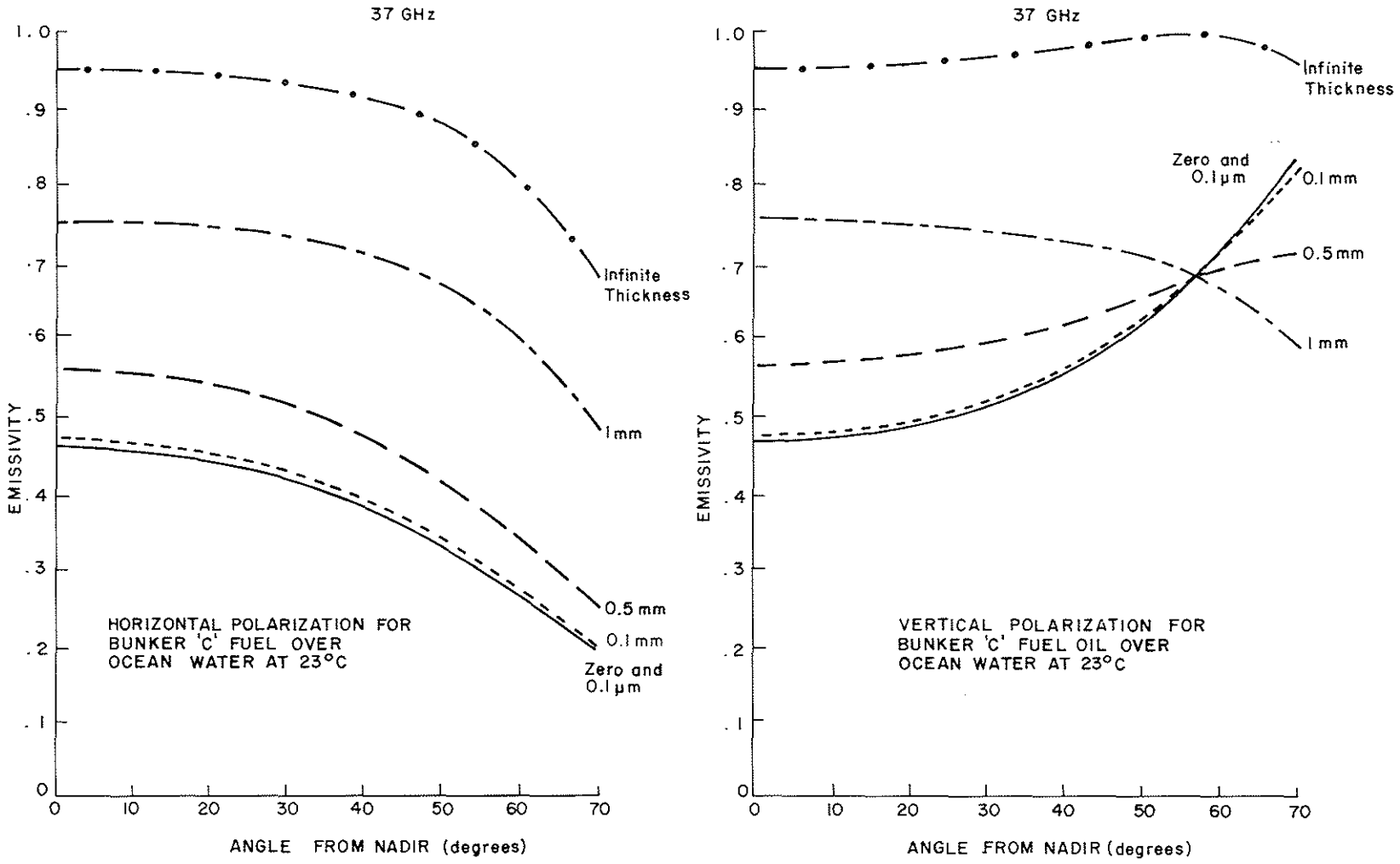

FIGURE A5-5 (Edgerton and Trexler, 1970)

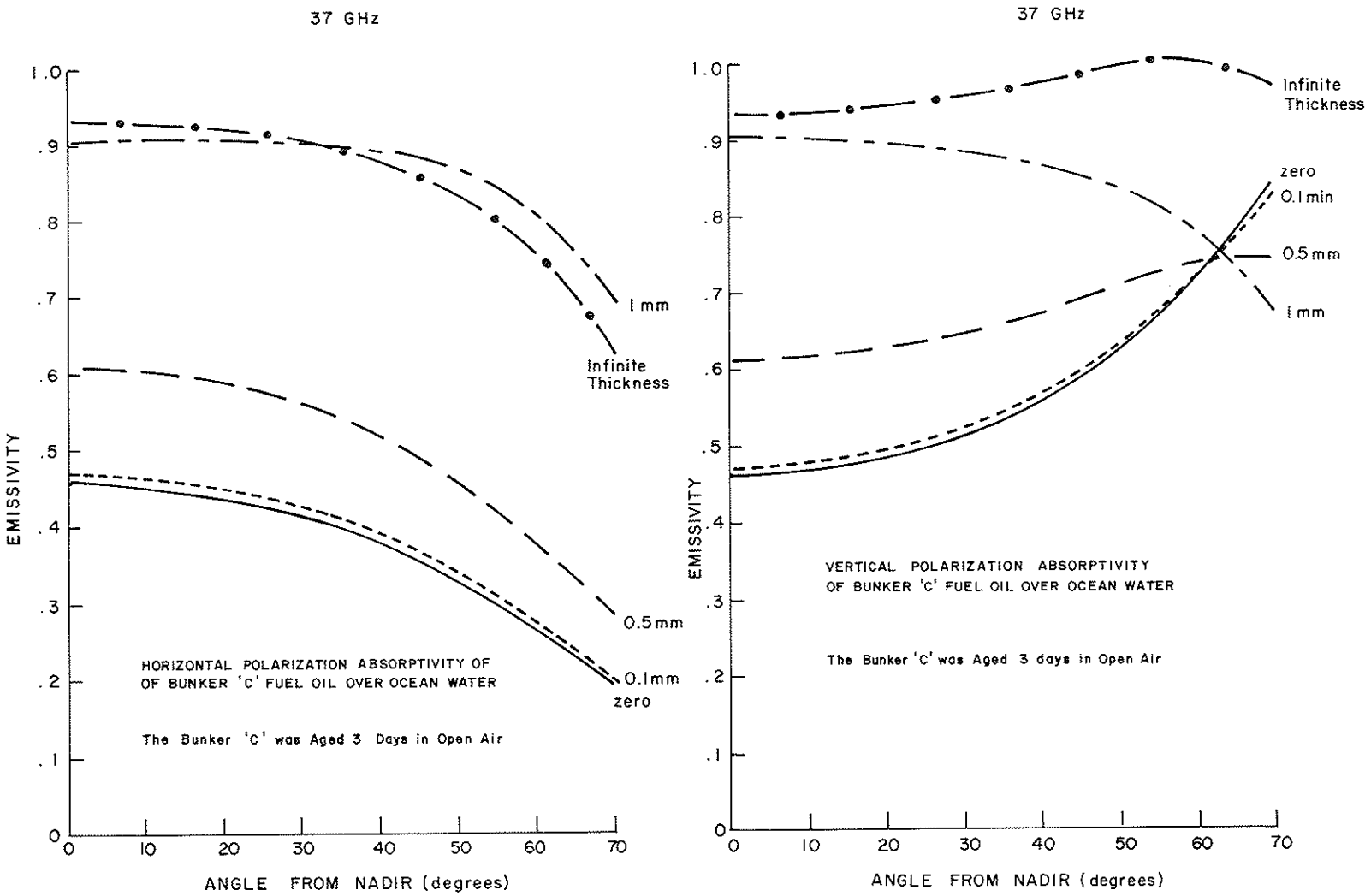

FIGURE A5-6 (Edgerton and Trexler, 1970)

the study. All "fresh" oils displayed almost exactly the same characteristics theoretically as Figure A5-5. The effect of "aging" is demosntrated in Figure A5-6 for bunker "C" crude oil.

Meeks et al.(1971), also with Aerojet General, undertook a further study of the emissive properties, using the previous study and theoretical calculations they derived Figures A5-7 to A5-11, showing the effect of incidence angle, polarization and sensor wavelength on the brightness temperature for increasing oil film thickness. The oscillatory effect is a result of the sinusoidal term, $e^{2i\Psi t}$, in the emissivity equation. From Figure A5-7, it can be seen that for vertical polarization, at an incidence angle of about 55^{o}, the emissivity is independent of oil slick thickness. Meeks et al.(1971) made the following relevant conclusions based on laboratory and field work:

(a) Oil slicks on the ocean surface provide unique and readily measurable signatures.
(b) The microwave emission characteristics of oil slicks vary with oil type and film thickness. The mass of oil per unit area is the parameter of most importance.
(c) Both theory and measurements demonstrate that horizontally polarized sensors are more responsive to oil film than vertically polarized sensors.
(d) The microwave brightness temperature signatures of oil slicks increase with sensor frequency.

Meeks et al.(1971) also noted a couple of discrepancies between theory and the actual experimental data. A large value for thickness calculations was always obtained when the vertical brightness temperature anomally is used as a basis for measuring slick thickness. They noted that it was probably due to disagreement in the theoretical and actual sky temperature values, which at the wavelength used, can be substantial. Any deviation from the standard atmospheric conditions could cause such an error. The oscillation of the brightness temperature with oil thickness only agreed in general with theory. This was due to uneven spreading of the oil and the fact that the ocean surface was not perfectly flat.

Hollinger (1974), undertook a detailed study of the microwave radiometric properties of petroleum oils at 19.36, 31.0 and 69.8 GHz. Figure A5-12 shows the typical brightness temperature variation with the angle of incidence for various oil thicknesses and both polarizations. Note that the curves are almost exactly the same in shape as those found by Aerojet General for different frequencies and oil types. Figures A5-13 and A5-14 demonstrate the effect of varying the real and imaginary parts of the complex permittivity, respectively. Decreasing the former reduces the brightness temperature and

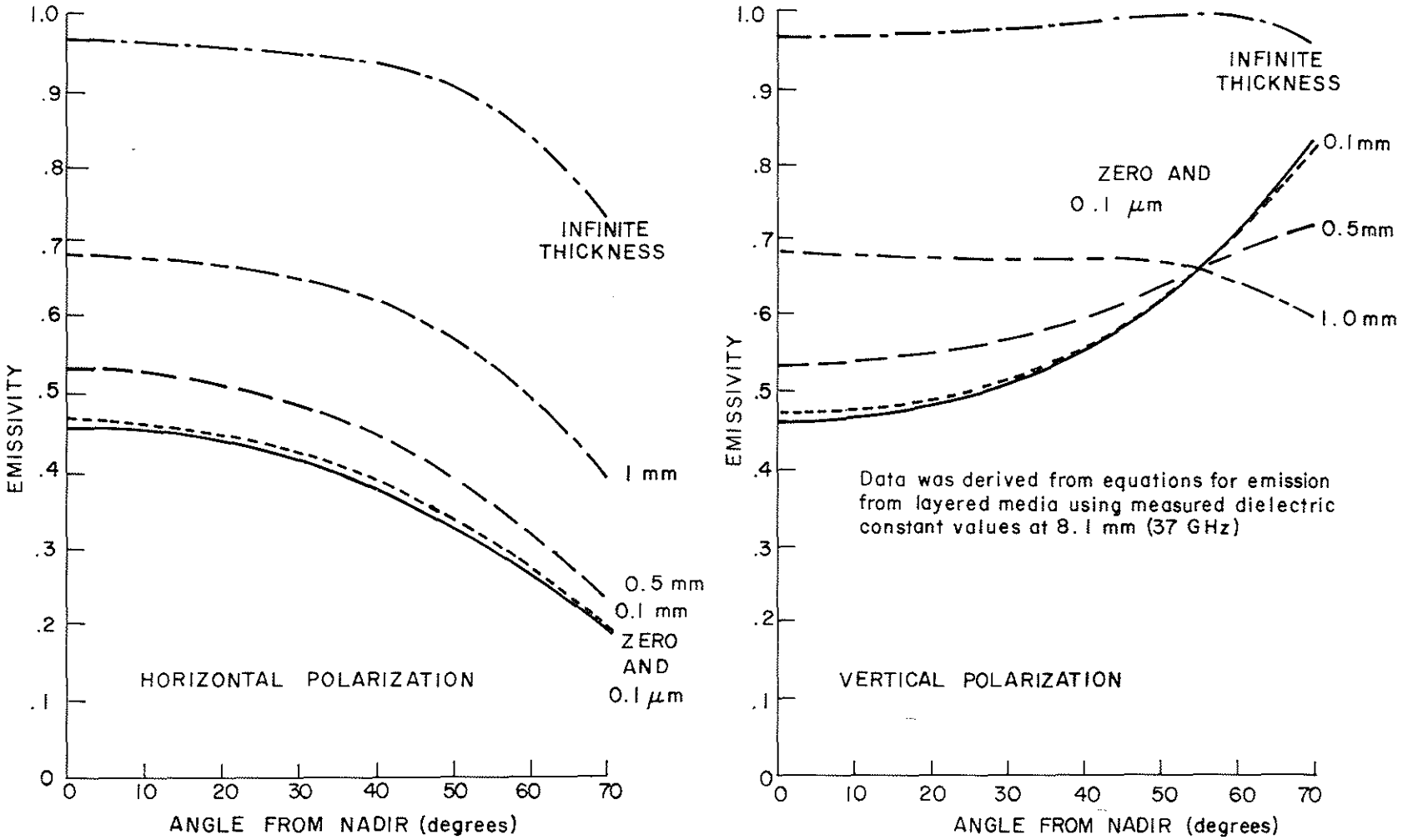

FIGURE A5-7 GRAPHS SHOWING EMISSIVITY VERSUS VIEW ANGLE FOR 30 API GRAVITY CRUDE OIL OVER FLAT OCEAN WATER. THERMOMETRIC WATER TEMPERATURE 296°K (Meeks et al, 1971).

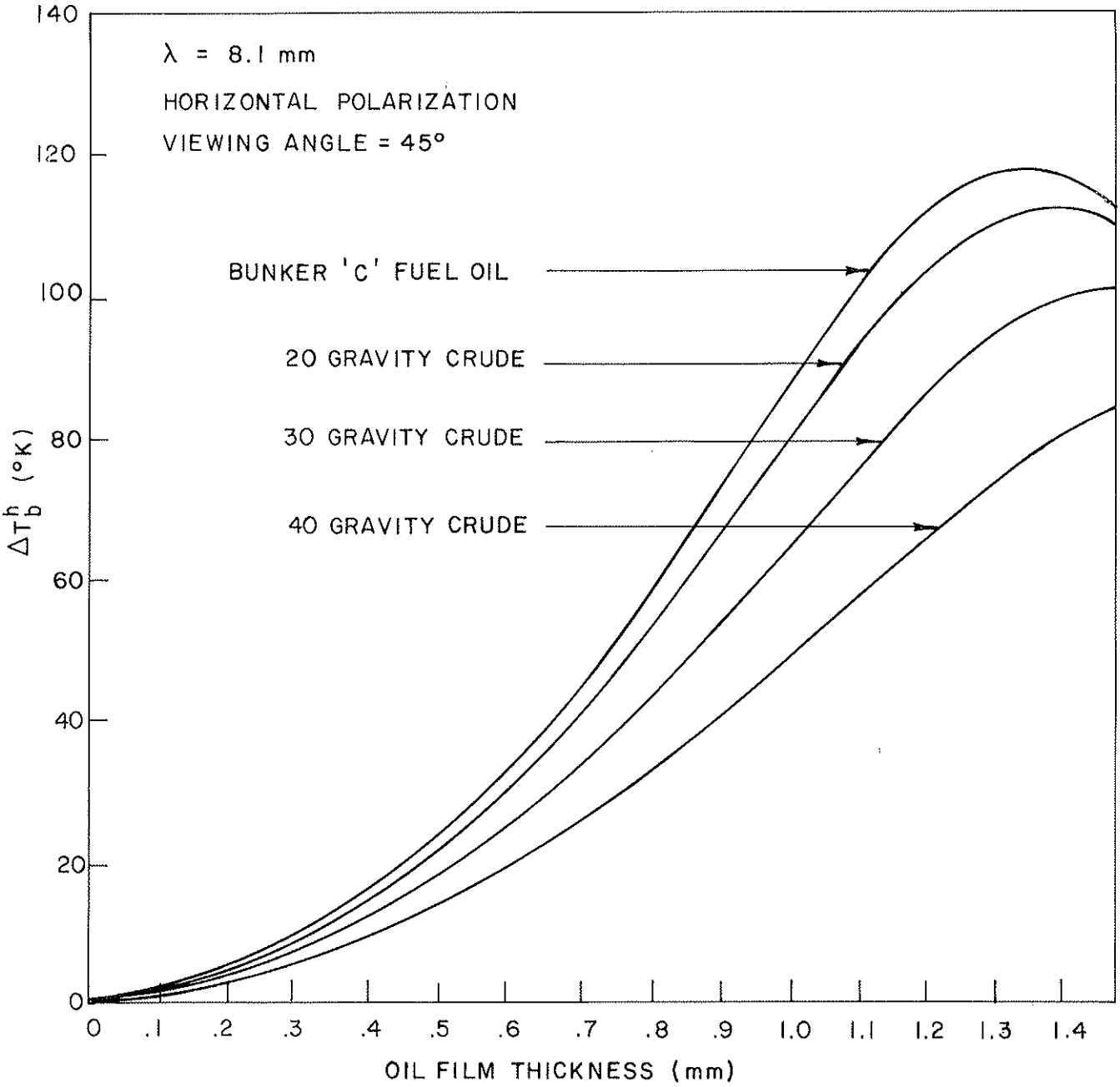

FIGURE A5-8 HORIZONTAL BRIGHTNESS TEMPERATURE INCREASE, ΔT_b^h, VERSUS OIL FILM THICKNESS AT 8.1 mm WAVELENGTH. FLAT WATER SURFACE (Meeks et al, 1971).

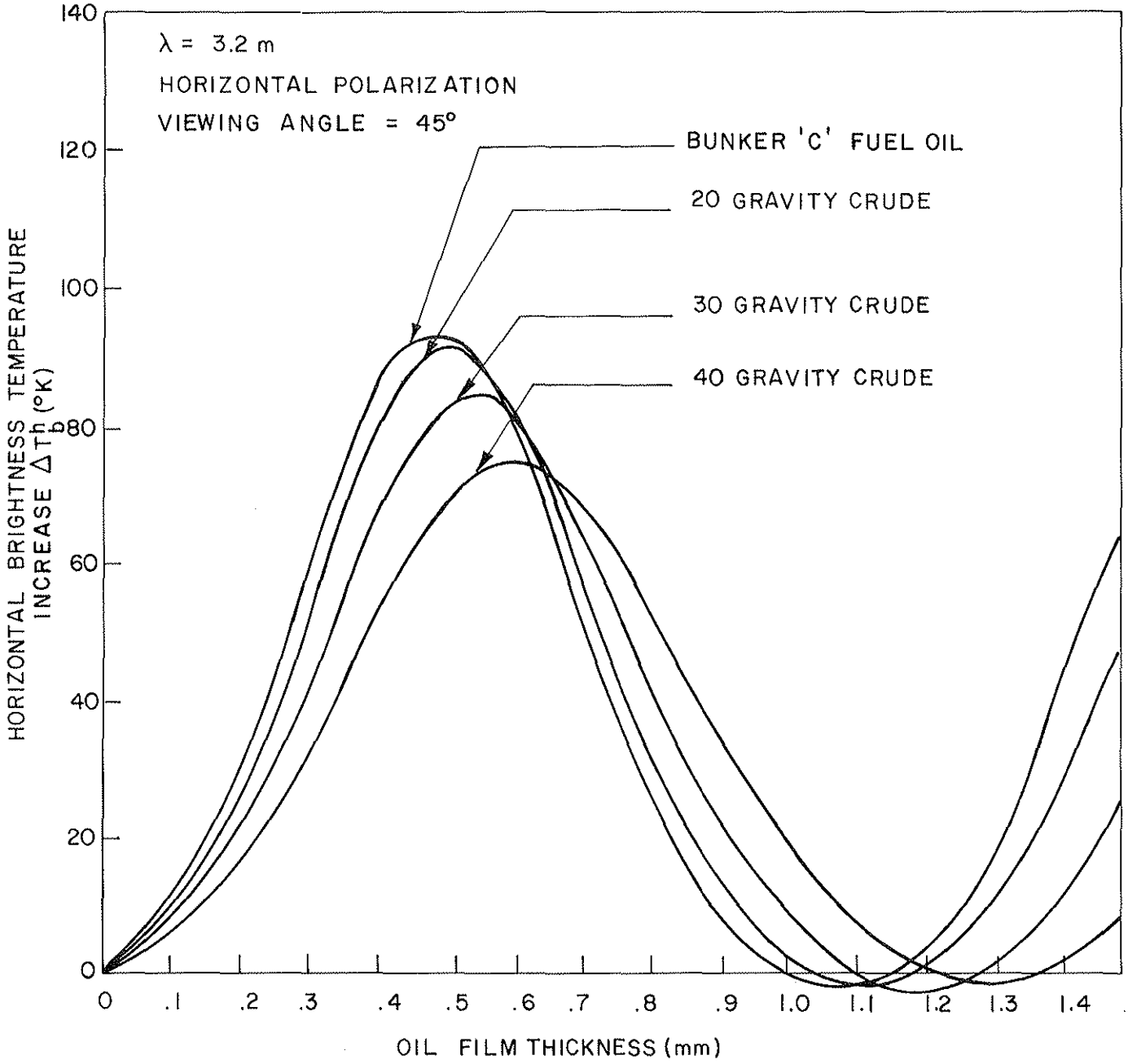

FIGURE A5-9 HORIZONTAL BRIGHTNESS TEMPERATURE INCREASE, ΔT_b^h, VERSUS OIL FILM THICKNESS AT 3.2 mm WAVELENGTH. FLAT WATER SURFACE. (Meeks et al, 1971).

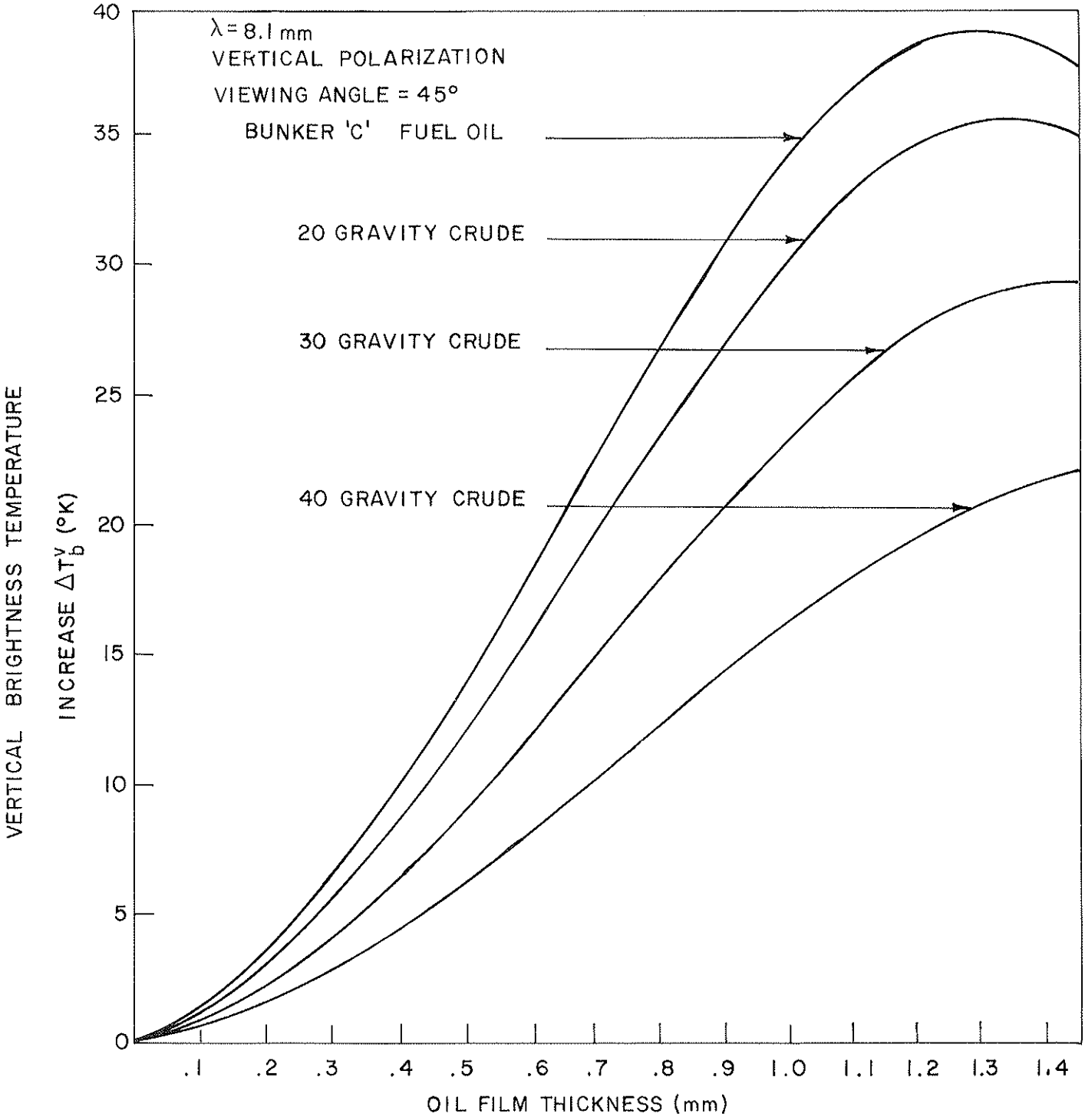

FIGURE A5-10 VERTICAL BRIGHTNESS TEMPERATURE INCREASE, ΔT_b^V VERSUS OIL FILM THICKNESS AT 8.1 mm WAVELENGTH. FLAT WATER SURFACE. (Meeks et al, 1971).

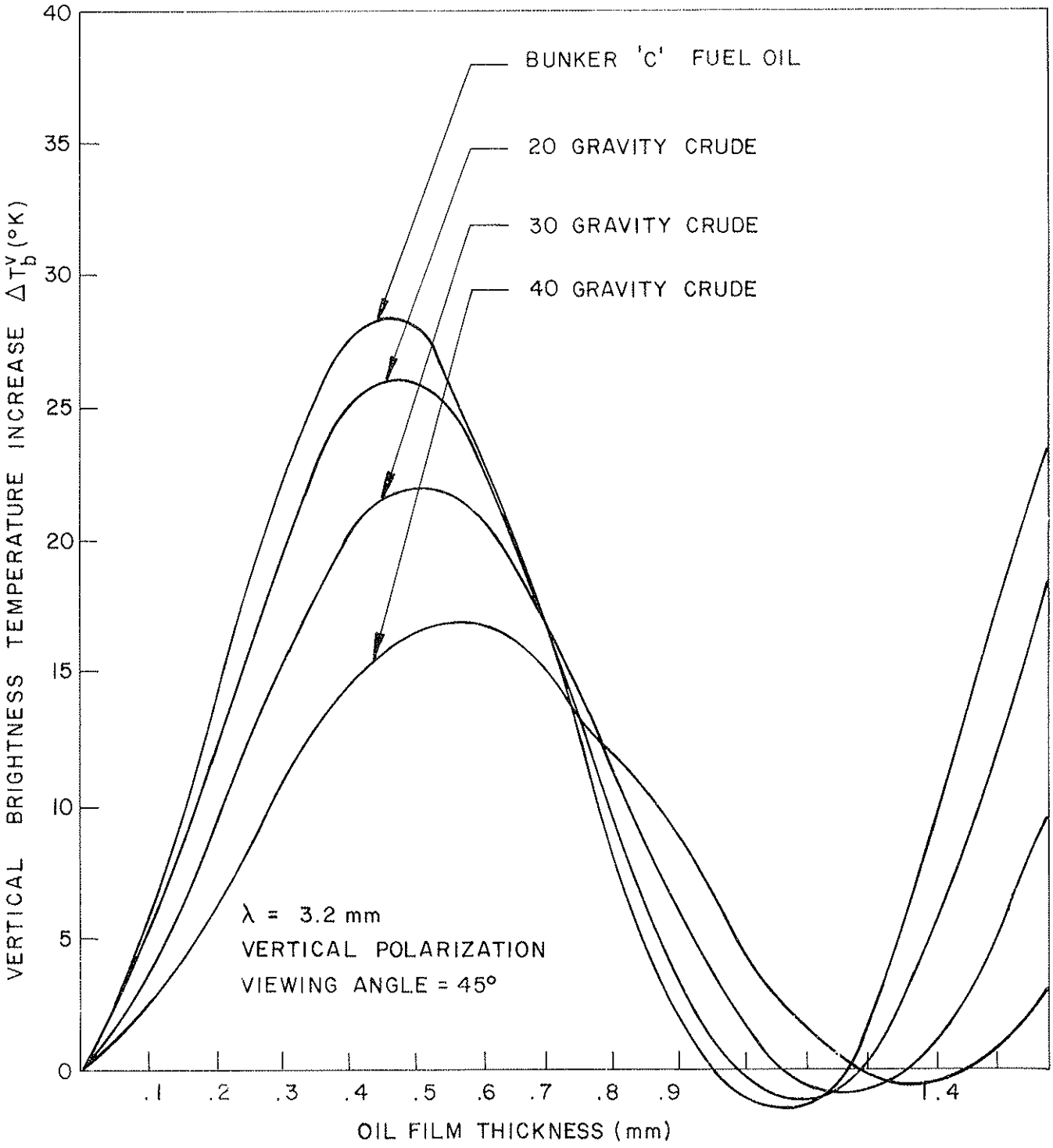

FIGURE A5-11 VERTICAL BRIGHTNESS TEMPERATURES INCREASE, ΔT_b^V, VERSUS OIL FILM THICKNESS AT 3.2 mm WAVELENGTH. FLAT WATER SURFACE. (Meeks et al, 1971).

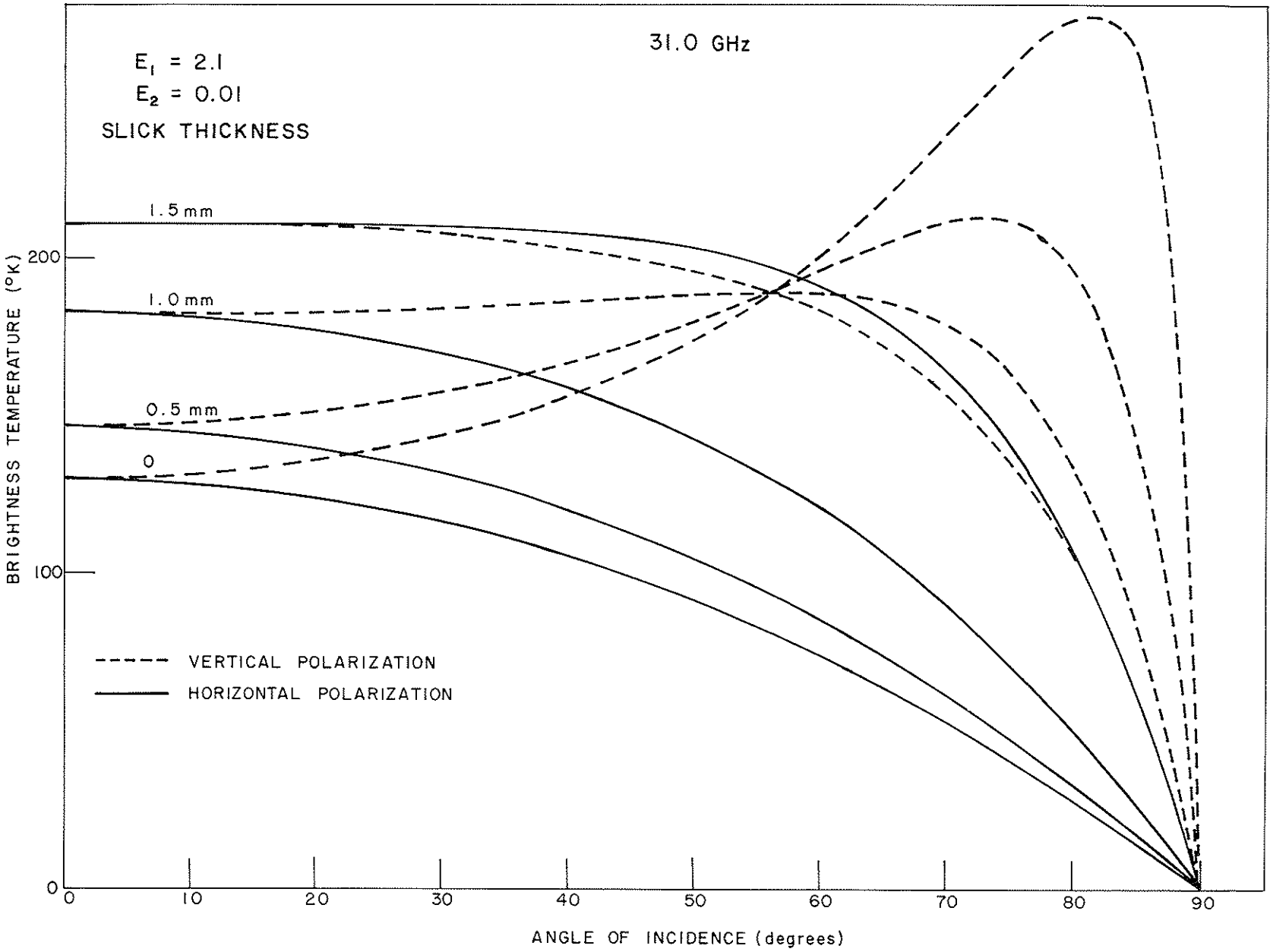

FIGURE A5-12 (Hollinger, 1974)

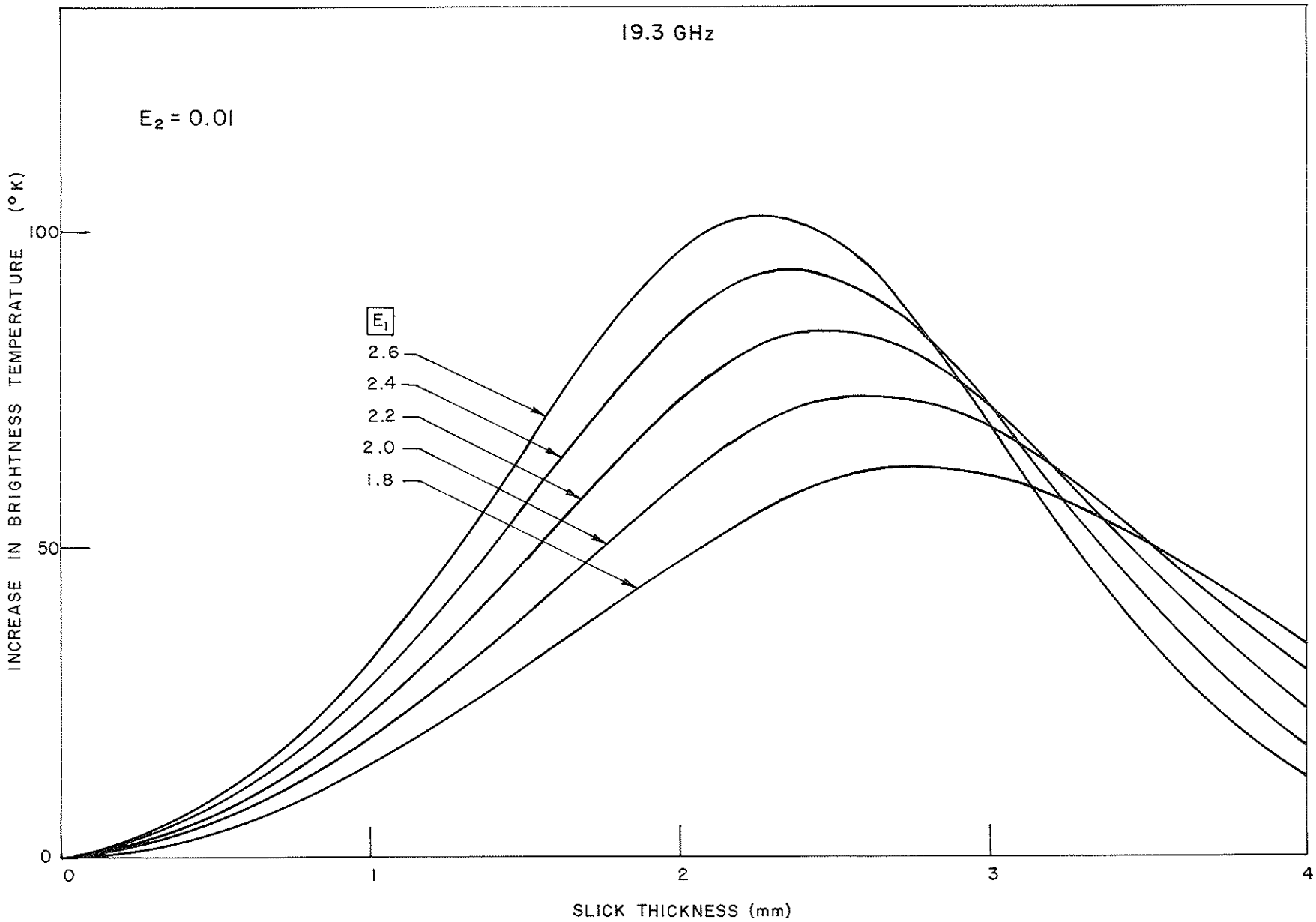

FIGURE A5-13 (Hollinger, 1974)

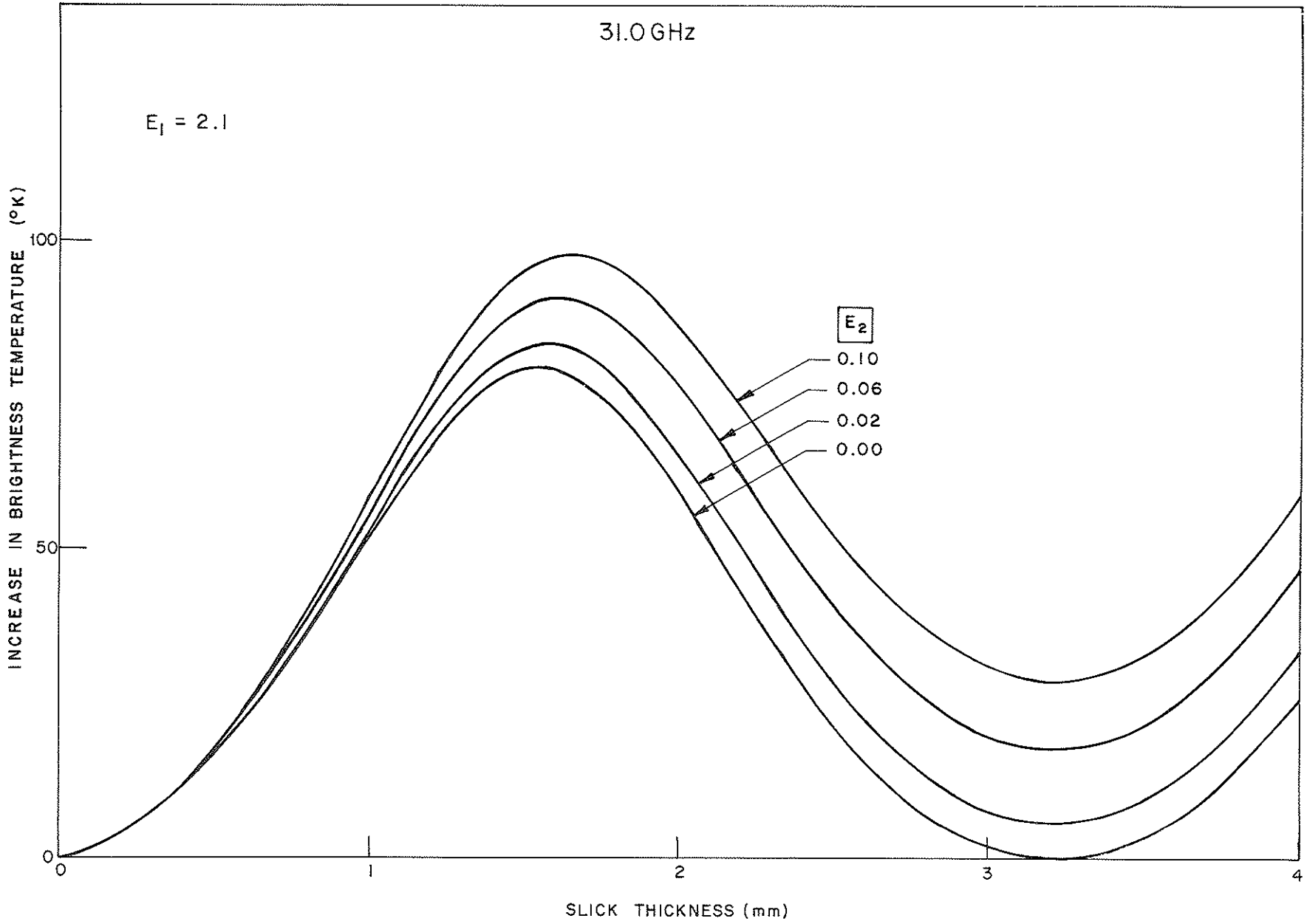

FIGURE A5-14 (Hollinger, 1974)

shifts the first peak to a greater thickness. Decreasing the latter has a similar effect on brightness temperature but shifts the first peak to a lower slick thickness. Hollinger also developed theoretical equations from which the volume of the oil spill through the change in the brightness temperature measurement can be calculated, taking into account main beam antenna efficiency and the case where the oil spill size is less than the resolution cell size. Tests performed under controlled oil spill conditions show that volume calculations were within about 25% of the known volume of oil spilled, even in rough seas.

The results and conclusions of this study agree with all the conclusions made by Aerojet General. They reinforce the conclusions relating brightness temperature (emissivity) to frequency, which was, based on Aerojet General's studies, possibly a little premature as they only studied the problem with two frequencies.

Finally, Kondratyev et al.(1975) undertook a similar study and their results were in agreement with the studies described here. It was observed that not only is the brightness temperature for horizontal polarization greater than that for vertical polarization but that the emissivity contrast between the oil and water is also greater. A summary of their emissivity data for horizontal polarization is given in Table A5.1. No oil type was specified.

A5.2.2 Rough Sea Conditions. In rough seas the dominant method enabling oil spills to be detected is the dampening of the capillary waves by the oil film. This causes a reversal effect as far as brightness temperature is concerned since the brightness

TABLE A5.1

	Film Thickness (mm)	Emissivity	Error
Water	-	0.37	-
Fresh-spilled oil	2.0	0.44	0.03
	3.0	0.51	0.03
	4.0	0.59	0.05
	5.0	0.62	0.01
Old oil	4.0	0.62	0.02

temperature of a rough sea is greater than that of a calm sea and could be greater than that of the oil slick. The oil slick, by reducing the roughness, lowers the effective brightness temperature of the polluted area creating a contrast and hence enables it to be detected. Detection by passive microwave techniques in this situation is dependent on the frequency of the sensor. As only the capillary (<0.025 m) and very short gravity waves (>0.050 m) are attenuated, only sensor operating at wavelengths comparable to or shorter than these will detect any change. For longer wavelengths this alteration in small-scale roughness will not have any significant effects. Thus, under rough sea conditions the increased emissivity of the oil may be counteracted by the increased ocean surface emissivity but the dampening effect still allows the slick to be detected. Aukland et al. (1969) noted the effect of sea surface roughness on oil detecting during experimentation. The reduction effect was reported to be able to produce a negative brightness temperature anomally of up to 10^{o}K. At an operating frequency of 38 GHz the crossover point between the increased temperature effect caused by the reduction in surface roughness was seen to be in the range of 0.1 to 0.3 mm oil film thickness.

Edgerton and Trexler (1970) examined to a small extent the above phenomena encountered during controlled oil spill conditions. At 37 GHz they found, for the conditions encountered, the additional emission from an oil slick overshadows the decrease in ocean emission associated with the reduction of surface roughness when film thicknesses were about 50 mm or more. For film thickness of 10 to 20 microns or less the surface roughness phenomena was dominant allowing the detection of these thin slicks. This reinforces other work finding that a "crossover" point exists where the two opposing mechanisms cancel each other. This would of course be dependent on such things as slick thickness, oil type and sea state.

Meeks et al.(1971) undertook a theoretical analysis of the dampening of ocean waves by an oil slick. Figure A5-15 shows the effect of a dense slick on the mean squared sea surface slope. One conclusion made was that very thin films (small fractions of sensor wavelength) do not appreciably increase the emissivity of the water surface and the only measurable way the slick could influence the brightness temperature is through the reduction in surface roughness. Figures A5-16 shows predicted 37 and 94 GHz brightness temperatures in response to ocean surface roughness (wind speed). Note that the horizontal polarization and the higher frequency provides the greatest difference between a clean and slick covered surface. The researchers also concluded that thick oil slicks would behave in a similar manner as thin slicks. This was confirmed in actual

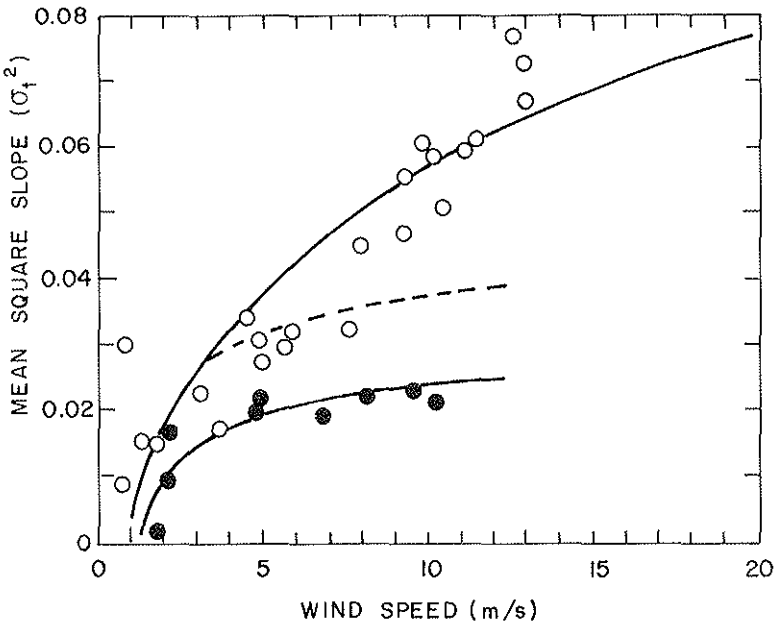

FIGURE A5-15 MEASUREMENTS OF THE MEAN-SQUARE SLOPE, σ_t^2 VERSUS WIND SPEED. (Cox and Munk (1954a, b). The open circles are for a clean water surface, the solid circles for a surface covered by a dense slick. (Meeks et al, 1971).

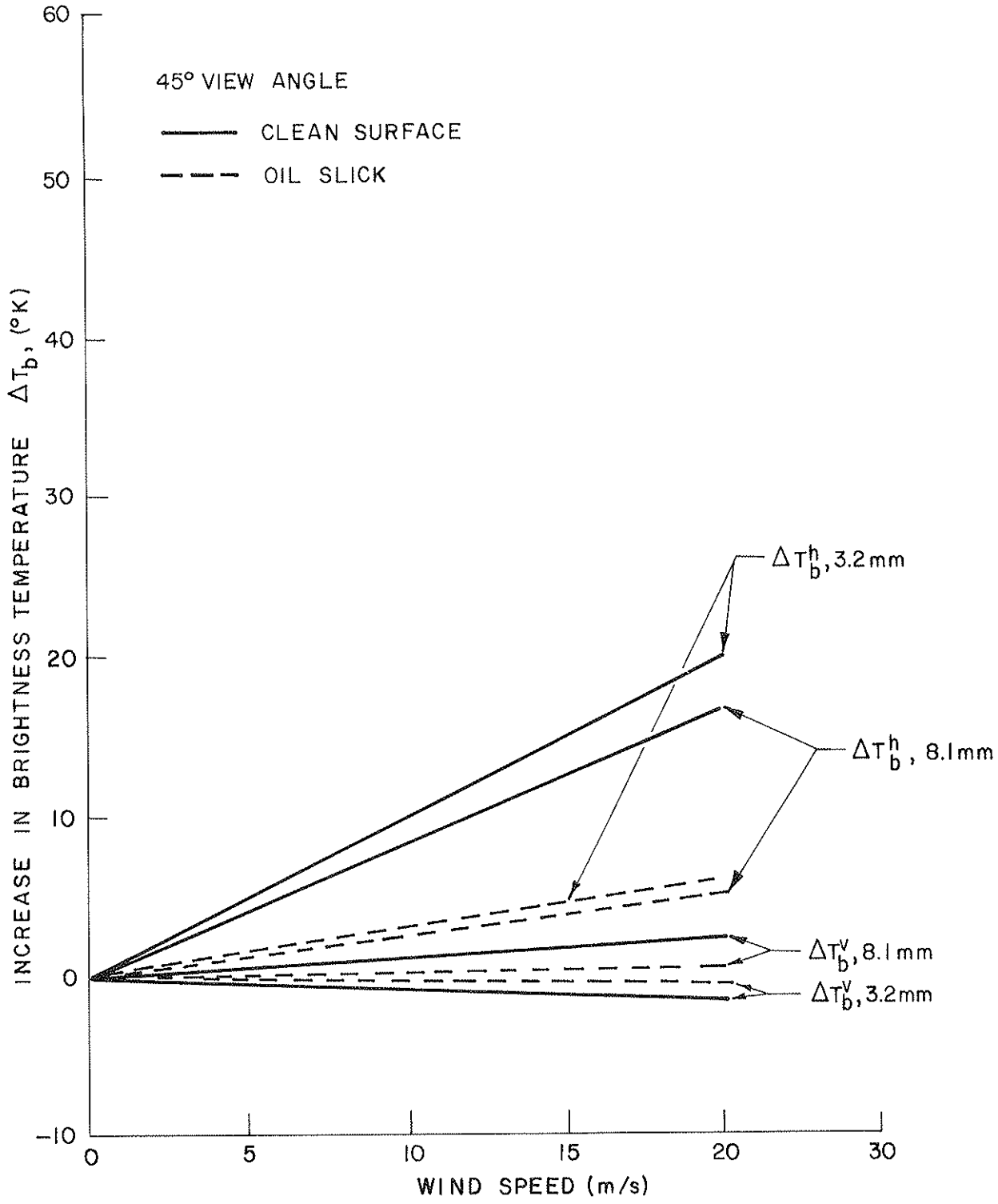

FIGURE A5-16 PREDICTED 8.1 AND 3.2 mm RESPONSE TO OCEAN SURFACE ROUGHNESS AS A FUNCTION OF WIND SPEED. (Meeks et al, 1971)

experiments. Finally, the effect of foam as briefly examined. Foam, with an emissivity of about 0.8 would give rise to a higher sea surface brightness temperature. The absence of foam caused by an oil slick's dampening effect on a normally covered sea would, therefore, increase the negative temperature anomally and aid in the detection of oil slicks.

Hollinger (1974) aslo examined the effect of surface roughness and sea foam on oil spill detection. He reported the calculations made by Cox and Munk (1954) which show that an oil slick dampened 30 cm wavelength waves by a factor of 10 and that waves shorter than this were essentially eliminated. The calculated depression in the antenna temperature due to the presence of oil on rough seas with and without foam for three sensor frequencies is given in figure A5-17. The look angle is nadir. Note that the effect is remarkably similar at all three frequencies.

In experimentation with an artificial mono-molecular slick in a surf-zone and a region of small ocean roughness Au et al.(1974) found that for horizontal polarization, the emission decreased below that of the surrounding ocean for all viewing angles. At vertical polarization the emission decreased below and increased above the viewing angle of approximately 60°. This is consistent with theoretical calcuations for thin oil slicks on calm seas (see Figure A5-13). The angle noted is approximately the same as found by Hollinger (1974) and Meeks et al.(1971). Au et al.(1974) used three frequencies, 14.5, 8.35 and 1.4 GHz, and found that temperature differences between the clean ocean and oil covered areas were detectable at 14.5 and 8.35 GHz but that at 1.4 GHz the difference was barely detectable. This is probably due to the fact that at 1.4 GHz the surface roughness detected by the instrument is on the order of 20 cm or more and dampening of ocean waves at these wavelengths is probably small compared to the shorter wavelengths viewing by the higher frequency sensors.

A5.2.3 Other Factors Affecting Emissive Detection. There are a number of other factors affecting the measured brightness temperature of an oil covered sea surface. These are: temperature variation, water salinity, frequency of detection, and resolution cell size. Meeks et al.(1971) concluded that for the temperature variation normally encountered in a given area the change in brightness temperature between an oil polluted and oil free area would not be significant. However, the variation in the emmissivity of oils with temperature has not been examined and may prove to be important at temperatures around $0^{\circ}C$ in order to distinguish it from surrounding water and ice.

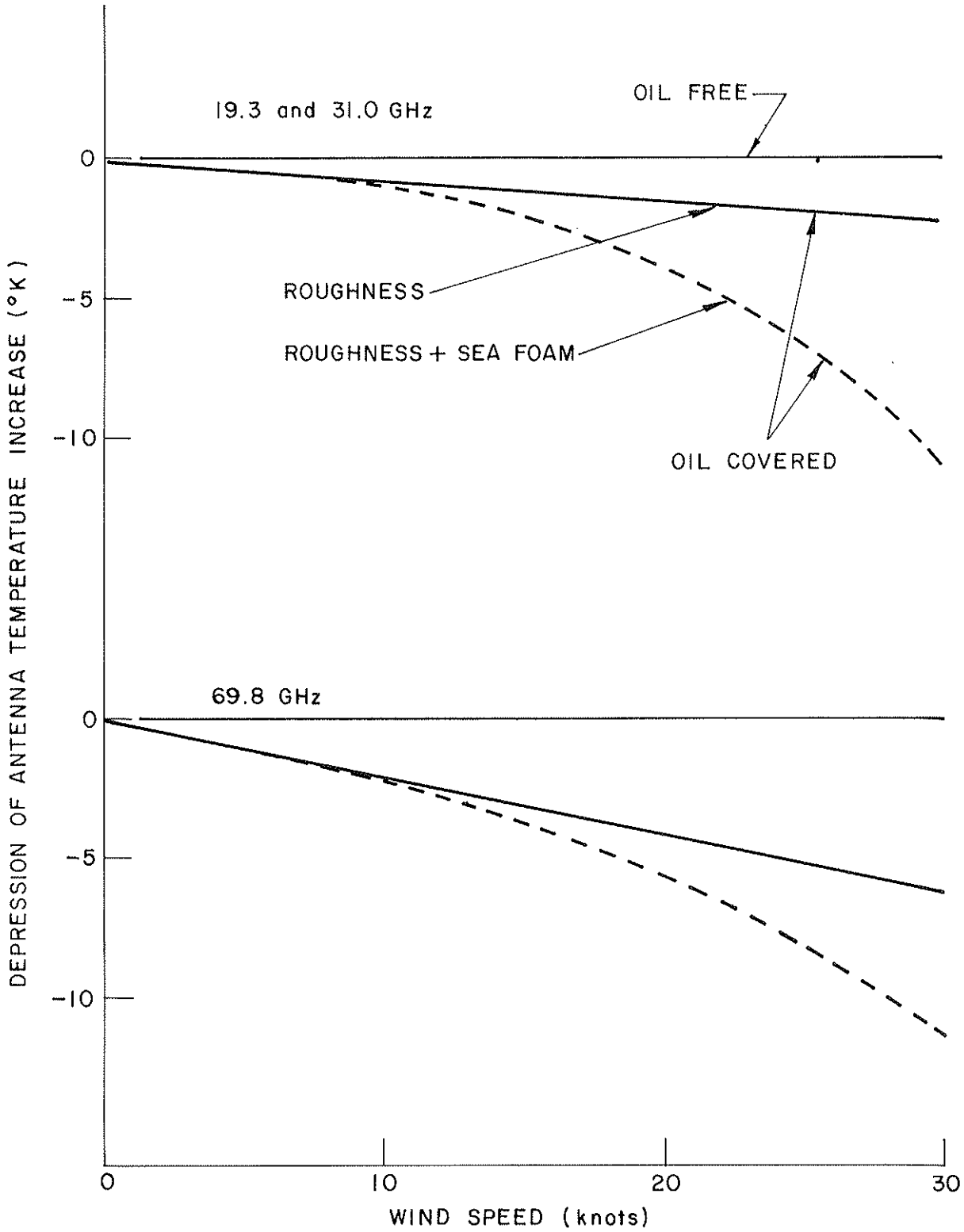

FIGURE A5-17 (Hollinger, 1974)

The variation in water salinity would not seem to have any significance on the brightness temperature of water at higher frequencies. Meeks et al.showed that through theoretical calculations expected salinity variations would not change the brightness temperature by more than a fraction of a degree at 37 GHz.

Previous work has shown that the microwave brightness temperature of oil increases with frequency. However, there have been no studies to better define this relationship. Because of atmospheric attenuation the next usable frequency above 37 or 38 GHz is 94 GHz (Edgerton and Trexler, 1970 and Kaski and Laaperi, 1976).

As oil does not spread evenly over an ocean surface, there will be areas within the polluted region that may be of widely different thicknesses and there may also be oil free areas. Therefore, the resolution cell of the sensor will probably be seeing a very diversified surface at any one time. This will result in an averaging effect causing volume and thickness calculation errors. Hollinger (1974) undertook an analysis of this problem in relation to volume measurement, and experimentation did demonstrate that the mathematical relationship derived was realistic.

A5.2.4 False Alarm Risks. Natural fish oils and other chemicals common to the ocean surface environment may also exhibit emissive and wave dampening properties very similar to those of petroleum oils. It may be, therefore, possible to mistakenly detect these slicks as accidental oil spills. Although there has been some mention of this by a number of researchers no detailed quantitative work has been undertaken up to now.

Large oil spills may extend over areas of sufficient size that the ocean roughness (wind speed) could vary significantly over the region. Therefore,under general surveillance monitoring the change in the surface conditions due to this phenomena may be sufficient to initiate a false alarm.

A5.2.5 Conclusions. A great deal of theoretical and experimental (both in the laboratory and on the open ocean) work has been undertaken to define the emissive properties of petroleum oils. Some of this work has led to recommendations on the design of, as well as the actual construction of, operational passive microwave sensors. Edgerton and Trexler (1970), as a result of their experience, recommended a 37 GHz microwave radiometer with a viewing angle between 30 and 45^{o}. Using a 40^{o} viewing angle the maximum half-power beamwidth would be 2.2^{o}. The sensitivity suggested was 3 standard deviations below the mean background noise (about 0.5^{o}K) with an integration time of 0.01 s, if flown on an aircraft with a cruise speed of 90 knots. Meeks et al.(1971) recommends a multibeam sensor operating at about 35 GHz with individual beamwidths of

1^{o} by 1.4^{o}, an integration time of 9.7 m/s and a signal-to-noise ratio of 10 dB. The United States Coast Guard (USCG) employs a 37 GHz horizontally polarized passive microwave imager which is deployed at an incidence angle of 45^{o}. This imagery is part of the USCG's Airborne Oil Surveillance System (AOSS).

No published work has been undertaken regarding the emissive properties of oils spilled in the Arctic and Subarctic regions, however, and there is a definite requirement to quantify these properties in such an environment. To be more specific temperature effects on the emissive properties around and below freezing must be examined. Also, false alarm risks need to be studied more closely because of, not only the presence of natural oils, but nilas and other ice types that may be mistakenly detected as oil.

Finally, insufficient research has been conducted to select an optimum frequency for detection of oil. This can be evaluated by defining the exact relationship between oil detectability and discrimination from the surrounding sea and ice environment, and frequency.

A5.3 Microwave Scattering

Guinard (1971a and b) was the first researcher to examine the feasibility of detecting oil spills with Radar. The Naval Research Laboratory (NRL) 4 Frequency Synthetic Aperture Radar (SAR) operating at 0.428, 1.228, 4.455 and 8.910 GHz was used for the study. The radar was equipped to transmit and receive simultaneously horizontal and vertical polarizations at each frequency. Therefore,both like and cross-polarizations could be examined for detection capability. The oil spills monitored were the Arrow spill in Chedabucto Bay, Nova Scotia, and controlled spills off Santa Barbara, California. Pertinent conclusions reached as a result of these studies are:

(a) Image contrast is a strong function of the polarization of the radar signal. Vertical polarized signals produce maximum contrast.

(b) There is a strong functional relationship between the incident radar wavelength, the sea state and the thickness of the oil film. The observed trends indicate that thin films (1 μm) are best detected in low sea states (10 knot winds or less) by low frequency transmissions (1 to 3 GHz) while there is some indication that thin films may be best detected in high sea states by higher frequency (5 GHz and above) transmissions.

(c) Oil film thicknesses of about 0.5 μm should be detectable.

(d) A spatial resolution of 100 to 300 ft in both range and azimuth directions is adequate for slick definition.

(e) There is some evidence that radar may be used to determine oil thickness; however, there has been no evidence that oil type yields a distinctive signature. Oil spreading rate may be used to gain some insight into oil type of two or more images can be acquired over a reasonable interval of time.

(f) The radar viewing angle should be within 45° of the horizontal to avoid specular returns. Since small grazing angles yield larger swath widths, an angular range from 2° to 20° seems suitable for radar design.

Pilon and Purves (1973) also reported on the NRI and SAR imagery obtained over Santa Barbara oil spills. They found that the vertical transmit-vertical receive polarization mode produced the highest contrast imagery and that oil films thicknesses less than 1 μm could be detected. Also streamers from the main spill region and wind blown films can also be imaged. They also found that at frequencies above 1.0 GHz the slicks are depicted with sharp boundaries while at lower frequencies the boundaries are indistinct. This was attributed to the ability of waves comparable to the radar wavelength to penetrate the oil slick a significant distance before being attenuated. Finally, it was also found that spills of less than 400 litres could be detected.

Van Kuilengerg (1975b) carried out a series of X-band SLAR ("Rijkswaterstaat" EMI SLAR, horizontal transmit - horizontal receive) observations of controlled oil spills in 1975. The slicks were almost always detectable as clearly defined patches showing contrast of 3 to 10 dB. No strong angle effects were observed in the range of grazing angles from 2° to 30°.

A detailed study to investigate the radar backscatter characteristics of an oil covered sea was undertaken by Krishen (1972). He used a 13.3 GHz vertically polarized scatterometer to gather data over a crude oil spill in the Gulf of Mexico. Figure A5-18 demonstrates the effect of an oil slick on the radar backscatter from the ocean surface. The decrease in the radar cross section at incidence angles between 25 and 50° was attributed to the dampening of small gravity or cappillary waves. Comparison of theoretical with experimental values of backscattering cross sections from this wave structure for oil free and oil covered areas showed close agreement.

Eklund et al.(1974) have reported measurements of the radar cross section of an oil covered sea in the Baltic. Using a vertically polarized X-band radar (10 GHz) they found that the reduction over the oil covered area was in the order of 5-7 dB at an incidence angle of 3.5°. Van Kuilenberg (1975a) conducted scatterometer tests under

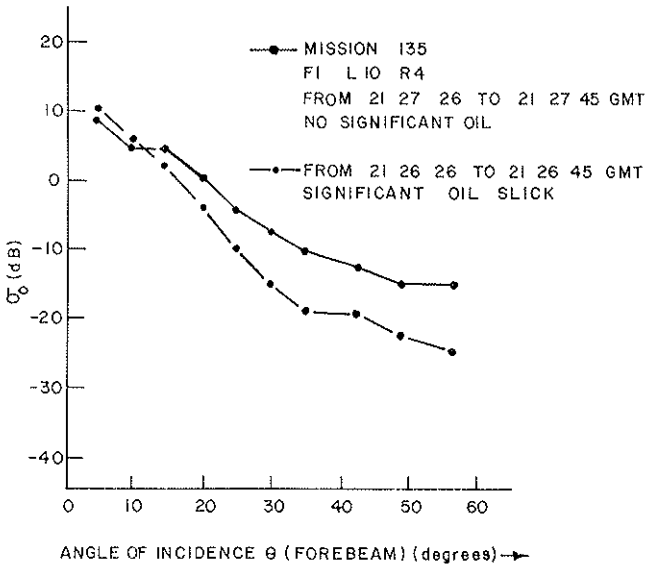

FIGURE A5-18(a) COMPARISON OF SCATTERING CROSS SECTION OF OIL SLICK AREA AND NO SIGNIFICANT OIL SLICK AREA FOR FLIGHT 1 (Krishen, 1972)

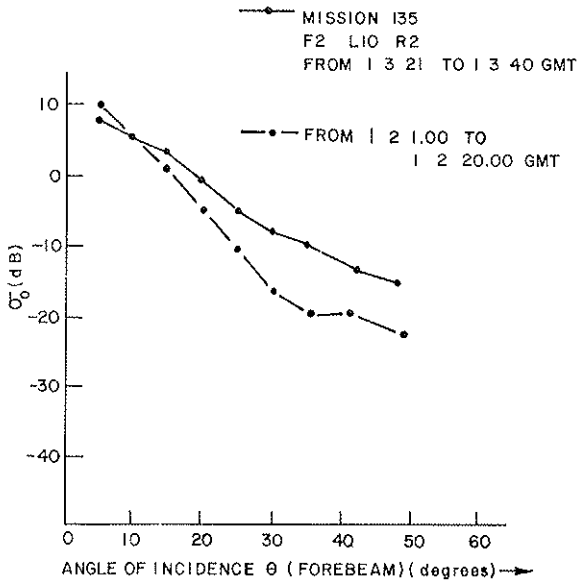

FIGURE A5-18(b) AVERAGE VALUE OF SCATTERING CROSS SECTION AT $\theta = 35°$ ALONG GROUND TRACK FOR F1 L10 R4 (Krishen, 1972)

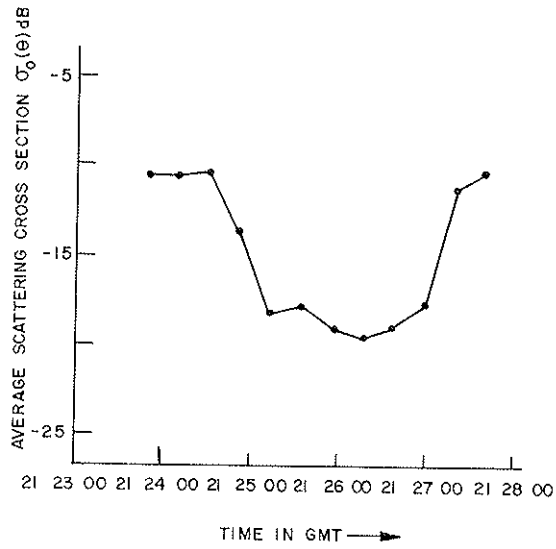

FIGURE A5-18(c) COMPARISON OF $\sigma_o(\theta)_{dB}$ OF OIL SLICK AND NO SIGNIFICANT OIL SLICK DATA FOR FLIGHT 2 (Krishen, 1972)

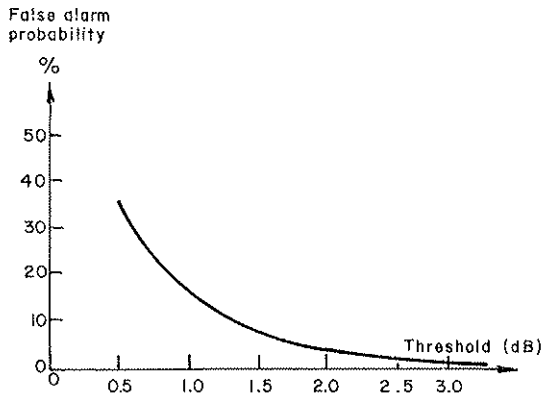

FIGURE A5-19 FALSE ALARM PROBABILITY vs THRESHOLD LEVEL (Eklund et al, 1974)

controlled conditions (tank) at 9.7 GHz. Qualitatively, his results agreed with other published data.

Finally, Pronk (1975) undertook an in-depth study of the dampening action of an oil film on an ocean surface. His relevant conclusions are:

(a) The water-waves influenced by oil films are in the range of 0.01 to 10 m.

(b) An oil layer always results in a dampening action on capillary waves and so is detectable by the relative weakening of the wave component.

(c) Thin oil films (μm thickness) only indicate their presence by their damping action on capillary waves; the nature of the oil (viscosity and layer thickness) at first instance cannot be deducted from this observation.

(d) The extent to which thick oil films (mm thickness) dampen the water-waves provides an opportunity for the estimation of the product of the oil viscosity and layer thickness which cannot be separated when applying water-wave amplitude measurements.

(e) The dampening of the waves that are influenced by an oil layer, takes place over a distance of typically 50 to 100 m upon entering into the oil slick.

A5.3.1 False Alarm Risks. The False Alarm condition applicable to oil detection by radar corresponds closely to those associated with passive microwave detection. In this case, however, it is only the modification of the ocean surface created by natural materials that will create the false alarm. Eklund et al.(1974) reported that a local reduction in the radar cross section of the order of 5 dB was considered a reasonable oil spill alarm threshold. They also state that the most difficult situation occurs at low wind speeds when space and time variations in the wind field alone may cause variations of the sea surface roughness that could be misinterpreted as being caused by oil slicks. This effect is more pronounced for cooler water surfaces. The critical wind speed below which false alarm risks could be of importance in an operational system using X-band radar is in the order of 3-5 m/s in summer and 8 m/s in winter. Sea surface temperature variations resulting in a surface roughness pattern alone do not seem to be important. Surface currents could also pose problems. Figure A5-19 shows the false alarm probability versus water cross section attenuation threshold level calculated for a 10 GHz vertical transmit-vertical receive polarized radar system.

A5.3.2 Conclusions. Experimental and theoretical studies indicate that X-band or higher frequency radars with vertical transmit - vertical receive polarization, a 100 by

100 ft to 300 by 300 ft resolution cell size, a 2^{o} to about 35^{o} angle of incidence show promise as operational oil slick detection systems. It is evident, however, that much more data is required to fully evaluate radar detection capabilities for oil spill monitoring. This will involve further studies on the effects of polarization, incidence angles and ocean surface conditions from calm to extreme sea states on the radar cross section. An optimum frequency must also be evaluated taking into account atmospheric attenuation, the wavelength of the damped capillary waves and the ability to detect oil in calm sea conditions. Operations in ice covered and ice-infested waters will require even more work, particularly for the problems of discrimination from certain ice types and "False Alarm" risks.

REFERENCES

Au, B., J. Kenney, and L.U. Martin, "Multi-frequency Radiometric Measurements of Foam and a Mono-Molecular Oil Slick," Proceedings of the Ninth International Symposium on Remote Sensing of Environment, II, Ann Arbor, Michigan, pp 1763-1773 , (April 1974).

Aukland, J.C., W.H. Conway, and N.K. Sanders, "Detection of Oil Slick Pollution on Water Surfaces with Microwave Radiometers," Proceedings of the Sixth International Symposium on Remote Sensing of Environment, II, Ann Arbor, Michigan, pp 709-719, (October 1969).

Edgerton, A.T., and D. Trexler, "Radiometric Detection of Oil Slicks," Report NO. SD1335-1, Aerojet General Corporation, El Monte, California, pp 130, (January 1970).

Eklund, F., J. Nilsson, and A. Blomquist, "False Alarm Risks at Radar Detection of Oil spill," Proceedings, USRI Commission II Specialist Meeting on Microwave Scattering and Emission from the Earth, Berne, Switzerland, pp 39-45, (September 1974).

Guinard, N.W., "The Remote Sensing of Oil Slicks", Proceedings of the Seventh International Symposium on Remote Sensing of Environment, Ann Arbor, Michigan, II, pp 1005-1026, (May 1971a).

Guinard, N.W., "Radar Detection of Oil Spills," Joint Conference on Sensing of Environmental Pollutants, Palo Alto, California, pp 8, (November 1971b).

Hollinger, J.P., "The Determination of Oil Slick Thickness by Means of Multifrequency Passive Microwave Techniques," NRL Memorandum Report No. 2953, Washington, D.C., pp 144, (1974).

Kaski, K., and A. Laaperi, "Remote Sensing of Oil Slicks with Microwave Radiometer," Report No. 583, Helsinki University of Technology, Helsinki, Finland, pp 16, (1976).

Kondratyev, K., Ya., Yu Rabinovich, V.V. Melenteyev, and E.M. Shulgina, "Remote Sensing Oil on the Sea Surface," Proceedings of the Tenth International Symposium on Remote Sensing of Environment, I, Ann Aobor, Michigan, pp 251-252, (October 1975).

Kotlarski, J.R. and H.R. Anderson, "Oil Slick Detection by X-band Synthetic Aperture Radar," Proceedings of the Ninth International Symposium on Remote Sensing of Environment, Ann Arbor, Michigan, II, pp 1774-1790, (April 1974).

Krishen, K., "Detection of Oil spills, Using a 13.3 GHz Radar Scatterometer," Proceedings of the Eighth Symposium on Remote Sensing of Environment, Ann Arbor, Michigan, II, pp 1105-1119, (October 1972).

Meeks, D.C., D.P. Williams, R.M. Wilcox, and A.T. Edgerton, "Microwave Radiometric Detection of Oil Slicks," Report No. 1335-2, Aerojet General Corporation, El Monte, California, pp 91, (March 1971).

Pilon, R.O., and C.G. Purves, "Radar Imagery of Oil Slicks," IEEE Transactions on Aerospace and Electronic Systems, AES-9,5, pp 630-636, (September 1973).

Pronk, A.C., "Remote Sensing of Oil Pollution of the Sea Surface II: Damping of water Waves by an Oil Layer as a Possible Indicator for SLAR Observations," Netherlands Interdepartmental Work Community for the Applications of Remote Sensing Techniques (NIWARS, NIWARS Pub. No. 22, Netherlands, pp 12, (July 1975).

Van Kuilenburg, J., "Radar Observations of Controlled Oilspills, Proceedings of the Tenth International Symposium on Remote Sensing of Environment," Ann Arbor, Michigan, I, pp 243-252, (October 1975a).

Van Kuilenburg, J., "Remote Sensing of Oil Pollution at the Sea Surface I, Review of Remote Sensing Methods Emphasizing Radar," Netherlands Interdepartmental Working Community for the Applications of Remote Sensing Techniques (NIWARS), NIWARS Publication No. 21, pp 28, (July 1975b).

APPENDIX 6

ANNOTATED BIBLIOGRAPHY

APPENDIX 6 - ANNOTATED BIBLIOGRAPHY

An annotated bibliography of available literature on the microwave emission and scattering from ice, oil, and water is presented here. Some publications are related to the behaviour of oil in the ice environment. The entries in the bibliography are arranged in alphabetical order.

A sample sheet from the bibliography is shown in Figure A6.1. This sample sheet is marked with letters and numbers to help understand the material presented with each bibliographic entry and to explain its organization. The notation on Figure A6.1 is described below:

(A) Bibliographic Entry - Contains - Name of Author(s) (Last name, Initials, for first author followed by Initials, last name for two or multiple authors), Title of Publication, Name of Journal, or Symposium Proceedings or Name of Agency or Company Name, Place or Address, Volume, Number, Page number or number of Pages, Month, Year of Publication:

(1) Affiliation of Author(s) at the Time of Publication;

(2) Affiliation of Author(s) marked with corresponding symbol * or **. (This is only presented in the case of two or more authors and their affiliations are not the same);

(3) Availability of the Publication - If the Publication had NTIS, AD, or any other number which would help in its retrieval. (For example, the Publication on the Sample sheet can be obtained from C-CORE);

(4) Contains Author's Abstract or Introduction, or Summary. (The Author's Introduction or Summary is only provided in the case where the Publication does not contain the Author's Abstract);

(5) Number of References in the Publication;

(6) Identification of each publication as Experimental, Theoretical, or Both, or General Review depending on its nature;

(7) Reviewer's Evaluation - High Significant, Significant, or Normal;

(8) Place of Data Collection for Experimental Work;

(9) Date or Time of Data Collection;

(10) System(s) used for Data Collection - Name, Frequency, and Polarization used;

(11) Key Words; and

(12) Reviewer's Comments - Significant Results, Conclusions, or Summary from the Publication, not included in the Abstract.

Ⓐ Gray, L., J. CIHLAR, S. PARASHAR and R. WORSFOLD*, Results from Shorefast and Floating Proceedings of the Eleventh International Symposium on Remote Sensing of Environment, Ann Arbor, Michigan, 1, pp. 645-657, (April 1977). ① CCRS, Ottawa; ② C- CORE*, St. John's. ③ C-CORE Publication No. 77-21.

Abstract - Multipolarized scatterometer sea ice measurements at 13.3 GHz obtained during the winter and spring of 1975-76 from a number of flight lines off the east coast of Canada were analyzed. Radar scattering coefficients, σ^o were calculated for several regions of sea ice as interpreted from aerial photographs. The variation in σ^o with incidence angle is presented for HH (Horizontal transmit - Horizontal receive) and HV (Horizontal transmit - Vertical receive) polarizations for the various ice regions. The depolarization ratio ($\sigma^o_{HH}/\sigma^o_{HV}$) as a function of incidence angle is also given. The sea ice regions studied included shorefast ice with varying degrees of snow cover and surface roughness and several varieties of floating sea ice with different thicknesses.

Ⓐ The value of σ^o for relatively thin ice can vary over a range of approximately 10 dB for both the like (HH) and cross (HV) polarized signals. Further, the returns for shorefast ice show a larger variation of approximately 20 dB and 25 dB for the HH and HV returns respectively. These results indicate clearly the difficulty in interpreting or correlating the magnitude of the backscattering coefficient with ice type or thickness. Nevertheless, there is some indication that radars operating with incidence angles of 60^o or less will acquire imagery on which the graytone will help in differentiating ice types. The scattering coefficient data also shows the contrasts between different ice regions is often a fee dB greater for the HV returns than for the HH returns. This was particularly true for the shorefast ice studies. A large dynamic range (30-35 dB) will be required by an imaging radar operating at incidence angles between 10^o and 60^o.

⑤ Seventeen; ⑥ Experimental; Highly Significant. ⑦

⑧ East Coast of Canada; Winter and Spring, 1975-76; ⑨

⑩ 13.3 GHz Multipolarized Scatterometer.

⑪ Radar, Scatterometer, sea ice, microwave, backscatter, polarization, Canadian East Coast.

⑫ Apart from the returns close to the vertical, the highest backscatter was observed from shorefast ice although some smooth surface ice showed returns lower than those obtained from much thinner ice, e.g. pancake ice and rafted young ice.

FIGURE A6.1 SAMPLE ENTRY IN THE BIBLIOGRAPHY

ANDERSON, V.H., "High Altitude, Side-Looking Radar Images of Sea Ice in the Arctic," Proceedings of the Fourth Symposium on Remote Sensing of Environment, Ann Arbor, Michigan, pp. 845-858, (April 1966). CRREL

Abstract - High altitude, side-looking radar was used to image sea ice patterns between Greenland and Ellesmere Island and within the Arctic Ocean, during the spring of 1962. Concurrent low altitude visual reconnaissance of sea ice patterns was conducted by the author over much of the same flight path flown by the radar aircraft. A comparison of the radar patterns with actual observed and photographed sea ice conditions is presented in this paper. A dramatic example of the eroding processes of polar ice as it moves southward to warmer environments is displayed by the radar imagery and is discussed in this paper. An example of radar imagery of sea ice in the Arctic Ocean, existing under a deteriorating environment during the summer of 1962, is also presented. Included is the radar image of Ice Island "T3" in the Beaufort Sea north of Alaska.

Nil, Experimental, Highly Significant.

Arctic (East); Spring, Summer, 1962; AN/APQ 56 (XAA) SLAR.

SLAR, Sea Ice, Arctic Ocean.

Polar ice (8 to 12 feet thick) with areas of very thick pressure ice exhibits a light tone on the radar image in contrast to refrozen leads, polynyas and smooth surface thin ice which gives dark tones.

Imagery shows the alignment of leads and refrozen cracks with a preferred orientation which is indicative of ocean currents affecting the ice drift, showing a potential for drift pattern studies.

The abraded remains of ice floes give light toned circular patterns with the darker tones surrounding these circular floes indicative of severely deformed winter ice which is extremely rough and unstable, consisting of brash fragments of ice and slush. The differences between angular ice and rounded floes is easily seen and icebergs are present throughout the imagery.

A potential method to differentiate between different thicknesses of ice is by inference. Slush ice and grease ice is extremely different from ice fragments. The thin ice breaks up and moves as a viscous mass and this mass can be easily imaged on the large-scale. This severely deformed ice corresponds to a fine texture on the imagery.

The radar return from ice islands like T3 is very strong. The less deformed a floe is the more photographic-like the radar image is. Pressure ridging can be seen in the larger floes. The radar return from first-year ice is very different from the return from polar ice. Observations are based on concurrent visual reconnaissance.

The relationship between the various frequencies of radar energy to composition, ice thickness and surface texture, and radar configuration all need further theoretical and field studies.

ANDERSON, V.H., R.B. AREND and M.J. LYNCH, "Interpretation of Winter Ice Conditions from SLAR Imagery," United States Coast Guard, Office of Research and Development, and Department of Transport, Washington, D.C., Report No. DOT-CG-14486-1A, 100 pp, February, (1972). Photographic Interpretation Corporation, Hanover, New Hampshire.

Abstract - Side-Looking Airborne Radar (SLAR) provides an all weather, all light level medium for imaging large areas of saline and freshwater ice. This report evaluates the use of SLAR imagery for determining winter sea and lake ice parameters and compares winter sea ice pattern "keys": with summer pattern "keys". The report also makes a preliminary evaluation of the effects of snow cover on the SLAR imagery and on the interpretation of ice conditions. In addition, an interpretation technique is developed which permits the interpreter to analyze ice environments to a greater degree than is possible through the use of image pattern keys. The study points out the requirement for additional research to correlate lake ice image patterns with age, thickness, condition, and snow cover parameters through a combined remote sensor and on-ice study.

Experimental, Significant.

Great Lakes, Beaufort Sea, Thule, Greenland to Goose Bay, Labrador; February-March, 1971; 16.5 GHz AN/DPD-2 (Modified) Philco-Ford SLAR.

SLAR, sea ice, lake ice, image interpretation.

Normally new and young ice yields dark grey to black tones on the radar imagery; however, under certain conditions new and young ice can display extremely bright tones as in the case of nilas. Many of the pattern indicators used in the interpretation on non-winter sea ice conditions are valid for winter ice conditions, but interpreters should not rely entirely on radar keys for their work. Multi-year ice can be separated from other ice types more rapidly than through use of aerial photos, and stress zones can also be quickly delineated. There was no apparent detrimental masking effects of sea ice conditions by snow cover on the Ku-band radar imagery.

Some large-scale features associated with icebergs in fast ice, and showing up as moderately bright streaks in the radar imagery were tentatively identified as snow drifts.

As with sea ice, there was no apparent detrimental masking effect by snow cover of lake ice conditions.

AU, B., J. KENNY and L.U. MARTIN, "Multi-Frequency Radiometric Measurements of Foam and a Mono-Molecular SLICK," Proceedings of the Ninth International Symposium on Remote Sensing of Environment, Ann Arbor, Michigan, III, pp. 1763-1773, (April 1974). NOAA, Florida.

Abstract - Microwave radiometric measurements have been made of both a surf-zone and of an ocean region where small-scale roughness was suppressed by an artificial mono-molecular slick. The foam measurements show near identical foam temperatures at 8.35 and 14.5 GHz, but large variations at 1.4 GHz. The resultant maximum foam emissivities at nadir range from 0.47 to 1.4 GHz to 0.84 to 14.5 GHz. The presence of the mono-molecular slick on the ocean had the same effect as a decrease in surface roughness. For horizontal polarization, the emission decreased below that of the surrounding ocean for all viewing angles. At vertical polarization, the emission decreased below and increased above a viewing angle of approximately 60 degrees. The change in temperature was observed at both 8.35 and 14.5 GHz, being barely detectable at 1.4 GHz.

Nil, Experimental, Significant.

Miami; April - June, 1973; 14.5, 8.35 and 1.4 GHz dual polarized radiometers on a NOAA C-130 aircraft.

Oil slick, foam, frequency, polarization, passive microwave, brightness temperature, emissivity.

Measurements or natural sea foam and a mono-molecular oil slick were made using both horizontal and vertical polarizations and various view angles. L-band was shown to be inadequate for slick detection. Foam measurements were made and compared with theory for emissivity.

AUKLAND, J.C., P.J. CARUSO, Jr., W.H. CONWAY and R.G. GROSHANS*, "Remote Sensing of the Sea Conditions with Microwave Radiometer Systems," Proceedings of the Sixth International Symposium on Remote Sensing of Environment, Ann Arbor, Michigan, II, pp. 709-719, (October 1969). Microwave Sensor Systems, Inc., California; RCA, New Jersey.*

Introduction - Information about the condition of the sea surface is of major importance to shipping, fishing, and naval operations. Likewise, other oceanographic activities and meteorological analyses and forecasts require sea surface data across the full expanse of the oceans. Two of the important parameters are sea state and sea-surface temperature.

To date, determinations of sea state and sea-surface temperature have been acquired as a result of local measurements and observations made either with in-situ devices or visually from surface craft, shore observations, and where possible, observations from low-flying aircraft. Obviously, only limited coverage is possible through the use of these techniques, and significant data cannot always be made available on a timely basis. What is needed is an operational remote sensing system through which measurements of sea state and sea temperature can be made from a spacecraft on a world-wide basis and reported in a timely fashion. It is believed that such a capability is possible through the use of passive microwave radiometry.

A microwave radiometric experimental program was proposed early this year by RCA Corporation as a result of a number of studies made for them by Microwave Sensor Systems, Inc. The purpose of the experimental program was to generate curves relating sea state and sea-surface temperature to apparent radiometric temperatures, providing the basic data to be used with remote microwave radiometric measurements for determining sea state and sea-surface temperature.

The experimental program consists of two types of measurements. The first experiments are a series of measurements on several closely controlled or monitored environments, such as water tanks and local piers. The results of the tank measurements may be used to establish the relationship between apparent (radiometric) and actual (thermometric) sea-surface temperature as a function of frequency, viewing angle, and signal polarity. The results of the pier or tower measurements may be used to obtain qualitative relationships between radiometric measurements and sea state. Following these measurements, a series of aircraft measurements coincident with ground truth

measurements will provide sea state data curves in an actual ocean environment. The results of the analysis for various aircraft altitudes can then be extrapolated to produce corresponding curves for satellite altitudes.

Following a discussion of theory for determining sea state and sea temperature the data taken to date will be presented.

Three, Experimental and Theoretical, Significant.

Experimental, 10.2, 30, and 38 GHz, Radiometers.

Horizontally polarized microwave radiometric signals are significantly sensitive to changes in sea state and incidence angle (and in lesser ways to sea temperature).

Vertically polarized microwave radiometric signals are invariant to sea state at or near an incidence angle of 40° to the surface.

Microwave radiometric signals (of both polarizations) are nearly invariant to changes in the water thermometric temperature at frequencies at or near that of water absorption.

The effects of non-polarized loss mechanisms like intervening atmosphere and, possibly, foam can be removed.

The ground based measurements indicate that foam and surface ripple must be considered in any system measuring sea state or sea temperature.

The presence of foam significantly modified the radiometric temperature by 20° - 100°, depending upon the quantity of foam in the beam.

AUCKLAND, J.C., W.H. CONWAY and N.K. SANDERS*, "Detection of Oil Slick Pollution on Water Surfaces with Microwave Radiometer Systems", Proceedings of the Sixth International Symposium on Remote Sensing of Environment, Ann Arbor, Michigan, II, pp. 789-796, (October 1969). Microwave Sensor Systems, Inc., California, University of California at Santa Barbara*.

Abstract - Examination of the theoretical and experimental body of information that is presently available leads to the conclusion that there are two mechanisms by which the presence of oil on a water surface may be detected. Both of these mechanisms create an apparent temperature anomaly when oil is present. It is the presence of this local anomaly in the relatively uniform background of the sea surface that will signify the detection of oil pollution. This paper develops an analytical basis for the mechanisms and presents the results of the experimental verifications.

The first phenomena to be considered is measuring the local change in sea due to the presence of the oil pollution. This phenomena presents very strong signals to microwave radiometers when winds of 6 knots or more are blowing. It is felt that this will be the primary detection mechanism for thin oil films. The second mechanism to be considered is the direct change in the emissivity of the water surface due to the presence of oil. This phenomena is slightly the weaker of the two, but offers the promise of measuring oil thickness. Because of the independence of these two potential detection mechanisms, they are described separately.

Five, Theoretical and Experimental, Significant.

Laboratory; Summer, 1960; 10.2 GHz and 38 GHz Experimental Radiometers.

Oil, microwave radiometer, sea state, pollution, water brightness temperature.

Examination of the obtained data reveals that oil on a water surface behaves in a manner that causes two separate and distinct effects. Thin layers of oil produce a lower radiometric temperature than the surrounding sea by reducing the number and size of small capillary waves produced by the wind. This effect can produce a signature of up to 10 degrees.

When the oil film becomes thicker, it causes the apparent temperature to increase due to the effects of a dielectric layer on the water surface. For an operating frequency of 38 GHz, the cross-over point for these two phenomena occurs in the range of 0.1 to 0.3 mm,

depending on the wind speed. Thicker oil concentrations caused very hot signatures, up to 100^{o} at 1.0 mm thickness, to be generated.

AUKLAND, J.C. and D.T. TREXLER, "Oil Pollution Detection and Discrimination by Remote Sensing Techniques", U.S.C.G. Office of Research and Development, Washington, D.C., Report No. 714104/A/006-1, 183 pp, (October 1970). Spectran, Inc., California. NTIS No. AD716349.

Abstract - Airborne remote sensing techniques were applied to the detection and discrimination of pollution by oil on the ocean surface. The tests were performed in the Gulf of Mexico during April, 1970. Pollutants investigated include No. 2 fuel oil, No. 6 fuel oil, 9250 lube oil, light crude oil, heavy crude oil, gasoline, and mixtures of gasoline and oil. A total of 103 oil slicks were produced as a function of spill rate and ship speed. Ship speeds were nominally 10, 14, and 17 knots and spill rates ranged from 0.02 to greater than 4.0 GPM (gallons per minute).

Sensors used during the airborne tests included; two dual polarized microwave radiometers operating at 10.2 and 30 GHz, an infrared scanner operated in both the 4- 5.5 μ and 8-14 μ regions, a dual 70 mm camera sensing visible colour and infrared colour, a 4-lens camera employed filters from the mid-visible to ultraviolet wavelengths.

Oil was detected on the sea surface at spill rates as low as 0.2 GPM for long wavelengths sensors and at the lowest spill rates for photographic imagery using an ultraviolet filter. Anomalously warm infrared radiometric temperatures were recorded in the 4-5.5 μ region for heavy crude oil while No. 6 fuel oil appeared radiometrically cooler.

Two, Experimental, Normal.

Gulf of Mexico; April, 1970; 10.2 and 30 GHz Dual-Polarized Microwave Radiometer, IR Scanner, Multispectral Cameras.

Oil spill, flow rate, multispectral detection.

The microwave radiometers pointed 46° off nadir aft of the aircraft. At an altitude of 2000 feet, the intercept areas were elliptical with major and minor axes of 302 and 230 and 170 and 120 feet for the 10.2 and 30 GHz radiometers, respectively. Most of the analysis involved the X-band system because the Ka-band system's signal magnitudes were questionable.

Detection capability was related to flow rate and a rate of 0.05 gallons per minute was detectable. Signals from the oil appeared colder than the unpolluted areas.

No conclusion could be reached as to whether different oil types could be discriminated.

BRADIE, RICHARD A., "SLAR Imagery for Sea Ice Studies", Photogrammetric Engineering, 33, 7, pp. 763-766, (July 1967). Raytheon/Autometric. American Society of Photogrammetry.

Abstract - The process of obtaining aerial photographic coverage of Arctic regions has been hampered by inclement weather, cost, and amounts of imagery necessary for adequate coverage. Recent studies utilizing Side-Looking Airborne Radar (SLAR) imagery have illustrated its value for collecting imagery during day or night, during periods of bad weather, and covering large amounts of land and water masses on relatively small amounts of film. The value of timely and continuous ice observations is evident for military and commercial applications. A brief historical background to the ice-observation program includes a comparison of radar versus conventional imagery acquisition and graphic examples of ice interpretation from radar flights.

Six, Experimental, Normal.

Alaskan Coast; pre 1967; SLAR.

SLAR, Sea Ice.

A basic explanation of radar returns from different ice types and why the tone varies, is given. The author cautions the interpreter to look beyond basic tonal variations to classify ice. It is implied by the paper that detailed texture analysis is required in the interpretation of sea ice. At the time the paper was published the term "texture analysis" was not in use.

BRADIE, R.A., A. BAY, A. BIACHE, C. MANN and C. PEPPARD, "Data Reduction of Airborne Sensor Records", Report No. DOT - CG - 01 - 800A, 196 pp, (July 1970). Autometric Operation Division, Raytheon Company.

Abstract - This report, through textural and graphic presentations, describes the capabilities of four remote sensors - panoramic camera, thermal infrared scanner, laser profiler and side-looking airborne radar - to detect sea and fast ice conditions and phenomena. Analysis of remote sensor records was accomplished in two modes: individual sensor record interpretation of the panoramic and thermal infrared; and interpretation of combination of sensor records. Generally speaking, the panoramic photography yielded more information on a unit area basis than any other sensor. Most ages of ice were interpreted from the available thermal infrared imagery. The laser profiler paper tapes were best utilized by correlation with an image forming sensor, thus yielding more definitive information than if examined alone. Side-looking airborne radar provides the greatest amount of information but the lowest per unit area.

In addition to the image analysis, an investigation of existing data bases was performed, resulting in recommendations for the implementation of a data base to encompass sea ice information from all sources.

Twenty-eight, Experimental, Normal.

Arctic, SS MANHATTAN; September 1969; AN/DPD - 2, Ka-band (16.5), SLAR.

Ice remote sensing, reconnaissance, Arctic Regions, Northwest Passage, SLAR, IR, laser profilometer, photographic.

This is a general report on the analysis of remotely sensed data collected during the SS Manhattan voyage through the Northwest Passage in September 1969. The significant results of this report are reported in other papers. This report was concerned with the establishing of a remote sensing data base.

BRADIE, R.A. and C.D. SHARP, "Analysis of SLAR Imagery of Arctic and Lake Ice," United States Coast Guard Office of Research and Development, Department of Transport, Washington, D.C., Report No. DOT-GG-11486-A, 169 pp, (April 1972). Raytheon Company, Equipment Division, Autometric Operations, Wayland, Mass.

Abstract - An evaluation of the capability of side-looking airborne radar to portray detail of ice covering sea and freshwater areas was accomplished using imagery collected over the Beaufort Sea, between Thule and Goose Bay and over portions of Lake Superior, Lake Michigan and Lake Huron. Interpretation techniques developed under previous studies were confirmed and enhanced. In addition, snow cover affects on the imaged appearance of sea and freshwater ice were investigated.

Experimental, Significant.

Baffin Bay and Beaufort Seas; February-March, 1971; 16.5 GHz, DPD-2 SLAR.

Remote sensing, sea and freshwater ice, SLAR, reconnaissance, Arctic regions.

Photography is indispensable for establishing tonal and textural signatures preliminary to SLAR imagery interpretation, and for verification of observed ice phenomena. New ice types were differentiated where possible with the aid of complementary photography. Slush, frazil and grease ice sometimes were not differentiated on the Lake or Arctic/Thule-Goose Bay imagery and at other times were certainly not detected in open water. Young ice could not generally be separated into dark grey and grey-white types on the Great Lakes, but had to be considered as one unit (Gray). Winter ice, the remaining major lake ice type, was interpreted with relative ease. In the Arctic and Thule to Goose Bay areas, first-year ice (winter ice on Great Lakes) was interpreted quite readily regardless of ridge and raft presence. Second-year and multi-year ice interpretation was also readily accomplished, but does require periodic photographic confirmation.

Ice type contact boundaries can be detected on the SLAR much more readily than on corresponding photographic coverage. The masking effects of snow cover on lake ice tends to complicate the identification of ice type. Effects of snow cover on sea ice are still to be determined. No masking was noted on sea ice images except for that of snow drift obliterating the return from ridges.

BRYAN, M.L., W.D. STROMBERG, and T.G. FARR, "Computer Processing of SLAR L-BAND Imagery", in Photogrammetric Engineering and Remote Sensing, XLII, pp. 1283-1294, (October 1977). JPL.

Abstract - A continuing problem with the interpretation of synthetic aperture radar (SAR) data, especially in the image format, is the fact that such radar systems generally are not calibrated. This tends to reduce the validity of computer processing in the form of automatic interpretation as it may be applied to SAR imagery. However, for some classes of targets, i.e. those which have especially constant and high or low returns, such automatic discrimination can be attained easily and quickly by digitally filtering and thresholding the data. We have applied such procedures to two scenes, one of sea ice and the other of freshwater lakes. The orientation of leads (through the entire sea ice scene) is quickly attained. For the lake scene, the areas of lakes were determined with a high accuracy by using the standard library routines in a General Electric Image 100 system. These techniques demonstrate the validity of machine processing for obtaining quantitative data from some classes of targets as seen by uncalibrated synthetic aperture radars.

Twenty-five, Experimental, Significant.

Beaufort Sea; October, 1975; JPL L-Band SAR, Frequency 1215 MHz, Digital HH, HV, or VV, VH.

Sea ice, lake ice, Image 100, processing, Fourier transform, uncalibrated SAR data.

To reduce the brightness gradient across each component strip and to equalize their average brightness, the mosaics were "high pass" filtered. Such an operation removes all low spatial frequency variations and sets the average data value to a specified level. The leads were isolated by simple brightness thresholding.

A measure of the orientation of leads was obtained through automated examination of the Fourier transforms of the binary lead pictures.

CAMPBELL*, W.J., P. GLOERSEN, W. NORDBERG and T.T. WILHEIT, "Dynamics and Morphology of Beaufort Sea Ice Determined from Satellites, Aircraft, and Drifting Stations," Proceedings of the COSPAR Symposium on Approaches to Earth Survey Problems Through Use of Space Techniques, P. Brock and others, eds., Constance, Germany, pp. 311-327, (May 1973). U.S. Geological Survey*, NASA/Goddard Space Flight Center.

Abstract - A series of measurements from drifting stations, aircraft, the ERTS 1, Nimbus 4 and Nimbus 5 satellites have jointly provided a new description of the dynamics and morphology of the ice cover of the Beaufort Sea. The combined analysis of these data shows that the eastern Beaufort Sea ice cover is made up of large multi-year floes while the western part is made up of small, predominantly first-year floes. The analysis suggests that this distribution might be quasi-steady-state and that the dynamics and thermodynamics of the region are more complex than hitherto known. The measurements consist of: (i) high resolution ERTS 1 imagery which is used to describe floe size and shape distribution, short-term floe dynamics, and lead and polynya dynamics; (ii) tracking by Nimbus 4 of IRLS drifting buoys to provide ice drift information which enhances the interpretation of the ERTS 1 imagery; (iii) Nimbus 5 microwave (1.55 cm wavelength) imagery which provides synoptic, sequential maps on the distribution of multi-year and first-year ice types; (iv) airborne microwave surveys and surface-based observations made during 1971 and 1972 in conjunction with the AIDJEX (Arctic Ice Dynamics Joint Experiment) program.

Nineteen, Experimental, Significant.

Beaufort Sea; 1970, 1971, 1972; ERTS 1, Nimbus 4, Nimbus 5, Passive Microwave Systems.

Sea ice, Beaufort Sea, Microwave Radiometer, Satellite, Nimbus, ERTS, AIDJEX.

Microwave (1.55 cm wavelength) images obtained during 1971 and 1972 AIDJEX experiments combined with those from Nimbus 5, permitted the delineation of first-year and multi-year ice types at several scales over the entire Arctic.

CAMPBELL*, W.J., W.F. WEEKS**, R.O. RAMSEIER*** and P. GLOERSEN****, "Geophysical Studies of Floating Ice by Remote Sensing", Journal of Glaciology, 15, 73, pp. 305-328, (1975). U.S.G.S.*, CRREL**, DFE***, NASA - Goddard****. International Glaciological Society.

Abstract - This paper presents an overview of recent remote sensing techniques as applied to geophysical studies of floating ice. The increase in scientific interest concerning floating ice has occurred during a time of rapid evolution of both remote sensing platforms and sensors. Mesoscale and macroscale studies of floating ice are discussed under these sensor categories: Visual, passive microwave, and active microwave. The specific studies that are reviewed primarily investigate ice drift and deformation, and ice type and ice roughness identification and distribution.

Fifty-Four, Theoretical/Experiment, Significant.

Arctic; Various.

AIDJEX, BESEX, SKYLAB, POLEX, LANDSAT, NOAA, ESMR, NIMBUS 5, DMSP, sea ice, radar.

This is a general paper giving a state-of-the-art overview of recent remote sensing techniques and their application to floating ice. Specifically, the authors deal with ice drift and deformation, ice type, ice roughness identification and distribution. Conclusions are that remote sensing is a valuable tool for all aspects of ice studies.

CAMPBELL*, W.J., R.O. RAMSEIER**, R.J. WEAVER** and W.F. WEEKS***, "SKYLAB Floating Ice Experiment", Department of Fisheries and the Environment, Fisheries and Marine Service, Ottawa, Miscellaneous Special Publication No. 34, pp 64, (1977). U.S.G.S*, DFE**, CRREL***. Printing and Publishing, Supply and Services Canada, Ottawa.

Introduction (Modified) - The following report describes the only SKYLAB experiment concerned with either lake ice or sea ice. The specific areas of study are of scientific and economic interest to both Canada and the United States in that they comprise part of the waters of the shipping route between the Atlantic Ocean and the Great Lakes.

In the following, we present a spacecraft-aircraft-surface multi-sensor view of sea ice in the Gulf of St. Lawrence and lake ice in the Thousand Islands-St. Lawrence River during January-February 1974. The ensemble of data is complex, including imagery and photography from Skylab-4 (SL-4); the Argus remote sensing aircraft of the Canadian Forces Maritime Proving and Evaluation Unit operating from Summerside, Prince Edward Island; the NASA NP-3A remote sensing aircraft operating from the Johnson Space Center, Houston; a Canadian Coast Guard helicopter operating from Prescott, Ontario, three hovercrafts of the Canadian Department of the Environment operating from Wolfe Island, Thousand Islands; and the Canadian oceanographic vessel CSS Dawson operating from the Bedford Institute of Oceanography, Dartmouth, Nova Scotia. The wide variety of sensor platforms that were used and the rather extreme environmental constraints that were encountered which caused various effects on sensors did not allow near-simultaneity of data sets in the three-level observing system to always be accomplished. However, we believe that the data collected gives a new view of the ice in these regions which we hope will serve as an aid to image interpretation of similar ice in other areas (Bering Sea, Baltic Sea, Sea of Okhotsk, Great Lakes, Lake Baikal) at the normal times when such multi-level, multi-sensor data are not available.

Seventeen, Experimental, Significant.

Gulf of St. Lawrence and Canadian East Coast; January-February, 1974; Skylab Sensors, Motorola APS-94D, X-band SLAR, 37.0 and 10.69 GHz Radiometers.

Passive Microwave Radiometer, SLAR, brightness temperature, sea ice, lake ice, Skylab.

The vertically polarized brightness temperature is invariably more than the horizontally polarized temperature for ice. As the age of the ice increases the brightness temperature increases in both polarizations with a decrease in the difference between the brightness temperatures for the two polarizations. Horizontally polarized brightness temperatures are the most sensitive to variation in ice type for both freshwater ice and sea ice.

CAMERON, H.L., "RADAR as a Surveying Instrument in Hydrology and Geology," Proceedings of the Third Symposium on Remote Sensing of Environment, Ann Arbor, Michigan, pp. 441-452, (October 1964). Acadia University.

Abstract - High-definition radar scope photography is investigated as a new means for studying the earth's surface. The radar is installed in an R.A.F. V-bomber and operated at approximately 41,000 feet; photographs of the scope are obtained at 5-minute intervals, providing adequate "stereo" overlap. The radar photos resulting from flights over Gaspé and Scotland are presented and discussed.

Nil, General, Normal.

Gulf of St. Lawrence; PPI.

Sea ice, PPI.

Ice survey work carried out over the Gulf of St. Lawrence near Gaspé and Prince Edward Island.

CATOE, CLARENCE E., "Remote Sensing Techniques for Detecting Oil Slicks", Journal of Petroleum Technology, pp. 267-278. (March 1973). NASA.

From Author's Introduction - There are a variety of devices for "seeing" oil on water - sensors that make use of both spatial and spectral dimensions. All of the devices are limited to a greater or lesser degree, but all are also considerably more reliable than the naked human eye.

We shall consider here the signature properties of oil slicks that make them amenable to remote sensing. We shall give particular attention to those signature properties of oil slicks that are useful in (1) detecting oil films on water surfaces; (2) mapping the aerial extent of the slicks, (3) measuring the thickness of the slicks, and (4) identifying oil types.

Thirteen, General, Significant.

NRL four-frequency dual-polarized radar system, Aerojet-General Corp. 0.81 cm radiometer.

Oil spill, SAR, microwave radiometer.

The emissive signature of petroleum products is significantly higher than that of a calm sea surface. Crude-oil pollutants have decreasing dielectric constants (increasing emissivity) with increasing API gravity. The horizontally polarized microwave signature of oil is twice the vertical polarized signature of an oil slick on a flat water surface. The detection of a slick usually becomes poorer as the sea state increases. Atmospheric cloud limitations are moderate to slight, and slicks less than 0.1 mm can be detected.

The physical phenomenon that makes an oil slick visible on radar imagery is the damping effect on the water waves in the 70 to 1.5 cm wavelength range. Radar observations of natural slicks have shown a decrease of three orders of magnitude in the return.

The Naval Research Laboratory has conducted several experiments on detecting and mapping oil slicks using the NRL four - frequency dual polarized pulsed coherent radar system. The ocean roughness acts as a depolarizer. Tests performed with the radar indicate that it is possible to map oil slicks using vertical transmit - vertical receive but horizontal transmit - horizontal receive is not responsive. The lack of detection in horizontal and cross-polarized modes is a characteristic of slightly rough surfaces viewed at shallow angles. Under such conditions, the horizontally polarized radar cross section

(RCS) is 20 dB lower than the vertically polarized RCS and the cross-polarized RCS is even lower.

With passive microwave imagery, oil slicks appear warmer than the surrounding ocean except at high sea states.

The ability to detect oil films using microwave radiometry is inversely proportional to sensor wavelength. Minimum detectable oil-film thickness using a dual-polarized 0.81 cm radiometer appears to be in the range of 10 to 20 cm calm under sea conditions. The roughness of the ocean surface affects the microwave signature. Microwave radiometers for oil-pollution detection must operate at wavelengths of 8 mm or less. Larger wavelength radiometers appear to be too insensitive to be useful for oil-pollution monitoring. Because of severe atmospheric attenuation, the nearest practical higher frequency radiometer would operate at 3 mm (94 GHz).

Low sea state conditions will prohibit the use of radar, and microwave techniques will be adversely affected by high sea states.

DUNBAR, M., "Interpretation of SLAR Imagery of Ice in Nares Strait and the Arctic Ocean", DREO Report No. 712, pp 33, (March 1975). DREO, DND. A shorter version is published in the Journal of Glaciology.

Abstract - SLAR imagery of Nares Strait was obtained on four flights carried out in January, March and August, 1973, and April, 1974, by Canadian Forces Marine Proving and Evaluation Unit in an Argus aircraft equipped with a Motorola APS-94D SLAR; the March flight also covered two lines in the Arctic Ocean, from Alert to the pole and from the pole down the 4^{o}E meridian to the ice edge at about 80^{o}N. No observations on the ground were possible, but some back-up was available on all flights from visual observations recorded in the air, and on the March flight from infrared line-scan and vertical photography.

The interpretation of ice features from the SLAR imagery is discussed, and the conclusion reached that in spite of certain ambiquities the technique has great potential which will increase with improving resolution. Extent of coverage per distance flown and independence of flight and cloud conditions make it unique among airborne sensors.

Ten, Experimental, Highly Significant.

Nares Strait North Water; Jan., March and Aug., 1973 and April, 1974; APS-94D SLAR, X-Band.

Ice observation, sea ice, Nares Strait, North Water, SLAR, IRLS, icebergs.

The range resolution was constant at about 30 m. The azimuth resolution varied with altitude and deteriorates across the range of the image. For example, at 2000 feet, the azimuth resolution is 40 m at 5 km and deteriorates at a rate of 8 m per kilometer. General image quality appears to deteriorate with range. It is concluded that the lower the flight altitude the more detail there is in the ice topography and the 25 km range gives more information than the 50 km range. The best altitude for image collection is between 1000 and 4000 ft. If extra coverage is more important, the 50 km range at a high altitude is better. These are only applicable to the APS-94D.

Multi-year ice does not have a characteristic appearance. There was no differentiation between multi-year ice and second-year ice so the term old ice is used. Certain characteristics of the particular ice regime under study were used to separate the old ice from the first-year ice, for example, the appearance of a floe within a floe which is an

outer "collar" of younger ice around an inner floe. Because old ice can be smooth or rough, gently undulating or hummocky, image reflectance can vary greatly. Frozen melt-puddles appear as dark patches on floes. Some tonal differences between the old floes were due to variation in the image quality across the range which is characteristic of the APS-94D. Floes tended to be brighter close to the track but this was not an invariable rule with the imagery. In imagery of areas other than the Nares Strait, it is more difficult to separate old ice from first-year ice. For example, in the Arctic Ocean the pack has not been subjected to melting or the jostling that results in rounded floes. Therefore, old ice is characterized by a wide range of grey-tones that can appear to be brighter or darker than the surrounding younger ice. Patterns of refrozen melt-puddles which appear very dark frequently assist in identifying old ice.

First-year ice is less varied in topography than old ice because it is relatively undeformed and very smooth. It can be broken by young pressure ridges which are sharply angular and present a good target to the radar signal. Rough first-year ice forms the cement that seals older floes together. Brash ice is very angular and gives very bright returns even though it may also contain ice from the previous open season.

Young ice forms occur in refrozen leads and in areas of open water that have just begun to freeze. Wind blown features in otherwise open water show streaks of slush ice and small cakes. The grey-tone between the strings of ice is a typical sea clutter return. Graduation from nilas to grey and grey-white ice can easily be seen. Some of the imagery appears to show backscatter due to wind formed small ripples in the open water areas. Young ice forms are difficult to interpret without the aid of surface verification or other sensor back-up.

Icebergs show up well on APS-94D imagery provided they are prominent enough and appear against a sufficiently uncluttered background. Some icebergs in the imagery visually sighted were lost in general bright clutter.

Ice concentration can be measured on summer imagery as open water areas appear black and all ice appears as various grey-shades. At other times of the year when young ice is present or leads refreeze, some difficulty is presented for interpretation because backscatter from new ice which is a smooth surface appears the same as backscatter from water which is smooth. Discrimination between smooth ice and water can often be made by the small roughness that commonly appears in ice surfaces or by noting similar lines in open water which are brash ice lined up by the wind.

Surface topography shows up as either discrete bright signals or variations in grey-tone due to minor roughness and surface undulations. Widely spaced ridges show up as bright lines but closely spaced ridges cannot be resolved. Visual truthing is required to increase the reliability in ridge detection. Topography shows up better in the middle and far ranges.

Dynamic features such as lead orientation, shear zones and drift patterns can easily be interpreted.

The most serious drawback of the APS-94D is its resolution. It is not adequate to resolve all necessary sea ice features. A comparison with the Goodyear APQ-102 synthetic aperture system shows that resolution and image quality can be improved across the whole range but smooth surfaces still remain a problem. A thorough ground truth program to observe all ice types is required.

DUNBAR, MOIRA and W.F. WEEKS*, "Interpretation of Young Ice Forms in the Gulf of St. Lawrence using Side-Looking Airborne RADAR and Infrared Imagery", CRREL Research Report 337, pp. 41, (July 1975). DREO and CRREL*. Also published as DREO Report 711.

Abstract - Ice conditions during mid-January 1974 in the Gulf of St. Lawrence and in the estuary as far upstream as Rimouski are described utilizing side-looking airborne radar, infrared and photographic imagery. The interpretations were verified by simultaneous surface observations on the ice by investigators operating from the CSS Dawson. The ice examined was undergoing rapid drift and deformation and showed a wide variety of thin ice (0-40 cm) features formed under the influence of strong winds and currents. These observations should serve as a guide in interpreting ice conditions in similar areas where ground truth data are not available.

Nine, Experimental, Normal.

Gulf of St. Lawrence; January, 1974; APS-94D X-band SLAR.

SLAR, IR scanner, sea ice, Skylab-4, ice experiment, radar, oceanography, aerial photography, Gulf of St. Lawrence.

For the Gulf of St. Lawrence ice only surface roughness effects are considered as the prime reason for the attained backscatter, as widely different ice types are not encountered.

When smooth areas are imaged there is no backscatter, thus it is not possible to distinguish between water or ice at X-band. The difference must be inferred by the shape of small roughness features on the ice or by ripples on the water surface.

The brightness returns cannot be directly related to the age of the ice or its thickness so shapes and patterns must be used to assist the interpretation. The estimate of thickness must be by reference, using other sensors as well as the SLAR. SLAR and IR are more useful in combination because they show different aspects of the ice.

EDGERTON, A.T. and D.T. TREXLER, "Oceanographic Applications of Remote Sensing with Passive Microwave Techniques," Proceedings of the Sixth International Symposium on Remote sensing of Environment, Ann Arbor, Michigan, II, pp. 767-788, (October 1969). Aerojet-General Corporation, California.

Abstract - Passive remote sensing in the microwave spectral region has proved to be a useful tool for determination of oceanographic phenomena such as sea state, pollution, and sea ice characteristics. Differences in radiometric brightness temperatures of the sea surface on the order of 15°K have been readily detected during air borne measurements of the Salton Sea, California and the North Atlantic using scanning phased array radiometers. Prediction of sea state (sea surface roughness) by microwave brightness temperature can be correlated with theoretical models for sea states less than 4 (Beaufort). Above sea state 4, white capping and the possibility of spray increase. The effects of foam on sea surface brightness temperature for a calm sea were investigated under controlled conditions. The brightness temperature for a sea surface with 50 percent foam cover increased approximately 40°K above temperatures recorded for the same surface without foam. Oil base pollutants on the ocean surface radically affect the radiometric response because of the distinctly different dielectric properties of the oil as compared to water. Laboratory and field investigations have examined the effects of different density oils and varying thicknesses on the microwave brightness temperature of the sea surface. Salinity variations in sea water between 30,000 and 34,000 ppm appear to be detectable with long wavelength radiometers. Theoretical studies indicate that small changes in the dissolved solid concentration in sea water can be determined by using radiometers operating at wavelengths greater than 10 cm. Another application of microwave radiometry is the delineation of various sea ice types based on surface roughness, thermal gradient in the ice, and the presence of absence of brine pockets. Mapping of sea ice types has a direct bearing on navigation in Arctic areas since various types of sea ice have a definite and predictable range of thicknesses.

Eight, General Review, Significant.

Passive Microwave radiometer, remote sensing, ocean, brightness temperature, sea state, oil, pollution, sea ice, salinity.

Microwave radiation observed over ocean surfaces is a function of water temperature and salinity, surface roughness, and atmospheric radiation and transmission in the observa-

tional bandwidth. Other factors to be considered include observational wavelength, antenna polarization, and viewing angle. Each of these variables is reviewed and potential oceanographic applications such as sea state determination, water temperature and salinity, oil pollution, and sea ice mapping are analyzed.

The emissivity for petroleum products is significantly higher than that of calm sea surface.

Crude oil pollutants have decreasing dielectric constants (increasing emissivity) with increasing API gravity.

Time of day and age of oil have only small effects on the radiometric response.

Detection of oil improved with decreasing sensor wavelength.

EDGERTON, A.T. and D.T. TREXLER, "Radiometric Detection of Oil Slicks," Aerojet-General Corporation, El Monte, California, Report No. SD1335-1, pp 30, (January 1970). Aerojet-General Corporation, California.

Abstract - A study has been performed to assess the feasibility of using microwave radiometry for detection of oil pollution. The investigations stems from the U.S. Coast Guard's requirement for an airborne surveillance system which can detect oil pollution during inclement weather and during the hours of darkness. Laboratory and airborne measurements were made of a variety of oil base pollutants. Laboratory investigations evaluated microwave response as a function of oil film thickness, physical temperature of the oil-water system, pollutant type, sensor wavelength, antenna polarization, and observation angle. These studies consisted of dual polarization radiometric measurements (observational wavelengths of 0.8 cm and 2.2 cm) of Bunker "C" fuel oil, gasoline, and 20, 30 and 40 API gravity crude oil. The dielectric properties of these pollutants were also measured by means of a 0.81 cm ellipsometer. The results of the laboratory measurements were used to select the most suitable microwave radiometer for the airborne measurements. The airborne experiments consisted of measurements of small oil slicks on the open ocean off the Southern California Coast. Measurements were made from a Cessna 210 aircraft instrumented with a dual-polarized 0.81 cm radiometer oriented with a forward antenna viewing angle of 45^{o} from nadir. Pollutants examined during the tests include marine diesel fuel; 20, 30 and 42 API gravity crude oils; and a mixture of diesel fuel and 20 gravity crude oil. Measurements were made under various atmospheric and low sea state conditions, including several at night.

Six, Experimental and Theoretical, Significant.

Laboratory and Southern California Coast; April, 1969; Dual-Polarized 0.8 cm and 2.2 cm Radiometers.

Oil slick, oil pollution, Microwave Radiometer, detection, emissivity, brightness temperature.

Results of radiometric measurements performed during the laboratory phase of the program showed that: 1) the microwave signature of an oil film is inversely proportional to sensor wavelength; 2) horizontally polarized signatures were twice the vertically polarized signatures for oil films of a flat water surface; and 3) all signatures were positive; i.e. greater than calm water without oil.

The airborne measurements using an 8.1 mm dual-polarized radiometer on small oil slicks showed that: 1) thinner oil-films than anticipated from laboratory findings could be detected, 2) ocean surface roughness affects the microwave signature of an oil slick since the radiometric brightness temperature of the sea increases with increased sea state, and 3) oil-films modify sea state conditions by reducing the surface roughness.

EDGERTON, A.T., D. MEEKS and D. WILLIAMS, "Microwave Emission Characteristics of Oil Slicks," Joint Conference on Sensing of Environmental Pollutants, California, American Institute of Aeronautics and Astronautics (AIAA) Paper No. 71-1071, pp. 6, (November 1971). Aerojet-General Corporation, California. AIAA Library, New York.

Abstract - The U.S. Coast Guard has sponsored microwave research for the detection, identification and surveillance of oil slicks. The dependence of microwave emission on oil type, age, film thickness, observational wavelength, antenna viewing angle and polarization was examined in the laboratory. Airborne measurements of controlled oil spills were subsequently performed at wavelengths of 8.1 and 3.2 mm for several refined and crude oil slicks, over a broad range of ocean surface and weather conditions. Microwave characteristics of slicks vary with oil type, film thickness and sea state, and provide measurable signatures over a wide range of sea state conditions.

Two, Theoretical and Experimental, Highly Significant.

Laboratory and Southern California Coast; Dual-Polarized 8.1 and 3.2 mm Wavelength Radiometers.

Oil pollution, oil slick, Microwave Radiometer, emission, brightness temperature.

Brightness temperature signatures ranging up to $70^{o}K$ were noted while overflying thick portions of oil slicks. The mass of oil per unit area is the parameter of most importance. Oil films with an average thickness of 1 μm are readily detected with 3.2 and 8.1 mm sensors. Both theory and measurements demonstrate that horizontally polarized passive microwave sensors are more responsive to oil films than vertically polarized sensors.

The microwave brightness temperature signatures of oil slicks increase with sensor frequency. However, the atmospheric attenuation also increases with frequency. The available atmospheric and oil film signature data indicate that a frequency of 37 GHz (8.1 mm wavelength) is optimal.

EDGERTON, A.T., A. STOGRYN, D.P. WILLIAMS and G. POE, "A Study of Microwave Emission Characteristics of Sea Ice," U.S. Department of Commerce, NOAA, NESS, Contract No. 1-35139, Summary Report No. 1741R-2, pp. 35, (July 1971). Aerojet-General Corporation, Azusa, California.

Abstract - A study of airborne microwave brightness temperature measurements of Arctic sea ice was conducted which consisted of (a) numerical modeling of sea ice emission, (b) identification of atmospheric effects, and (c) comparative analysis of measured results. Aircraft data were acquired by NASA/Goddard Space Flight Center, Greenbelt, Maryland during the middle of June, 1970 near Point Barrow, Alaska. Microwave measurements were performed at observational wavelengths of .51, .55, .81, .96, 1.35, 2.81, and 3.2 cm at low (150) and high (9 km) altitudes. Only the low altitude data were considered in the present study since a solid cloud deck existed during most of the overflights. Lack of "surface-truth" information (e.g. salinity and temperature profiles) precluded direct quantitative comparisons of measurements and theory. A major result of the present study is the general classification of sea ice brightness temperatures into categories of "high" (~240°K) and "low" (~200-210°K) emission corresponding to young and weathered sea ice, respectively. Several mechanisms were advanced to explain this phenomenon using available aircraft supporting data (photographic infrared and geodolite data). However, none could be determined to be more valid than the other. Based on computed estimates (using aircraft meteorological data), the present study indicates that the effects of atmospheric attenuation (and re-radiation) will degrade but not eliminate the mapping of gross ice type and ice-water boundaries using passive microwave radiometry.

Nil, Theoretical and Experimental, Highly Significant.

Off P. Barrow, Alaska; June, 1970; Microwave Radiometer at 0.51, 0.55, 0.81, 0.96, 1.35, 1.55, 2.81 and 3.2 cm wavelengths.

Young ice, weathered ice, theoretical model, microwave radiometer, skin depth.

The theory of vertically structured media, which incorporates subsurface salinity and temperature gradients and neglects non-specular scattering, was employed to establish the dependence of sea ice emissions on salinity and temperature for several observational wavelengths and view angles. By using linear distributions of salinity and temperature, it was found that a relatively large range of sea ice emissions (or brightness temperature)

may arise as a result of either surface temperature or salinity changes. The computer sea ice brightness temperature exhibited the largest changes at temperature near $0^{o}C$ due to the fact that changes in the brine volume in sea ice are especially rapid near $0^{o}C$.

Two different atmospheric models were investigated, one derived from measured meteorological data incorporating clouds, and another using Arctic Summer Atmospheric Model having no clouds. In both cases, the computed brightness temperature of seawater ($0^{o}C$ and $35^{o}/oo$ salinity) due to atmospheric contributions between seawater and a 9 km altitude were on the order of 3 to $4^{o}K$ at 2.81 cm, 10 to $12^{o}K$ at 1.55 cm, 10 to $18^{o}K$ at 1.35 cm, 8 to $10^{o}K$ at 0.96 cm, 15 to $17^{o}K$ for the horizontal polarization at 0.91 cm (45^{o} from nadir) and 10 to $13^{o}K$ for the vertical polarization at 0.81 cm (45^{o} from nadir). The increases due to increases in cloud wave content (0 to 0.3 kg/m^{2}) were on the order of $4^{o}K$ at 2.81, $7^{o}K$ at 1.55 cm (nadir), $9^{o}K$ at 1.35 cm, $15^{o}K$ at 0.96 cm, and $30^{o}K$ and $18^{o}K$ at 0.81 cm for, respectively, the horizontal and vertical polarization (45^{o} from nadir).

It was noted that the atmospheric attenuation will be significantly reduced when viewing substances whose emissivities are larger than sea water.

The contrast in brightness temperatures between young and weathered older ice types decreased significantly as the observational wavelength increased. A significant contrast in the brightness temperatures of ice and water was observed at all wavelengths greater than (or equal to) 0.81 cm and increased with wavelength, being largest at 2.81 cm.

EKLUND, F., J. NILSSON and A. BLOMQUIST, False-Alarm Risks at Radar Detection of Oil Spill, Proceedings, USRI Commission II Specialist Meeting on Microwave Scattering and Emission from the Earth, Berne, Switzerland, pp. 39-45, (September 1975). National Defence Research Institute, Stockholm, Sweden.

Introduction (excerpt) - The potential of radar in detecting and mapping oil spills at sea is well demonstrated, and plans are underway to use radar in operational systems for large area surveys of oil spills at sea in various countries.

In such systems possible false alarm sources should be well known, facilitating the development of equipment and interpretation techniques with an acceptable level of false oil spill alarms.

For a slightly rough sea the radar back scatter cross-section, σ^o, is proportional to the two dimensional energy density spectrum, Ψ (K_x, K_y) of the sea surface height variations. Here K_x and K_y are the wave numbers for water waves in the x- and y-directions, respectively.

Only water wave components propagating in the same direction as the radio wave, (the x-direction), contribute to the back scattered power.

For cm wave radar the water waves responsible for backscattering are in the region of capillary and short gravity waves.

When the sea is rough the theory must be modified in different ways: Large-scale waves modify the local θ value, shadowing effects must be included, spray and foam contribute etc.

An oil film on the surface increases the attenuation rate of water waves for all wavelenghts of interest. The result is that capillary and short gravity waves either are damped out or grow more slowly than on a clean water surface resulting in a decrease of Ψ (K) of σ^o within the area of an oil slick.

Only few measurements of the amount of the decrease in σ^o are reported. At experiments in the Baltic the decrease in σ^o was found to be of the order of 5-7 dB at a radar wavelength of 3 cm, vertical polarization and at $\theta = 3.5^o$. The measurements were made within the first hour of small intentional spills of 150 gallons of heavy fuel oil at wind speed 6-10 m/s, sea surface temperature 0^oC and air temperature 0^oC.

In this discussion of possible risks for false oil spill alarms, a local reduction in σ^o of the order of 5 dB will be considered as a reasonable oil spill alarm threshold.

Five, Experimental, Significant.

Baltic Sea; Summer and Fall, 1972; Airborne Vertically polarized X-band radar.

Oil spill, radar, backscattering, cross-section, windspeed, temperature, false alarm, probability.

There may be many different reasons for false alarms in radar oil spill surveying. The most difficult situation occurs at low wind speeds when space and time variations in the wind field alone may cause variations of the sea surface roughness that could be misinterpreted as caused by oil slicks. This effect is more pronounced the cooler the water surface is.

The critical wind speed below which false alarm risks could be of importance in an operational system using X-band radar is of the order of 3-5 m/s in summer and 8 m/s in winter.

It does not seem very likely that sea surface temperature variations alone could result in sea surface roughness patterns that could be misinterpreted as oil slicks except in some extreme cases. Possible other reasons for false oil spill alarms such as currents and algae belts have been mentioned but a quantitative estimate of their effects remains to be made.

ENGLAND, A.W., "The Effect Upon Microwave Emissivity of Volume Scattering in Snow, in Ice and in Frozen Soil," Proceedings, URSI Commission II Specialist Meeting on Microwave Scattering and Emission from Earth, Berne, Switzerland, pp. 273-287, (September 1974).

U.S. Geological Survey, Denver, Colorado.

Abstract - Radiative transfer theory has been applied to volume scattering in relatively low loss dielectric media. The theory and its inherent assumptions are reviewed. Conclusions are that volume scattering dominates the microwave emissive properties of dry snow, but that scattering will, in general, be irrelevent to longer wavelength emission from ice over freshwater and from frozen soil. Consequently, the variation of emisivity with wavelength probably cannot be used to infer the thickness of a dry snowpack but can be used to infer thicknesses of ice over freshwater and of seasonally frozen soil.

Twenty-six, Theoretical, Significant.

Microwave emissivity, volume scattering, ice, snow.

The model of Rayleigh scatterers embedded in a dielectric layer of nonuniform thickness provides an adequate and self-consistent characterization for computing the microwave emissivity of low-loss media containing relatively small scatterers.

ESTES, J.E. and B. GOLOMB, "Oil Spills: Method of Measuring their Extent on the Sea Surface," Science, 169, pp. 676-678, (May 1970). University of California.

Abstract - It is difficult to estimate the area affected by an oil spill at sea, the degree of coverage by oil pollutants within the affected area, and the quantity of pollutants involved. Estimates of volumes and flow rates are based on estimated change in arrival extent of the spill. Uncertainties in measurement of area degrade the accuracy of estimating other parameters. To resolve this problem, available stock components have now been assembled into a system that yields repeatable, economical measurements of the arrival extent of oil spills at acceptable levels of accuracy. The system comprises overflights with a thermal infrared imaging system, densitometric colour enhancement of the infrared images, and automatic digital planimetry of the areas of specified image densities.

Four, General Experimental, Normal.

Santa Barbara; February, 1969; Bendix 8-14 um thermal mapper, data colour film reader system.

Oil, arrival extent, densitometry, enhancement.

It is difficult to estimate the area affected by a given oil spill, the degree of concentration of the pollutants within the affected area, and the quantity of pollutants involved. Oil on the sea surface does not image well in the spectral bands recorded by conventional black and white or colour photography. A thermal infrared mapper combined with densitometric colour enhancement and automatic digital planimetry can be used to obtain automatic and repeatable accurate measurements or arrival extent of an oil spill.

There are conflicting explanations for the apparent thermal anomalies that can be seen on images of oil patches in thermal infrared. Because it is darker than the ambient sea water oil should have a higher emissivity and show a lighter tone on the imagery.

Opposingly, reflectivity of oil films and their interference with heat exchange at the air/sea interface substantiates expectations that oil patches should register as darker (cooler) tones. Darker areas are areas around the blowout where cooler fluids from the ocean bottom are displacing the warmer surface waters.

Outside the main body of the blowout are diffuse patches, which are occasionally lighter but are generally darker than the background. These are thinner oil film areas whose

iridescence makes them efficient reflectors and whose interposition at the air/sea interface reduces heat exchange and leads to a cool (darker) thermal infrared tonal image.

ESTES, J.E., L.W. SENGER and P.R. FORTUNE, "Potential Applications of Remote Sensing Techniques to the Study of Marine Oil Pollution, Geoforum, 9, pp. 69-81, (1972). University of California.

Abstract - The detection and measurement of oil pollution in the marine environment are procedures requiring a broad range of instrumentation capabilities within an equally broad range of environmental conditions. Due to the complex behaviour of oil on water, its susceptibility to transport and modification forces, and the physiochemical anomalies associated with its presence, both aerial and surface sensors are necessary to establish a complete and effective monitoring system. Remote sensors, operating in the ultraviolet, thermal infrared, and microwave portions of the electromagnetic spectrum, exhibit potentially good oil detection capabilities. Radar in particular, possesses strong capability for the mapping of an oil slick's arrival extent since it is operative even under adverse weather conditions, day or night. Since no remote sensor system is presently capable of providing accurate information on the type or thickness of an oil slick, surface-based mechanisms must be utilized to gather ground truth data. These measurements, including the collection of radiometric, meteorological, and oceanographic information, are essential for a comparative analysis of remotely sensed data and their interpretation. More research is needed in the realm of remote sensing and ground truth data collection systems, including their co-ordination, if an operationally feasible system for monitoring marine oil pollution is to be developed.

Twenty-three, General review, Significant.

Aerojet-General Corporation, 8.1 mm Dual-Polarized Radiometer; Dual-Polarized P, X, L and C Synthetic Aperture Radar.

Microwave radiation is more linearly dependent upon temperature than infrared radiation. Water has an emissivity of 0.41 throughout the microwave region and exhibits a low equivalent black body temperature.

Laboratory tests indicate that the microwave radiometric signature of an oil film is inversely proportional to sensor wavelength. For a flat water surface, the horizontally polarized signatures are twice the vertically polarized signatures. Oil signatures are greater than those for calm water without oil. Airborne measurements with an 8.1 mm dual polarized radiometer show that oil films thinner than those in the laboratory can be detected.

The presence of an oil film modifies or reduces the ocean's surface roughness thereby changing its equivalent black body temperature and microwave signature. The detection ability of both active and passive microwave systems is dependent upon surface roughness which serves to enhance the object to background contrast ratios, with passive systems more applicable for oil thickness detection. The ability of radar to detect oil increases with sea state because damping of capillary waves increases the contrast between oil polluted and uncontaminated seawater with increasing sea state.

For an imaging radar, vertical transmit-vertical receive polarization is more suitable for oil spill detection than horizontal transmit-horizontal receive polarization.

Altitudes from 165 to 1650 m have proven adequate for most oil imaging purposes.

GLAESER, J.L. and G.P. VANCE, " A Study of the Behaviour of Oil Spills in the Arctic, United States Coast Guard, Office of Research and Development, Applied Technology Division, Washington, D.C., Final Report, Project No. 714108/001,002, pp. 60, (February 1971). USCG. AD717142.

Abstract - A program to investigate the behaviour of oil spills in the Arctic was conducted off the Northern Coast of Alaska in July 1970. Numerous small oil spills were made to obtain data on the following subjects; the spreading behaviour of crude oil on ice and water surfaces; the interaction characteristics of crude oil with ice, on water, and under ice; and the effectiveness of burning and absorption as methods of removal.

Both Prudhoe Bay ("Sag" River) crude oil and diesel oil were used in the test program. Results quantify spreading and interaction characteristics in addition to presenting qualitative information on each area of interest. Promise is shown for both burning and absorption as methods of oil removal in the summer. Data is presented on both the physical and chemical properties of aged crude oil.

Six, Theoretical and Experimental, Significant.

Off Alaska; July, 1970.

Oil Pollution, Arctic oil pollution, oil in ice, oil under ice.

It was found that an upper layer of recrystallized ice in the test area absorbed up to 25 percent of its volume in oil which had been released on the surface. The oil travelled through the upper layer seeking the lowest possible level and eventually migrating to the melt ponds present. Measurements showed recrystallized ice thickness to average approximately two inches, and core samples showed the density of the upper layer to range from 0.46 to 0.61 g/cm^3. Data from the spreading experiments on ice show power law relationships between length of spill and time.

The spreading of the crude oil, when released on water, was significantly affected by the wind. As a result of a net negative spreading coefficient, the crude would not spread out as a thin film. Crude oil which was released under an ice cover rose to the surface, where it remained without dispersing to any great extent.

The North Slope crude burned easily under all conditions except when in a thin film. Burning resulted in the estimated removal of 90 to 98 percent of the oil spilled. Straw and peat moss were also used as absorbants.

An investigation into the effect of an oil spill on the arctic heat budget showed general agreement with past work done on the subject.

GLOERSEN, P., J.J. SCHMUGEE and T.C. CHANG, "Microwave Signatures of Snow, Ice and Soil at Several Wavelengths, Proocedings, URSI Commission II Specialist Meeting on Microwave Scattering and Emission from Earth, Berne, Switzerland, pp 101-111, (September 1974). NASA Gooddard.

Abstract - Analyses of data obtained from aircraft-borne radiometers have shown that the microwave signatures of various parts of the terrain depend on both the volume scattering cross section and the dielectric loss in the medium. In soil, it has been found that experimental data fit a model in which the scattering cross section is negligible compared to the dielectric loss and the surface reflectivity with regard to the observed emissivity. The data and a subsequent analysis show that the moisture content in the top of 0.2 of a wavelength in the soil primarily determines the emissivity of the soil at a given wavelength. Because the flow of water to the soil surface is dependent on the moisture content of the subsurface, the radiometers appear to be responding to the plant available water in the soil. On the other hand, the volume scattering cross section in snow and continental ice was found, from analyzing data obtained with aircraft and spacecraft borne radiometers, to be more important than the dielectric loss or surface reflectivity in determining the observed microwave emissivity. A model which assumes Miel scattering of ice particles of various sizes was found to be the dominant volume scattering mechanism in these media. Both spectral variation in the microwave signatures of snow and ice fields, as well as the variation in the emissivity of continental ice sheets such as those covering Greenland and Antarctica appear to be consistent with this model.

Five, Theoretical and Experimental, Normal.

Greenland, Antarctica; Nimbus 5 Radiometer, 1.5 cm wavelength Radiometer.

X-band, Ka-band, Snow, ice, emissivity, brightness temperature, snow particle size, soil moisture.

The Miel scattering theory has been used to calculate the microwave extinction efficiency for spherical snow particles of various radii near the melting point. In general, the extinction efficiency increases with particle size, largely as a result of the increase in scattering cross section.

GLOERSEN, P., W.J. WEBSTER, Jr., T.T. WILHEIT, T.C. CHANG, and D.B. ROSS*, "Spectral Variation in the Microwave Emissivity of the Roughened Sea", Proceedings, URSI Commission II Specialist Meeting on Microwave Scattering and Emission from Earth, Berne Switzerland, pp 11-15, (September 1974). NASA, Goddard Space Flight Centre, Maryland, and NOAA, Florida*.

Abstract - Recently acquired microwave data obtained from the NASA CV 990 research aircraft over a wavelength range from 0.8 to 21 cm for various ocean surface wind conditions have yielded the variation of the sea surface emissivity as functions of the wavelength, polarization, the viewing angle, and the surface wind speed. Data acquired at a wavelength of 1.5 cm, horizontal polarization, agree with the data obtained earlier by Nordberg et al. and Hollinger at nadir and 50° viewing angles respectively; and ratio of brightness temperature change to wind speed change was found to be approximately 1°K per metre per second over a wind speed range of 5 to 26 metres per second. Combining these recent measurements with the earlier measurements, it is evident that microwave radiometry can be used as a remote sensing anemometer over all wind speed ranges of interest. Analysis of the data revealed that for nadir-viewing instruments, the ratio of the brightness temperature change to wind speed change was approximately constant for the wavelength range of 0.8 to 2.8 cm, about three quarters of that value at 6 cm, and nearly zero at 21 cm. A model which assumes a thin transition layer with continuously varying dielectric constant between the foam or streak bubbles or actively breaking waves and the sea surface leads to calculated surface emissivities which are consistent with the observations.

Six, Experimental, Normal.

Radiometers over a wavelength range from 0.8 to 21 cm, Passive Microwave Imager at 1.55 cm.

Storm cell, microwave brightness temperature, radiometer, ocean surface wind speed.

For nadir viewing radiometers, the sensitivity of brightness temperature changes to changes in the surface windspeed are independent of wavelength above the wavelength of 2.8 cm, and the sensitivity drops to nearly zero at a wavelength of 21 cm.

GOWER, J.F.R., "Microwave Sensing of Sea Surface Wave Patterns, Proceedings of the Fourth Canadian Symposium on Remote Sensing, I, Quebec City, pp 395-406, (May 1977). Inst. of Ocean Sci., Patricia Bay, Victoria, B.C. Canadian Aeronautics and Space Institute.

Abstract - Data from the GEOS-3 altimeter and from an airborne synthetic aperture radar have been obtained for the North East Pacific off the British Columiba Coast. Both these instruments are forerunners of sensors to be included in SEASAT, NASA's prototype all weather oceanographic satellite.

The waveheight measurements deduced from the altimeter have been compared with ship wave and weather reports. The satellite waveheights appear at present to be accurate to $\pm$ 1 m, but possibility for improvement exists in the computation methods used in correcting for effects other than waveheight that also change the average shape of the radar pulse reflected by the sea surface. Examples of different processing methods are shown. The preferred technique is based on the results of a simple model of the pulse variations and allows timing or tracking loop errors to be compensated.

The accuracy of waveheights deduced using the preferred processing technique is estimated as about 0.5 m.

High resolution radar imagery complements the altimeter by showing wave patterns and hence their wavelength and direction. The radar imagery to be presented was taken with the Jet Propulsion Laboratories L-band synthetic aperture radar flying on the NASA Convair 990 aircraft. The unit roughly duplicates the SEASAT instrument but has slightly higher resolution. The direction and wavelength of the predominant surface waves can be seen, and comparisons are made with the limited ground truth available at the time of the flight. Surface markings due to internal waves are particularly clearly seen, and SEASAT radar imagery should be very suitable for studying the frequency of occurrence of these.

Five, Experimental, Normal.

NE Pacific; April-July, 1976, April-May, 1975; JPL L-band SAR, GEOS-3 Radar Altimeter.

GOES-3, radar altimeter, JPL L-band SAR, ocean waves, internal waves, tidal fronts, SEASAT.

This is a general study evaluating the radar altimeter data and L-band SAR data which will be available on SEASAT A for studies on ocean waves. The paper shows that surface

waves cannot always be detected on radar and shows that repetitive coverage is needed to determine internal wave effects.

GRAF, K.A., D.E. TREMAIN and H. GUTHART, Induced Current Effects on Microwave Backscatter, IEEE Journal of Oceanic Engineering, OE-2, pp 36-42, (January 1977). Stanford Research Institute.

Abstract - Microwave measurements have been made with a coherent radar in a wind-wave tank to determine the effect of induced current on backscatter. Perturbations were introduced into the wave structure by inducing a current in the water that flowed either with or against the wind. The effect of that flowed either with or against the wind. The effect of current on radar cross section was slight; the effect on the Doppler was much more pronounced. It was found that the wave components responsible for radar backscatter are predominately free waves (that is, wave which travel at the dispersion velocity) rather than waves which are parasitic (or locked) to the dominant waves.

Six, Experimental, Normal.

Menlo Park, California; wind-wave tank 6 x 6 x 30 ft, Coherent 9.6 GHz and 31 GHz Radars with horizontal polarization.

Backscatter, Doppler, current, free wave, parasitic waves, wind.

The angle of incidence of the radar was 45^{o}. The Doppler shift was comparatively small Doppler associated with the flow against wind cases, larger with no flow cases and largest in the flow with wind cases. The wind ranges were 5 m/s to 10 m/s and correspond to 6.8 m/s and 13.1 m/s on the open ocean 10 m above the surface. The surface current flow was sinusoidal due to the bottom. The mean velocities were 0.018 m/s in one direction and 0.022 m/s in the other. It was inferred that the wind induced additional surface currents of 0.05 m/s and 0.1 m/s when the nominal wind velocities were 5 m/s and 10 m/s, respectively. Cross sections obtained for various windspeeds (Figures) changed rapidly for a wind speed of less than about 4 m/s because of a tendency for the induced current to perturb the waves in regions where they were developing. Induced currents retarded or speeded up the development of the ave spectra at any particular fetch and corresponding wind speed.

These curves and similar data for $\theta = 70^{o}$ indicate that the cross-section tends to be greater when the water is being pumped against the wind than when it is being pumped with the wind for the range of wind speeds indicated. The Doppler shifts for this data are plotted and show the tendencies noted above.

The parameters representing the derived relationship between Doppler shift and wind speed (with or against flow) for the X and Ka-band radar for incidence angles of 45^{o} and 70^{o} are given in a table. The Doppler spread tended to increase linearly with wind speed and can be related to the orbital velocity of the dominant wave.

The dominant wave and the components locked into it contribute very little to the radar return. Most of the radar return is due to capillary waves, which travel at velocities independent of the longer gravity waves. A comparison of measured Doppler shift against calculated Doppler shift shows that at $\theta = 45^{o}$ the Doppler shift is independent of the dominant wave and there is a strong dependency on the capillary waves. Similar results were obtained at $\theta = 70^{o}$. Attempts to find the Doppler frequency predicted for the parasitic waves (waves moving with the dominant wave) failed at both incidence angles on other cases when parasitic signals should have been resolvable. They were not observed and were, therefore, at least 30 dB below the main peak in the spectrum. Previous studies show that for $\theta \leq 60^{o}$ free waves (capillary) are predominately responsible for backscatter and this is in agreement with these results. The previous study also states that for $\theta \geq 70^{o}$ parasitic waves are predominately responsible. This is contrary to these results.

GRAY, A.L., R.O. RAMSEIER and W.J. CAMPBELL, "Scatterometer and SLAR Results obtained Over Arctic Sea Ice and Their Relevance to the Problems of Arctic Ice Reconnaissance," Proceedings of the 4th Canadian Symposium on Remote Sensing, I, pp 424-443, (May 1977). CCRS, DFE, U.S.C.G., Canadian Aeronautics and Space Institute.

Abstract - Although side-looking airborne radars (SLAR's) have been shown to be a valuable tool in ice reconnaissance, the optimum parameters for microwave frequency resolution, look angle and polarizations have not been determined. For example, experience gained with imagery obtained from the DND Motorola APS-94D SLAR has shown that there can be ambiguities and overlap in the magnitude of the backscatter from regions of first year and multi-year sea ice over much of the imaged swath. This observation appears to be consistent with the fact that the surface roughness of both forms of sea ice is highly variable and one of the dominant mechanisms related to microwave backscatter is the surface roughness and relief. Nevertheless, the results obtained in the Arctic with the 13.3 GHz scatterometer operated by the Canada Centre for Remote Sensing have shown systematic changes in microwave backscatter which have a strong correlation with fairly gross ice type categories. In particular, in the spring 1975 AIDJEX and Beaufort Sea offshore programes multi-year ice showed significantly higher backscatter were 8-10 dB for the like polarized signals and 15-18 dB for the cross-polarized signals. Some of these results, together with supporting visible and infrared imagery will be used to illustrate the variation in backscatter with incidence angle and to compare and discuss the sensitivity to ice type that should be obtainable with imaging radars operating in the 2-3 cm wavelength range. On the basis of the 1975 active microwave remote sensing data and other available imagery, an attempt will also be made to choose operating parameters for an airborne imaging radar to be used as part of an ice reconnaissance sensor package.

Twenty-one, Experimental, Highly Significant.

Arctic-Beaufort Sea AIDJEX; Ryan 720 Scatterometer (13.3 GHz) and APS-94D X-band SLAR.

SLAR, Scatterometer, backscatter, AIDJEX, Beaufort Sea, sea ice.

It has been demonstrated that a SLAR operating at a 2-3 cm wavelength with incident angles of less than 80^{o} will acquire imagery on which the grey scale or image tone information will help signigicantly in Arctic ice type identification.

It appears that for ice reconnaissance, a cross-polarized radar channel will have more grey scale information and contrast than the equivalent like polarized channel.

Ideally, a dynamic range of 30 to 35 dB for the like and cross-polarized channels for an ice reconnaissance imaging radar would be desirable though to implement.

GUINARD, N.W., "The Remote Sensing of the Sea and Sea ice," Proceedings of the Sixth International Symposium on Remote Sensing of Environment, Ann Arbor, Michigan, II, pp 737-754, October, (1969). Naval Research Laboratory.

Abstract - The Naval Research Laboratory has developed a unique data collection facility, the Four-Frequency Radar (4FR) System which is an experimental radar installed in an EC-121 (super Constellation) aircraft. The system has a wavelength capability spanning the range from UHF to X-band, and linear polarization diversity, pulse width and repetition rate flexibility and the ability to illuminate terrain and targets at various angles of incidence and with near simultaneity. This system has been used to measure the radar returns scattered from both sea and ice surfaces both for the purpose of identifying sea states and ice types and to determine effective models of the scattering processes to aid in the design of optimum sensors. Data collected over the ocean in low sea states at Puerto Rico and in the higher sea states observed in the North Atlantic have been used to verify the predictions of the slightly rough surface model. Polar ice has been mapped in synthetic aperture mode to determine roughness and contour. Some penetration effects have been noted.

Nine, Experimental, Highly Significant.

Off Puerto Rico, North Atlantic, off Alaska; July, 1965, February, 1969, April, 1968; NRL 4FR Experimental radar system, X-C-L- and P-bands.

NRL, Four-Frequency Radar, radar cross section, sea state, sea ice.

The measurement of the radar energy scattered from the sea surface over a wide range of wind/height conditions have resulted in the establishment of the upper limit for the radar cross section.

A prediction of the trend followed by the bandwidth of the doppler spectrum with wave height has been developed from basic hydrodynamic principles and verified by data.

The varying shades of grey on the radar imagery at X-band may be associated with the differing roughness of the ice. From a knowledge of the ice roughness, ice analysts are able to infer the age and thus the melting rate of the ice patch.

The L-band radar responds more strongly to the boundaries of the ice patches than to the roughness of the ice.

GUINARD, N.W., "The Remote Sensing of Oil Slicks," Proceedings of the Seventh International Symposium on Remote Sensing of Environment, Ann Arbor, Michigan, II, pp 1005-1026, (May 1971a). Naval Research Laboratory. CCRS 1000904 M5-7.

Abstract - Radar is presently being used by the Naval Research Laboratory to detect the area of coverage of oil spills. The effort is being sponsored by the U.S. Coast Guard. In the first phase of the study, two types of measurement programs were conducted. The first was the mapping of the accidental spill produced when the tanker ARROW collided with Cerberus Rock in Chedabucto Bay, Nova Scotia, while the second was conducted over a programmed spill off the California coast. In both cases, imagery was acquired as a function of radar frequency, polarization and viewing angle by the NRL Four-Frequency Radar System. As a result, both the feasibility and utility of the radar approach has been established and various characteristics of the oil signature have been determined. Experiments are continuing over both programmed and accidental spills to accumulate a data base from which the relationships between image contrast and radar variables, sea state and oil type and thickness can be obtained as well as to acquire operational data which can provide guidance into the deployment and utilization of the technique.

Seven, Experimental, Operational, Highly Significant.

Nova Scotia, California; Febr. 17, 1970, Oct. - Dec., 1970; NRL 4-Frequency Radar.

Oil spill, thickness, SAR polarization, sea state, radar wavelength, scope, incidence angle.

Image contrast is a strong function of the polarization of the radar signal. Vertically polarized signals produce maximum contrast.

There is a strong functional relationship between the incident radar wavelength, the sea state and the thickness of the oil film. Although there is insufficient data at present to define this relationship, the observed trends indicate that thin films (1 micron) are best detected in low sea states (10 knot winds or less) by low frequency transmissions (1 to 3 GHz), while there is some indication that thin films may be best detected in high sea states by higher frequency (5 GHz and above) transmissions.

The minimum thickness of oil detected in the SCOPE tests was 1.0 micron in low sea states. Since the contrast of the slick image was large under these conditions, 0.5 microns should be detectable.

A spatial resolution of 100 to 300 feet in both range and azimuth direction is adequate for slick definition.

There is some evidence that radar may be used to determine oil thicknesses; however, there has been no evidence that oil type yields a distinctive signature. Oil spreading rate may be used to gain some insight into oil type if two or more images can be acquired over a reasonable interval of time.

The radar viewing angle should be within 45 degrees of the horizontal to avoid specular returns. Since small grazing angles yield larger swath widths, an angular range from 2 to 20 degrees seems suitable for radar design.

GUINARD, N.W., "Radar Detection of Oil Spills," Joint Conference on Sensing of Environmental Pollutants, California, pp 8, (November 1976b). NRL. AIAA Library, CCRS No. 1001282.

Abstract - The Naval Research Laboratory (NRL) under sponsorship of the U.S. Coast Guard has been investigating the potential of synthetic aperture radar in the detection and monitoring of oil spills on the ocean surface. The four frequency radar system has been used to map the accidental spill produced by the tanker ARROW in Chedabucto Bay, N.S. and also programmed spills off the California coast (SCOPE). Results have shown the feasibility of the technique in low to moderate sea states and have shown the capability of radar to reliably detect 1 micron average oil thickness in low sea states. Oil spreading rates have also been determined by repeated mapping runs over an expanding spill.

Seven, Experimental, Significant.

Chedabucto Bay, Santa Barbara, February 17, 1970, Oct. - Dec. 1970; NRL 4 Frequency SAR.

SCOPE, Chedabucto Bay, Four Frequency Radar, oil thickness sea state, polarizations, radar wavelength, incidence angle.

Radar imagery of two oil spills was analyzed to determine the functional relationship between the image contrast and the radar parameters of wavelength, polarization and viewing angle and the sea state and oil thickness. Conclusions based upon this experiment are:

Image contrast is a strong function of the polarization of the radar signal. Vertically polarized signals produce maximum contrast. There is a strong relationship between the incident radar wavelength, the sea state and the thickness of the oil film, but it is not possible to define this relationship because of insufficient data.

Observed trends indicate that thin films (1 micron) are best detected in low sea states (10 knot winds or less) by low frequency transmissions (1 to 3 GHz). There was some indication that thin films might best be detected in high sea states by higher frequency transmissions (5 GHz and above).

The minimum thickness of oil detected was 1.0 microns in low sea states. Spatial resolution of 100 to 300 feet in both range and azimuth directions is adequate for slick

detection. There is some evidence that radar can be used to determine oil thickness. There is no evidence that oil type yields a distinctive signature. Radar viewing angles should be within 45^{o} of horizontal to avoid specular returns. An angular range from 2 to 20 degrees appears suitable for radar design.

HALLIKAINEN, M., "Analysis of Dielectric Properties and Noise Temperature of Sea Ice for Microwave," Remote Sensing Applications, Proceedings of the European Microwave Conference, Brussels, No. C.15.3, pp 4, (September 1973). Helsinki University of Technology, Radio Laboratory, Otanieni, Finland.

Introduction - Remote sensing by using microwave radiometers is becoming an important new method for mapping the characteristics of sea ice. In order to determine the physical properties of sea ice from the measured noise temperature data, knowledge of the dielectric properties of sea ice is required. Some results of the analysis of dielectric properties at microwace frequencies have been reported earlier /1/ and a method for calculating the noise temperature of sea ice has been suggested /2/.

In this paper, the dielectric properties of sea ice have been studied considering the effects of temperature, salinity and frequency. The results obtained have been used for calculating the noise temperature of sea ice. Calculations are based on experimental salinity profiles measured along the Finnish coast.

Six, Theoretical, Normal.

Microwave Radiometer, sea ice, noise temperature, brightness temperature, dielectric properties.

The dielectric loss of sea ice depends strongly on frequency, salinity and temperature above $-10^{\circ}C$. The radiation received by a microwave radiometer is the sum of the components from seawater and sea ice. The contribution of the second order reflections is negligible even at moderate salinities of sea ice.

The noise of the temperature signal increases with ice thickness until the attenuation is so high that the lowest ice layers do not contribute to the radiation received by the antenna.

HAMMOND, D.L., R.A. MENNELLA and E.J. WALSH*, "Short Pulse Radar Used to Measure Sea Surface Windspeed and SWH," IEEE Journal of Oceanic Engineering, OE-2, 1, pp 61-67, (January 1977). Naval Research Laboratory, NASA Wallops Flight Center.*

Abstract - A joint airborne measurement program is being pursued by NRL and NASA Wallops Flight Center to determine the extent to which wind speed and sea surface significant wave height (SWH) can be measured quantitatively and remotely with a short pulse (2 ns), wide-beam (60^{o}), nadir-looking 3 cm radar. The concept involved relative power measurements only and does not need a scanning antenna, doppler filters, or absolute power calibration. The slopes of the leading and trailing edges of the averaged received power for the pulse limited altimeter are used to infer SWH and surface wind speed. The interpretation is based on theoretical models of the effects of SWH on the leading edge shape and rms sea-surface slope on the trailing-edge shape. The models include the radar system parameters of antenna beam width and pulse width. Preliminary experimental results look promising and indicate that it may be possible to design a relatively compact airborne radar to infer, in real-time, the sea surface SWH and surface wind speed.

Twenty-three, Theoretical, Normal.

NRL 3 cm, 2 ns (60^{o}) wind-wave radar.

Slope, direction, SWH, wind-speed, backscatter, sea-surface.

The slopes of the leading and trailing edges of the averaged received power for a pulse limited nadir or near nadir, looking altimeter can be used to determine SWH and surface wind speed, respectively. The SWH is determined directly from its effect on the slope of the leading edge. Wind speed is inferred from the trailing edge slope which depends on surface roughness (radar backscatter properties) which is influenced by the surface wind field.

The attraction of this system is that it provides a means of determining the wind speed without the necessity of an absolute calibration of the radar. The theory is compared with actual data obtained and shows excellent correlation. There is very little scatter for the mean power returned.

HOFER, R. and E. SCHANDA, "Emission Properties of Water Surfaces at 3 mm Wavelength," Proceedings, URSI Commission II Speciality Meeting on Microwave Scattering and Emission from Earth, Berne, Switzerland, pp 17-23, (September 1974). University of Berne, Switzerland.

Abstract - Antenna temperature and forward scattering measurements at 94 GHz on water surfaces in a temperature range between 7 and 43°C are compared and discussed. The angular dependence of the considerable contribution of the atmosphere in this frequency region according to the secans law is verified and taken into account for all measurements. An oil polluted water surface and surface waves are studied.

Five, Experimental, Significant.

Laboratory; Experimental Radiometer at 3 mm wavelength.

Forward scattering, microwave emission, oil film, Brewster angle, waves and water.

The reflection coefficient of fresh water increases with increasing water temperature over the angular range of 0 to 80°.

For horizontal polarization, the measured antenna temperature increases nearly linearly with the quantity of the oil. For vertical polarization the angular dependence is reduced with increasing oil quantity.

For homogeneous materials and smooth surfaces forward scattering and antenna temperature measurements are absolutely equivalent in laboratory experiments.

For rough or inhomogeneous materials, the determination of the emission coefficients can only be achieved by radiometer techniques, but scattering measurements may give additional information on the irregularities of the sample.

HOLLINGER, J.P., "Passive Microwave Measurements of Sea Surface Roughness," IEEE Transactions on Geoscience Electronics, GE-9, pp 165-196, (July 1971). NRL.

Abstract - Passive microwave measurements of the sea surface were made from Argus Island tower at 1.41, 8.34 and 19.34 GHz over a range in wind speed from calm to 15 m/s. These measurements show a definite frequency-dependent correlation between the microwace brightness temperature and wind speed. This dependence results from roughness effects of the compact sea surface associated with wind-driven waves.

Sixteen, Experimental, Significant.

Argus Island Tower; March-April, 1969 and March, 1970; Radiometers at 1.41, 8.36, 19.34 GHz.

Wind speed, microwave brightness temperatures, geometric optics, mean square slope.

The observations of the microwave brightness temperature of the sea dependence on wind speed is due to the roughness effects of the compact surface associated with wind-driven waves.

The wind speed dependence decreases with observational frequency and any theoretical models used to interpret the microwave characteristics of the sea must be frequency dependent.

Surface roughness effects will dominate at the lower wind speeds.

The microwave characteristics of the sea will be determined by sea foam at very high wind speeds. The transition wind speed between the two effects is not known but will probably lie in the region between 15 and 20 m/s.

HOLLINGER, J.P., "Remote Passive Microwave Sensing of the Ocean Surface," Proceedings of the Seventh International Symposium on Remote Sensing of Environment, Ann Arbor, Michigan, III, pp 1807-1817. (May 1971). NRL.

Abstract - The important potential of all weather determination of ocean surface wind fields by means of remote passive microwave sensing is discussed. The wind speed dependence of the microwave brightness temperature of the sea is interpreted as resulting primarily from small-scale wave structure at wind speeds below 15 to 20 m/s and from the increasing coverage of sea foam at higher wind speeds. Measurements of these two effects are presented and the characteristics of each described separately. The two effects are combined to estimate the total microwave brightness temperature dependence of a wind driven sea as viewed from a satellite. Taken together the two effects allow the determination of ocean surface wind fields over the entire range of winds speeds. The sensitivity to wind speed increases with observational frequency and is most pronounced for horizontal polarization at larger incidence angles.

Thirteen, Experimental, Normal.

Argus Island Tower; March, 1969 and 1970; Radiometers at 1.41, 8.36 and 19.34 Ghz.

Wind speed, microwave brightness temperatures, surface roughness, foam.

The effect of surface roughness on the microwave brightness temperature is shown to depend upon observational frequency, increase with increasing frequency and is a function of the angle of observation and polarization of the radiation received. Increases of $1.1^{\circ}K$ per m/s of the horizontally polarized brightness temperature at 19.34 GHz and 55 degrees incidence angle with wind speed have been measured.

The surface roughness effect is closely coupled to the local wind field; rapidly responsive to changes in the local wind and hence is relatively insensitive to the energy content of low frequency gravity waves.

A possible interpretation of the observations based on a geometric optics model of the rough surface is made and implies that surface waves shorter than the observational wavelength are relatively unimportant.

The data available at present are insufficient to describe the microwave characteristics of foam in detail as a function of frequency, polarization and incidence angle. Foam is known to have a very high brightness temperature approaching the physical temperature

of the sea. The brightness temperature is apparently relatively independent of polarization and incidence angle and should decrease with decreasing observational frequency for foam layers whose depth is less than about one fourth of the observational frequency.

HOLLINGER, J.P., "Microwave Properties of a Calm Sea," Naval Research Laboratory, Washington, D.C., Report No. 7110-2, pp 66, (August 1973). Naval Research Laboratory, Washington, D.C.

Introduction - This report presents calculations of the following: (I). the dielectric properties of water as a function of the salinity and temperature of the water and the frequency of observation; (II). the propagation characteristics of microwave radiation in water for these dielectric properties as a function of salinity, temperature, and frequency; and (III). the brightness temperature of a calm sea, based on these dielectric properties, as a function of salinity and temperature of the water and the frequency, polarization, and angle of incidence of observations.

One, Theoretical, Significant.

Dielectric properties, microwave properties, water, ocean, salinity, temperature, brightness temperature.

The devised analytic expressions of dielectric properties are shown to be in excellent agreement with experimental values reported by other researchers over the salinity range of 0 to 55.9 parts per thousand (PPT) and the temperature range of 0 to 40°C.

Calculations of parameters such as skin depth, wavelength in water, indices of refraction and absorption as a function of frequency are given for salinities of 0 and 35 PPT and temperatures of 0 and 20°C.

HOLLINGER, J.P., "The Determination of Oil Slick Thickness by Means of Multifrequency Passive Microwave Techniques," NRL Memorandum Report 2953, pp 144, (June 1974). Naval Research Laboratory, NTIS No. AD-A001302, CCRS No. 2001924.

Abstract - A technique for the remote determination of the thickness and volume of sea surface oil spills using multifrequency microwave radiometry was investigated. Aircraft-borne measurements were made at 19.3 and at 31.0 or 69.8 GHz of a total of fifteen controlled marine oil spills. The spills consisted of from 200 to 630 gallons of either No. 2 fuel oil or No. 4 or No. 6 crude oil. The first eight spills were conducted under calm sea conditions with surface winds of less than 10 knots. A second group of seven spills were subsequently carried out to investigate the effects of rougher seas and higher marine wind speeds. Measurements were obtained with seas of up to 5 feet, swell of up to 8 feet and winds of up to 24 knots during this group of spills.

The microwave measurements of the oil spills of each oil type showed very similar results. The slicks formed an identifiable region with film thicknesses of a millimeter or more and containing the majority of oil which was surrounded by a very much larger and thinner slick which contained very little of the oil. In general, the thick region contained more than 90 percent of the oil in less than 10 percent of the area of the visible slick. It was always possible to locate and delineate the thick region solely from the microwave observations. The total volume of oil present derived from the microwave measurements was within about 25 percent of the volume of oil spilled. Multifrequency passive microwave radiometry offers the potential to measure the distribution of oil in sea surface slicks, locate the thick regions, and measure their thickness and volume on an all weather, day or night, and real-time basis. As such, it should prove a useful tool in the confinement, control, and clean up of marine oil spills.

Twenty-Five, Experimental and Theoretical, Highly Significant.

Off Virginia; August 1972 to February 1974; 19.3, 31.0 and 69.8 GHz Passive Microwave Radiometers.

Oil Slick, thickness, volume, microwave radiometry, sea state, wind, dielectric properties, mixing spreading.

Information regarding dielectric properties is given. 19.3, 31.0 and 69.8 GHz were used in the calculations. Results indicate that the real part of the dielectric constant of the majority of the oils is near 2.1 but ranges from 1.8 to 2.6. The imaginary part is usually

less than 0.02 except for aged 40 gravity crude and Bunker C fuel oil where it may be as large as 0.3.

The oil film acts as a matching layer between free space and the sea. Reflection is minimized and emission is a maximum when the film has a thickness equal to odd multiples of a quarter wavelength. The brightness temperature of an oil slick at first reaches a maximum and then oscillates with increasing slick thickness. The oil slick can increase the brightness temperature by 80^{o}K or more above the oil free sea surface. The use of the above group of 3 frequencies will allow oil film thicknesses between about 0.1 and 3.0 mm to be unambiguously determined.

For the 3 frequencies, the largest increase in brightness temperature occurs for the horizontal component with a somewhat larger difference between frequencies in the region of 60^{o} than at 0^{o}. The initial larger decrease in the vertical component near Brewster's angle at 80^{o} with increasing film thickness is not of practical significance since a slightly rough sea would greatly reduce the decrease and measurements would be very difficult at such a large incidence angle.

The brightness temperature of the vertical component is independent of thickness at about 55^{o} for thin films and low loss oils. As the loss in the oil is increased by forming very thick films, the brightness temperature will increase and approach the physical temperature of the oil.

The maxima and minima occur at increasing film thicknesses as the incidence angle increases. The maximum value of the increase in brightness temperature also increases with incidence angle for the horizontal component and offsets the decrease at small thicknesses due to the shift of the maximum to a greater thickness so that the sensitivity to very thin films is roughly independent of incidence angle.

As the real part of the permittivity increases the maximum brightness temperature increases and reduces the thickness at which the maxima and minima occur. The depth of the minima increases slightly and the separation of the maxima decreases markedly with increasing dielectric constant.

Increasing the imaginary part raises the brightness temperature increase and greatly reduces the depth of successive minima. The spacing and separation of the maxima and minima are unaffected by changes in the imaginary part.

The microwave brightness temperature is dependent on the surface roughness and the sea foam effect. Cox and Munk (1954) calculated that an oil slick damped waves of 30 cm wavelength by a factor of 10 and that waves shorter than this were essentially eliminated.

Also, an oil slick reduced the mean square slope with respect to a clean surface by a factor of 2 or 3. The damping is essentially independent of oil film thickness. The effect of the damping of surface waves by an oil slick is to reduce the microwave brightness temperature in the region of the slick below its value from the adjacent unpolluted sea. This decrease is in addition to and counters the increase in brightness temperature due to the increased emssivity of the oil slick over the clean water surface.

A graph is given showing the calculated depression of the antenna temperature increase resulting from an oil spill due to the effects of sea surface roughness as a function of wind speed. The results are practically independent of oil thickness, less than 20% of the total effect.

The sea foam effect is due to the relatively high brightness temperature of sea foam compared to the average sea surface and to the increasing surface coverage of sea foam with wind. An oil film will inhibit the production of white caps hence the sea foam effect will result in a decrease in the brightness temperature. For the frequencies given, $100^{o}K$ is said to be a reasonable estimate for the increase in brightness temperature for foam. The presence of foam is dependent on wind speed, the air-sea temperature difference, the duration and fetch of the wind, and the history of the wave spectrum of the sea area being observed. The maximum effect due to sea foam plus surface roughness is given in a graph. The total sea state effect at nadir is remarkably similar at all three frequencies. It can be reasonably correct below wind sppeds of 37 km/h but serious error will occur above it.

Because of the poor resolution, thickness variations much smaller than the surface resolution may be anticipated. Theoretical calculations are made for the case of many small puddles of the same thickness randomly distributed over the main beam. The antenna temperature increase is proportional to the fractional area of the beam filled by the oil puddles. Since a single thickness is associated with each puddle the antenna temperature is proportional to the volume of oil.

Using a highly directive antenna beam and assuming that the total brightness temperature is linearly proportional to oil thickness, the volume of oil is proportional to the integral of

the measured antenna temperature increase over the oil slick. The volume calculation is independent of the detailed distribution of thickness present or the spatial scale of thickness variations over the slick.

Laboratory passive microwave measurements were made. Measurements of No.2, No. 4 and No. 6 crude oils were made. The behaviour of the No. 2 oil closely followed that of theoretical predictions; No. 4, oil behaviour followed them roughly and No. 6 showed little correlation.

Dielectric measurements were made and a simple technique for measuring these properties for any material which may be formed in uniform layers of variable depth was demonstrated.

Airborne measurements were made of 15 spills - 8 were done under calm sea conditions and 7 were done under rough sea conditions. Ground truth data was available. The results of the calm sea tests showed that a clearly defined region with thicknesses of a millimetre or more and containing the majority of the oil always formed. This region was surrounded by a very much larger slick, hundreds of times thinner, which contained very little of the oil. It was always possible to locate and delineate the thick region solely from the microwave observations. The thickness derived from the microwave data are consistent with in situ thickness measurements and the total volume of oil present determined from the microwave observations was within about 25% of the known volume of oil spilled. In general, the microwave measurements determined that more than 90% of the oil was contained in less than 10% of the area of the spill. In one case No. 2 and No. 6 were used and they spread too rapidly to get any real extent information.

The results of the rough sea oil spills were generally the same as those obtained from the calm sea spills with the exception of two. No thick patches were detected for these two.

It seems likely that the thick regions are formed and maintained by small quantities of surface active materials present in the oil itself which spread more rapidly than the bulk of the oil, surround it, inhibit its growth and act as a control agent.

Oil slick growth was more rapid at higher wind speeds (quantitative measurements made). A relationship is derived and shown graphically. In general, the growth rate was primarily in the upwind-downwind direction with the slick taking on a characteristic roughly oblong shape with thick patches in the downwind end.

The measured depression of the microwave signal in the region of the oil slick with increasing wind speed, due to the damping of small-scale surface waves and the reduction of the amount of white caps and foam, agreed well with the calculations. This permits the entire slick to be delineated by the microwave signal.

It appears that if the range of thicknesses present is reasonably less than the thickness of the first maximum, increased distribution of thicknesses caused by sea roughness will not result in significant errors.

Oil-in-water emulsions are not of much practical concern because of the great dispersal and very low concentration of the oil and the near impossibility of detecting or recovering the oil.

Water-in-oil emulsions would, in general, be expected to have a higher dielectric constant at microwave frequencies due to the high dielectric constant of water (equation given for calculating). The dielectric constant of the mixture does not increase linearly with the percentage of water (see graph). The major effect on the brightness temperature is that the maxima of the increase are increased and occur at smaller oil film thicknesses. The minima are also increased. The net result would be to cause the oil film thickness to be over estimated. The effect should be negligible for distillates since they do not form stable emulsions.

HOLLINGER, J.P. and R.A. MENNELLA, "Oil spills, Measurements of Their Distributions and Volumes by Multifrequency Microwave Radiometry," Science 181, pp 54-56, (July 1973). Naval Research Laboratory, Washington, D.C.

Abstract - Aircraft-borne multifrequency passive microwave observations of eight marine oil spills revealed that, in all cases, over 90 percent of the oil was confined in a compact region comprising less than 10 percent of the area of the visible slick. These measurements show that microwave radiometry offers a means for measuring the distribution of oil in sea-surface slicks; for locating the thick regions; and for measuring their volumes on an all weather, day or night, and real-time basis.

Twelve, Experimental and General Review, Normal.

East Coast of Virginia; 1971-72, 19.4, 31.0 and 69.8 GHz Microwave Radiometers.

Brightness temperature, oil spill, Microwave Radiometer, volume distribution.

Microwave radiometry offers a unique potential for the determination of oil slick thicknesses greater than about 0.05 mm.

HOULT, D.P., S. WOLFE, S. O'DAE and J.P. PATUREAU, "Oil in the Arctic," Department of Transportation, U.S. Coast Guard, Office of Research and Development, Washington, D.C., Report No. CG-D-96-75, Task No. 4108.2.3, pp 218, (March 1975). MIT. NTIS.

Abstract - This report describes the results of several researchers on the behaviour of oil spilled in the Arctic. Included are studies on evaporation, spreading and maximum extent of oil spilled on ice, and the behaviour of oil spilled under ice. Physically sound theories are developed which correlate well with laboratory and field data.

Thirteen Theoretical and Experimental, Highly Significant.

Laboratory.

Oil pollution, Arctic, behaviour, oil on ice, oil under ice.

Oil in even a very large Arctic spill will be confined to a very small area due to natural processes. Two principle modes of behaviour of interaction of sea ice with trapped oil under it are observed: sea ice entraps the oil causing the formation of a matrix of oil and ice, and ice will entrap the oil in a pool and proceed to form beneath it. The actual method by which the crude and diesel oils are trapped in the sea ice is a combination of the two modes.

The presence of an oil pool under the ice causes a marked change in the temperature distribution in the ice and affects its growth rate because the oil pool acts as an insulating layer between the cold air and the relatively warmer sea water.

An order of magnitude estimate of the maximum extent to which oil can spread under Arctic conditions can be deduced from the measurements of the thickness of the adhering oil layer.

A simplified model of oil spreading on ice has been developed by considering the random nature of surface roughness of ice, its auto-correlation function and power spectrum.

HOWARD, D.L., N.A. THOMAS, and M.C. LICITRA, "Microwave Monitoring of Seawater," Contamination of Navy Fuel Oils, pp 15, (June 1967). NRL. NTIS AD65 819.

Abstract - Seawater contamination of Navy Special Fuel oil is a major problem in oil-burning naval ships. The main cause of the contamination is the use of the fuel bunkers for ballast by filling them with seawater when they are emptied of fuel. Thus, even though "Burner fuel oil - Navy Special" is supplied under Mil-F-859E specification, which permits only 0.5% water content, much higher percentages are experienced in the fleet. The contamination is one of the major factors causing slag deposits on boiler tubes which lower efficiency, reduce ability to get under way rapidly, and increases maintenance costs. Under certain conditions of severe contamination, it has even caused furnace explosions. The detection and accurate monitoring of the degree of salt water contamination of Navy Special fuel oil is therefore of prime importance in the readiness and efficient operation of Navy marine boilers.

Prior approaches to electronic monitoring of the contamination, that have been investigated at UHF and low frequencies, have given insufficient accuracy in that the percentage sea water could be determined only within several percent. The major problem is that boiler fuel oils, including Navy Special fuel oils, are extremely impure and relatively uncontrolled mixtures of compounds. The oil comes from all parts of the world differing greatly in content, and consequently dielectric constant, from one source to the next. With the stipulation that the source of the oil be an unknown, the difference in characteristics of oils from different sources masks the indication used to sense the water content.

Studies of microwave monitoring techniques have resulted in a potential method of monitoring the percentage of seawater contamination to an accuracy of $\pm$ 0.25%. Investigation was made by both the dielectric constant and the characteristics of contaminated fuel. The dissipation method gave the greater accuracy which improved with increasing microwave frequency. The dissipation measured for all samples of uncontaminated fuels was very small compared to the sensitivity to water, so that the effects of the differences in the different sources of fuel were minimized. Testing of samples from all parts of the world with accurately mixed percentages of seawater showed that this microwave technique can be used to monitor the percentage of seawater to within $\pm$ 0.25% of the actual value regardless of the source of the oil. The ability to measure to this order of accuracy was limited, in part, by the difficulty of preparing

sufficiently precise sample mixtures for testing the technique. The microwave technique also lends itself readily to convenient practical implementation of continuous monitoring of fuel flowing to the furnaces.

Eight, Experimental, Significant.

Laboratory.

Oil-water mixture, dielectric properties, microwave techniques.

The real part of the complex permittivity for various Navy Fuel oils (categorized by source) is given for the 4.0-4.5 GHz range.

JACKSON, F.C., "Directional Spectra of Ocean Waves from Microwave Backscatter," Proceedings, URSI Commission II Specialist Meeting on Microwave Scattering and Emission from Earth, Berne, Switzerland, pp 257-272, (September 1974). General Electric Co., Space Division.

Abstract - The paper presents an analysis of two proposed microwave radar techniques for measuring ocean wave directional spectra. Tomiyasu's short pulse idea and Barrick's two-frequency correlation idea are regarded - independent of transmitted wave form - as essentially two alternative detection systems for modulated noise. Together, the two systems constitute a "general detection system" for modulated noise described some years ago by Parzen and Shiren. A frequency domain analysis for backscatter on arbitrary incident wave form is given, and an interesting physical optics solution for the generalized fourth-order moments of the scattering matrix is obtained. It is shown that the present narrow band version of Barrick's two-frequency idea is impractical, and that the proper application of Barrick's idea is to wide band signals. Both short pulse and wide band two-frequency techniques appear to be entirely feasible for aircraft application, but feasibility for satellite application is doubtful.

Seventeen, Theoretical, Significant.

Ocean waves, microwave, backscatter, directional spectra, radar.

The backscatter of a short pulse (that is short compared to the dominant ocean wavelength) is envelope detected and spectrum analyzed (say with a bank of band pass filters) for the modulation impressed on the return by the large gravity wave structure.

A current version of the two-frequency technique calls for the cross-correlation of the backscattered powers of two long coherent pulses that are separate in frequency. The signal (or modulating spectrum) at the difference frequency is detected as the difference of the cross-correlation and the product of the two average backscattered powers. Repeated measurements with pairs of pulses over a range of differences then yields the modulation spectrum at the set of discrete difference frequencies. Using a composite surface model Barrick showed that for large angle backscatter the modulation spectrum is proportional to the large wave slope spectrum.

JOHNSON, J.D. and L.D. FARMER, "Use of Side-Looking Airborne Radar for Sea Ice Identification," Journal of Geophysical Research 76, 9, pp 2138-2155, (March 1971). USCG.

Abstract - An experiment was conducted to assess the performance of side-looking airborne radar (SLAR) in mapping and identifying sea ice parameters. A Philco-Ford AN/DPN-2 (modified) SLAR was installed on a Coast Guard C-130 aircraft and flown on an experimental basis during September 1969 in conjunction with the S.S. Manhattan's transit of the Northwest Passage. In addition to the research effort to determine its feasibility as an ice observational technique, the SLAR was also used as a routing aid to the Manhattan. The results of its experiment indicate that SLAR can readily be used to detect ice concentrations, floe size and number, and water openings, and to identify, through careful image interpretation, ice age, ice drift, surface topography, fractures, and pressure characteristics. SLAR's broad aerial coverage all weather, day and night capability make it an effective means of observing sea ice, and for many purposes it provides observations superior to information obtained by a visual ice observer. SLAR imagery can be used in research efforts to study the formation, growth, and decay of sea ice and can be used operationally for ship routing and ice forecasting. It will be necessary to conduct similar experiments during other seasons of the year to determine whether there is a seasonal influence on an imaged appearance of sea ice.

Four, Experimental, Significant.

SS Manhattan Project (Northwest Passage, Arctic); Sept. 1969; Philco-Ford AN/DPD-2 (Modified) SLAR 16.5 Ku-band.

SLAR, sea ice, SS Manhattan, ice concentration, floe size, water openings.

Noncoherent radar is more effective than non-focused coherent radar for ice pack mapping. The imagery contained dark and light bands which are the result of sensor malfunctions or gain changes.

Ice concentration is easily observed, because, where there are black returns or no radar return, water is present. The various grey shades of ice in the black areas represent the deformed character of the ice and hence can be a clue in determining its age.

Floe size and some inference into the structure of the floe can be obtained but the tonal differences are not always true reflections of the surface being viewed.

Water openings are normally black indicating that there is no radar return but thin ice often gives the same black return at this frequency.

The age of the ice can often be determined by the presence of ponds and drainage channels on the surface which are characteristic of the development of older ice forms. These can be identified, especially at the near range of the radar. The tonal difference between first year ice (new forms) and water (black return) are an indication of age. Ground truth information concerning the thickness and salinity of the ice is required to make judgements concerning the differences between second year ice and multi-year ice. Differentiation is difficult as the second year ice displays a somewhat smooth grey-tone while multi-year ice displays a varying mottled grey tone.

Ice drift is measured on the basis of repeated coverage by examining changing floes with formations that do not appear to have any changes. Many pressure ridges that are close together will appear as one bright return. The identification of a single pressure ridge is limited by the resolution of the system. Older ridges do not image as brightly as younger ridges. The older ridges are grey linears becoming more white the younger the ridge.

Fractures appear as alternate dark and light returns depending on the width and orientation to the radar beam. Sometimes the radar energy is reflected from the ice edge giving a light return rather than from the water which would give a dark edge return. If the fractures contain brash, slush or black ice, they will appear as light grey. The width of the fracture and the oririentation will result in different image effects.

Pressure in the ice pack is indicated by very few water openings with bright returns caused by small ice fragments jammed together. Wide water openings indicate little or no pressure.

SLAR contains more information than the normal visual ice map.

JONES, W.L., L.C. SCHROEDER, and J.L. MITCHELL*, "Aircraft Measurements of the Microwave Scattering Signature of the Ocean," IEEE Journal of Oceanic Engineering, OE-2, 1, pp 52-61, (January 1977). NASA Langley Research Centre, Vought Corporation*.

Abstract - Microwave scattering signatures of the ocean have been measured over a range of surface wind speeds from 3 m/s to 23.6 m/s using the AAFE RADSCAT scatterometer in an aircraft. Normalized scattering coefficients are presented for vertical and horizontal polarizations as a function of incidence angle (nadir to 55^{o}) and radar azimuth angle (0^{o} to 360^{o}) relative to surface wind direction. For a given radar polarization, incidence angle, and azimuth angle relative to wind direction, these scattering data exhibit a power law dependence on surface wind speed. The relation of the scattering coefficient to azimuth angle obtained during aircraft circles (antenna conical scans) is anisotropic and suggests that microwave scatterometers can be used to infer both wind speed and direction. These results have been used for the design of the SEASAT A Satellite Scatterometer (SASS) to be flown in 1978 on the first NASA oceanographic satellite.

Fourteen, Experimental, Significant.

Pacific and Atlantic; 1973-1974; AAFE RADSCAT (13.9 GHz).

Scattering coefficient, incidence angle, azimuth angle, AAFE RADSCAT, wind speed, polarization, ocean.

For a smooth sea and light winds the dynamic range of the backscattered signal is approximately 60 dB from measurements made at near nadir to a 55^{o} incidence angle.

A combined microwave radiometer - scatterometer (RADSCAT) operating at 13.9 GHz was used. Only the scatterometer data is analyzed. The pulse is long and the area illuminated is beam limited (1.5^{o}). A typical plot for upwind observation and a low surface wind speed is shown. The mean cross section decreases with incidence angle. The values are nearly equal for both polarizations from nadir to above 25^{o}. The shape of the curve from nadir to 15^{o} agrees with those predicted by geometric optics scattering theory.

Beyond 30^{o}, the separation of the polarized scattering coefficients and the general shape of the curves agree qualitatively with first order Bragg scattering calibrations. In a figure showing upwind downwind and crosswind σ^{o} versus incidence angle for a wind speed

of 6.5 m/s (V-pol.) the values are approximately equal at nadir. In the Bragg scattering region, the three scattering characteristics are different, i.e. maximum for upward, minimum for crosswind and in between for downwind. For higher wind speed (14.0 m/s) a plot shows a decrease in the range of σ^{o} versus angle of incidence. Only after about 30^{o} does the V and H polarizations curves begin to separate. RADSCAT ocean scattering signature measurements were made over a wind speed range of 3 to 24 m/s. The data conform to a power law wind speed response. Wind circle lines were also flown showing the variation in σ^{o} for both H and V polarization for different wind speeds. The graphs show an overall increase with windspeed and a cyclic (quasi-sine) variation with direction.

These results were used for the design of the scatterometer for SEASAT A.

KASKI, KIMMO AND ANTTI LAAPERI, "Remote Sensing of Oil Slicks with Microwave Radiometer," Report No. 583, pp 16, (1976). Helsinki University of Technology, Radio Laboratory.

Introduction - In the beginning of September, the year 1974-09-10... 12 many field tests were carried out to declare how to detect the oil slick on the surface of the sea with remote sensing methods. The experiments took place in the Baltic Sea near Stockholm.

Experiments were made with optical devices, such as multispectral photography, colour photography and low light television system, IR-scanner (thermal IR region), near IR photography, thermal IR radiometer, microwave radiometer, airborne radar and ship borne radar. The experiment was carried out in co-operation between Swedish Coast Guard, the Swedish Research Institute of National Defence, the National Land Survey of Sweden, the Radio Laboratory of the Helsinki University of Technology and Swedish Saab-Scania. The Swedish Space Corporation was responsible for the coordination of the experiment.

This report will deal only with the microwave radiometer. This radiometer has been developed in the Radio Laboratory of the Helsinki University of Technology for ice measurements and has, therefore, a centre frequency of 4.75 GHz. This frequency is not very suitable for oil measurements as can be seen later.

At field tests, several different oil types were released from boats. Normally, the airborne measurements started shortly after than the oil was released and continued for about two hours. The experiments also included a release behind the oil barrier. This test was very successful for microwave radiometer, because the thickness of oil slick became great enough to become clearly detected.

The main aims of the experiments were to a) detect the oil slick on the water surface; b) map the volume, thickness and total area of the oil slick; and c) identify the oil type.

The profits of microwave radiometer are the mapping capability at almost all kinds of weather both day and night and the fact that it is possible to find the thickest part of the oil slick representing the biggest volume of the slick, which must be cleaned up.

Two, Experimental, Significant.

Baltic Sea; September 10-12, 1974; 3 Channel passive microwave radiometer (4.65, 4.77 and 4.8 GHz) developed by Helsinki University of Technology for sea ice measurements.

Oil spill, volume, thickness, radiometer, frequency, detection.

This is part of a major experiment for oil spill detection. The authors admit that the radiometer is not optimum and that frequencies up to 38 and 94 GHz would be better.

KLEMAS, VYTAUTAS, "Detecting Oil on Water: A Comparison of Known Techniques," Proceedings of Joint Conference on Sensing of Environmental Pollutants, Palo Alto, California, pp 6, (November 1971).

Excerpt - This paper reviews new developments in oil pollution detection and compares available techniques according to their effectiveness. Emphasis is on in situ and remote sensing techniques, with a potential for real-time, automated operation. No mention is made of traditional methods, requiring that a sample be taken to a laboratory for test or solubility, chemical reactions, or their properties.

Thirteen, General Review, Significant.

Aerojet-General Radiometer; 0.428, 1.228, 4.455 and 8.910 GHz pulsed coherent imaging radars with 2 polarizations (JPL).

Oil, thickness, wind, microwave radiometer, SAR, polarization.

The physical, electrical, and optical properties of oils and sea water are given along with the source of the data.

The thermal emission at microwave frequencies from thin oil films is in direct opposition to that at infrared wavelengths. In the microwave region, an oil film appears warmer than seawater. In this region, oil films on water create apparent anomalies by two mechanisms: the change in sea state caused by the calming effect of the oil film, and the increase in the emissivity of the surface due to the low loss and high emissivity of the oil. The first is the dominant of the two and presents strong signals to microwave radiometers when winds exceed 6 knots. The second gives an indication of oil film thickness (Figure given). Edgerton found that minimum detectable oil film thicknesses were of the order of 10 to 20 microns, and that for such thin films the additional emission from the oil was more than offset by a reduction in ocean emission because of reduced surface roughness. When film thicknesses exceed 50 mm, the additional emission from an oil slick over shadows the decrease in ocean emission associated with a reduction of surface roughness. Edgerton also recommends horizontal polarization, viewing angles 30 to 40 degrees above nadir and wavelengths shorter than 8 mm.

Microwave radiometers, however, detect thin films and light oils poorly and gives weak contrast in calm seas.

The scattering of radar signals at incident angles other than the normal is primarily due to the capillary and small gravity waves generated on the surface by wind. The oil coatings damp out these waves and thus strongly reduce the echoes returned for the oil covered areas, decreasing the effective radar cross section of the surface.

Guinard used four pulsed coherent imaging radars at 0.428 GHz, 1.288 GHz, 4.455 GHz and 8.910 GHz, including two polarizations. Although a variety of frequency polarization combinations was employed, no characteristic signatures of the spills imaged were obtained. Calm conditions eliminated horizontally polarized transmissions.

KENNEDY, J.M. and R.T. SAKAMOTO, "Passive Microwave Determinations of Snow Wetness Factors," Proceedings of the Fourth Symposium on Remote Sensing of Environment, Ann Arbor, Michigan, pp 161-171, (December 1966). Space-General Corporation, California.

Abstract - A mobile field unit, designed and constructed by Space-General Corporation, was utilized to measure the microwave radiometric emission characteristics of snow at 13.5 GHz and 37 GHz. Analyses of the data and theoretical considerations show that variations in free water content affect significant changes in the radiometric brightness temperature of snow. By making measurements with suitable combinations of frequency, polarization, and incidence angles, the free water content of natural snow may be determined.

Four, Experimental and Theoretical, Normal.

Crater Lake National Park, Oregon; 13.5 GHz, 37 GHz and 94 GHz Experimental Radiometers.

Snow, brightness temperature, radiometer, microwave.

An empirical relationship is derived for the radiometric brightness temperature and the percentage of free water contained in snow. The measurements were made under semi-controlled conditions.

KENNEDY, J.M. and G.G. WERMUND, "Oil Spills, IR and Microwave," Journal of the American Society of Photogrammetry, XXXVII, 12, pp 1235-1242, (December 1971). TRW Systems and Remote Sensing Inc., Houston, Texas.

Abstract - Examples indicate that the utilization of thermal infrared and microwave radiometric data, approached from a systems point of view are of value to operational groups charged with cleaning up oil pollution in ocean and coastal water environments. In addition, this system may be used to upgrade and increase the value of theoretical models so that they more nearly agree with field observations. The preliminary findings of this study point to fruitful areas of directed applications research and the techniques should be pursued with vigor and proper governmental finding. This would ultimately result in greatly reduced costs for spill tracking, source identification, determining the terminal destination and determining the efficiency of clean-up operations.

Six, Theoretical and Experimental, Highly Significant.

110 Miles SE of New Orleans; March, 1970; 13.6 GHz (22 mm) microwave radiometers.

Oil spill, thickness, volume, flow rates, radiometric temperature, IR temperature.

The reasoning behind the oscillatory nature of the signal received from an oil slick for both active and passive microwave systems is discussed. References to previous tests are made. Flights were made over an oil slick at 10,000 and 35,000 ft with an IR imager and a microwave radiometer. The resolution of the radiometer was too poor for it to be of any value at 35,000 ft. Thickness and volumetric calculations were made using both instruments and certain assumptions which are not all necessarily valid. No surface truth work was undertaken to compare the calculations with the actual situation.

A discussion of theoretical surface diffusion of oil was given and seemed to be in excellent agreement with the actual spill measurements.

KETCHUM, Jr., R.D. and S.G. TOOMA, Jr., "Analysis and Interpretation of Airborne Multifrequency Side-Looking Radar Sea Ice Imagery," Journal of Geophysical Research, 78, 3, pp 520-538, (January 1973). Naval Oceanographic Office. American Geophysical Union.

Abstract - During April 1968, the Naval Oceanographic Office conducted an airborne side-looking radar experiment over the sea ice fields north of Alaska using the four-frequency radar system of the Naval Research Laboratory. The shorter wavelength X-band radar appears to have the greatest potential for sea ice study when more definite information is required, such as mapping, distributions of stages of ice development, and fracture pattern analysis. Pressure ridge patterns can sometimes be identified when they are present on a low backscatter background. The L-band radar has potential value for mapping the aerial distribution for surface topography. This wavelength does not receive discriminative backscatter from various ice types but sees only the more prominent topographic features, such as ridges and hummocks. The P band does not appear to have any characteristics that would make it valuable for sea ice mapping. Only the most prominent features, such as large fractures and floes, were imaged by this radar.

Four, Experimental, Very Significant.

North Alaska; April, 1968; NRL Four Frequency Dual-Polarized SLR X, C, L and P bands, 8910 MHz, 8910 MHz, 4455 MHz, 1228 MHz, and 428 MHz, respectively, (Synthetic Aperture).

SLR, four frequencies, synthetic aperture, photographic ground, truth, sea ice.

Because the NRL radar was a one-of-a-kind experimental device, the quality of the imagery obtained was affected by many factors. The main shortcoming was that the C-band transmitter was so weak that no usable C-band data could be collected. Other factors which reduced the quality of the imagery were the lack of dynamic range of the data film which was used to record the Doppler phase histories. The full radar system capabilities could not be used. Imagery was degraded in the far range and this was attributed to inadequate transmission power and the low grazing angles at this range. False backscatter cross sections occurred at extended boundaries. Where the contrast was great (i.e. high and low backscatter areas) a low return was achieved if the movement is from high backscatter to low backscatter and a high return was achieved when movement was from a low to high backscatter. This effect was caused by the automatic

gain control of the system. The last major factor was fluctuation in the system parameters which caused the quality of the images to vary.

Imagery at X-band showed discrimination between old ice and young ice but could not provide discrimination between open water and first-year ice forms such as young ice and new ice. Multi-year floes gave a continuous high backscatter which produced a smooth textured light grey image which is characteristic of this type of ice during winter months. Pressure ridges in this types of ice cannot be identified owing to the high background backscatter from the underlaying zones of recrystallized snow. It was hypothesized that summer melt conditions may allow discrimination of pressure ridges in this type of ice. Underformed first-year ice appears smooth at this wavelength. Ridges can be identified but closeness of ridges have a stringy appearance. Identification of ice ridges and hummocks depend on the degree of backscatter from the target and background and the spatial distribution of the targets with respect to the system resolution. Some areas of first year ice with high concentrations of new pressure ridges and hummocks provide a high backscatter similar to multi-year ice thus reducing the confidence for correct ice type identification. Where new pressure ridges can be resolved from nearby ridges distinct light grey lineations identify them. Fractures and fracture patterns are also identifiable but their low backscatter reduces the confidence of interpretation as the background backscatter increases.

For the L-band images, it was noted that the micro roughness of multi-year ice does not appear to have been affected by the long wavelenghts. New ridges with irregular angular surfaces stand out well but older ridges smoothed with age tend to have little reflectance. Old ridges and hummocks of multiyear ice provide little or no radar backscatter. Multi-year ice floes are interpreted because of their roundness and continuous low backscatter surfaces. Areas between multi-year ice contain new ridges and have a high backscatter which helps to set off the low backscatter areas. The image texture is determined by degree of concentration and backscatter. First-year ice has a low backscatter thus a field of multi-year ice and first-year ice is very difficult to detect and interpret. Radar energy at L-band is a function of the concentration of new ridges and hummocks. Some fractures can be discerned and others cannot and identification depends on the conditions of the ice surface bounding the fracture and the fracture size. Narrow fractures can sometimes not be detected. At both horizontal and vertical polarizations, the only targets giving significant backscatter are new features. Stronger energy returns are being received in

the horizontal mode than the vertical mode. It was not certain if the polarization variations were not influenced by inadequencies in the system operation.

P-band radar appeared inadequate in providing useful information about the distribution of sea ice conditions. At this longer wavelength, the sea ice surfaces produced lower backscatter and less discriminating returns than the X and L bands. The only prominent features observed were major water openings or fractures of vast ice floes or very rough areas. More energy appears in the horizontal mode than in the vertical from areas of extremely rough ice.

In a comparison with Johnson and Farmers K-band data, it is felt that X and K-band data provide the most information.

KETCHUM, Jr., R.D., and A.W. LOHANICK, "Passive Microwave Signatures of Sea Ice Features," Naval Ocean Research and Development Activity (NORDA), NSTL Station Mississippi, NORDA Technical Note 9, pp 16, (September 1977). Oceanographic Division, Naval Oceanographic Laboratory, Washington, D.C.

Abstract - An evaluation has been conducted of passive microwave imagery which displayed many different sea ice forms and features of varying age and thickness, and in various stages of formation, deformation, and weathering. The lowest radiometric temperatures, (i.e. brightness temperatures) were displayed by open water, some areas of new ice which presumably had moist surfaces, and dome multi-year ice floes and other forms which apparently had experienced considerable internal stress. It has been hypothesized that internal ice structure changes brought about by severe stresses result in a lowered emissivity. The highest radiometric temperatures were displayed by areas of thin ice which presumably no longer had a wet surface, new ice ridges, and frozen melt ponds. The older, thicker areas of first-year ice appeared to have lower radiometric temperatures than the thinner areas of first-year ice. Single multi-year ice floes often display a wide radiometric temperature range. This has been attributed to physical property changes which resulted from summer melting and erosional processes, and from stresses produced by the interaction of floes.

The detection of stress fields and/or stress lines through the use of microwave techniques is a new concept developed by evaluation of this data. This concept invites further investigations.

Six, Experimental, Significant.

Chukchi and Beaufort Seas; March-April, 1976; Ka-band (33.6 GHz) Passive microwave Imaging System (MICRAD).

Passive Microwave, Sea ice, radiometric temperatures, imagery, interpretation, ice stress, brightness temperature.

Relatively thicker areas of first-year ice show a brightness temperature between the nilas and young ice categories. There is no evident distinction on the MICRAD data between ridged areas of first year ice and the relatively underformed first year ice. The ridges in the first-year ice cannot be distinguished from their background. However, rafted ice appears radiometrically cooler than its background of similarly aged, deformed ice.

Identification and discrimination of multi-year ice can be done easily and accurately on the NICRAD imagery. Multi-year ice, on average, displays cooler radiometric temperatures than the younger ice types, although a wide spectrum of radiometric temperatures may be present on a single multi-year ice floe.

KONDRATYEV, K. YA., YU. RABINOVICH, V.V. MELENTEYEV and E.M. SHULGINA, "Remote Sensing of Oil on the Sea Surface," Proceedings of the Tenth International Symposium on Remote Sensing of Environment, Ann Arbor, Michigan, I, pp 251-252, (October 1975). Hydrometeorological Service of the USSR, Leningrad, USSR.

Summary - The increasing pollution of the aquatic regions is a consequence of continuous growth of industry. Oil and oil products are the most serious sources of sea and ocean pollution.

Together with elaboration of the methods of struggle against the sea and ocean surface pollution, the development of techniques for remote sensing of this pollution, with the aim of its timely localization, is quite essential. The paper considers the possibility of microwave remote sensing of the ocean surface pollution by oil products.

To calculate the oil-film covered sea surface microwave emission, the data on the oil dielectric constants obtained over the range of 2.5 - 3.4 cm, have been used. The real part of the oil dielectric constant does not practically change over this range (2.24- 2.27), but the imaginary part of the dielectric constant increases with decrease of frequency (0.0126-0.0150).

Calculations of the "oil product-water" system microwave emission are performed over the wavelength region of 1.6 - 3 cm at the temperature of 20°C and salinity of 40°/oo. The results of calculations have shown that for the horizontal polarization, the emissivity contrasts due to the presence of oil products on the sea surface are greater than for the vertical polarization. However, they do not exceed the analogous contrasts at nadir observations. The emissivity contrast can reach 0.06, which corresponds to ratio-brightness temperature variation by approximately 20°K. The microwave emission dependences on the oil product type and age, and on film thickness are considered in this paper; recommendations are made on the wavelength selection which is optimum for remote sensing of the sea surface pollution.

Measurements of emissivity of the water surface covered with oil layers of different thicknesses have been made at the 3.2 cm wavelength, by measuring the radiation coefficients for various natural surfaces under laboratory conditions. The radiating properties of the fresh-spilled oil and old oil were investigated at the environmental temperature of 17-20°C.

The observations have shown that the emissivity of the oil contacting with air during three days, increases. This is due to the increase of the imaginary part of the oil dielectric permeability at the expense of the moisture absorption from air.

Comparison of the laboratory measurements results with the data on the "oil product-water" system radiating properties calculated from the observed oil film constants, have shown their good agreement.

The aircraft multi-channel measurements of the sea surface pollution confirmed the possibility of remote sensing of regions with intensive pollution.

Nil, Summary (Experimental), Normal.

Laboratory; Experimental radiometer at 3.2 cm.

Oil, dielectric properties, emissivity, thickness.

A table giving emissivity values for freshly spilled and old oil is given.

KONG, J.A., "Microwave Remote Sensing of Ice and Snow," Proceedings, URSI Commission II Specialist Meeting on Microwave Scattering and Emission from Earth, Berne, Switzerland, pp 239-243, (September 1974). MIT, Cambridge, Massachusetts.

Abstract - A composite theoretical model is proposed to account for effects on emissivity caused by layering, absorption, anisotropy, surface roughness, inhomogeneities and sub-surface scattering. The emissivity as a function of frequency is calculated for a two layer model simulating ice or snow covered water or land. The theoretical results are compared with experimental data.

Four, Theoretical and Experimental, Normal.

Laboratory; Summer, 1973; Experimental simulation.

Ice, snow, emissivity, scattering, theoretical model, microwave.

The scattering point in the composite theoretical model is the stratified model which accounts for absorption, layering, and anisotropy. The solution is exact and in closed form. It is proposed that the reflectivity at each interface in the solution be modified to include rough surface effects. The effects due to buried scattering centres can be treated by a statistical model which is very convenient in obtaining root mean height and correlation length of the submerged scatterers and a flux method which is programmed to give numerical results. The scattering reduced the emissivity. In the experiment styrofoam balls wrapped with aluminum foil are used to simulate conducting spheres.

KOTLARSKI, J.R. and H.R. ANDERSON, "Oil Slick Detection by X-band Synthetic Aperture Radar," Proceedings of the Ninth International Symposium on Remote Sensing of Environment, Ann Arbor, Michigan, III, pp 1775-1790, (April 1974). Hughes Aircraft Company.

Abstract - The results of two oil slick detection experiments made with an X-band real-time synthetic aperture radar are presented. In each case the slicks were small, on the order of 0.2 to 0.6 square km, and they were detected in calm seas, with wind speeds of less than 5 knots.

Two, Experimental, Significant.

Point Arguello and Santa Barbara, Cal., Hughes/Navy Fighter Attack Reconnaissance Modular Adaptive Radar (FARMAR) (X-band, synthetic aperture radar).

Oil slick, backscatter, SAR, X-band.

A forward looking synthetic aperture imaging radar (x-band) is shown to be able to detect oil spills and give a real-time display. With its forward coverage the radar can be used to dynamically cue, position, and track a very narrow field of view sensor.

KRISHEN, K., "Detection of Oil Spills Using a 13.3 GHz Radar Scatterometer," Proceedings of the Eighth Symposium on Remote Sensing of Environment, Ann Arbor, Michigan, II, pp 1105-1119, (October 1972). Lockheed Electronics Company, Inc.

Abstract - This paper describes the results of an analysis of 13.3 GHz single polarized scatterometer data collected during NASA/MSC Mission 135, flown on March 16, 1970. Data were gathered over a crude oil spill on the Gulf of Mexico (test Site 128) off the Mississippi Delta. With the aid of RC-8 Camera photographs, the scattering cross section was correlated with the extent of the oil spill (25^{o} to 50^{o}) decreased by 5 to 10 dB in the presence of the oil spill. This was attributed to the oil's damping of small gravity and capillary waves. The composite scattering theory and the scatterometer-acquired data were used to obtain an expression of radar scattering over ocean surfaces with oil spills. The study demonstrates that the presence and extent of oil spills can be detected using high frequency radar systems.

Twelve, Experimental, Highly Significant.

Gulf of Mexico, Mar. 16, 1970; 13.3 GHz Single-Polarized Scatterometer (NASA).

Backscattering, cross section, oil, waves, scatterometer.

13.3 GHz (VV) Scatterometer data over an oil spill was compared to that of a calm sea and excellent agreement was found. Indications show that in the presence of oil the high surface wind velocity ocean radar scattering cross section is similar to that of an ocean with low surface wind speed.

Comparison of σ^{o} for a surface with and without oil slicks shows that at incidence angles of 25^{o} and above σ^{o} decreases about 7 dB in the presence of oil. This implies that the power returned from an oil slick is decreased by a ratio of 5 over the return from an oil free surface.

Maintaining a constant incidence angle a graph of average σ^{o} as a function of time/distance was plotted. A definite dip showed the presence of oil. This is one possible way of determining aerial extent.

Experimental and calculated values of backscattering cross sections from the sea's small gravity - capillary structure for oil free and oil covered areas showed close agreement.

Repeated coverage of an affected area with radars and presentation of the data as false - color photography can be used to detect and monitor the spread of an oil spill.

LARSON, R.W., R. RAWSON, D. AUSHERMAN, L. BRYAN and L. PORCELLO, "Multi-Spectral Microwave Imagery Radar for Remote Sensing Applications," Proceedings, URSI Commission, II Specialist Meeting on Microwave Scattering and Emission from Earth, Berne, Switzerland, pp 305-315, (September 1974). ERIM, Ann Arbor, Michigan.

Abstract - A multispectral airborne microwave radar imaging system, capable of obtaining four images simultaneously is described. The system has been successfully demonstrated in several experiment and one example of results obtained, freshwater ice, is given. Consideration of the digitization of the imagery is given and an image digitizing system described briefly. Preliminary results of digitization experiments are included.

Nine, Experimental and General, Normal.

Northern Great Lakes; ERIM Four Channel SAR, X & L-band.

SAR, Digitized data, texture analysis, radar backscatter.

Four channel radar data has been digitized and registered. The combination of the digitization system and digital data processor provides a powerful tool for the analysis of radar data and for the handling of the large volume of radar data to be expected from spacecraft radar systems such as SEASAT.

Many complex operations can be carried out with the microwave data in a digital format. Various statistics of returns in the radar imagery can be calculated and used in recognition algorithms. Texture analysis can be accomplished to provide additional capabilities in identification and classification of various factors such as ice types, fields or crops, and others.

LE VINE, D.M., "Monitoring the Sea Surface with a Short Pulse Radar," Proceedings, URSI Commission II Specialist Meeting on Microwave Scattering and Emission from Earth, Berne, Switzerland, pp 67-75, (September 1974). Goddard Space Flight Centre, Greenbelt, Maryland.

Abstract - A solution is presented for the scattering of short pulses from a stochastic, corrugated surface apropos of the sea for the case of a narrow beam transmitting antenna pointing near nadir. The spectrum of the received power and its time history are calculated and this solution is used to show that a measure of the variance of the surface ordinant can be obtained from the backscatterer power. A composite model is employed for the surface with the Kirchoff approximation being used for the large-scale surface undulations and a perturbation method employed to account for the small-scale structure. Included explicity in the analysis is the finite nature of the source and the role of the small-scale wave structure (capillary wave range). It is shown that when sufficiently short pulses are transmitted, one can obtain a measure of the variance of the large-scale surface ordinant from either the temporal spacing of the peaks in the returned power or from the envelope of the spectrum of the received power. Assuming an appropriate model for the statistics and spectrum of the surface ordinate, the variance can be used to compute the wind speed and the significant wave height of the surface.

The theoretical work is part of a program at the Goddard Space Flight Center (NASA) to evaluate the potential of a short pulse radar for active sensing of the sea. An experiment of a preliminary nature has been performed and another experiment using more suitable equipment is underway. Comparison of the theory with some preliminary experimental data will be given.

Seven, Theoretical and Experimental, Significant.

Atlantic; Janaury, 1974; NRL Altimeter, X-band.

JONSWOP, spectrum, received power, sea surface, scattered field, significant wave height, wind speed, radar, altimeter.

Both the temporal history and the spectrum of the power scattered by a short pulse can be expressed in terms of the solution for complex (analytic) representation of the scattered field. The solution employed to obtain the complex representation of the scattered fields is basically a physical optics solution modified to include the effects of small-scale

surface roughness. The calculations are executed for the case of a Gaussian distributed (large-scale) surface.

LOWRY, R.T., D.G. GOODENOUGH, J.S. ZELENLKA* and R.A. SHUCHMAN*, "On the Analysis of Airbrone Synthetic Aperture Radar Imagery of the Ocean," Proceedings of the Fourth Canadian Symposium on Remote Sensing, Quebec City, I, pp 480-505, (May 1977). CCRS, ERIM*. Canadian Aeronautics and Space Institute.

Abstract - As part of the National Aeronautics and Space Administration (NASA) SEASAT/Marineland experiment, scientists from the Canada Centre for Remote Sensing (CCRS) and the Environmental Research Institute of Michigan (ERIM), using the ERIM optical/digital correlator, digitized selected portions of the data taken with the ERIM 4-channel synthetic aperture radar (SAR) off the coast of Florida. The CCRS objectives were to obtain data with which to:

(a) study the implications of wave train velocity on SAR correlator design and operations;
(b) investigate the relationship between the two-dimensional transform of a spectrum of waves as measured by buoys;
(c) investigate at various resolutions ocean wave and ship imagery at both X-band (3 cm) and L-band (25 cm) wave length and both parallel and cross polarization to predict which would be best for various surveillance tasks, and
(d) examine the electromagnetic/water wave interactions by which waves are imaged.

In examining these questions, CCRS developed software to do geometric and radiometric correction and two dimensional transforms of the radar imagery.

The presentation will include an outline of the problems presented and the software developed. Results will be presented of a comparative study of wave visibility as a function of radar wavelength, polarization, look angle, focus, and resolution. A similar study to determine what parameters might be best for ship surveillance will be discussed and results presented. We shall also show results of our investigation of two dimensional spectra and discuss wave imaging models.

Twenty-Six, Experimental, Significant.

Marineland Experiment; December, 1975; ERIM 4-Channel SAR.

SAR radar data correction, wave train, velocity implications, Fourier analysis.

The paper is concerned with a digital study carried out on Marineland data. The program included radar data correction for geometric distortion and radiometric non-uniformity as a function of range.

MAURER, LT. A. and A.T. EDGERTON*, "Flight Evaluation of U.S. Coast Guard Airborne Oil Surveillance System," Conference on Prevention and Control of Oil Pollution, San Francisco, California, pp 30, (March 1975). U.S. Coast Guard and Aeroject Electrosystems Company*.

Abstract - A prototype airborne oil surveillance system was developed for the U.S. Coast Guard by Aerojet ElectroSystems Company. The multisensor system permits real-time day/night, all weather detection, mapping and documentation of oil spills at sea. The system was installed aboard a Coast Guard HU-16 Albatross and flight tested off the California Coast. Surveillance data were obtained from natural seeps, a series of controlled oil spills, routine shipping and targets of opportunity.

The system reliably detected and mapped oil spills and seeps for conditions ranging from dense undercast to clear, wind speeds from 0 to 25 knots and daytime to total darkness. Test results demonstrate that a practical airborne oil surveillance system is feasible and can be invaluable to other Coast Guard missions.

Nine, Experimental, Highly Significant.

California Coast; July through October, 1974; AOSS.

SLAR, passive microwave imager, oil, ocean, wind, sea state.

The approximate minimum detectable oil film thickness for each of the detection instruments are given. The relationships are rather qualitative since precise techniques for the measurement of oil film thickness have not yet been perfected.

Radar systems detect oil slicks by measuring a reduction in radar backscatter resulting from calming effect oil films on small-scale water waves. The radar signatures are dependent on wind speed, especially for winds less than 3 knots. Small-scale wave damping by oil films is a boundary layer phenomenon and it is theoretically possible for a radar to detect monomolecular layer oil films.

Passive microwave systems measure the natural microwave energy emitted and/or reflected by surfaces. This natural microwave energy is a function of surface roughness and the dielectric constant of the surface. Oil slicks affect the radiometric response in two ways. In the presence of moderate to high winds, thin films of oil (0.1 mm and greater) emit more microwave energy than unpolluted water (due to the significantly lower dielectric constant of oil). The increase in microwave emission from oils films

0.1 mm thick and greater overshadows the decrease in ocean roughness and produces positive contrasts for low to moderate wind conditions. The microwave emission from oil films of 0.1 mm or more is a function of the film thickness and this information may be inferred from the relative brightness temperature measured. Use of multiple-frequency radiometers can produce more accurate thickness data and enable quantification of the volume of the discharge.

Controlled spills were conducted for conditions ranging from dense undercast (760 m marine layer) to clear, wind speeds from 0 to 13 m/s, calm to 4 metre seas, and daytime to total darkness. Discharges used in the testing varied from static (point source), spills of 1900 litres, to dynamic spills (vessel underway) of less than 13.5 liters per km. In all instances the discharges were reliably detected and mapped (all ranges up to 22 km). Multisensor evaluation of the slicks encountered in the test program permitted a first order approximation of the volume of the discharges and/or seepage. Multisensor evalution also permitted differentiation between oil slicks and false alarms.

Large ships were detected at ranges in excess of 74 km and smaller craft were also detected at substantial ranges. Vessel identification and documentation proved to be difficult in many instances due to the small size or apparent absences of markings on some ships.

The testing also verified that every individual sensor has at least one blind spot such that an intergrated multisensor system is required for the surveillance task.

MAURER, A.T., A.T. EDGERTON, and D.C.MEEKS, "U.S. Coast Guard Airborne Oil Surveillance System Status Report," Proceedings of the Eleventh International Symposium on Remote Sensing of the Environment, Ann Arbor, Michigan, II, pp 1639-1640, (April 1977). USCG, Aerojet Electro Systems Company.

Summary - The U.S. Coast Guard, through the provisions of legislation such as the Federal Water Pollution Control Act and the Marine Sanctuaries Act, is assigned the responsibility of enforcing anti-pollution discharge laws and regulations in the navigable waters of the United States. To meet this responsibility, the Coast Guard has embarked on a program to equip a number of new Medium Range Surveillance (MRS) aircraft with operational sensor systems designed to detect, quantify, identify, map and document oil spills on the open ocean. A major step in that program was the development of the Airborne Oil Surveillance System (AOSS).

The prototype AOSS was developed by Aerojet ElectroSystems Company for the Coast Guard through a program initiated in 1972. The AOSS was designed to be a real-time all weather, day/night sensor system with the capability to (1) detect oil slicks; (2) indicate the magnitude of spills - aerial extent and approximate thickness; (3) identify and document the source(s) of discharge; (4) assess cleanup operations; and (5) gather data regarding the frequency and magnitude of significant spills.

The prototype system was installed aboard a Coast Guard HU-16E Albatross and flight tested off the California coast. Controlled testing of the system was completed in October 1974. During 1975 the prototype AOSS aircraft was used operationally by the Coast Guard to evaluate the system effectiveness in detection; monitoring and assessment of offshore oil discharges; search and rescue operations; ice reconnaissance missions; and monitoring of foreign fishing activities in coastal waters. Approximately 350 hours of operational experience were realized.

The results of both the controlled testing and opertional evaluation prompted a decision by the Coast Guard to incorporate several improvements to the system and transfer the improved version to an operational C-130 as a permanent installation.

The operational version of the AOSS is an integrated multisensor system configured to provide effective airborne oil surveillance over a wide range of operating conditions. The system uses a sidelooking radar system and a passive microwave imager for long range ship-spill surveillance up to 25 miles from each side of the aircraft. The combination permits effective detection and oil slick mapping day or night and under all

but extreme weather conditions. The system also includes an aerial reconnaissance camera and a multichannel line scanner for high resolution documentation of discharges and oily suspected violators. This total sensor combination permits multispectral false target discrimination and an approximation of the magnitude (area and thickness) of slicks.

The side-looking radar system is a modified APS-94D system which uses a unique 8 foot, vertically polarized antenna for oil detection and mapping. A standard 16 foot horizontally polarized antenna complements the 8 foot antenna to provide a 50 nautical mile swath width. This system produces a near real-time radar map on film. The 37 GHz passive microwave imager is horizontally polarized and scans in a conic arc with a constant incidence angle of 45^{o}. The dual beam imager has internal calibration sources and is Dicke-switched. The RS-18 MS multispectral line scanner operates in three bands: 8 to 14 micrometres, 8.0 to 9.5 micrometers and 0.32 to 0.38 micrometres. The camera is a standard KS-72 aerial reconnaissance camera.

The four sensors and a position reference system are integrated by means of a software controlled operator console with real-time video displays. This arrangement permits the operator to select the best sensor(s) for the prevailing conditions so that the unique advantages of each sensor can be used and their individual limitations avoided. All imagery is automatically annotated using an airborne data annotation system interfaced with the computer console. Sensor data from any of the sensors can be converted to a common display format by the processing display subsystem to facilitate operator interpretation of the data. Data displayed can also be recorded on a video tape recorder.

Nil, General (Summary), Normal.

AOSS.

Oil spill, multispectral.

MEEKS, D.C., D.P. WILLIAMS, R.M. WILCOX, and A.T. EDGERTON, "Microwave Radiometric Detection of Oil Slicks," Aerojet General Corporation, Report No. 1335-2, pp 177, (March 1971). Microwave Division, Aerojet General Corporation, El Monte, California.

Abstract - Two years of research have been conducted to determine the feasibility of using microwave radiometry for the detection, identification, and surveillance of oil pollution. The research can be divided into three main areas: (1) theoretical studies; (2) laboratory experiments; and (3) airborne measurements. Theoretical studies consisted of a review of contemporary theory concerning parameters that influence microwave emission from both unpolluted and oil covered seas. Laboratory investigations confirmed results obtained from earlier studies and established the response characteristics of the 3.2 mm sensor to continuous oil films. Airborne measurements of controlled spills off the Southern California Coast were performed with dual-polarized 3.2 and 8.1 mm sensors oriented with a forward antenna viewing angle 45^{o} above nadir. Four sets of oil spills, or missions, were performed to obtain data over a variety of sea surface conditions. Pollutants used for the tests included No. 2 diesel fuel, 26.1 and 21.6 API gravity crude oils, and 9.7 API gravity fuel oil. For each set of spills, both ocean surface observations and airborne measurements were performed for three days, or until the slicks dissipated. Significant microwave brightness temperature oil slick signatures were noted for a wide range of ocean conditions (sea states 1-4) and oil film thickness (thickness <1 micron and greater). Based on the experimental results, a passive microwave imaging system configuration has been recommended for oil pollution surveillance.

Thirty-four, Theoretical and Experimental, Highly Significant.

South California; 1969-1970; Aerojet General 3.2 mm and 8.1 mm passive microwave radiometers and laboratory facilities, Piper Apache aircraft 35 mm camera and K-17 aerial camera.

Oil, sea state, damping, brightness temperature, thickness, passive microwave, dielectric properties, emissive properties.

Theoretical work is undertaken to determine microwave emissivity under rough and calm sea conditions for oil of varying thicknesses and type. Polarization and incidence angle effects are examined. A detailed analysis of the damping of waves by an oil film is also

undertaken. The effects of salinity, temperature and foam on ocean surface brightness temperature are also discussed.

Numerous curves are given for all the above.

A description of the laboratory tests is provided and in general confirm theoretical analyses for calm sea conditions. However, viscous oils were found not to spread evenly and the film thickness tends to be non-uniform so that brightness temperatures oscillations associated with real oil slicks are not as prevalent.

A detailed description of the airborne experiments were given along with a discussion of results.

The theoretical and experimental data are compared and a list of conclusions given.

A general list of conclusions is given and a 37 GHz (8.1 mm) imager is recommended. Additional observations are noted, especially that natural oil films may give a high false alarm rate.

A description of a proposed system is provided and techniques for calibrations are given.

MEEKS, D.C., G.A. POE, and R.O. RAMSEIER*, "A Study of Microwave Emission Properties of Sea Ice - AIDJEX," Aerojet Electrosystems Company, California, Final Report No. 1786 FR-1, pp 103, (January 1972). Aeroject Electrosystems Company, California; DOE*, Ottawa. University of Washington, AIDJEX Program Office, Seattle, Washington.

Abstract - Results derived from a comparative study of surface-based 13.4 GHz passive microwave measurements and detailed surface truth measurements concerning the physical properties of sea ice performed during the 1972 AIDJEX pilot study are reported in detail. Data obtained illustrate distinct decreasing microwave emissions for first-year, transitional and multi-year sea ice types. For transition and multi year ice, a structural relationship for microwave emission by sea ice type exists. Both vertically and horizontally polarized measured brightness temperatures decrease linearly with increasing average ice porosity. In the case of first-year ice, however, measured brightness temperatures are comparatively uniform and microwave emission appears to be more strongly influenced by high near surface salinity concentrations combined with the occurrence of uniform porosity. Detailed substantiation for these results and their relationship in the determination of ice thickness is offered. Evaluations of the effects of physical sea ice temperature and Arctic snow cover upon microwave emission are made and the structural complexity of the sea ice in terms of measured brightness temperature is illustrated.

Eleven, Experimental and Theoretical, Highly Significant.

AIDJEX Camp off Pt. Barrow, Alaska; April, 1972; Experimental 13.4 GHz Dual Polarized Radiometer.

Sea ice, microwave, radiometer, brightness temperature, AIDJEX, brine, volume, porosity.

Warm and cool microwave brightness temperatures are quantitatively related to first-year and multi-year sea ice, respectively. These ice types represent the upper and lower bounds of sea ice passive microwave signatures and are easily identifiable from high flying aircraft and satellite altitudes. In addition to these ice types, open water (leads and polynyas), thin ice, transition ice, and refrozen melt ponds are quantifiable when using high resolution microwave radiometry.

The first-year ice and melt ponds that have grown through the ice cover are not radiometrically distinguishable and in terms of microwave emission are both considered to be first-year ice. Measured brightness temperatures obtained for these ice types are comparatively uniform (average = 255^{o}K) and microwave emission is mostly influenced by high near surface salinity ($\geq 2^{o}/_{oo}$) concentration with the occurrence of uniform porosity.

For transitional sea ice, brightness temperature decreases as a function of increasing average ice porosity and decreasing ice salinity.

The brightness temperature for multi-year ice and melt ponds decreases linearly as a function of increasing average ice porosity, amounting to about a 2^{o}K decrease per one percent increase in average porosity.

Freeboard height (ice above sea level) for transitional ice, refrozen melt ponds, and multi-year ice can be inferred from measured brightness temperature.

The horizontally polarized brightness temperature is more affected by surface roughness than the vertically polarized brightness temperature.

It can tentatively be concluded that Arctic snow cover has no significant effect upon brightness temperature when making a differentiation between ice types. It is noted, however, that this conclusion is only valid during the non-melt Arctic seasons and is not applicable during the summer months when free water exists within the snow cover.

MEEKS*, D.C., R.O. RAMSEIER**, and W.J. CAMPBELL***, "A Study of Microwave Emission Properties of Sea Ice - AIDJEX 1972," Proceedings of the Ninth International Symposium on Remote Sensing of Environment, Ann Arbor, Michigan, I, pp 307-322, (April 1974). Aerojet Electrosystems Company*, COE (Canada)**, USGS***.

Abstract - Results derived from a comparative study of surface based 13.4 GHz passive microwave measurements with detailed surface truth measurements concerning the physical chemical and structural properties of Arctic Sea ice illustrate distinct decreasing microwave emissions for first-year, transitional and multi-year sea ice types. For transitional and multi-year ice, a structural relationship for microwace emissions by sea ice exists. Both vertically and horizontally polarized measured brightness temperatures decreases linearly with increasing average ice porosity. In the case of first-year ice, however, measured brightness temperatures are comparatively uniform and microwave emission appears to be more strongly influenced by high near surface salinity concentrations combined with the occurrence of uniform porosity.

Eight, Experimental, Highly Significant.

Beaufort Sea; April, 1972; 13.4 GHz Microwave Radiometer (Dual Polarized).

Sea Ice, classification, salinity, porosity, brightness temperature, passive microwave.

The radiometer was mounted on a 13 ft tower with a view angle of 40°. It was moved to different areas of a designated target site. Cores were used to classify the ice types via salinity profiles. The ground resolution was 0.31 by 0.58 meters.

Some discussion and results are given correlating skin depth and brightness temperature with ice types (salinity). The brightness temperature is related to physical properties and ice thickness. Various graphs are provided.

The problem of the lower aircraft resolution is examined. A list of conclusions are given.

MEYER, M.A., "Remote Sensing of Ice and Snow Thickness," Proceedings of the Fourth Symposium on Remote Sensing of Environment, Ann Arbor, Michigan, pp 183-192, (December 1966). Adcole Corporation, Massachusetts.

Abstract - A high resolution monocycle VHF radar has been developed and tested over lake ice. Tests were conducted with the U.S. Army Cold Regions Research and Engineering Laboratory using a boom as the antenna support in 1965, and using a moving helicopter as a support in 1966.

Ice thickness and snow thickness were rapidly measured by visual data reduction. Thickness measurement accuracies of the order of 1 cm are possible utilizing this technique. Results of measurements and the data taken are discussed as well as the expected results for such a measurement. The application of these measurements to the determination of dielectric constant is discussed.

Two, Experimental, Significant.

Lake Mascoma, New Hampshire; February, 1965; Experimental Monocycle VHF Radar.

Ice thickness, snow thickness, VHF, monocycle radar, impulse radar, remote sensing.

The work to date has clearly demonstrated the utility of a monocycle radar for fresh lake and snow thickness measurements. Further measurements will indicate its effectiveness for media with complex dielectric constants introducing attenuation such as sea ice.

MOORE, R.K., J.P. CLAASSEN, J.D. YOUNG, W..J. PIERSON, Jr., and V.J. CARDONE*, "Preliminary Analysis of Skylab RADSCAT Results over the Ocean," Proceedings, URSI Commission II Specialist Meeting on Microwace Scattering and Emission from Earth, Berne, Switzerland, pp 47-53, (September 1974). University of Kansas, Centre for Research Inc. City University of New York.

Abstract - Preliminary observations at 13.9 GHz of the radar backscatter and microwave emission from the sea have been analyzed using data obtained by the radiometer-scatterometer on Skylab. Results indicate approximately a square-law relationship between differential scattering coefficient and windspeed at angles of 40^{o} to 50^{o}, after correction for directional effects, over a range from about 4 up to about 25 m/s. The brightness temperature response was also observed, and considerable success was achieved in correcting it for atmospheric attenuation and emission.

Measurements reported here were made in June, 1973, over Hurricane Ava off the west coast of Mexico and Caribbean Sea. Many other observations were made with the Skylab instrument, but analysis awaits corrections to the data.

Three, Experimental, Normal.

Pacific Ocean; June, 1973; Skylab RADSCAT at 13.9 GHz.

Skylab, RADSCAT, ocean, wind speed, Hurricane Ava, scattering.

The preliminary Skylab data from June of 1973 indicate good correspondence between radar and radiometric signals received from the ocean and wind speed. Apparently, much of the scatter of the data points is caused by coarseness of the available meteorological data rather than by deviations in the response of the scatterometer to the local wind speed.

MOORE, ROBERT P. and JOHN, O. HOOPER, "Microwave Radiometric Characteristics of Snow Covered Terrain," Proceedings of the Ninth International Symposium on Remote Sensing of Environment, Ann Arbor, Michigan, III, pp 1621-1632, (April 1974). Naval Weapons Centre, China Lake, Cal.

Summary - A very sensitive Ka-band microwave radiometer has been used to map agricultural areas during winter, spring and summer seasons, and at various altitudes. Preliminary analysis of these data indicate possible use of microwave radiometric maps in the remote sensing of agricultural, geological, and geographical parameters.

The microwave radiometer utilized in this program employs a parametric amplifier to achieve its ultra-high sensitivity. The mapping function is accomplished by rotating parabolic antennas which scan the beam in the cross-track direction. The area mapped is a strip which has a width four times the altitude of the aircraft. The system is capable of rapid installation and removal. The radiometer will operate automatically over a wide range of speeds and altitudes and is capable of either a Dicke or high-speed mode of operation. The temperature sensitivity and spatial resolution are sufficient to produce detailed images of the terrain.

A number of mapping flight tests have been conducted over cultivated terrain during the winter, spring (both thawing and freezing states), and the summer seasons. Maps were obtained at 300, 740, 1,400 and 3,000 metres during each season. Ground truth data includes aerial photographs taken (1) simultaneously with the radiometric maps, (2) a short time after the flight tests, and (3) 2 to 8 years before the flight tests. Agricultural information, contour maps, and observer comments have also been obtained.

Preliminary analysis of these data show that most of the field structure is visible through the snow cover. Small lakes and sloughs are detectable in the winter data, although most are frozen solid and covered with snow. Some contrast reversals occurred in the data during the spring melting season. In spite of some seasonal variability of the radiometric map, almost all terrain features are detectable during all seasons; field patterns, sloughs and lakes, roads, forested areas, and buildings are among the detectable items. There are reasons to believe that a strong correlation exists between the field patterns and crop plants, cultivation state, and soil types.

Harvested fields that were planted in oats, for example, tend to produce very cold radiometric temperatures during the winter. Radiometric images of sloughs and drainage areas correlate well with contour maps.

The visibility of these features may be due not only to the transparency of the snow at these frequencies, but the physical characteristics of the snow as affected by the nature of the terrain beneath it. The terrain roughness and its thermal characteristics are believed to modulate the effect of sun and temperature on the snow. The present data is insufficient to establish such a relationship; however, such a possibility should be investigated further, since it has important implications for remote sensing. For example, if the radiometric signature of a certain soil type could be tied to its thermal characteristics, moisture content and other information could possibly be deducted.

In addition to solving the problem of terrain remote sensing through snow cover, the technique provides a means by which to survey large areas in a short period of time. For example, the present system covers a 12,000 metre swath width when flying at 3,000 metres. This swath could be covered for speeds in excess of 700 kilometres per hour, if so desired.

Seven, Experimental, Significant.

Agricultural Area; 1970; 33.6 GHz Passive Microwave Imaging Radiometer.

Snow, weather effects, terrain, emissivity, reflectivity, passive microwave.

The reasons for being able to "see through" snow cover terrain are hypothesized. Design considerations are discussed for optimizing for weather effects. Some data is provided regarding these effects.

O'NEIL, R.A., "The Application of Presently Available Sensors for Airborne Oil Pollution Surveillance," Requirements for the Control of Vessel Source Pollution, Appendix A, pp 49, (April 1976). CCRS. CCRS 1009076.

Abstract - A survey is made of a number of sensors which may be suitable for the airborne surveillance of Canadian territorial waters. Emphasis is made on the application of these sensors to the detection and identification of oils spills. The following sensors are considered: a side looking radar, an infrared/ultra-violet line scanner, a forward looking radar, an infrared/ultra-violet line scanner, a forward looking surveillance radar, a low light level television, a profiling microwave radiometer, a camera system, an illumination system for night-time photography, a laser fluorosensor and a forward looking infrared radiometer. While not all of these sensors may be necessary at any one time, it is noted that the data from the individual sensors is usually complementary; and thus, one sensor does not make the others redundant. As well as real time displays, a suitable method of data acquisition and annotation must be provided for the data.

Fourteen, General, Highly Significant.

AOSS, Motorola APS-94 Series SLR's, Goodyear APD-10 SLR, Westinghouse K-band APQ-10 SLR.

Oil spill, SLAR, passive microwave.

Two thirds of the oil appearing on the oceans and lakes come from a shore source. An oil slick may consist of many different types of oil. Wind and wave action form the slick into a series of streamers with very little oil between them. Dispersion is mainly governed by wind and wave action. The shape of an oil spill is a major clue to its identity and its origin, thus, imaging sensors are desirable for oil pollution detection.

A Side Looking Radar (SLR) is able to detect an oil spill on the ocean because of the oil stills the capillary waves. Vertical polarization has been used to maximize the clutter. The Airborne Oil Surveillance System (AOSS) SLR was able to detect oil slicks under a wide variety of conditions from a minimum thickness of 3.5 μm to a very thick state spill of 1900 litres of Bunker C. Slicks were detected at 32 km. Spills were not detected over glassy oceans (no wind), but identified at wind speeds between 0.8 and 10 m/s. Some doubt exists as to whether oil can be seen in the stormy waters which frequently occur off

Canada's coasts. A blind area exists directly under the aircraft which is the greater of 2.2 times the altitude or 1330 m wide.

A microwave radiometer can give some indication of oil thickness. At 37 GHz, passive microwave techniques can measure oil thickness between 0.05 to 1.5 mm. The signature is dependent on the thickness no contrast is seen when a microwave radiometer views a thin oil slick on a calm sea.

A thick oil slick will exhibit a higher brightness temperature. The brightness temperature decreases with increasing sea state. The oil tends to be swept into regions of varying thickness in a rough sea. Interference effects within the oil films can cause ambiguous values for the thickness measurement; but this can be resolved by equipping the radiometers with receivers tuned to different microwave frequencies. There will be some ambiguity in the AOSS Passive Microwave Imager for thicknesses greater than 1.5 mm.

PAGE, D.F., and R.O. RAMSEIER, "Application of Radar Techniques to Ice and Snow Studies," Journal of Glaciology, 15, 73, pp 171-191, (1975). Communication Research Centre and Department of Environment (1) Reprint from authors (2) International Glaciology Society.

Abstract - This paper presents an overview of the active microwave tools becoming available to the glaciologist with emphasis on recent radar developments as applied to floating ice. Sufficient theory is presented for the user to understand the techniques. Side-looking radar imagery is discussed using a number of examples resulting from the use of real and synthetic aperture, single and dual polarization. Recent studies of the microwave properties of ice and snow are reviewed, and are shown to be leading to significant advances in high-resolution radar techniques for accurate sounding of these materials. Remote sensing of freshwater ice thickness is shown to be well established and operational, with similar techniques feasible in the near future for sea ice. It is pointed out that both imaging and probing radars applied to studies of sea ice and snow usually must be used in association with data from other sensors.

Forty-five, Theoretical and Review, Significant.

Rotating scan radar, SLR, scatterometer, radar sounding, impulse radar probes.

Using rotation scan radar or plan position indicator (PPI) sea ice can be imaged. The ability to distinguish adjacent objects depends on the resolution of the radar used. A limitation of PPI radars is very coarse azimuthal resolution. Good range resolution can be obtained. The azimuthal resolution is determined by antenna size and usually cannot be made large enough for remote sensing purposes.

The X-band real aperture system is discussed. The imagery shows that this frequency lacks the ability to distinguish between open water and new ice. This is characteristic at X-band and results from both open water and new ice having flat specularly reflecting surfaces. Also shown was imagery of smooth floes of grey ice showing a radar return from the edges only. Stronger returns are shown from rougher older ice. The authors point out that a distinct characteristic of wide area SLAR imagery is the tendency for the amplitude of radar returns to decrease at longer cross-track ranges which results from the substantial decrease in backscatter energy as the radar angle increases from nadir. The authors also discuss synthetic aperture systems. These systems are capable of greater azimuthal resolution.

The authors state that SLR images tend not to show reflections from snow surfaces. What is shown are the stronger reflections from underneath the snow surface although old, perennial snow is sometimes visible.

The authors discuss other sensors which can be used to "calibrate" the SLR system, with a special section on the microwave scatterometer. There is also a section on radar probes such as the impulse radar and radio sounder for attempts to measure ice thickness.

PARASHAR, S.K., A.K. FUNG and R.K. MOORE, " A Theory of Wave Scatter from an Inhomogeneous Medium with a Slightly Rough Boundary and its Application to Sea Ice," Proceedings, URSI Commission II Specialist Meeting on Microwave Scattering and Emission from Earth, Berne, Switzerland, pp 245-255, (September 1974). University of Kansas.

Abstract - An analytical of electromagnetic wave scattering from an inhomogeneous medium with a slightly rough boundary surface is formulated. The inhomogeneity in the medium is assumed to vary continuously in the vertical direction. In addition, it is also assumed to have a small random variation in the horizontal direction. The medium is assumed to consist of two layers. Maxwell's equations are solved by using the small perturbation method together with Fourier transfrom technique. The resulting differential equations are solved by using WKB and variation of parameter methods. Field amplitudes in each medium are determined by taking boundary conditions into account. The expressions for first order polarized radar backscatter cross-section, σ^o, are obtained.

An attempt is made to apply the developed theory to compute sea ice scatter. The complex permittivity of sea ice, which depends on both the temperature and salinity, varies with the depth of sea ice. In addition, there is certainly some variation in the horizontal direction. Thus, the developed model may be able to give useful estimates when applied to sea ice scattering. Numerical calculations are performed for polarized radar backscatter cross section σ^o_{VV} and σ^o_{HH} at two frequencies, 13.3 GHz and 400 MHz. It can be shown that WKB method is applicable at both of these frequencies. These theoretical results are compared with the experimental results obtained from NASA Earth Resources Program mission 126. Theoretical results give the same absolute value of σ^o and the relative variation among the six ice types as is given by the experimental results.

Three, Theoretical and Experimental, Highly Significant.

Off Pt. Barrow, Alaska; April, 1970; 0.4 and 13.3 GHz Scatterometer, 16.5 GHz, SLAR.

Theoretical scattering model, sea ice, wave scatter, radar, scatterometer, inhomogeneous, surface roughness, radar scattering coefficient.

The theoretical model developed gives results that coincide reasonably well in order of magnitude and in order of responses from different types of ice. The theoretical

responses calcuated vary somewhat more rapidly with angle of incidence than do the experimental responses, with the difference being greater at 13.3 GHz than at 0.4 GHz.

PARASHAR, S.K., B.A.W. BIGGS, A.K. FUNG, and R.K. MOORE, "Investigation of Radar Discrimination of Sea ice," Proceedings of the Ninth International Symposium on Remote Sensing of Environment, Ann Arbor, Michigan, I, pp 323-332, (April 1974). University of Kansas, Centre for Research Inc.

Abstract - The ability of radar to discriminate sea ice types and their thickness was studied. Radar backscatter measurements at 400 MHz (multi-polarization) and 13.3 GHz (VV polarization) obtained from NASA Earth Resources Aircraft Program Mission 126 were analyzed in detail. The mission was conducted in April, 1970, off the coast of Alaska near Pt. Barrow. The scatterometer data were separated into seven categories of sea ice according to age and thickness as interpreted from stereo aerial photographs. The variations of radar backscatter cross section (σ^o) with sea ice thickness at various angles are presented at the two frequencies. There is a reversal of angular character of radar return from sea ice less than 18 cm thick at the two frequencies. Multi-year ice (sea ice greater than 180 cm thick) gives strongest return at 13.3 GHz. First-year ice (30 cm to 90 cm thick) gives strongest return at 400 MHz. Open water can be differentiated at both the frequencies.

Four polarization 16.5 GHz radar imagery was obtained from Mission 126. Open water and three categories of sea ice can be identified on the images. The results of the imagery analysis are consistent with the radar scatterometer results. There is some indication that cross-polarized return may be better in discriminating sea ice types and thus thickness.

An analytical theory of radar scatter from sea ice was developed. Sea ice was considered an inhomogeneous medium in which the dielectric properties vary continuously in the vertical direction. In addition, a small random horizontal variation was considered. Polarized radar backscatter cross-section (σ^o) was computed for six ice types at 400 MHz and 13.3 GHz by taking surface roughness into account. The results thus obtained are presented and are shown to be in general agreement with the experimental results.

Automatic classification techniques were applied to scatterometry data. Using the four categories (as in the SLAR analysis), a correct classification of 85 percent can be achieved. The results presented here may be important in understanding the nature of radar return from sea ice and in design of ice mapping imaging radars.

Fifteen, Experimental and Theoretical, Highly Significant.

Near Pt. Barrow, Alaska; April, 1970; 13.3 GHz and 400 MHz Scatterometer, 16.5 GHz SLAR.

Sea ice, SLAR scatterometer, radar microwave, scattering coefficient polarization, theoretical model.

13.3 GHz signals can be used with high certainty to identify ice thickness categories: open water, less than 18 cm, 18 to 90 cm, greater than 90 cm.

Greater ambiguity exists between radar returns from the thinnest ice layer (under 18 cm) and a moderately thick layer (90-180 cm), but differencies in the character of images for the two kinds of ice should permit resolving ambiguity with an imaging system. A tentative conclusion can be reached that this ambiguity does not exist with cross-polarized signals, but the quality of images used is not sufficient to guarantee that this result is valid rather a consequence of saturation in the images. Although 400 MHz is not a satisfactory for ice identification as 13.3 GHz, combining a 400 MHz and 13.3 system definitely eliminates the ambiguity regarding the very thin ice.

The developed theory of radar scattering from sea ice should be useable to permit extrapolation of the presented results to other situations where the ice temperature may be different.

PARASHAR, S.K., R.M. HARALICK, R.K. MOORE, and A.W. BIGGS, "Radar Scatterometer Discrimination of Sea Ice Types," IEEE Transactions on Geoscience Electronics, GE-15, 2, pp 83-87, (April 1977). University of Kansas, Centre for Research, Inc.

Abstract - Experiments with 400 MHz and 13.3 GHz radar scatterometers indicate that these all-weather remote sensors provide some information which may be used to discriminate between some types of sea ice categories. Using 12 incidence angles. First-year and multi-year ice were distinguished with greater than 90 percent correct identification accuracy on the basis of 13.3 GHz VV polarization scatterometer data taken in May 1967, near Pt. Barrow, Alaska (NASA Mission 47). Thin first-year and multi-year ice were distinguished with about 87 percent correct identification accuracy on the basis of the 13.3 GHz VV polarization scatterometer data taken in April, 1970, also near Pt. Barrow, Alaska (NASA Mission 126) and about 75 percent correct identification accuracy on the basis of the 400 MHz VV polarization scatterometer taken during the same mission.

Ten, Experimental, High Significant.

Near Pt. Barrow, Alaska; April, 1970; 13.3 GHz and 400 MHz Scatterometers.

Sea ice, radar, scatterometer, MISSION 126, classification, radar backscatter, prediction set, training set, Bayes Decision Rule.

A multiangle 13.3 GHz vertically polarized radar scatterometer is able to distinguish sea ice types better than a 400 MHz scatterometer. Using a Bayes decision rule assuming a multi-variate density function, the 13.3 GHz scatterometer achieved a 92 percent correct identification accuracy in distinguishing water or thin ice, first-year ice, and multi-year ice. Other automatic classifying techniques had identification accuracies less than 90 percent for the 13.3 GHz scatterometer.

PARIS, J.F., "Salinity Surveys Using an Airborne Microwave Radiometer," Proceedings of the Eighth International Symposium on Remote Sensing of Environment, Ann Arbor, Michigan, I, pp 665-675, (October 1972). Lockheed Electronics Company, Inc.

Abstract - Surface water salinity is an important parameter to be measured and surveyed in many environmental quality and resource inventory programs. These include coastal circulation, river outflow, marine ecological, salt springs pollution, disease vector and fisheries studies.

Studies of the electric properties of water with dissolved salts revealed that the thermal microwave emission of surface water is affected significantly by changes in water salinity for microwave frequencies less than 3 GHz. Surface water temperature affects the relationship also.

An L-band (1.42 GHz microwave radiometer was on the NASA 927 (NP-3A) aircraft as a part of the multifrequency microwave radiometer (MFMR). Also, an airborne infrared radiometer (PRT-5) was available on the NASA 927 aircraft. It was, therefore, feasible to use these two remote sensors to conduct surveys of water surface temperature and salinity using the NASA 927 aircraft.

An error analysis of the MFMR system was made. As a result it was determined that large systematic errors were present in the determination of (1) the scale factor for the response curve of the radiometer and (2) the antenna transmission factor. To remedy this problem, a scheme was developed such that MRMF data taken during a flight could be used along with a supporting surface measurement and an atmospheric sounding of temperature and humidity to determine the correct values of scale factor and antenna transmission factor. This scheme involved the use of computer models for water surface emission and reflection, atmospheric absorption, transmission, and emission; and sensor transmission and self-emission.

It was further determined that the same models could be used to obtain the salinity of the surface water from a given set of MFMR and PRT-5 data. In general, this information is gained from the remotely sensed data by a three step process. First, measurement of sky brightness and water brightness over a selected surface truth point and used to determined the correct values of scale factor and antenna transmission factor. Second, the PRT-5 measurement is used to determine water surface temperature. Last, the L-band measurement of water brightness is used with the surface temperature measurement to determine surface water salinity. An iteration technique is used for the

latter step with the use of the computer models of the microwave properties of water and of the atmosphere.

These methods were tested by using MFMR and PRT-5 data taken over a line intersecting South Pass and Southwest Pass, La., in the region of the outflow of the Mississippi River into the Gulf of Mexico. The flight took place at 262 m above the sea surface in November, 1971 during Mission 190 on a clear day with light winds. A computer program incorporating the above methods was used to produce a plot of water surface temperature and salinity along the aircraft flight line. The surface truth point was taken to be the outflow area at Southwest Pass, La., where the salinity and temperature had been measured to be 9.0 ppt and 22.2°C. A surface survey of the lines was conducted shortly after the aircraft survey. The surface measurements showed good agreement with the airborne measurements. Also, gradients in the remotely determined salinity were associated with surface convergence fronts marked by foam lines.

These investigations showed that water surface salinity and temperature may be surveyed accurately with an airborne infrared radiometer and an L-band microwave radiometer.

Ten, Theoretical and Experimental, Significant.

Gulf of Mexico; November 11, 1971; NASA Multifrequency Microwave Radiometer, one channel at 1.42 GHz.

Sea surface salinity, microwave radiometer, PRT-5, surface effects, atmospheric effects, temperature effects.

The theory of microwave emission and reflection of water is developed. Salinity and temperature effects are introduced into the dielectric constant. A curve is given for brightness temperature versus water temperature for various salinities at 1.42 GHz. Atmospheric effects are examined, including the effects of rain. Calibration equations are also given for the radiometer.

Results based on one flight pass are given showing close agreement between the salinity calculated and the actual value. One drawback of the technique is that the surface temperature is required. A PRT is used and this limits the total system capability in cloud covered areas.

PARRY, J.T., "Interpretation Techniques for X-band SLAR," Proceedings of the Fourth Canadian Symposium on Remote Sensing, Quebec City, I, pp 376-394, (May 1977). McGill University. Canadian Aeronautics and Space Institute.

Abstract - Only in recent years has high resolution SLAR imagery become available with the result that there has been little time for the elaboration and testing of interpretation procedures and techniques. In 1972, X-band synthetic aperture SLAR imagery was obtained for parts of eastern Quebec and Ontario covering a range of terrain types and cultural landscapes. System limitation parameters, operation parameters, and terrain parameters were assessed in terms of their effect on the information content of the imagery. A basic methodology of SLAR imagery interpretation was elaborated and a simple, inexpensive viewing system has devised. The various image elements such as tone, speckle, texture, shadow, shape, and association were examined and procedures were developed for the semi-quantitative assessment of tone, speckle and shadow texture. Tone and speckle can be analyzed using incremental scales which are "fixed" at various points by matching field and image detail for different types of terrain and ground cover. Radar signatures can be checked against reference sets of backscattering curves for various categories of surface material. Shadow texture can be related to terrain roughness by densito-metric and particle size analysis. Other image characteristics such as cardinal effects, blooming, corner reflector effects, and resonance can be treated deductively to yield useful information about particular objects and their response to microwave energy.

Twenty-two, Theoretical, Significant.

Ontario and Quebec; 1972; Goodyear X-band AN/UPD-4 SAR.

Synthetic Aperture, range display, swath width, scale, resolution, complex dielectric constant, surface geometry, corner reflections, resonators, roughness, local relief slope, tone, speckle, texture, pattern, size, shape, shadow, association, detection signatures, identification.

This is a theoretical paper which describes synthetic aperture systems, system limitation parameters, operational parameters, terrain parameters, and radar imagery interpretation in clear concise terms in the language of the layman and beginner. This is a useful document to read before undertaking an interpretation task using radar imagery.

PILON, R.O. and C.G. PURVES, "Radar Imagery of Oil Slicks," IEEE Transactions on Aerospace and Electronic Systems, AES-9, 5, pp 630-636, (September 1973). Naval Research Laboratory.

Abstract - A joint agency controlled oil slick experiment, sponsored by the United States Coast Guard, was conducted in the Pacific Ocean in the Fall of 1970. The Naval Research Laboratory's synthetic aperture radar was used to detect and monitor the slicks at frequencies of 428, 1228, 4455 and 8910 MHz during the low sea state conditions encountered. At frequencies of 1228 MHz and higher, the slicks were depicted with sharp boundaries. At 428 MHz, the boundaries were indistinct. Approximately 400 litres of oil was detected as it was being mapped from the initial thickness to equilibrium thicknesses of 1 micron or less. Thin streamers of oil and wind blown films were also imaged. Area growth rates were determined for 2500 litre spills of API 26.1 crude oil and API 9.7 fuel oil on a calm sea. The respective rates from approximately 1 to 4 hours after the spills, were 134 m^2/s and 16 m^2/s.

Nine, Experimental, Significant.

Santa Barbara; Fall, 1970; NRL four frequency Radar.

Oil, backscatter, waves, radar.

Radar imagery, vertically polarized, is capable of detecting and mapping oil from the initial thickness of the polluting spill to equilibrium thicknesses of 1 μm or less. Streamers from the main bodies of oil and wind blown films can also be imaged. At frequencies above approximately 1 GHz, the slicks are depicted with sharp boundaries. At lower frequencies, the boundaries are indistinct, possibly due to the intrusion of radar backscatter water wavelengths to a significant distance within the slick.

Results indicate that it is possible to image less than 400 litres during the period of spillage.

Aerial growth rates of 134 and 16 m^2/s were recorded on two of the spills showing that the lighter oil was spreading at a rate of 8.4 times faster than the more viscous oil.

PLANT, W.J., "Studies of Backscatter Sea Return with a CW, Dual-Frequency, X-band Radar," IEEE Journal of Oceanic Engineering, OE-2, 1, pp 28-35, (January 1977). Naval Research Laboratory.

Abstract - A coherent, CW, dual-frequency, X-band radar was used to study microwave sea return from the Chesapeake Bay. It is shown that the product of the backscattered fields depends strongly on long surface wave properties. In particular, a sharp line is found in the product power spectrum whose frequency is that of the water wave whose wavelength is in resonance with the spatial period of the beat frequency between the two transmitted signals and whose wave vector is parallel to the horizontal line of sight. Thus, gravity wave dispersion relations can be obtained with the system. Furthermore, the degree of modulation of short waves by long ones is given by the intensity of the line. A broad background corresponding to the convolution of the single frequency Doppler spectral is also seen in the product power spectrum. These results are shown to be interpretable in composite surface scattering theory.

Ten, Experimental and Theoretical, Normal.

Chesapeake Bay; October, 1974 to January, 1975; Coherent, CW, Dual-Frequency, X-band Radar.

Waves, backscatter, dual-frequency radar.

Each individual return in the dual-frequency system yields Doppler spectra which show mean large wave orbital velocities as well as small wave amplitudes, mean speeds, and radial directions of motion. The product of the return field gives large wave dispersion relationships and power spectra of the spatial modulation of the short waves. By offsetting the frequency of an individual return, an indication of the relative intensities of advancing and receding long waves and the strength of surface current components parallel to the horizontal viewing direction may be found.

Dual frequency radars can detect long gravity waves.

POE, G., A. STOGRYN and A.T. EDGERTON, "A Study of the Microwave Emission Characteristics of Sea Ice," U.S. Department of Commerce, NOAA, NESS, Contract No, 2-34340, Technical Report No. 1749R-2, pp 141, (September 1972). Aerojet General Corporation.

Abstract - A study is made of the applicability of presently available theories of the microwave emission properties of sea ice in explaining representative portions of the 1971 airborne passive microwave measurements taken over the Arctic ice-based AIDJEX camp. Results indicate that non-specular surface or volume (or both) scattering phenomena must be incorporated in theories of sea ice emissions before satisfactory explanations of present experimental results can be achieved. Since present theories do not include volume scattering effects, a theory of the scattering by random dielectric constant fluctuations (in a bounded medium) applicable to sea ice is derived. A theory of surface scattering for slightly rough surfaces is also derived. Interesting new theoretical results are obtained for both types of scattering. Computer programming of the volume scattering problem is partially completed and interesting new results are obtained for the one and two dimensional correlation functions needed in the theory of volume scattering.

One hundred and five, Theoretical, Highly Significant.

Volume scattering, theoretical model, microwave emission, sea ice, random medium, small-scale surface roughness, sensor dielectric constant.

In the theory of the effects of volume inhomogeneities, it was discovered that the random medium may be replaced by a non-random medium which is described not by a scalar dielectric constant, but by a tensor dielectric constant when considering the specularly reflected wave. This non-ramdom medium has a dielectric constant which is a function of depth even if the mean dielectric constant of the random medium is independent of depth.

A basic function occurring in the case of volume scattering is the Fourier transform of the three dimensional correlation function of the inhomogenieties. Since definite measurements of this correlation function have not been made, simple geometries of the inhomogenieties were employed to examine the behaviour of one and two dimensional correlation functions which can provide the basis for examining the more difficult three dimensional correlation function.

In the theory of the effects of small-scale surface roughness, it was shown that self-consistent results for brightness temperature calculations based on Rice's method of small

perturbations can be achieved only by keeping terms through second order. A basic parameter in the theory is the surface roughness spectral density function. No direct measurements relating to this quantity have been made in the case of sea ice.

PRONK, A.C., "Remote Sensing of Oil Pollution at the Sea Surface II: Damping of Water Waves by an Oil Layer as a Possible Indicator for SLAR Observations," NIWARS publication No. 22, pp 12, (July 1975). NTIS N77-23483.

Summary - The damping action of oil pollution on sea waves is discussed in view of observation from the air. It is found that oil layers of all thicknesses damp a part of the wave spectrum. Only in case of thicker layers is the damping related to the nature of the oil. The distance over which the sea waves damp out after an oil slick has entered seems a useful indicator for the oil properties.

Twenty-One, Theoretical, Significant.

Netherlands; 1974.

Oil, water waves, damping, viscosity, thickness, frequency, spectrum.

The water waves influenced by oil are in the range of 0.01 to 10 m. Only these waves can provide information about the oil layer. An oil layer always results in a damping action on capillary waves and so is detectable by the relative weakening of that wave component. Thin oil films (μm's thickness) only indicate their presence by their damping action on capillary waves; the nature of the oil (viscosity and layer thickness) at first instance cannot be deducted from the observation. The extent at which oil films (mm's thickness) damp the water waves, provides an opportunity for the estimation of the product of the oil viscosity and layer thickness. These magnitudes cannot be separated when applying water wave amplitude measurements. The damping of the waves that are influenced by an oil layer, takes place over a distance of typically 50 to 100 m upon entering of the waves into the oil slick. The relation between radar backscatter and wave spectra in general, and the deduction of the wave spectrum from the radar detection in particular, is of a great importance for gaining information on the nature of the oil layer, as the oil properties mainly show up by the deformation of the wave spectrum. The oil viscosity is highly temperature dependent such as has been found from the experiments. So, for a quantitative interpretation of the observation of an oil layer, a simultaneous absolute temperature measurement with some precision (0.2 to 0.4^{o}C) is necessary.

RAMSEIER, R.O.*, P. GLOERSEN** and W.J. CAMPBELL***, "Variation in the Microwave Emission of Sea Ice in the Beaufort and Bering Sea," Proceedings, URSI Commission II Specialist Meeting on Microwave Scattering and Emission from Earth, Berne, Switzerland, pp 87-93, (September 1974). DOE, Canada*, NASA Goodard**, USGS, Washington***.

Abstract - Analysis of microwave and physical data obtained on the surface of the sea ice and from aircraft sensors in 1972 and 1973 over the Beaufort and Bering Seas have revealed sea ice properties in addition to those reported earlier by Gloersen et al, and Nordbert et al, based on 1971 and earlier surface and aircraft data. The sea ice emissivity at 1.55 cm wavelength was found to be about 0.94 for the Bering Sea, where physical surface temperatures between 260°K and 265°K were encountered, and about 0.97 for the Beaufort sea ice where the physical surface temperature encountered were some 10°K lower. Since the physical properties i.e. salinity profiles, for the sea ice observed in the two seas were quite similar, the variation of the microwave emissivity with physical temperature has been indicated. In addition, a sea ice signature similar to that reported earlier by Gloersen et al, and Nordbert et al, for multi-year ice has been found in one case to correspond to grey ice with a thin moisture film of high salinity on the surface. Finally, analysis of surface-based measurements have shown that the composition of the sea ice in the 1972 AIDJEX test area, which appeared from the aircraft data to consist mostly of first-year sea ice with an emissivity of about 0.90, in reality was a mixture of first-year ice and relatively small fragments of multi-year ice, the order of 100 metres in diameter, or smaller.

Five, Experimental, Normal.

Beaufort and Bering Seas; Radiometer at 1.55 cm (Nimbus-5).

AIDJEX, Brightness temperature, polar ice, sea ice, BESEX, salinity, Nimbus-5, scanning microwave radiometer, emissivity, ERTS.

The microwave properties of sea ice have been reviewed illustrating that the microwave emissivity of sea ice is a function of its age, its physical temperature, its salinity, and its thickness.

RAMSEIER, R.O., M.R. VANT, L.D. ARSENAULT, L. GRAY*, R.B. GRAY**, and W.J. CHUDOBIAK***, "Distribution of Sea Ice Thickness in the Beaufort Sea," Beaufort Sea Project, Technical Report 30, pp 98, (December 1975). DOE, DEMR*, CRC**, Carleton University***. Beaufort Sea Project Office, Ottawa.

Abstract - Although it was not possible to measure sea ice thickness directly, monthly maps indicating the distribution of first year and multi-year ice for the entire Beaufort Sea region were prepared from NIMBUS-5 passive microwave imagery. Detailed investigation of the sheer zone was performed using 13.4 GHz scatterometer and X-band SLR imagery for April, 1975. A description of the various sensors employed and an outline of the development of a UHF radar for direct measurement of sea ice thickness are included.

Forty-six, Experimental, Significant.

Beaufort Sea; April, 1975; UHF Impulse Radar, SLR, Scatterometer, Passive Microwave Radiometer (NIMBUS-5).

Sea ice, X-band SLR, 13.4 GHz scatterometer, passive microwave, UHF impulse radar.

The aim of this study to make direct thickness measurements of sea ice but the results were not satisfactory. Dielectric properties of ice were intensively studies and significant advances were made. Scatterometer results provided σ^{o} vs θ curves for various sea ice types for the spring season, which allowed the identification of different types of sea ice. Cross polarized data at one angle in the 20^{o}-60^{o} range seem significant for ice type determination if visible or infrared observations are also available. SLR and scatterometer results were demonstrative in nature. The shear zone, shorefast ice, first-year ice and multi-year floes were easily identified. SLR data was not completely analyzed but it was used to ground truth the passive microwave imagery. The Nimbus-5 PMI enabled analysis of the ice cover with percentages of first-year ice, multi-year ice and open water to be determined.

RAYTHEON COMPANY, VIRGINIA, "Data Reduction of Airborne Sensor Records," Sections 1 and 8, United States Coast Guard, Office of Research and Development, Department of Transportation, Washington, D.C., Report No. DOT-CG-01-800-A, pp 11, (July 1970). Raytheon Company, Autometric Operation, Alexandria, Virginia.

Abstract - This report, through textural and graphic presentation, describes the capabilities of four remote sensors - panoramic camera, thermal infrared scanner, laser profiler and side-looking airborne radar - to detect sea and fast ice conditions and phenomena. Analysis of remote sensor records was accomplished in two modes: individual sensor record interpretation of the panoramic and thermal infrared; and interpretation of combination of sensor records. Generally speaking, the panoramic photography yielded more information on a unit area basis than any other sensor. Most ages of ice were interpreted from the available thermal infrared imagery. The laser profiler paper tapes were best utilized by correlation with an image forming sensor, thus yielding more definitive information than if examined alone. Side-Looking airborne radar provided the greatest amount of information but the lowest per unit area.

In addition to the image analysis, an investigation of existing data bases was performed, resulting in recommendations for the implementation of a data to encompass sea ice information from all sources.

General Review, Significant.

Ice, remote sensing, reconnaissance, Arctic Regions, Northwest Passage.

In general, the panoramic photography yeilded more information on a unit area basis than any other sensor. Most ages of ice were interpreted from the available thermal infrared imagery. The laser profiler data were best definitive information than if examined alone. SLAR provided the greatest amount of information but the lowest per unit area.

ROYER, G.M., "The Computer Analysis of CW Scatterometer Data with Particular Reference to the Ryan Model 720 System," CRC Report No. 1265, pp 63, (March 1975). Department of Communications.

Abstract - Scatterometer data can be analyzed to obtain the normalized backscatter coefficient, σ^{o}, a variable much used in radar theory to express the scattering properties of terrain. In this document, the equations which are required to analyze CW scatterometer data are developed. Errors in the computed values for σ^{o} are investigated as functions of imperfections arising in practical scatterometer systems. Also when computing σ^{o}, it is necessary to know certain system characteristics precisely. Measurements of these characteristics for the Ryan Model 720 system are presented.

Seven, Technical, Highly Significant.

Ryan Model 720 CW Scatterometer, 13.3 Ghz.

Data processing, scatterometer, analysis, radar detection.

This report contains the equations required for computer analysis of the CW scatterometer owned and operated by Canada Centre for Remote Sensing System parameters have been given and the combiner which has been added to the system is explained.

SCHANDA, E. and R. HOFER, "Microwave Multispectral Investigations of Snow," Proceedings of the Eleventh International Symposium on Remote Sensing of Environment, Ann Arbor, Michigan, I, pp 601-607, (April 1977). Institute of Applied Physics, University of Berne.

Abstract - A long-term observational program on the microwave emission and scatter behaviour under controlled conditions has been started at a high altitude alpine test site. All stages of development of the snow cover during the whole season are under investigation. The purpose of this study is to achieve the required knowledge on the microwave radiative properties of snow for the optimization of the microwave payloads of air and space borne snow sensors and for the interpretation of large-scale snow maps obtained by these sensors.

Preliminary results of the first month of our investigation obtained with the radiometers at 4.9, 10.5, 21 and 36 GHz are presented.

Two, Experimental, Significant.

Switzerland; March/April, 1977; 4.9, 10.4, 21, 35, and 94 GHz Microwave Radiometers.

Snow, emissive properties.

Passive microwave observations were made of snow under spring conditions at horizontal and vertical polarizations and varying incidence angles. Diurnal variations in the emissive properties are shown and related to the snow structure. The variation over a five day period is also shown, graphs are given.

SHCELL, J.A., J.W. ROUSE, Jr., J.A. PERMENTER and W.D. NORDHAUS," On the Development of a Prototype System for the Real-Time All Weather Classification of Arctic Sea Ice." Oceans 73, Seattle, Washington, pp 500-503, September. Remote Sensing Centre, Texax A & M University.

Abstract - The Arctic Region is of significance to meteorological military, mineral exploration, and transportation application. The development of an all weather system possessing the capability to classify Arctic ice in real time of potential benefit to these diverse interests.

Analysis of airborne 2.25 cm radar measurements from the Beaufort Sea have established the feasibility of the all weather radar measurement and classification of Arctic sea ice. These investigations have demonstrated the grouping of these radar measurements according to ice age. An electronic radar signal processor/ice classification system has been developed using signal conditioning and linear discriminant classification techniques to provide real time identification of sea ice by type. The processing of actual and simulated radar data by this prototype system has shown the applicability of the system design criteria in the real time classification of Arctic sea ice.

Six, Theoretical, Significant.

Beafuort Sea; Ku-band (2.25 cm) radar.

Sea ice, Ku-band, SLAR, backscatter.

The feasibility of real time classification of Arctic ice using the 2.25 cm wavelength radar scatterometer measurement is explored.

SITTROP, H., "X- and Ku-Band Radar Backscatter Characteristics of Sea Clutter," Proceedings, URSI Commission II Specialtily Meeting on Microwave Scattering and Emission for Earth, Berne, Switzerland, pp 25-37, (September 1974). Physics Laboratory TNO, The Hague, The Netherlands.

Abstract - An experimental model is demonstrated which describes the radar backscatter of sea clutter per unit area (σ^o), and the spectrum bandwidth f(0.5), as a function of grazing angle, and wind velocity. A series of parameters is incorporated in the model, to relate on the dependency of radar wavelength, polarization and observation angle with respect to wind directions.

The influence of grazing angle on σ^o and f(0.5) characteristics is quite significant and is demonstrated by a variety of slopes related to σ^o resp. f(0.5), vs wind velocity, and indicating their increase in dB's/decase. An interesting discovery is the more rapid increase of σ^o with wind velocity at X-band, compared with Ku-band.

An attempt is made to give a qualitative analysis of σ^o and f(0.5) characteristics, based on the Bragg scattering mechanism.

The measurements are carried out at the west coast of Norway, with a non-coherent measuring radar, rigidly mounted on a rock, 450 m above sea level. A sector of 180^o of sea area is covered. The influence of coastal effects on wind velocities and directions has been incorporated in the results of measurements. A calibration accuracy with 1 dB has been obtained.

Twelve, Experimental, Significant.

West Caost of Norway; 1968-1973; Experimental non-coherent pulsed radar at X- Ku-Bands.

Radar scattering, X-band, Ku-band, wind speed, spectrum, bandwidth, experimental model, polarization.

Radar backscatter coefficient, σ^o, increase with wind velocity is larger for X-band, then for Ku-band. σ^o values at X-band will become larger than those at Ku-band at wind velocities of 13 m/s and 15 m/s, for cross and upwind observations, respectively.

σ^o polarization ratios for horizontal and vertical polarization show to be dependent on observation angle, wind velocity and frequency band; for upwind at X- and Ku-band, they are more sensitive for horizontal polarization; for crosswind at X-band they show a

tendency to be more sensitive for vertical polarization and at Ku-band, they are independent of wind velocity.

The slope of the spectrum vs wind velocity curve decreases at X-band, but increases at Ku-band for larger grazing angles.

Upwind/crosswind ratios of spectrum bandwith differ significantly at X- and Ku-band. At X-band these ratios are >0dB for wind velocity (WV) <20 knots and <0dB for Wv >20 knots. At Ku-band they are <0dB for all measured wind velocity.

In general, spectrum bandwidth is larger at Ku-band. X/Ku-band ratios increase with wind velocity. The Bragg resonant capillary waves have proven to be the dominant backscattering mechanism. An increase of surfce layer viscosity (oil spills), reduces capillary waves and results in a decrease in radar backscatter.

The observed grazing angle region shows significant discrepancies between X- and Ku-band characteristics. The influence of attenuation by spray is dominant at Ku-band. The tilt dependence of scattering surfaces, due to the interaction of the larger sea structure with the short gravity and capillary waves proves to result in a radar return which is polarization dependent. The Bragg resonant rough surfaces are more easily excited at Ku-band for lower wind velocities. Together with screening effects, in particular for upwind observations, these mechanisms provide a basis for a qualitative explanation of the results obtained.

THAMAN, R.R., J.E. ESTES, R.W. BUTLER and C.M. RYERSON, "The Use of Airborne Imagery for the Estimation of Area and Thickness of Marine Oil Spills: An Operational Example," Proceedings of the Eighth International Symposium on Remote Sensing of Environment, Ann Arbor, Michigan, II, pp 1039-1104, (October 1972). University of California.

Abstract - On March 8 and 10, 1972, 27,500 gallons of biodegradable soybean oil were spilled off Point Conception, California by the United States Coast Guard as part of an experiment to evaluate a prototype high seas oil containment system. In conjunction with this experiment, both multi-spectral remote sensing imagery and surface sampling data were acquired. Using these data it was possible to: (1) evaluate a number of sensors (ranging from ultraviolet scanner imagery through photography to synthetic aperture radar) with respect to their overall usefulness for the detection, identification, measurement and monitoring of marine oil spills; (2) evaluate the usefulness of remote sensing imagery for the determination of aerial extent, thickness, and volume of oil by preparing a time-dependent budget for oil loss durng the experiment; and (3) to improve existing methods for co-ordinating surface sampling data with remote sensing overflights.

Sixteen, Experimental, Normal.

Point Conception, California; March, 1972; Various sensors, including Hughes Aircraft Company SAR (only microwave instrument used).

Soybean oil spill, detection, area, thickness, photography, infrared, ultra-violet, multi-spectral scanner, SAR.

SAR was shown to be able to detect the oil spill but because of the low sea state conditions the contrast was low. No frequencies, polarization, or resolution information is given. The altitude was 2286 m and the squint angle was 45^{o}.

THOMSON, K.P.B., S. ROSS*, and H.E. HOWARD-LOCK**, "Remote Sensing of Oil spills," Economic and Technical Review Report EPS-3-EE-74-2, Environmental Emergency Branch, Environment Canada, pp 829-840, (1974). CCRS, DOE*, McMaster University**, Information Canada Cat. No. En 46-3/1974-2.

Abstract - The Canadian Federal Government, working together with agencies of other governments, is conducting a number of programs related to detection and cleanup of oil spills in the environment.

In both the environmental assessment and clean-up aspects, remote sensing technology provides a vital input. The paper discusses the state-of-the-art in the remote detection of oil spills especially in terms of Canadian experience and needs. Three basic types of sensor "packages" are discussed. These are: passive imagery techniques operating in the visible range of the spectrum, microwave systems and active or specialized techniques. Each of these three categories has certain advantages and disadvantages. For example, simple aerial photography or airborne multi-spectral scanner systems, operating in the visible range of the spectrum, are limited by meteorological conditions and to daytime operations.

Requirements of quasi-operational airborne systems include all weather capability which can be accommodated by microwave systems. Microwave systems can also be used for night-time surveillance and, under certain conditions, for estimating the thickness of oil. The third category covers instrumentation such as active laser line-scanner systems (useful for night operations) and laser fluorosensors which may provide means of identification of the type of oil as well as distinguishing between oil and chemical effluents.

General, Normal.

Oil, Multispectral.

At microwave frequencies the emissivity of water is 0.4 while oil has an emissivity of about 1.0. For passive microwave instruments, it is found that the horizontally polarized component gives better definition.

SLAR can best detect oil slicks at surface wind speeds greater than 2 m/s. Vertical polarization is desirable.

At present there is no dedicated or even readily available remote sensing aircraft system for oil spill emergencies in Canada.

TIURI, M., M. HALLIKAINEN, and K. KASKI, "Experiments on Remote Sensing of Sea Ice Using a Microwave Radiometer," Proceedings, URSI Commission II Specialist Meeting on Microwave Scattering and Emission from Earth, Berne, Switzerland, pp 95-100, (September 1974). Helsinki University of Technology.

Abstract - Investigations have been started in Finland to find out if microwave radiometers can be used in surveying sea ice for controlling ice breakers in the Baltic Sea. Based on theoretical calculations of the brightness temperature of sea ice, the frequency of the radiometer was selected to be 4.7 GHz. The radiometer uses a novel travelling wave antenna with a beam direction depdendent on the frequency. A three-channel radiometer carried by a helicopter measures the brightness temperatures of three adjacent ice strips. An auxiliary radiometer at 605 MHz is used for checking purposes. During the winter of 1974 several measurements of different ice types were made, the results of which are described and discussed.

Seven, Experimental and Theoretical, Significant.

Baltic Sea, Bothnian Bay; March, 1974; 4.7 GHz and 605 MHz radiometers.

Microwave brightness temperature, multi-channel radiometer, sea ice, noise temperature, ice types.

Open water (with surface temperature close to $0^{\circ}C$) has a low brightness temperature of about $100^{\circ}K$ which is over $100^{\circ}K$ smaller than the temperature of thick ice, hence rifts and open leads are easily detected using the microwave radiometer.

A relatively thin ice layer increases the brightness temperature of the surface considerably ($8^{\circ}C$ ice has a brightness temperature which is only about $30^{\circ}K$ lower than that of thick ice when the surface temperature is $-3^{\circ}C$).

The effect of ice thickness on the brightness temperature seems to be relatively small for thicknesses over 500 mm. Hence, accurate ice thickness measurements are not possible in the case of thick ice.

Pressure ridges have brightness temperatures about $10^{\circ}K$ less than those of surrounding areas with normal ice. This indicates that it should be possible to detect ice ridges, which is important in guiding the ice breakers.

605 MHz and 4.8 GHz brightness temperatures do not differ very much and show similar characteristics.

TIURI, M. M. HALLIKAINEN and A. LA APERI, "Remote Sensing of Sea Ice," Microwave Radiometry, Sahko, 50, 4, pp 149-152, (April 1977). Helsinki University of Technology.

Summary - Remote Sensing of sea ice has been studied at the Radio Laboratory at Helsinki University of Technology since 1972. In addition to theory this article presents results obtained in measurements in the Gulf of Bothnia using UHF and microwave radiometry. Theory and experiments show that the UHF band is superior to microwave frequencies in the remote sensing of sea ice. It has been theoretically proved that using a 3-channel UHF radiometer, the thickness of ice can be measured with sufficient certainty. Measurements using a radiometer such as this are being conducted in winter 1977.

Five, Theoretical & Experimental, Significant.

Bay of Bothnia; Spring, 1976; Dicke-type Radiometers, 610 MHz and 4.75 GHz.

Ice Thickness, UHF, Brightness Temperature, Helicopter, low salinity.

Theoretical analysis and experimental results show that the brightness temperature of low salinity sea ice increases, oscillating with the thickness of ice when measured with a narrow band UHF radiometer.

Calculated brightness temperature, by adding the radiometric temperature at frequencies of 505, 870 and 1000 MHz, increases almost monotonously with the ice thickness for thickness as exceeding 300 mm.

The maximum measured brightness temperature at 610 MHz is about 200^{o}K for 0.111 m thick ice with a surface temperature of -3^{o}C. The minimum brightness temperature is about 145^{o}K, corresponding to an ice thickness of 270 mm.

The brightness temperature variation in the 4.75 GHz radiometer was small with a total variation of 10^{o} and 15^{o}K around 240^{o}K. Ice ridges gave lower brightness temperatures than the surrounding ice areas.

TOMIYASU, K., and W.L. JONES, "Near Nadir Radar Cross Section of Ocean," Proceedings, Remote Sensing of Earth Resources, II, University of Tennessee, Tullahoma, pp 521-527, (March 1973). General Electric Company, NASA LRC, Virginia.

Abstract - The strongest reflections of microwave signals from the ocean surface occur near nadir incidence angles, and at nadir the radar cross section decreases monotonically with increasing wind field over the ocean surface. With a calm sea, the maximum normalized radar cross section is about 8 dB less than the antenna gain. Preliminary measurements taken by using the AAFE RADSCAT sensor installed in a C-130 aircraft indicate a Nadir Radar cross section reduction of about 1/2 dB per knot of wind speed over the ocean. Further, heading dependence measurements show a difference between upwind, downwind and crosswind radar cross section for identical incidence angles. There is a possibility of measuring remotely the wind velocity over the ocean surface by using a multibeam microwave scatterometer.

Twelve, General Review, Normal.

Radar cross section, ocean, AAFE RADSCAT, specular reflection.

The theoretical value of the normalized radar cross section for a calm sea surface is reviewed and is compared with measurements. There is a possibility of determining the wave direction by making radar scattering coefficient measurements at incidence angles of about 40° from nadir with various headings.

TOOMA*, S.G., R.A. MENNELLA, J.P. HOLLINGER, and R.D. KETCHUM*, Jr., "Comparison of Sea Ice Type Identification between Airborne Dual Frequency Passive Microwave Radiometry and Standard Laser/Infrared Techniques," Journal of Glaciology, 15, 73, pp 225-239, (1975). U.S. Naval Oceanographic Office*, U.S. Naval Research Laboratory.

Abstract - During December 1973, the Naval Oceanographic Office (NAVOCEANO) and the Naval Research Laboratory (NRL) conducted a joint remote sensing experiment over the sea ice fields off Scoresby Sound on the east coast of Greenland using NAVOCEANO's RP -A Birdseye aircraft laser profiler, and infrared scanner, and NRL's 19.34 and 31.0 GHz nadir-looking radiometers. The objectives of this mission were: (1) to develop skills for interpreting sea ice passive microwave data; (2) to expand, if possible, the two category capability (multi-year ice and first-year ice) of passive microwave sensors over sea ice; (3) to compare two frequencies (19 and 31 GHz) to determine which may be more useful in a scanning radiometer now under development at NRL; and (4) to determine the value of multi-frequency as compared to single frequency study of sea ice.

Since, because of darkness and remoteness, no photography or in situ ground truth were possible for this mission, it was necessary to rely on the interpretations of the laser and infrared (IR) data to evaluate the performance of the microwave radiometers. Fortunately, excellent laser and IR data were collected, and a confident description of the ice over-flown was possible.

Five ice conditions: (1) open water/new ice; (2) smooth first-year ice; (3) ridged first-year ice; (4) multi-year ice; and (5) a higher brightness temperature form of multi-year ice interpreted as second-year ice were identifiable, regardless of weather conditions, by comparing the average of the two microwave brightness temperatures at the two frequencies with their difference.

Eight, Experimental, Highly Significant.

Off Scoresby Sound on the east coast of Greenland; December, 1973; NRL's 19.34 and 31.0 GHz Nadir Looking Radiometer.

Sea ice types, emission, brightness temperature, laser, IR.

Using two frequencies, passive microwave appears capable of distinguishing between five distinct ice types and forms. Delineation between smooth first-year ice and ridged year

ice seemed to be independent of age or thickness, but to depend rather on surface roughness.

The broad-based ridges and hummocks of multi-year ice did not appear to significantly influence the brightness temperature; rough multi-year ice was observed to have the same radiometric temperatures as smooth multi-year ice.

The $30^{o}K$ range in brightness temperature observed for multi-year ice is probably attributable to the inhomogeneity of multi-year ice caused by its make up of ice of various ages and from surface irregularities created by summer melt.

By plotting average brightness temperature versus temperature difference, it appears possible to describe the ice field generally in terms of the five categories independent of weather conditions.

VAN KUILENBERG, J., "Radar Observations of Controlled Oil Spills", Proceedings of the Tenth International Symposium on Remote Sensing of Environment, Ann Arbor, Michigan, I, pp. 243-252, (1975a). NIWARS.

Abstract - A report is given of studies and experiments concerning the radar detection of oil slicks at the sea surface. From scatterometer observations of oil slicks in a wave tank, it is concluded that oil is always detectable, but also that oil type and thickness are of little influence on the radar echo. The radar observations of the damping of water waves which travel into the polluted area is proposed as an indicator of the physical oil properties. A radar operating in the VV polarization mode is shown to be optimal because of the strength of the radar echo, the observed contrast and the low noise. However, experiments using a SLAR operating in the HH mode, showed this polarization combination to perform well enough for the purpose of oil detection. In general, the conclusion is drawn that the SLAR performs well for detection and mapping of oil spills but that other sensors are needed for classification and quantification of oil spills.

Eleven, Experimental, Significant.

Netherlands; 1975; 9.7 GHz (variable) FM-CW Scatterometer, EMI X-band SLAR.

Oil damping, polarization, scatterometer, backscatter, SLAR.

Scatterometer tests (10 GHz) were conducted under laboratory conditions for oil spilled on the surface of water subjected to various wind speeds. Qualitatively the observations are in accordance with other published results. σ^{o} grows proportional to the logarithm of the wind speed and VV polarization shows less dependence than on any other polarization combination. The dependence varies with orientation w. r. t. the wind direction. It appears that the dominant water frequency could be found as a secondary effect in the radar echo frequency spectrum. It appeared that the drift speed of the oil spill was about 2% of the wind speed at 1 m above the surface, independent of the oil type.

SLAR observations were made of controlled oil spills using HH polarizations at low sea states and wind speeds. They were almost always detectable as clearly defined patches showing contrasts of 3 to 10 dB.

No strong angle effects are observed in the range of grazing angles from 2° to 30°.

A table of the microwave properties of water are given for various salinities and temperatures. The specifications for the scatterometer and SLAR are given. Radar echo and spectrum graphs are also shown.

VAN KUILENBERG, J., "Remote Sensing of Oil Pollution at the Sea Surface, I, Review of Remote Sensing Methods emphasizing Radar," Netherlands Interdepartmental Working community for the applications of Remote Sensing Techniques (NIWARS), NIWARS Publication No. 21, pp 28, (July 1975b). NIWARS. NTIS N77-23582.

Summary - The problem of monitoring oil pollution is stated and the remote sensing methods applicable for that purpose are reviewed. A more detailed discussion is presented on radar observations of oil slicks and of the surrounding sea surface. A selected bibliography is presented.

Forty-Five, General Review, Significant.

Backscatter, oil, sea surface, SLAR scatterometer, passive microwave.

The temperature contrast between oil and water in the thermal spectral domain (3-12 μm) results from (1) initially the oil being at a different temperature when discharged; (2) at equilibrium the conduction of heat to the surface, evaporation at the sea surface, the turbulent heat transport regime of the water and air and the specific heat budget components of the slick due to radiation; and (3) the emissivity difference between the oil (0.972) and the water (0.993).

In the thermal microwave spectral domain (0.8-10 cm), the emission coefficient of water and oil is typically 0.4 and 0.8, respectively. The penetration depth of the microwaves is in the order of millimetres. As the radiation power of a passive microwave mapping system is very low the spatial resolution will be low unless a large antenna is used. This can only be improved by using a large antenna.

Foam can be confused with oil because its emission coefficient is also higher than water. thus at high wind speeds and in the wake of ships, the detection capability degrades.

Passive microwave imaging has a proven utility for thicker layers.

For active radars (8-1000 mm wavelengths) the penetration does not exceed approximately 1/10 of the radar wavelength. The damping by oil of capillary and short gravity waves should carry some information about oil types and thickness. Limited near real time performance is a drawback.

Radar scattering is mainly determined by waves which have approximately the same wavelength as the radar. The sea can be considered a scattering agent which is composed of two components. One wave changes slowly with periodicities of seconds and

amplitudes of metres and the other wave component changes more quickly with periodicities of tenths of a second and amplitudes in millimetres.

A figure showing the general trend of the scattering of the sea surface is given (σ^o versus incidence angle). At angles near vertical (0^o - 30^o) the backscatter is specular with high σ^o (5 dB) dependent of sea state and wind speed. From 30^o to 85^o a plateau region of non-specular diffuse scattering is responsible for σ^o (-40 dB). After 85^o for L-band and 89.5^o, X-band, destructive interference from directly scattered radiation and from radiation scattered after one reflection causes the return to drop about -50 dB.

The plateau region is the region where SLAR imaging occurs. For a scatterometer (0^o - 60^o) the specular region dominates.

The wind effect on σ^o is given in figures. For vertical polarization the wind effect is less (0.27 dB/km/h) than for horizontal polarization (0.43 dB/km/h). Above wind speeds of 15 m/s the sensitivity decreases. The radar cross section is always greatest in the upwind direction.

In the range of grazing angles where SLAR operates the return of the vertical polarization is 5 to 10 dB higher than that of horizontal polarization (figures).

The dependence of radar frequency on σ^o is not very pronounced. The horizontal polarization component seems to decrease roughly inversely proportional to the wavelength. Vertical polarization seems to be roughly independent of wavelength. These relations are influenced by the sea state and the polarization differences diminish with increasing sea state. The main property that is expected to be determined from multi-wavelength observations of oil slicks is the difference in damping of the different sea wavelengths running into the slicks.

The penetration into the water surface is important if an estimate is to be made of how much of the surface layer contributes to the obseved scattering (see table for typical penetration depths). Seawater has a resistance of 16 MΩ/m and a dielectric constant of bout 65 at X-band. The scattering is effectively from the surface (table given for penetration of different wavelengths).

The first unclassified observations of oil pollution were made by NRL with their four frequency experimental SAR (30 - 700 mm). Imagery taken specially for the purpose of pollution detection is of much better quality than that not specifically tuned for sea return.

Results of experiments show that spills of a few hundred litres are clearly visible near the ship which is dumping them while the estimates of the aerial extent can be made within 10% error bounds. The spreading of the spill is clearly visible and amounts to 0.5 km^2/h for lighter types. At higher sea state the oil patch breaks up and the visibility becomes less - caused by the limited spatial radar resolution.

At moderate sea states oil patches have been observed down to a thickness of 0.5 μm. These thin layers are indirectly of interest because they lag behind the thicker core of the slick and thus provide the general direction of the slick movement. The slick boundary is sharp at high frequencies (above 1 GHz) and more fuzzy at longer wavelengths. As higher frequencies mainly respond to shorter water wavelengths, multi-spectral observations indicate how far sea waves run into the slick before being damped. It was estimated that the 1.3 GHz observations (mainly 350 mm water waves) are damped after travelling 160 m. These observed differences are directly related to oil thickness and viscosity.

Graphs of scatterometer returns (10 GHz, VV) are given. There is about a 10 dB difference between an oil-covered surface and a clean one. The graphs fit the theoretical model well. There is a strong similarity between the scatter diagram of an oil slick with strong wind, and the scatter diagram of a clean sea surface with little wind. This supports the idea that mainly wave damping is observed and that the wave generating mechanism within the oil slick area is of the same character as that outside the slick area.

VV mode radar is the only sensor rated fairly good for detecting and mapping of oil slicks when day and night and all weather properties are required. All other techniques map far smaller areas.

The U.S. Coast Guard is the only agency which evaluates the remote sensing of oil pollution in a semi-operational program. A list of other systems is given.

VICKERS, R.S. and G.C. ROSE, "High Resolution Measurements of Snowpack Stratigraphy Using a Short Pulse Radar", Proceedings of the Eighth International Symposium on Remote Sensing of Environment, Ann Arbor, Michigan, I, pp 261-277, (October 1972). Colorado State University.

Summary - The measurement of snowpack thickness, density and stratigraphy has been the subject of many remote sensing papers in recent symposia. In this paper, a system is described which can be used to derive either the snow thickness, or the average snow density by measurement of the transit time of a one nanosecond radar pulse. Data is given which shows that the radar system is capable of providing an accuracy of better than 10% when used to measure the density of the snow pack. Operations in the Rocky Mountain Watershed are reported in which the system was used in both static and mobile configurations to measure snow depth.

The use of the radar system to detect horizontal layering within the snowpack is also reported and the radar data for this application is compared with that from simultaneous measurements with gamma ray density profiling equipment. The limitations of the method are presented.

Eight, Experimental, Significant.

Colorado; March-April, 1972; Short pulse radar system 2-7 GHz, 1 watt into antenna (Usable range of 12-15 m), Gamma Ray Density Profiler.

Snow density, dielectric properties, thickness, radar.

This paper describes results obtained using a short pulsed radar system to obtain snow density and thickness. A table is given showing dielectric properties and attenuation rates for snow and ice for various frequencies is also provided. A permittivity versus density curve is also given showing a direct linear relationship.

WADHAMS, P. and R.T. LOWRY, "A joint Topside - Bottomside Remote Sensing Experiment on Arctic Sea Ice," Proceedings of the Fourth Canadian Symposium on Remote Sensing, Quebec City, 1, pp 407-423, (May 1977). Canadian Aeronautics and Space Institute.

Abstract - A joint operation took place in October 1976 in which a long range Arctic patrol aircraft and a nuclear submarine undertook a detailed study of the ice cover on the Arctic Ocean from above and below. The data collected from the two platforms provides the basis for a large scale comparison of the topography above and below the Arctic sea ice canopy.

The Royal Naval submarine H.M.S. "Sovereign" entered the Arctic Ocean between Spitsbergen and Greenland and followed an under ice track of about 4,000 km extending from the offshore province near Greenland and Ellesmere Island as far as the North Pole. She was equipped with a narrowbeam upward-looking sonar to obtain a sea ice bottom profile, and a sidescan sonar mounted on her upper casing which provided some imagery out to 140 m to port and starboard. At the same time, a Canadian Armed Forces Argus aircraft of Maritime Command overflew an identical track, obtaining imagery from a laser profilometer, an infrared line scanner (IRSL) and a side looking airborne radar (SLAR/SAR).

The main goal of the experiment is a statistical comparison of the surface profiles taken from the top by laser and bottom by sonar, for identical ice provinces, allowing us to formulate the relationship between ridge height and keel draft distributions. The techniques for, analyzing sonar profiles and laser profiles has been developed and some comparisons have been made, but never on the scale of this experiment. By careful planning between aircraft and submarine and by using sophisticated navigation techniques and multiple flights, the timing and positional overlap were maximized despite the difficulties in communication and the very great difference in speed between the two platforms. In view of the high accuracy of the navigation systems used, some overlap took place between the image swathes, permitting a direct comparison of certain ice features.

We will be reporting on the data collected, which will form a datum for future work on remote sensing of ice; on a preliminary comparison of ridge and keel size and spacing distributions; on a comparison of sonar and IRLS and sonar and SLAR/SAR imagery; and we will show examples of the imagery taken by all sensors.

Sixteen, Experimental, Normal.

Arctic Ocean between Greenland and Svalbard; October, 1976; APS/94D SLAR.

Sonar, Radar, Infrared Scanner, Laser Profilometer, Sea Ice.

SLAR imagery was used in this paper to determine the direction of future studies and data manipulation. The SLAR image interpretation in this paper is in contradiction to other APS/94D interpretations. This is most likely the result of interpretation being made on a print that was a positive to negative image transfer instead of a positive to positive transfer.

WEISSMAN*, D.E., C.T. SWIFT, W.L. JONES, JR., J.W. HONSON, W.L. GRANTHAM, J.Q. HOWELL, J.C. FEDORS and J.J. DAVIS, "A Dual Frequency Radar for Ocean Roughness Sampling," Proceedings, URSI Commission II Specialist Meeting on Microwace Scattering and Emission from Earth, Berne, Switzerland, pp 55-65, (September 1974). Hofstra Univ., Hempstead, N.Y.*, NASA, Langley Research Centre, Hampton, Virginia.

Abstract - A microwave technique for determining the roughness (RMS wave height) of a randomly varying air-water interface has been developed theoretically, verified with laboratory wavetank studies and is currently being implemented for ocean surface measurements in a series of applications flight experiments. These aircarft observations will be near the Chesapeake Light Tower and will include a range of altitudes and sea conditions.

The measurement concept involves cross-correlating the envelope fluctuations on two received carriers that are monochromatic when transmitted in a normal direction to the interface and are observed in a backscatter direction after reflection by the large number of randomly distributed specular points on the surface. The measured correlation coefficient (normalized covariance) as a function of carrier frequency separation will depend on height. This correlation is equal to the square of the magnitude of the characteristic function of the specular point height from which both the RMS value and the p.d.f. can be determined.

Laboratory measurements using an X-band radar at the NASA Langley Research Centre wavetank have verified the theoretical development and now aircraft based measurements will further explore the usefulness of this method for the actual sea geometry and flight conditions. Details of the flight system are discussed and preliminary flight results are presented.

Six, Experimental and Theoretical, Significant.

Laboratory and Caribbean, June, 1974; Experimental Radar at X-band.

RMS wave height, surface roughness, dual frequency, cross-correlation, probability density function, RADSCAT.

The objective of the program is to develop a radar technique that can measure the statistical height properties of a randomly rough, surface, and to apply this capability to the observation of oceans from an aircraft or spacecraft.

The statistical quantities that can be measured are the probability density function of the height of specular points and its root mean square value.

The two frequency correlation function senses the density and relative cross section of the scattering elements (specular points) along the propagation path of the radar wave. In effect, the scattering cross section per unit area as a function of depth (or range) is observed.

WILHEIT, T., W. NORDBERG, J. BLINN*, W. CAMPBELL** and A. EDGERTON**, "Aircraft Measurements of Microwave Emission from Arctic Sea Ice," Remote Sensing of Environment, 2,3, pp 129-139, (March 1972). NASA, JPL*, USGS**, Aerojet-General Corp.***

Abstract - Measurements of the microwave emission from Arctic Sea ice were made with aircraft at 8 wavelengths ranging from 0.510 to 2.81 cm. The expected contrast in emissivities between ice and water was observed at all wavelengths. Distributions of sea ice and open water were mapped from altitudes up to 11 km in the presence of dense cloud cover.

Different forms of ice also exhibited strong contrast in emissivity. Emissivity differences of up to 0.2 were observed between two types of ice at the 0.81 cm wavelength. The higher emissivity ice type is tentatively identified as having been formed more recently than the lower emissivity ice.

Twelve, Experimental, Highly Significant.

Off Pt. Barrow, Alaska, May 1967, June 1970; 8 Microwave Radiometers ranging from 0.510 to 2.81 cm wavelength.

Microwave Radiometer, sea ice, Arctic, brightness temperature.

For typical atmospheric conditions, brightness temperatures over open water are 55 and 40 percent lower than those over ice at 30 and 10 mm wavelengths, respectively.

Two ice types, one with more emissivity termed "new" and the other termed "old" with lesser emissivity, can be identified. The contrast in emissivity between the two ice types is as much 25 percent near the 10 mm wavelenght.

Wavelengths near 10 mm are recommended for satellite use.

ZAGORODNIKOV, A.A., V.S. LOSHCHILOV, and K.B. CHELYSHEV, "Relationship between Sea Wave Parameters and The Spectra of Aerial Photography and Radar Imagery of Sea Surface," Proceedings of the Eight International Symposium on Remote Sensing of Environment, Ann Arbor, Michigan, II, pp 1083-1091, (October 1972). Arctic and Antarctic Research Institute, USSR.

Abstract - Algorithms relating sea waves spectra with two dimensional spectra of aerial photo pictures and radar imagery of sea surfaces are discussed. Examples are given how different parameters of sea waves can be obtained by means of two dimensional and one dimensional spectra of sea surface imagery.

Nine, Theoretical, Normal.

USSR

Wave spectra, two dimensional, one dimensional, directional data, SLAR, filter effects.

SLAR and aerial photography are compared for their ability to measure ocean wave spectra. The effect of the filter characteristics of the SLAR are demonstrated.

ZAGORODNIKOV, A.A., V.S. LOSHCHILOV, and K.B. CHELYSHEV, "Two Dimensional Statistical Analysis of Radar Imagery of Sea Ice," Proceedings of the Eighth International Symposium on Remote Sensing of Environment, Ann Arbor, Michigan I, pp 279-290, (October 1972). The Arctic and Antarctic Research Institute (USSR).

Abstract - Theoretical assumptions and operational techniques for obtaining morphometric characteristics of sea ice cover using airborne remote sensing (SLAR) data are discussed. The technique is based on two dimensional Fourier transformation of small scale SLAR images of the ice cover by means of optical image filtering.

Examples of optical image filtering and spectral analysis of images of different areas of ice cover are given. It is shown that the optical method is apparently the most appropriate for operational statistic analysis of ice images, obtained by a side looking airborne radar "TOROS".

Seven, Theoretical and Experimental, Normal.

TOROS SLAR.

Sea ice, spectral analysis, statistical analysis, floe size, SLAR, optical processing, remote sensing, image processing.

A technique is developed where by Fourier spectral analysis of SLAR sea ice imagery provides floe size information and whether the distribution is isotropic.